HARVARD UNIVERSITY
Graduate School of Arts and Sciences

DISSERTATION ACCEPTANCE CERTIFICATE

The undersigned, appointed by the

Department of Physics

have examined a dissertation entitled

Emergent gapless fermions in strongly-correlated phases of matter and quantum critical points

presented by Alexandra Rose Thomson

candidate for the degree of Doctor of Philosophy and hereby certify that it is worthy of acceptance.

Signature _____

Typed name: Professor Subir Sachdev, Chair

Signature _____

Typed name: Professor Daniel Jafferis

Signature _____

Typed name: Professor Ashvin Vishwanath

Date: May 3, 2018

Emergent gapless fermions in strongly-correlated phases of matter and quantum critical points

A DISSERTATION PRESENTED
BY
ALEXANDRA ROSE THOMSON
TO
THE DEPARTMENT OF PHYSICS

IN PARTIAL FULFILLMENT OF THE REQUIREMENTS
FOR THE DEGREE OF
DOCTOR OF PHILOSOPHY
IN THE SUBJECT OF
PHYSICS

HARVARD UNIVERSITY
CAMBRIDGE, MASSACHUSETTS

MAY 2018

Thesis advisor: Subir Sachdev Alexandra Rose Thomson

Emergent gapless fermions in strongly-correlated phases of matter and quantum critical points

Abstract

States with gapless degrees of freedom are typically more complicated and less well-understood than systems possessing a gap. In this thesis, we study strongly-correlated systems described by gapless fermions. In most of the systems we consider, the fermionic excitations are emergent, *i.e.* they are not adiabatically connected to the electrons which constitute the fundamental building blocks of the system in question.

We start by proposing several novel states of matter which we claim are relevant to strongly-correlated systems. The first state we present is a fractionalized Fermi liquid on the surface of a topological Kondo insulator. A Kondo insulator is a material which becomes insulating at low temperatures as a result of strong electron-spin interactions. When spin-orbit coupling is present, this insulator might be topological and, consequently, host robust gapless surface modes. Given the strong interactions and the decreased dimensionality of the surface, we propose that the spins and electrons there may decouple, resulting in the formation of a fractionalized Fermi liquid.

We next argue that quantum electrodynamics in 2+1 dimensions (QED_3) with $N_f = 4$ fermion flavours may describe a continuous, deconfined phase transition connecting the 120° coplanar Néel phase and the $\sqrt{12} \times \sqrt{12}$ valence bond solid phase of the triangular lattice antiferromagnet (AF). In addition to being a critical point, QED_3 is also believed to describe a critical phase of matter called the Dirac spin liquid. Regardless of whether QED_3 is manifest as a phase or a critical point, impurities and imperfections are always present in the real world, and it is therefore important to understand what effects this may have. We show that when QED_3 is perturbed by weak disorder, under certain circumstances, it flows to a new critical point in which both interactions and disorder are present.

Conclusively identifying a system described by QED_3 has proven to be a difficult task, not only experimentally, but in numerical studies as well. Since QED_3 is a critical theory, its spectrum on a torus is a universal quantity dependent only on low-energy degrees of freedom, such as the torus area. It follows that this data is accessible via exact diagonalization and can serve as an identifying signature of the theory. To this end, we calculate the QED_3 torus spectrum using path integral methods.

We conclude this thesis with a comprehensive study of gapped $\mathbb{Z}_2$ spin liquids of the square lattice antiferrogmagnet, using a critical theory of Dirac fermions coupled to an SU(2) gauge field as a starting point. There are many different $\mathbb{Z}_2$ spin liquid groundstates which preserve the same symmetry group. Even if one knows that a system has a $\mathbb{Z}_2$ spin liquid groundstate, it is by no means obvious *which* $\mathbb{Z}_2$ spin liquid is being realized. By starting from a gapless theory, the set of possibilities can be reduce considerably. Further, using certain recently proposed dualities, comparisons with theories formulated using bosons can be made.

Contents

Citations to previous work

Chapter 2:

A. Thomson, S. Sachdev, *Fractionalized Fermi liquid on the surface of a topological Kondo insulator*, Physical Review B **93**, 125103 (2016) [arXiv:1509.03314]

Chapter 3:

C.-M. Jian, A. Thomson, A. Rasmussen, Z. Bi, C. Xu, *Deconfined Quantum Critical Point on the Triangular Lattice*, Physical Review B **97**, 195115 (2018) [arXiv:1710.04668]

Chapter 4:

A. Thomson, S. Sachdev, *Quantum electrodynamics in 2+1 dimensions with quenched disorder: quantum critical states with interactions and disorder*, Physical Review B **95**, 235147 (2017) [arXiv:1702.04723]

Chapter 5:

A. Thomson, S. Sachdev, *Spectrum of conformal gauge theories on a torus*, Physical Review B **95**, 205128 (2017) [arXiv:1607.05279]

Chapter 6:

A. Thomson, S. Sachdev, *Fermionic spinon theory of square lattice spin liquids near the Néel state*, Physical Review X **8**, 011012 (2018) [arXiv:1708.04668]

Figures

Tables

To Barco, Kitty, Cat-Two, Tiger, Mischief, Tumbles, Pita, and Peaches. You aren't with us anymore, but I know you would be proud.

(Also, to Mom and Dad. I love you.)

Acknowledgments

I couldn't have completed this PhD without the help and support of numerous people.

First, I would like to thank my advisor, Subir Sachdev. Under his guidance, I have learned a tremendous amount across a number of topics. His breadth of vision and creativity stand as a marker towards which I strive. I have both benefitted from our work together and greatly enjoyed the experience. I would also like to acknowledge the comments and advice provided by my other committee members, Ashvin Vishwanath and Daniel Jafferis. I thank Bert Halperin for his involvement in my committee during the first few years of my graduate studies.

There are many other people at Harvard whose assistance has been invaluable. I am incredibly grateful for everything Lisa Cacciabaudo has done for me. She has always been kind and incredibly helpful, even when the problem at hand is primarily the result of my own poor organizational skills. I also greatly appreciate the support and guidance provided by Jacob Barandes, especially at the beginning of graduate school. The administrative staff of the department has significantly facilitated my PhD and I'd like to specially recognize Carol Davis, Liz Alcock, and Barbara Drauschke. Finally, I'd like to thank Melissa Franklin for her occasional advice and constant off-beat sense of humour.

I would also like to thank my collaborators, from whom I have learned very many things. While our project was ultimately unsuccessful, I am grateful to Yejin Huh for her assistance at the beginning of my research career at Harvard. Later, I was fortunate enough to spend some months at KITP, where I was fortunate enough to work Cenke Xu and his group: Chao-Ming Jian, Alex Rasmussen, and Zhen Bi. Working with Cenke, it was impossible not to be inspired by his enthusiasm and originality. I also thank Chao-Ming Jian for his readiness to talk physics and patience answer my questions.

Many of the friendships I formed over the course of graduate school have centred around physics. I owe a special thanks to Seth Whitsitt, Shubhayu Chatterjee, and Dan Kapec for many informative and thought-provoking physics conversations, in addition to many good

nights out with friends – I hope to continuing learning and partying with them down the road. Many graduate students and postdocs in the condensed matter theory group have also had an important impact on my life: Wenbo Fu, Aavishkar Patel, Richard Davison, Mathias Scheurer, Andreas Eberlein, Andy Lucas, and Chong Wang. Similarly, there are many condensed matter physicists outside of Harvard who I am very happy to have met: Alex Rasmussen, Ryan Thorngren, Raquel Aueiroz, Zhen Bi, Dominic Else, Christina Knapp, Peter Lunts, Danny Bulmash, Hart Goldman, Justin Wilson, Jason Iaconis, Anushya Chandran, and Chris Laumann.

I am also grateful to the many people who enriched my life (largely) outside of physics. Among people in Boston, this includes the condensed matter theorists mentioned above, as well as Anders Andreassen, Yuliya Dovzhenko, Jacob Baron, Maria Carierro, Zidi Chen, Kevin Thompson, and Fionnuala Connolly.

The friendships that have persisted since my time in Montreal have also been very important to me. In particular, I especially acknowledge my best friend, Katrina Fast, who I have known since kindergarten. She has provided a getaway in Montreal, complete with fantastic food. I also greatly appreciate her tolerance of my poor roommate skills over the course of my undergraduate degree. And, more generally, I would like to thank her for being wonderful in all ways.

I am very happy (and slightly surprised) that Florian Shkurti still tolerates Katrina and my antics. In addition, I would also like to recognize the friendships of Tereza Jarnikova, Aynsley Merk, Dieter Fishbein, and Matthew de Courcy-Ireland. While I often go a long time without seeing them, I always enjoy catching up.

In addition to Katrina, many of my most important friendships date back to high school. I greatly value the friendship of Amelia Rajala and Tasha Rennie, and I fully expect to be drinking wine with them years down the road. Similarly, I always enjoy my time with Kirsten Dohmeier in Vancouver – hopefully, we will not be so constrained by time in the future.

I would also like to thank M. Djavad Mowafaghian and Hamid Eshghi for their continued support of my education. It has made an enormous difference, and I am extremely grateful.

Last, but certainly not least, I'd like to thank my family: my grandmother, Rose Sparks; my brother, Reid Thomson; and my parents, Margaret and Jim Thomson. I'm especially grateful for my mom's unwavering encouragement and insistence that I never feel lesser for being a woman. I also particularly appreciate my dad for always encouraging curiosity and for his continued willingness to consider and answer whatever question I cook up. Most of all, I'd just like to thank them for all the love and support they have shown me. I really can't imagine better parents.

Chapter 1

Introduction

1.1 Quantum states of matter

Our understanding of matter is founded on the identification and classification of different phases. In the standard Landau-Ginzburg approach, this assignment is determined by the symmetries of the system. The standard example is that of the (classical) Ising model,

$$H_{ising}^{(cl)} = -J \sum_{\langle \boldsymbol{ij} \rangle} \sigma_{\boldsymbol{i}}^z \sigma_{\boldsymbol{j}}^z, \tag{1.1}$$

where $\sigma_{\boldsymbol{i}}^z = \pm 1$ on each site $\boldsymbol{i}$ and $J > 0$. This Hamiltonian is invariant under the global $\mathbb{Z}_2$ transformation, $\sigma_{\boldsymbol{i}}^z \to -\sigma_{\boldsymbol{i}}^z$. At high temperatures, to maximize entropy, the system chooses a paramagnetic state, *i.e.* one in which the average magnetization vanishes: $m = \langle \sigma_{\boldsymbol{i}}^z \rangle = 0$. Conversely, in dimensions $d \geq 2$, at low temperatures, the system prefers to minimize its energy by selecting one of its two groundstates and spontaneously breaking the $\mathbb{Z}_2$ symmetry. The resulting phase is a ferromagnet, with either $m \to +1$ or $m \to -1$ as the temperature approaches zero.

A direct analogue exists in a (zero temperature) quantum model. The Hamiltonian is

$$H_{ising}^{(qm)} = -gJ \sum_{\boldsymbol{i}} \sigma_{\boldsymbol{i}}^x - J \sum_{\langle \boldsymbol{ij} \rangle} \sigma_{\boldsymbol{i}}^z \sigma_{\boldsymbol{j}}^z, \tag{1.2}$$

where both J and g are positive and $\sigma_{\boldsymbol{i}}^z$ now represents a 2×2 Pauli matrix. As in the classical case, $H_{ising}^{(qm)}$ is invariant under a global $\mathbb{Z}_2$ transformation. The action of this symmetry on the operators of the theory is implemented though conjugation by $\mathcal{O} = \prod_{\boldsymbol{i}} \sigma_{\boldsymbol{i}}^x$. In particular, $\mathcal{O}$ acts on the Pauli operators as $\sigma_{\boldsymbol{i}}^z \to -\sigma_{\boldsymbol{i}}^z$ and $\sigma_{\boldsymbol{i}}^x \to \sigma_{\boldsymbol{i}}^x$, establishing that $\mathcal{O}$ commutes with $H_{ising}^{(qm)}$. Instead of the temperature, the transition is tuned by the strength of the transverse field g. When $g \gg 1$, $\langle\sigma_{\boldsymbol{i}}^x\rangle \to +1$ in the groundstate: $|\text{gnd}\rangle_{g=\infty} = \bigotimes_{\boldsymbol{i}} \frac{1}{\sqrt{2}}\left(|\uparrow\rangle_{\boldsymbol{i}} + |\downarrow\rangle_{\boldsymbol{i}}\right)$. Since the magnetization then vanishes, $\langle\sigma_{\boldsymbol{i}}^z\rangle = 0$, this is the paramagnetic phase. In the opposite limit, $g \ll 1$, the groundstate is ferromagnetic with either $\langle\sigma_{\boldsymbol{i}}^z\rangle \to +1$ or $\langle\sigma_{\boldsymbol{i}}^z\rangle \to -1$.

While certain phases may be characterized by their symmetries in this way, it is by no means a sufficient method of classification when quantum mechanics is considered.In particular, quantum entanglement often plays a very important role, and its inclusion results in a much richer set of states. We briefly review some of the more important examples, placing special emphasis on those relevant for this thesis.

1.1.1 $\mathbb{Z}_2$ TOPOLOGICAL ORDER

A gapped phase is said to have 'long-range entanglement' when there is no set of local transformations which can map the groundstate to a product state without closing the gap or exiting the phase [181, 182]. $\mathbb{Z}_2$ spin liquids (SLs) are among the the best-known long-range entangled phases [145, 183]. These phases possess what is know as '$\mathbb{Z}_2$ topological order.' This topological character becomes evident when a $\mathbb{Z}_2$ spin liquid is placed on a manifold with nonzero genus, g, such as torus: provided the surface is large enough, one finds 4^g (essentially) degenerate grounstates. Tunnelling between these states can only occur via non-local operators that stretch around one of the cycles of the manifold. For instance, for a square torus with lengths L in both the x and y directions, it follows that the energy splitting between the four degenerate groundstates is of the order $\sim e^{-\Delta L}$ where Δ is the gap to the excited states.

A more striking aspect of the $\mathbb{Z}_2$ SL is that it hosts nonlocal excitations that satisfy

fractional statistics. There are two distinct bosonic excitations, e and m, which have semionic mutual statistics, *i.e.* the wavefunction picks up a minus sign when an m particle is taken around an e particle. A third particle, ε, can be formed as a bound state of the first two, $\varepsilon \sim e\,m$. It also has mutual semionic statistics with e and m, but its self-statistics are fermionic.

These nontrivial properties may be interpreted as consequences of an emergent $\mathbb{Z}_2$ gauge field under which all the excitations are charged. This $\mathbb{Z}_2$ gauge redundancy is not a physical property, and it follows that the total wavefunction must always be invariant under its action. For this to be true, excitations must always appear in pairs. Notably, this implies that $\mathbb{Z}_2$ spin liquids have no fermionic excited states even though there is a fermionic excitation ε. Nevertheless, the theory is deconfined, and the excitations may be arbitrarily far from one another, with the region separating them indistinguishable from the groundstate.

The $\mathbb{Z}_2$ SL structure becomes much more complicated when symmetries are included: in addition to obeying fractional statistics, the excitations may also carry fractional quantum numbers of the symmetry group. To see why, consider the action of an unbroken symmetry G on a state containing two ε excitations located at $\boldsymbol{r}$ and $\boldsymbol{r}'$. G will exclusively affect the region immediately surrounding the excitations: $G\,|\boldsymbol{r},\boldsymbol{r}'\rangle = \mathscr{G}_\varepsilon(\boldsymbol{r})\mathscr{G}_\varepsilon(\boldsymbol{r}')\,|\boldsymbol{r},\boldsymbol{r}'\rangle$, where $\mathscr{G}_\varepsilon(\boldsymbol{r})$ are local operators with support near $\boldsymbol{r}$. Since $\mathscr{G}_\varepsilon(\boldsymbol{r})$ always appears with a partner, it need only satisfy the group relations of G up to a minus sign. For instance, both $\mathscr{G}_\varepsilon(\boldsymbol{r})\mathscr{G}_\varepsilon(\boldsymbol{r}) = +\mathbb{1}$ and $\mathscr{G}_\varepsilon(\boldsymbol{r})\mathscr{G}_\varepsilon(\boldsymbol{r}) = -\mathbb{1}$ are consistent with $G^2 = \mathbb{1}$. This is referred to as 'symmetry fractionalization' [43] and is discussed in greater detail in Chapter 6.4.1. (The 'projective symmetry group' [184], a related concept, is reviewed in Chapter 6.3 and Appendix E.2.)

When symmetry fractionalization is possible, classifying states solely by their physical symmetries is no longer an option: numerous $\mathbb{Z}_2$ SLs with distinct symmetry fractionalizations may exist for a single set of physical symmetries.

1.1.2 Quantum critical points and conformal field theories

Quantum correlations are also especially strong at a quantum critical point (QCP) – *i.e.* a continuous phase transition at zero temperature [155]. Not only are critical points interesting in their own right, but they also provide a natural way to probe the adjoining phases and study the full phase diagram. At a QCP, a description in terms of quasi-particles is often meaningless, and these 'strongly-interacting' critical theories will be the focus of the following discussion.

The critical point separating the disordered and ordered phases of the quantum Ising model in $d = 2$ spatial dimensions is probably the best-known example of a quantum phase transition. It is described by ϕ^4 theory [193]:

$$\mathcal{L}_{wf} = \frac{1}{2}\left(\partial_\mu \phi\right)^2 - \frac{1}{2} r \phi^2 - \frac{\lambda}{4!}\phi^4, \tag{1.3}$$

where ϕ is a scalar field and μ is summed over both space and time directions. Like the transverse field Ising model in Eq. (1.2), $\mathcal{L}_{wf}$ possesses a global $\mathbb{Z}_2$ symmetry under which $\phi \to -\phi$. The phase transition is tuned via the mass r. When $r > 0$, $\langle\phi\rangle = 0$, indicating that this is the paramagnetic phase, whereas when $r < 0$, $\langle\phi\rangle \neq 0$ and the $\mathbb{Z}_2$ symmetry is broken. The phase transition occurs exactly at the point where the mass r vanishes (in the appropriate renormalization scheme). Its most salient feature is the presence of a scaling symmetry, resulting in the algebraic decay of correlation functions [191, 192]. This is indicative of the critical theory's strongly-correlated nature.

In addition to the scaling symmetry, a number of symmetries that are not present at the microscopic level may emerge at a quantum critical point. Notably, the strongly-interacting theories of interest frequently have an emergent Lorentz symmetry. For instance, while the Ising model presented at the being of this chapter is quite clearly non-relativistic, the theory describing its phase transition, Eq. (1.3), is Lorentz-invariant. One reason this occurs so frequently in strongly-interacting theories is simply that non-relativistic theories are more

likely to be weakly interacting. In a non-relativistic theory, the action typically possesses a linear time derivative and quadratic space derivatives. time typically scales linearly and momentum scales quadratically. This raises the *effective* dimension of the field theory, making it more likely to behave like a free theory at low energies [155].

In conjunction with the scaling symmetry, the emergent Lorentz symmetry typically implies the existence of a larger conformal symmetry, and this has actually been proven in both 1+1 and 3+1 dimensions [39, 125]. When this is the case, the critical point is described by a conformal field theory (CFT) [36, 151, 173].

The conformal symmetry imposes rather stringent consistency conditions, so it is typically assumed that two CFTs with the same symmetries are equivalent. For this reason, it is perhaps not overly surprising that many of the (lower-dimensional) field theories studied by high energy theorists have applications to condensed matter. In particular, when a QCP has Lorentz symmetry and is expressed in terms of fermions, we expect these fermions to take a Dirac form.

In this thesis we focus primarily on gauge theories with Dirac fermions transforming in the fundamental representation of the gauge group. We will see why this is natural below in Sec. 1.2. In Chapter 6 we work with quantum chromodynamics in 2+1d (QCD_3) with an SU(2) gauge group and $N_f = 2$ fermion flavours, while in Chapters 3, 4, and 5 we look at quantum electrodynamics in 2+1d (QED_3). We also mention that QED_3 has the distinction of potentially describing an extended phase of matter, instead of a critical point.

As was the case with the $\mathbb{Z}_2$ spin liquid considered above, the SU(2) and U(1) gauge fields are not physical symmetries, and so the Hilbert space only contains charge-neutral objects. It follows that the fermionic operators themselves are emergent, and that these field theories are bosonic like the $\mathbb{Z}_2$ spin liquids in spite of appearances.

The presence of the gauge field distinguishes the theories we consider from the Ising transition in an important respect. The Ising model describes a transition between a symmetry preserving and a symmetry broken phase. However, phase transitions with emergent sym-

metry are not constrained in this manner. They can connect different topological phases, ordered phases, and more [166, 170]. Since the gauge field mediate long-range interactions, their presence is indicative of the enhanced correlations these theories possess.

1.1.3 Fractionalized Fermi liquid

The most ubiquitous example of a phase hosting gapless degrees of freedom is the Landau Fermi liquid (FL). While the bare Coulomb interaction between electrons in a metal is very large, this force is screened at low energies, and the electron behaviour is, in many ways, completely analogous to that of a free particle [**?**].

In this thesis, we will be interested in a more exotic version of the FL, called the *fractionalized* Fermi liquid (FL*) [169, 171]. This phase can be thought as the coexistence of an FL with a $\mathbb{Z}_2$ or U(1) spin liquid. Note, however, that unlike the $\mathbb{Z}_2$ spin liquids and continuous gauge theories mentioned above, the FL* does support fermionic states. While the spin liquid component of the FL* may admit a description in terms of gapless, emergent fermionic operators, this need not be the case. The actual fermionic states are essentially electrons.

1.2 Parton constructions

In the previous section, we discussed various long-range entangled states of matter. This naturally lends itself to the question of how and where such states are found. A generic Hamiltonian capable of describing many of these systems is the frustrated spin-1/2 Heisenberg model in 2+1d:

$$H_H = \sum_{i,j} J_{ij} \boldsymbol{S_i} \cdot \boldsymbol{S_j}. \tag{1.4}$$

The presence of the phases of interest is typically argued via a parton construction [186] (this is also discussed in Chapter 6.2.2 and Appendix E.2). The spins are rewritten either

in terms of Schwinger bosons, $b_{\boldsymbol{i}}$, or slave (or Abrikosov) fermions, $f_{\boldsymbol{i}}$ [11, 186]:

$$\boldsymbol{S_i} = \frac{1}{2} b_{\boldsymbol{i}}^\dagger \boldsymbol{\sigma} b_{\boldsymbol{i}} = \frac{1}{2} f_{\boldsymbol{i}}^\dagger \boldsymbol{\sigma} f_{\boldsymbol{i}}. \tag{1.5}$$

These are accurate representations of the spin Hilbert space provided the constraints

$$\sum_\alpha b_{\boldsymbol{i}\alpha}^\dagger b_{\boldsymbol{i}\alpha} = 1, \qquad \sum_\alpha f_{\boldsymbol{i}\alpha}^\dagger f_{\boldsymbol{i}\alpha} = 1 \tag{1.6}$$

are imposed. Since $b_{\boldsymbol{i}}$ and $f_{\boldsymbol{i}}$ carry spin, both are frequently referred to as 'spinons,' with the modifiers 'bosonic' and 'fermionic' sometimes used to distinguish the two. Inserting this expression into H_H results in either a four-boson or four-fermion term. The Hamiltonian can then be decoupled via a Hubbard-Stratonovich transformation and treated using the standard mean field theory procedure. Provided the mean field ansatz is stable and preserves the spin symmetry, a spin liquid phase is obtained.

In this thesis, we primarily use the slave-fermion approach, and so we focus on this case for the remainder of the section. The unit constraint on the number of fermions introduces a gauge redundancy. For instance, it's clear that local phase rotations, $f_{\boldsymbol{i}} \to e^{i\phi_{\boldsymbol{i}}} f_{\boldsymbol{i}}$, do not alter the physical operator, the spin $\boldsymbol{S_i}$, and therefore cannot constitute a real symmetry of the Hamiltonian. For slave-fermions, the constraint in Eq. (1.6) actually implies two other constraints:

$$\sum_{\alpha\beta} \epsilon_{\alpha\beta} f_{\boldsymbol{i}\alpha} f_{\boldsymbol{i}\beta} = 0, \qquad \sum_{\alpha\beta} \epsilon_{\alpha\beta} f_{\boldsymbol{i}\alpha}^\dagger f_{\boldsymbol{i}\beta}^\dagger = 0, \tag{1.7}$$

where $\epsilon_{\alpha\beta}$ is the two-component Levi-Civita symbol. These in turn generate two more gauge transformations, demonstrating that the introduction of slave fermions results in an SU(2) gauge redundancy in total. Depending on the mean field ansatz, the gauge group can be Higgsed to either U(1) or $\mathbb{Z}_2$.

When only a $\mathbb{Z}_2$ gauge redundancy remains, the resulting state is precisely the $\mathbb{Z}_2$ spin

liquid discussed in Sec. 1.1.1. The ε excitations of the $\mathbb{Z}_2$ topological order should be associated with the excitations created by the slave fermions $f_{\boldsymbol{i}}^\dagger$. Similarly, both QCD_3 and QED_3 can be obtained from this construction when the mean field ansatz either preserves the full gauge group or Higgses it down to U(1). The fermionic spinon is naturally associated with the Dirac fermion operator of the field theories.

Since the original theory, the Heisenberg model, has no fermionic excitations, its low energy description cannot either regardless of whether we choose to express the theory in terms of fermionic operators. These observations are consistent with our earlier statements at the ends of Secs. 1.1.1 and 1.1.2.

We also apply the fermionic parton construction in the context of the Kondo lattice model. In this model, there is a one-to-one correspondence between electrons and spins. Before including interactions, the electrons and spins are governed by a tight-binding Hamiltonian and a Heisenberg Hamiltonian, respectively. They are coupled through a term of the form

$$\frac{J_K}{2}\sum_{\boldsymbol{i}} c_{\boldsymbol{i}}^\dagger \boldsymbol{\sigma} c_{\boldsymbol{i}} \cdot \boldsymbol{S}_{\boldsymbol{i}}, \tag{1.8}$$

where $c_{\boldsymbol{i}}$ is an electron annihilation operator and $\boldsymbol{S}_{\boldsymbol{i}}$ is a spin-1/2 operator (in Chapter 2 we work with a minor variant of this Hamiltonian). Representing the spin operators in terms of spinons, this becomes, $\sim -\frac{1}{4}J_K \sum_{\boldsymbol{i}} f_{\boldsymbol{i}\alpha}^\dagger c_{\boldsymbol{i}\alpha} c_{\boldsymbol{i}\beta}^\dagger f_{\boldsymbol{i}\beta}$. Performing a Hubbard-Stratonovich transformation, we obtain

$$\sim -\frac{1}{2}\sum_{\boldsymbol{i}} V_{\boldsymbol{i}} f_{\boldsymbol{i}}^\dagger c_{\boldsymbol{i}} + h.c. \tag{1.9}$$

where $V_{\boldsymbol{i}} = \frac{1}{2}J_K \left\langle c_{\boldsymbol{i}}^\dagger f_{\boldsymbol{i}} \right\rangle$ is typically referred to as the hybridization. When $V_{\boldsymbol{i}}$ is nonzero, depending on both the chemical potential and the form of the band structure, a heavy Fermi liquid or a Kondo insulator is obtained. The FL* phase described in Sec. 1.1.3 is realized precisely in the opposite limit when the hybridization, $V_{\boldsymbol{i}}$, vanishes. This is discussed further

in Chapter 2.2.

1.3 Organization of thesis

We now provide an outline of the thesis.

We start by proposing a number of novel states in Chapters 2, 3, and 4. Chapter 2 discusses the possibility that a topological Kondo insulator (TKI) may host a highly entangled phase on its surface. If we ignore the unusual origin of the spinons, f_i, and the hybridization, V_i, the TKI is completely analogous to a conventional topological insulator [18, 47, 57, 84, 114, 135, 150]. The Hamiltonian is a simple 4-band model, which, depending on its symmetries, may or may not admit a topologically non-trivial band structure. It turns out that the spin-orbit coupling typically necessary for this to occur is present in Kondo lattice systems, substantiating proposals for the existence of TKI's in real materials. A TKI is gapped everywhere except for the robust states at the surface originating from the topological band structure. We propose that the hybridization vanishes at the surface and that these surface states are unstable to the FL* theory discussed above.

In Chapter 3, we discuss the phase diagram of the triangular lattice antiferromagnet. We demonstrate that a direct, continuous transition between two ordered phases is possible. Such a phase transition must necessarily be deconfined. The presence of a proximate $\mathbb{Z}_2$ spin liquid indicates that a description in terms of fermionic spinons may be natural. This leads us to show that the phase transition may be described by QED$_3$ with $N_f = 4$ Dirac fermions.

In Chapter 4, we study QED$_3$ on more general grounds. In the large-flavour limit, we investigate its stability against a variety of disorder perturbations. We observe that provided the disorder satisfies certain restrictions, the theory flows away from the clean fixed point to one in which both disorder and interactions are present. At this new fixed point, we calculate the universal flavour conductivity to subleading order. We find that generic disorder becomes strong under the renormalization group flow, taking the theory away from the perturbatively

accessible regime.

We change focus in Chapter 5, where we address the problem of identifying strongly correlated phases of matter. Numerical simulations of highly entangled states is a difficult task. One issue for CFTs is that the first method by which we may attempt to identify the theory, a measurement of the critical exponents and their anomalous dimensions, is severely limited by system size. The spectrum is another, arguably more accessible, universal CFT data which can be used to identify the theory being simulated. With this in mind, we calculate the spectrum on the torus of QED_3. We also consider theories containing a Chern-Simons term, as these may be relevant to quantum Hall transitions.

We conclude in Chapter 6 with a study of $\mathbb{Z}_2$ spin liquids proximate to the π-flux phase of the square lattice antiferromagnet, whose low-energy description is QCD_3 with an SU(2) gauge group and $N_f = 2$ fermion flavours. Ref. 184 showed that when approaching the problem from a lattice perspective, 58 $\mathbb{Z}_2$ spin liquids can be found. With access to the continuum theory, the set of spin liquids under consideration can be restricted in a number of natural ways. Further, QCD_3 is related to $\mathbb{CP}^1$, a bosonic CFT describing the Néel-VBS transition on the square lattice [179]. The spin liquids obtained by perturbing about QCD_3 can be matched with those obtained by perturbing about $\mathbb{CP}^1$ and new dualities inferred.

Chapter 2

Fractionalized Fermi liquid on the surface of a topological Kondo insulator

We argue that topological Kondo insulators can also have 'intrinsic' topological order associated with fractionalized excitations on their surfaces. The hybridization between the local moments and conduction electrons can weaken near the surface, and this enables the local moments to form spin liquids. This coexists with the conduction electron surface states, realizing a surface fractionalized Fermi liquid. We present mean-field solutions of a Kondo-Heisenberg model which display such surfaces.

2.1 Introduction

An important development of the past decade has been the prediction and discovery of topological insulators (TI) [18, 47, 57, 84, 114, 135, 150]. These materials are well-described by traditional band theory, but possess strong spin-orbit interactions that result in a non-trivial winding of the ground state wavefunction in a manner analogous to the integer quantum Hall effect. Since their discovery, the multitudinous effects of interactions have been a prominent topic of study. One compelling proposal to emerge is the notion of a topological *Kondo* insulator (TKI) [40–42]. In contrast to a band insulator, a Kondo insulator only develops an insulating gap at low temperatures, and the magnitude of the gap is controlled by electron-electron interactions. Doniach explained this phenomenon through the Kondo lattice model

[37] in which a lattice of localized moments is immersed within a sea of conduction electrons. At high temperatures, RKKY-type exchange interactions dominate and an ordered magnetic state results. Conversely, at low energies, strong interactions between localized moments and conduction electrons become important; the system crosses over into either a metallic phase well-described by Fermi liquid theory (FL) or, if the chemical potential is appropriately tuned, a Kondo insulator. As strong spin-orbit coupling is often present in these materials, the possibility that a Kondo insulator may have a nontrivial topological character is well-justified.

Of specific interest has been the Kondo insulator samarium hexaboride (SmB_6). A number of experiments have examined the proposal that it is a TKI: transport measurements have established the presence of metallic surface states [92, 93, 124, 195, 209], and angle-resolved photoemission spectroscopy (ARPES) results appear consistent with the expected Dirac surface cones [34, 80, 122, 201, 202]. Nonetheless, the spin-polarized ARPES measurements [201] remain controversial.

However, as the TKI phase is well-described within a mean field framework [42], its topological properties are not expected to be markedly different from what has already been observed in its uncorrelated cousins. More intriguing is the potential the topologically protected surface states present for new interesting phases [4, 20, 70, 149]. In SmB_6, this expectation is motivated experimentally by ARPES measurements which find light surface quasiparticles [80, 122, 202] in contradiction to current theories which predict heavy particles at the surface [5, 40, 41, 105]. Ref. 4 proposes "Kondo breakdown" at the surface as an explanation. They show that the reduced coordination number of the localized moments at the surface may lead to a suppressed Kondo temperature. At low temperature these moments are thermally decoupled from the bulk.

In this paper, we propose the existence of a fractionalized Fermi liquid (SFL*) on the surface of a TKI. This state is characterized by "*intrinsic* topological order" on the surface of a TKI, in which the local moments form a spin liquid state which has 'fractionalized'

excitations with quantum numbers which cannot be obtained by combining those of one or more electrons [13]. Rather than being thermally liberated, as in Ref. 4, the surface local moments exploit their mutual exchange interactions to decouple from the conduction electrons, and form a spin liquid state, as in the fractionalized Fermi liquid state (FL*) [169, 171]. We will present mean-field computations on a Kondo-Heisenberg lattice model which demonstrate the formation of mutual singlets between the surface local moments, while conducting surface states of light electronic quasiparticles are also present.

Somewhat confusingly, our SFL* state is 'topological' in two senses of the word, a consequence of unfortunate choices (from our perspective) in the conventional terminology. As in conventional TI, it is 'topological' because it has gapless electronic states on the surface induced by the nature of the bulk band structure. However, it is also 'topological' in the sense of spin liquids [13], because of the presence of fractionalized excitations among the local moments on the surface.

The outline of this chapter is as follows. We specify our Kondo-Heisenberg model in Section 2.2. In Section 2.3, we present the mean-field solution of this model for the case of a translationally-invariant square lattice with periodic boundary conditions. The effect of the surface on the mean field solutions is addressed in Section 2.4 where the presence of the SFL* state is numerically demonstrated. We conclude in Section 2.5 with a discussion of our results and their relevance to physical systems.

2.2 Model

Here we present the specific form of the Kondo-Heisenberg lattice model to be studied:

$$H = H_c + H_H + H_K \,. \tag{2.1}$$

The first terms represents the hopping Hamiltonian of the conduction electrons,

$$H_c = -\sum_{\langle ij \rangle} t_{ij} \left(c^\dagger_{i\alpha} c_{j\alpha} + h.c. \right), \tag{2.2}$$

where the operator $c^\dagger_{i\alpha}$ creates an electron at site $\boldsymbol{r}_i$ of spin $\alpha = \uparrow, \downarrow$. The remaining two terms establish the form of the interactions: H_H is a generalized Heisenberg term which specifies the inter-spin interaction while H_K is a Kondo term and describes the electron-spin exchange.

The spin-orbit coupling of the f-orbital imposes a classification in terms of a $(2J+1)$ multiplet, where J is the total angular momentum. In general, this degeneracy is further lifted by crystal fields and we will consider the simplest case of a Kramers degenerate pair of states. We start from an Anderson lattice model [7] with hopping t_f between f-orbitals and onsite repulsion U_f. To access the Kondo limit ($U_f \to \infty$), we perform a Schrieffer-Wolff transformation [162] and obtain a term of the form

$$H_H = -\frac{J_H}{2} \sum_{\langle ij \rangle} f^\dagger_{i\alpha} f_{j\alpha} f^\dagger_{j\beta} f_{i\beta}\,, \tag{2.3}$$

where $f_{i\alpha}$ creates a spinon at site $\boldsymbol{r}_i$, and $J_H \sim t_f^2/U_f$. This limit imposes the constraint $\sum_\alpha f^\dagger_{i\alpha} f_{i\alpha} = 1$ and further ensures that the correct commutation relations for the "spin" operators $S^a_j = \frac{1}{2} f^\dagger_{j\alpha} \sigma^a_{\alpha\beta} f_{j\beta}$ are obeyed. By using the Fierz identity (and dropping a constant) we can verify that we indeed have the familiar Heisenberg term:

$$H_H = \frac{J_H}{4} \sum_{\langle ij \rangle} f^\dagger_{i\alpha} \boldsymbol{\sigma}_{\alpha\beta} f_{i\beta} \cdot f^\dagger_{j\gamma} \boldsymbol{\sigma}_{\gamma\delta} f_{j\delta} = J_H \sum_{\langle ij \rangle} \boldsymbol{S}_i \cdot \boldsymbol{S}_j\,, \tag{2.4}$$

where $\boldsymbol{\sigma} = (\sigma^x, \sigma^y, \sigma^z)$. It is important to note that the spinon operators $f_{j\alpha}$ do not have a uniquely defined phase. In fact, by choosing to represent the spins in terms of constrained fermion operators, we are formulating the Kondo lattice model as a U(1) gauge theory. This emergent gauge structure is what permits a realization of the fractionalized phases we will

discuss [169, 171].

For the electron-spin interaction, H_K, we follow the construction of Coqblin-Schrieffer [31] for systems with spin-orbit coupling. In order for the interaction to transform as a singlet, the electron and spin must couple in a higher angular momentum channel. For simplicity, we assume a square lattice and that the spins and conduction electrons carry total angular momentum differing by $l = 1$. In the Anderson model, an appropriate interaction term is then

$$H_{int} \sim \mathcal{V} \sum_{\boldsymbol{k},\alpha} \left(\alpha \sin k_x - i \sin k_y\right) c^\dagger_{\boldsymbol{k}\alpha} \left|f^0\right\rangle \left\langle f^1; \alpha\right| + h.c. \tag{2.5}$$

For instance, the interaction between moments with total angular momentum $J = 3/2$ and spin-1/2 electrons would take this form. We will verify in the next section that for the purpose of obtaining a TKI, this coupling is sufficient. We next define the electron operators

$$d_{\boldsymbol{k}\alpha} = 2\left(\alpha \sin k_x + i \sin k_y\right) c_{\boldsymbol{k}\alpha}, \qquad d_{i\alpha} = -i\alpha(c_{i+\hat{\boldsymbol{x}},\alpha} - c_{i-\hat{\boldsymbol{x}},\alpha}) + (c_{i+\hat{\boldsymbol{y}},\alpha} - c_{i-\hat{\boldsymbol{y}},\alpha})\,. \tag{2.6}$$

and, taking the same $U_f \to \infty$ limit as above, again implement the Schrieffer-Wolff transformation [162] to obtain

$$H_K = -\frac{J_K}{4} \sum_i f^\dagger_{i\alpha} d_{i\alpha} d^\dagger_{i\beta} f_{i\beta} \tag{2.7}$$

where $J_K \sim \mathcal{V}^2/U_f$.

We next perform a Hubbard-Stratonovich transformation of the Kondo and Heisenberg

terms:

$$\begin{aligned} H' =& H_1 + H_0 \\ H_1 =& -\sum_{\langle ij\rangle}\Big((t_{ij}-\delta_{ij}\mu_i)c^\dagger_{i\alpha}c_{j\alpha}+h.c.\Big)+\frac{1}{2}\sum_{j\alpha}\Big[V_j f^\dagger_{j\alpha}d_{j\alpha}+V_j^* d^\dagger_{j\alpha}f_{j\alpha}\Big] \\ & -\frac{1}{2}\sum_{j\alpha\hat{\boldsymbol{\mu}}}\Big[\chi_{j\mu}f^\dagger_{j+\hat{\boldsymbol{\mu}},\alpha}f_{j\alpha}+\chi^*_{j\mu}f^\dagger_{j\alpha}f_{j+\hat{\boldsymbol{\mu}},\alpha}\Big]+\sum_j \lambda_j f^\dagger_{j\alpha}f_{j\alpha} \\ H_0 =& \sum_j\left[-\lambda_j+\frac{|V_j|^2}{J_K}+\sum_{\hat{\boldsymbol{\mu}}}\frac{|\chi_{j\mu}|^2}{2J_H}\right]. \end{aligned} \tag{2.8}$$

We proceed with a saddle-point approximation, and treat the fields V_j, $\chi_{j\mu}$, and λ_j as real constants subject to the self-consistency conditions

$$V_j = -\frac{J_K}{2}\left\langle d^\dagger_{j\alpha}f_{j\alpha}\right\rangle, \qquad \chi_{j\mu} = J_H\left\langle f^\dagger_{j\alpha}f_{j+\hat{\boldsymbol{\mu}},\alpha}\right\rangle, \tag{2.9}$$

$$1 = \left\langle f^\dagger_{j\alpha}f_{j\alpha}\right\rangle. \tag{2.10}$$

This can be formally justified within a large-N expansion of Eq. (2.1), with N the number of spinons. As we are specifying to the case of an insulator, it further makes sense to require perfect half-filling. Since $n_f = 1$ already, this results in a final equation for the chemical potential μ_j:

$$1 = \left\langle c^\dagger_{j\alpha}c_{j\alpha}\right\rangle. \tag{2.11}$$

2.3 Translationally invariant system

We begin by solving Eqs. (2.9) – (2.11) in a translationally invariant system with periodic boundary conditions on a square lattice. Letting $V_j = V$, $\chi_{jx} = \chi_{jy} = \chi$, $\lambda_j = \lambda$ and $\mu_j = \mu$,

we perform a Fourier transform:

$$H_1 = \sum_{\boldsymbol{k}} \Psi^\dagger_{\boldsymbol{k}} \mathcal{H}(\boldsymbol{k}) \Psi_{\boldsymbol{k}} \qquad \Psi^\dagger_{\boldsymbol{k}} = \left(c^\dagger_{\boldsymbol{k}\uparrow}, f^\dagger_{\boldsymbol{k}\uparrow}, c^\dagger_{\boldsymbol{k}\downarrow}, f^\dagger_{\boldsymbol{k}\downarrow} \right) \tag{2.12}$$

$$\mathcal{H}(\boldsymbol{k}) = \begin{pmatrix} h(\boldsymbol{k}) & 0 \\ 0 & h^*(-\boldsymbol{k}) \end{pmatrix} \qquad h(\boldsymbol{k}) = \begin{pmatrix} \epsilon_c(\boldsymbol{k}) & V(\sin k_x + i \sin k_y) \\ V(\sin k_x - i \sin k_y) & \epsilon_f(\boldsymbol{k}) \end{pmatrix}. \tag{2.13}$$

For simplicity, we only consider nearest-neighbour coupling between spins; for the electron dispersion, a slightly more general description is required, and we also take next-nearest neighbour hopping into account. The dispersions are given by

$$\epsilon_c(\boldsymbol{k}) = -t_1(\cos k_x + \cos k_y) - 2t_2 \cos k_x \cos k_y - \mu, \quad \epsilon_f(\boldsymbol{k}) = -\chi(\cos k_x + \cos k_y) + \lambda \tag{2.14}$$

where the subscripts "c" and "f" refer to the electrons and spinons respectively. In the following, we will use units of energy where $t_1 = 1.0$.

Since TI's exist as a result of a band inversion, it's important to ask which sign χ will take. Naturally, when $V = 0$, the particle-hole symmetry of our mean field *ansatz* implies that $\chi > 0$ and $\chi < 0$ have the same energy. At finite hybridization, however, one will become preferable. We note that when χ and t_1 have opposite signs, the energy of the lower band will be less than the Fermi energy and hence occupied throughout most of the Brillouin zone (BZ): an increase in V will push most of these states to lower energies. Conversely, if χ and t_1 take the same sign, in one of part of the BZ no states will lie below the Fermi energy while in another both the upper and lower band will. It therefore makes sense to expect $\text{sign}\,(\chi) = -\text{sign}\,(t_1)$. In the parameter regime explored, the numerics always find this to be the case.

By construction, the Hamiltonian H_1 supports a non-trivial topological phase and is in fact the familiar Bernevig-Zhang-Hughes model [18] used to describe the quantum spin Hall

effect in HgTe wells. We can see this by studying the eigenfunctions of $h(\boldsymbol{k})$:

$$\psi_{\pm}(\boldsymbol{k}) = \frac{1}{\sqrt{2d(d \pm d_3)}} \begin{pmatrix} d_3 \pm d \\ V(\sin k_x + i \sin k_y) \end{pmatrix} \tag{2.15}$$

where $d(\boldsymbol{k}) = \sqrt{d_3(\boldsymbol{k})^2 + V^2(\sin^2 k_x + \sin^2 k_y)}$, and $d_3(\boldsymbol{k}) = (\epsilon_c(\boldsymbol{k}) - \epsilon_f(\boldsymbol{k}))/2$. If $d_3(\boldsymbol{k}) > 0$ or $d_3(\boldsymbol{k}) < 0$ for all $\boldsymbol{k}$, these functions are well-defined on the entire BZ and the system is in a topologically trivial phase [17]. If this is not the case then it is impossible to choose a globally defined phase – the ground state wavefunction has nontrivial winding and characterizes a topological insulator. From Eq. (2.14), we see that this occurs when

$$-2 < \frac{\mu + \lambda + 2t_2}{t_1 - \chi} < 2\,. \tag{2.16}$$

Alternatively, we can obtain the same result by calculating the $\mathbb{Z}_2$ invariant ν [46]: when Eq. (2.16) holds, $\nu = -1$ and the system is a TI.

We will typically be studying systems with $|t_1| \gg |\chi|$ and $|t_2/t_1|$ small (implying μ and λ small as well), so Eq. (2.16) is not difficult to fulfill. In Fig. 2.1 the energy spectrum of the system in a slab geometry is shown for $J_H = 0.15$, $J_K = 0.3$. Half-filling is maintained on every site (see Appendix A.1), but V and χ were determined by self-consistently solving Eq. (2.9) in a periodic system. In Fig. 2.1(b), the topologically protected Dirac cone is clearly visible.

If we ignore the effect the boundary will have on the values of V, χ, and λ, we can calculate the Fermi velocity of the Dirac cone [17]:

$$v_F = 2V\sqrt{\frac{|\chi(t_1 - 2t_2)|}{|t_1 - 2t_2| + |\chi|}} \sim 2V\sqrt{|\chi|} \tag{2.17}$$

where we've assumed $|\chi| \ll t_1$ in the second equation. This is consistent with the prediction that the quasiparticles at the surface be heavy [5, 40, 41, 105]. For the parameters shown

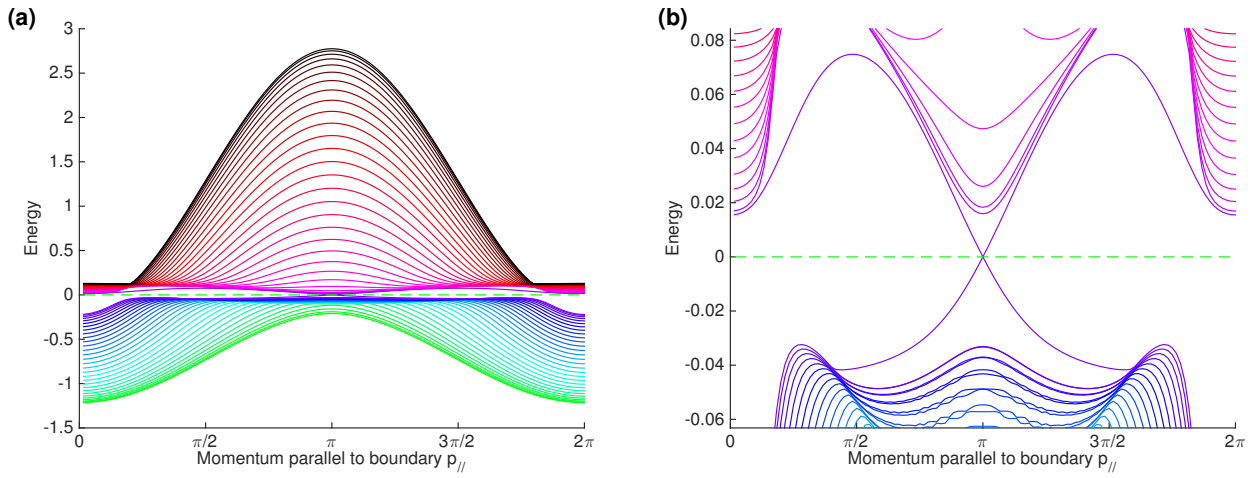

Figure 2.1: Energy spectrum for $J_H = 0.15$, $J_K = 0.3$. Both V and χ are constant throughout the bulk, but both μ_i and λ_i have been self-consistently solved to ensure that $n_c = n_f = 1$ on every site (see Appendix A.1). (a) The full spectrum is shown. (b) A closer view of the insulating gap, where the Dirac cone is clearly visible. We use units with $t_1 = 1.0$. Calculations were done with $t_2 = -0.25$ and at a temperature of 10^{-5}.

in Fig. 2.1, this formula predicts $v_F = 0.0592$, consistent with the numerically determined value $v_F = 0.0585$.

2.4 System with boundary

We now consider the effect the boundary will have on the mean field configuration and demonstrate the presence of two new fractionalized phases. Generally, we expect that the lower coordination number at the boundary will suppress the (nonlocal) hybridization: $V_{\text{surf}} \sim 3V_{\text{bulk}}/4$. While the decrease in V_{surf} will induce an increase in the spinon bond parameter $\chi_{i\mu}$ [123] both parallel and perpendicular to the surface, the parameter parallel to the surface will be more strongly affected. Since Heisenberg coupling ultimately favours an alternating bond order, in the absence of hybridization V, this anisotropy will result in a further decrease in the magnitude of the spinon bond parameter perpendicular to the surface, $|\chi_\perp|$.

When these effects are predominant, an FL* on the surface is realized: the hybridization V_i vanishes on one or more layers at the surface and $\chi_\perp$ vanishes on the innermost

layer. The existence of the SFL* phase is shown numerically by self-consistently solving Eqs. (2.9)−(2.11) in a slab geometry and comparing ground states energies (some details are given in Appendix A.1). The resulting phase diagram is shown in Fig. 2.2(a). In fact, we find two distinct SFL* phases: a decoupled spin chain and a decoupled spin ladder, which are depicted in Figs. 2.2(b) and 2.2(c) respectively. In Fig. 2.3 we plot the spatial dependence of the mean field parameters in both SFL* states. The plots in the left column correspond to a spin chain SFL* state whereas the right column corresponds to a spin ladder SLF* state. The phases are distinguished by whether V vanishes on the first site only or on both the first and second site, shown in Fig. 2.3(a) and (b) respectively. In Figs. 2.3(c) and (d) our intuition regarding the behaviour of χ near the boundary is confirmed: $|\chi_\perp|$ is suppressed to zero whereas $|\chi_\parallel|$ increases to the value it would assume in a single dimension. The fluctuations of the Lagrange multiplier field λ (Figs. 2.3(e) and (f)) are a reflection of the on-site requirement of half-filling for both the spinons and electons.

In Fig. 2.4(a), the spectrum of the spin chain SFL* state is shown. The red dash-dotted curve is the dispersion of the spinons calculated at mean field. While we do not claim that this accurately represents the Heisenberg chain, we nonetheless expect gapless spin excitations [53]. The remaining in-gap states can be understood as the result of the mixing of the surface layer of conduction electron with the Dirac cone. Consistent with its topology, even if the Dirac cone is no longer present at the chemical potential, two chiral bands traverse the gap from the conduction to the valence band and the surface is metallic. In this case, an additional four metallic surface states per spin are present, but these are not topologically protected and we can imagine pushing them below the chemical potential in a number of ways, such as, for instance, softening the restriction imposed by Eq. (2.11).

The spectrum corresponding to the second surface FL* state, the decoupled spin ladder, is shown in Fig. 2.4(b). The red curve representing the spinons is now two-fold degenerate per spin (a small splitting is hidden by the thickness of the line). Even more so than for the

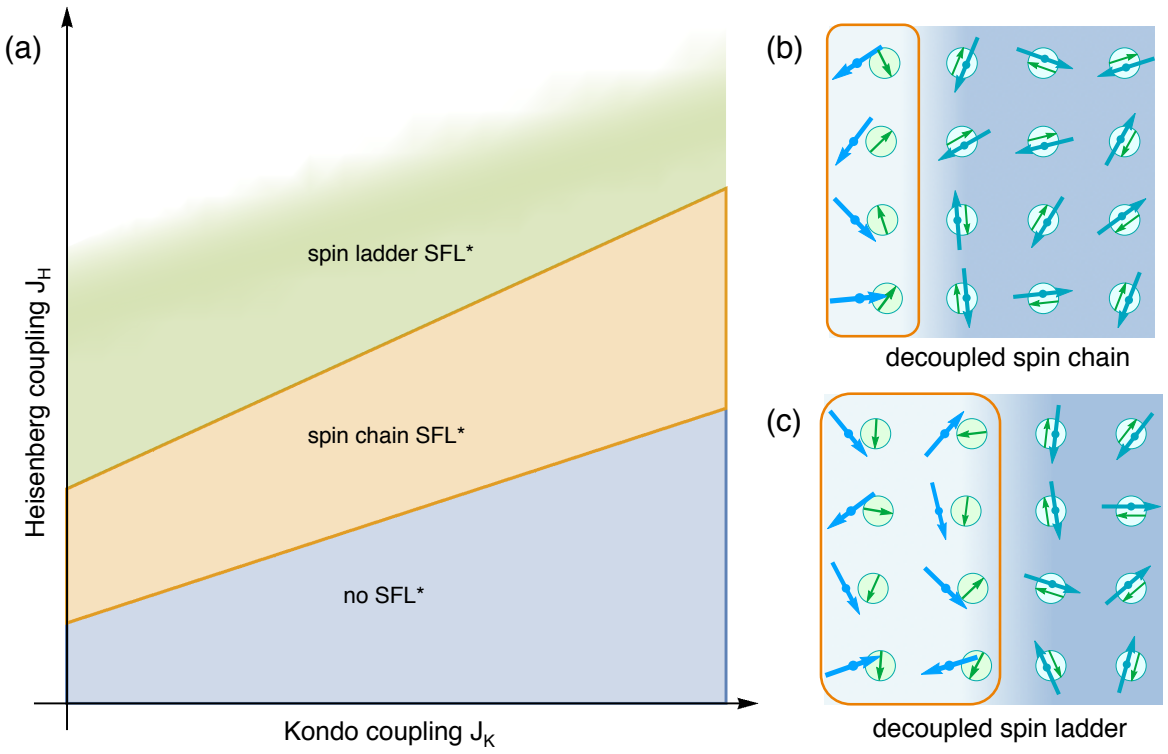

Figure 2.2: (a) Schematic phase diagram of surface states. (b),(c) Cartoon depictions of surface FL* states. In the dark blue region, the electron spins and localized moments are locked into singlets. Towards the edge (the pale blue region outlined in orange) the conduction electrons decouple from the moments, and the latter form a spin liquid. Naturally, the conduction electrons remain coupled to each other at all sites.

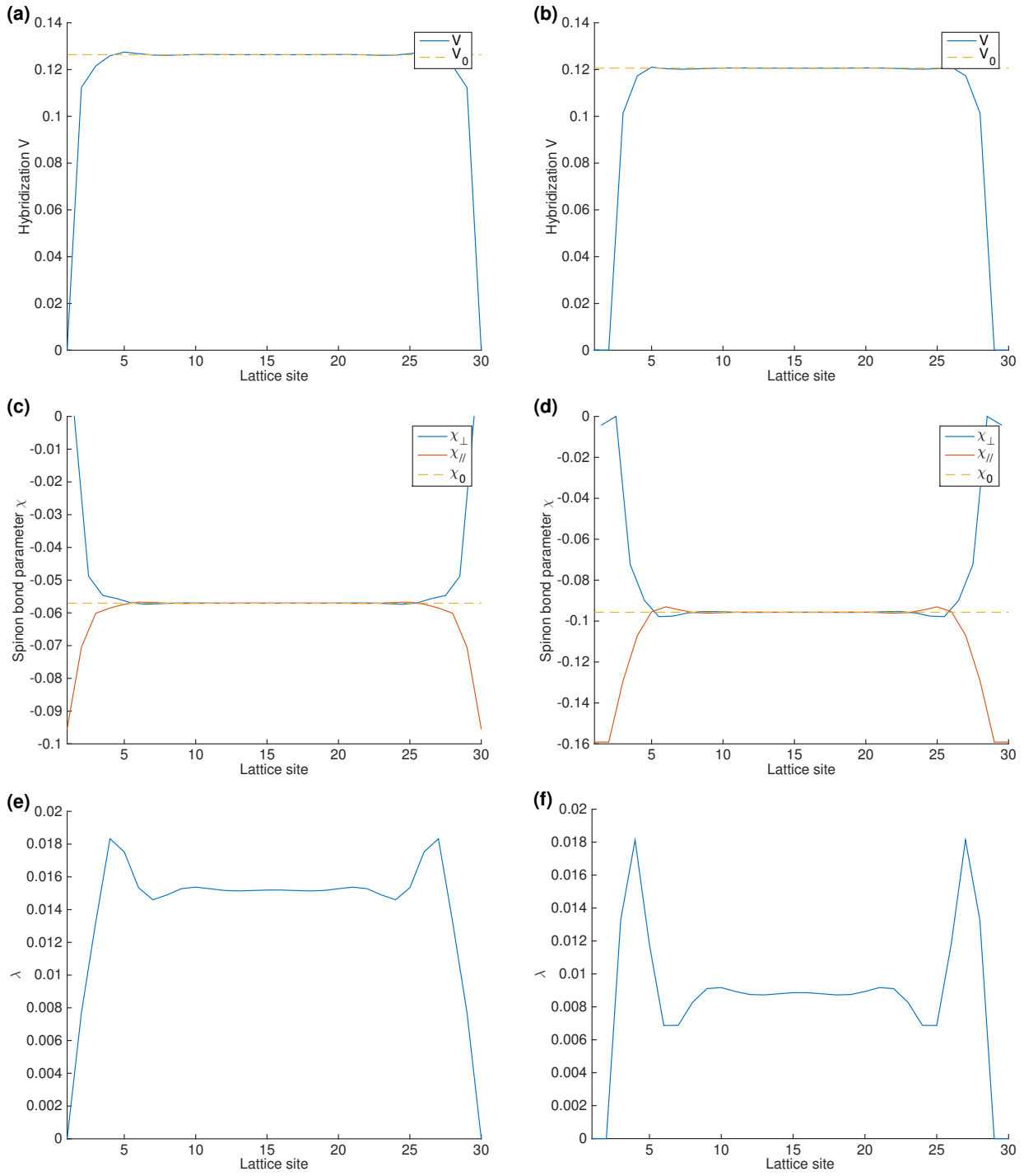

Figure 2.3: Spatial dependence of mean field parameters in SFL* phases. In the left column, we plot values corresponding to the spin chain SFL* ($J_H = 0.15$, $J_K = 0.3$) while on the right values corresponding to the spin ladder SFL* ($J_H = 0.25$, $J_K = 0.3$) are shown. (a),(b) Hybridization V_i. (c),(d) Spinon bond parameters $\chi_{i\mu}$ in the direction perpendicular (blue) and parallel (red) to the boundary. (e),(f) The Lagrange multiplier field λ_i. In (a)−(f), the yellow dashed line plots the value obtained in the translationally invariant case. We use units with $t_1 = 1.0$. Calculations were done with $t_2 = -0.25$ and at a temperature of 10^{-5}.

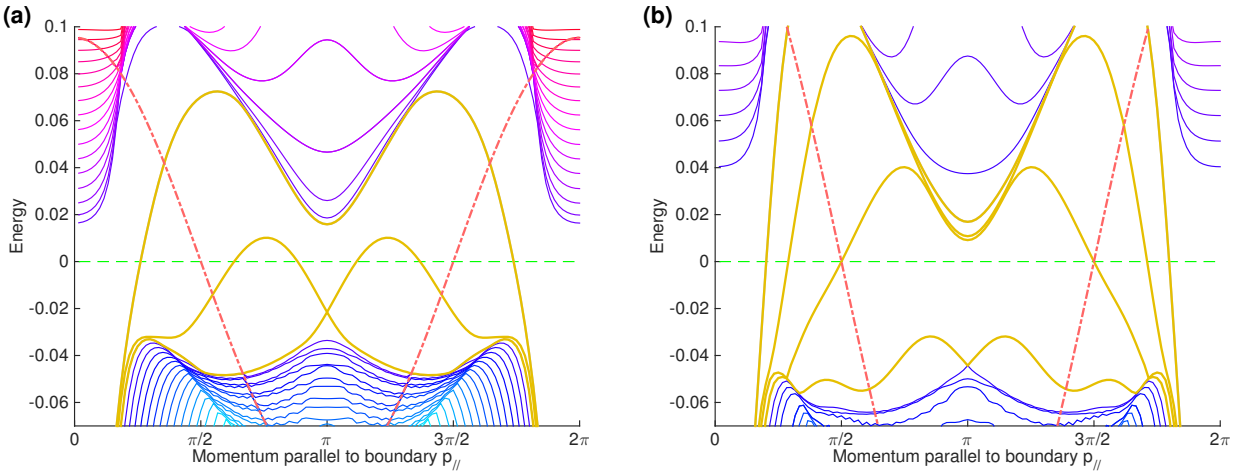

Figure 2.4: Energy spectra in SFL* phases. (a) Spin chain SFL* ($J_H = 0.15$, $J_K = 0.3$). The ground state has $V_i = 0$ on the first surface layer and the moments form a spin chain decoupled from the bulk. (b) Spin ladder SFL* ($J_H = 0.25$, $J_K = 0.3$). The ground state has $V_i = 0$ on the first two layers and a spin ladder is present on the surface. In both figures, the dash-dotted red curve represents the one-dimensional cosine dispersion found for the spinons and is merely an artifact of the *ansatz*. We use units with $t_1 = 1.0$. Calculations were done with $t_2 = -0.25$ and at a temperature of 10^{-5}.

spin chain, this result is an artifact of the mean field calculations: save in the limit where the legs of the ladder are completely decoupled, a ladder of spin-1/2 particles is gapped [50**?**].

In both phases, the metallic bands have lighter quasiparticles than predicted by the translationally invariant theory in Eq. (2.17). For the spin chain, the surface velocity of the leftmost state in Fig. 2.4(a) is $v_F = 0.095$, compared to $v_F = 0.052$ for the Dirac cone of Fig. 2.1(b). For the spin ladder, the effect is even more pronounced. There, the lightest state has a Fermi velocity of $v_F = 0.48$ compared to the translationally-invariant value $v_F = 0.072$.

The structure of the fractionalized excitations in the SFL* states found here is rather simple: just a free gas of neutral $S = 1/2$ spinon excitations. We view this mainly as a 'proof of principle' that such SFL* states can exist on the surface of TKI. Clearly, more complex types of spin liquid states are possible on the surface, and also in three-dimensional TKI with two-dimensional surfaces.

2.5 Discussion

The strong electron-electron interactions in topological Kondo insulators make them appealing candidates for searching for novel correlated electron states. In many heavy-fermion compounds, the strong interactions acting on the f-electron local moments are quenched by the Kondo screening of the conductions electrons, and the resulting state is eventually a Fermi liquid, or a band insulator for suitable density. The topological Kondo insulators offer the attractive possibility that the hybridization between the local moments and the conduction electron states can be weakened near the surface [4, 149], and this could explain the light effective masses associated with the surface electronic states [80, 122, 202]. With the weakened hybridization, we have proposed here that the local moments may form a spin liquid state with 'intrinsic' topological order. As the fractionalized excitations of such a spin liquid co-exist with the conduction electron surface states similar to those of a conventional TI, the surface realizes a fractionalized Fermi liquid [169, 171].

This paper has presented mean-field solutions of Kondo-Heisenberg model on a square lattice which act as a proof-of-principle of the enhanced stability of the such surface fractionalized Fermi liquids (SFL*). We fully expect that such solutions also exist on the surfaces of three-dimensional lattices, relevant to a Kondo insulator like SmB_6.

The recent evidence for *bulk* quantum oscillations in insulating SmB_6 [174] is exciting evidence for the non-trivial many-electron nature of these materials. It has been proposed [98] that these oscillations appear because the magnetic-field weakens the hybridization between the conduction electrons and the local moments, and this releases the conduction electrons to form Fermi surfaces leading to the quantum oscillations. The fate of the local moments was not discussed in Ref. 98, but a natural possibility is that they form a bulk spin liquid, similar to the surface spin liquid we have discussed here. Thus, while we have proposed here the formation of a SLF* states in SmB_6 in zero magnetic field, it may well be that a bulk FL* state forms in high magnetic field.

Chapter 3

Deconfined quantum critical point on the triangular lattice

We first propose a topological term that captures the "intertwinement" between the standard "$\sqrt{3} \times \sqrt{3}$" antiferromagnetic order (or the so-called 120° state) and the "$\sqrt{12} \times \sqrt{12}$" valence solid bond (VBS) order for spin-1/2 systems on a triangular lattice. Then using a controlled renormalization group calculation, we demonstrate that there exists an unfine-tuned direct continuous deconfined quantum critical point (dQCP) between the two ordered phases mentioned above. This dQCP is described by the $N_f = 4$ quantum electrodynamics (QED) with an emergent PSU(4)=SU(4)/Z_4 symmetry only at the critical point. The topological term aforementioned is also naturally derived from the $N_f = 4$ QED. We also point out that physics around this dQCP is analogous to the boundary of a $3d$ bosonic symmetry protected topological state with on-site symmetries only.

The deconfined quantum critical point (dQCP) [166, 170] was proposed as a direct unfine-tuned quantum critical point between two ordered phases that is beyond the standard Landau's paradigm, as the ground state manifold (GSM) of one side of the transition is not the submanifold of the other ordered phase (or in other words the spontaneously broken symmetry of one side of the transition is not the subgroup of the broken symmetry of the other side). A lot of numerical work has been devoted to investigating the dQCP with a full SU(2) spin symmetry [55, 104, 119–121, 133, 134, 159–161, 165, 172]. Despite early numerical evidence indicating models with in-plane spin symmetry lead to a first order transition

[32, 33, 49, 101], recent studies with modified models [137, 210] demonstrate that a continuous dQCP could exist with even inplane spin rotation symmetry, and at the easy-plane dQCP there may be an enlarged emergent O(4) symmetry which becomes more explicit after mapping this dQCP to the $N = 2$ noncompact QED [85, 131, 179], which enjoys a self-duality and hence has a more explicit O(4) symmetry [67, 116, 200]. This emergent O(4) symmetry is also supported by recent numerical simulations [88, 137].

Let us summarize the key ideas of the original dQCP on the square lattice [166, 170]:

(1) This is a quantum phase transition between the standard antiferromagnetic Néel state with GSM S^2 (two dimensional sphere) and the valence bond solid (VBS) state on the square lattice. Although the VBS state only has four fold degeneracy, there is a strong evidence that the four fold rotation symmetry of the square lattice is enlarged to a U(1) rotation symmetry at the dQCP, and the VBS state has an approximate GSM S^1, which is *not* a submanifold of the GSM of the Néel state on the other side of the dQCP. Thus we can view the dQCP as a S^2-to-S^1 transition.

(2) The vortex of the VBS order parameter carries a bosonic spinor of the spin symmetry, and the Skyrmion of the Néel order carries lattice momentum. This physics can be described by the NCCP^1 model [166, 170]: $\mathcal{L} = \sum_\alpha |(\partial_\mu - ia_\mu)z_\alpha|^2 + r|z_\alpha|^2 + \cdots$, where the Neél order parameter is $\vec{N} = z^\dagger \vec{\sigma} z$, the flux of a_μ is the Skyrmion density of $\vec{N}$, and the flux condensate (the photon phase of a_μ) is the VBS order. Thus there is an "intertwinement" between the Néel and VBS order: the condensation of the defect of one order parameters results in the other order.

(3) If we treat the Néel and the VBS orders on equal footing, we can introduce a five component unit vector $\vec{n} \sim (N_x, N_y, N_z, V_x, V_y)$, and the "intertwinement" between the two order parameters is precisely captured by a topological Wess-Zumino-Witten (WZW) term of the nonlinear sigma model defined in the target space S^4 where $\vec{n}$ lives [51, 168].

The goal of this paper is to study a possible dQCP on the triangular lattice. Let us first summarize the standard phases for spin-1/2 systems with a full spin rotation symmetry

on the triangular lattice. On the triangular lattice, the standard antiferromagnetic order is no longer a collinear Néel order, it is the $\sqrt{3} \times \sqrt{3}$ noncollinear spin order (or the so-called 120° order) with GSM SO(3)= S^3/Z_2. The VBS order discussed and observed in numerical simulations most often is the so-called $\sqrt{12} \times \sqrt{12}$ VBS pattern with a rather large unit cell [89, 113, 138]. This VBS order is the most natural pattern that can be obtained from the condensate of the vison (or the m excitation) of a Z_2 spin liquid on the triangular lattice. The dynamics of visons on the triangular lattice is equivalent to a fully frustrated Ising model on the dual honeycomb lattice [112], and it has been shown that with nearest neighbor hopping on the dual honeycomb lattice, there are four symmetry protected degenerate minima of the vison band structure in the Brillouin zone, and that the GSM of the VBS order can be approximately viewed as SO(3)= S^3/Z_2 (just like the VBS order on the square lattice can be approximately viewed as S^1). Thus the $\sqrt{3} \times \sqrt{3}$ noncollinear spin order and the $\sqrt{12} \times \sqrt{12}$ VBS order have a "self-dual" structure. Conversely on the square lattice, the self-duality between the Néel and VBS order only happens in the easy-plane limit [115].

The self-duality structure on the triangular lattice was noticed in Ref. 199 and captured by a mutual Chern-Simons (CS) theory:

$$\mathcal{L} = |(\partial - ia)z|^2 + r_z|z|^2 + |(\partial - ib)v|^2 + r_v|v|^2 + \frac{i}{\pi} a \wedge db + \cdots \tag{3.1}$$

z_α and v_β carry a spinor representation of $\mathrm{SO}(3)_e$ and $\mathrm{SO}(3)_m$ groups respectively, and when they are both gapped ($r_z, r_v > 0$), they are the e and m excitations of a symmetric Z_2 spin liquid on the triangular lattice, with a mutual semion statistics enforced by the mutual CS term [199]. Physically z_α is the Schwinger boson of the standard construction of spin liquids on the triangular lattice [107, 153, 180], while v_β is the low energy effective modes of the vison.

Eq. (3.1) already unifies much of the physics for spin-1/2 systems on the triangular lat-

tice [199]: (1) When both z_α and v_β are gapped, the system is in the Z_2 spin liquid mentioned above. (2) When v_β is gapped, it can be safely integrated out of the partition function, generating a standard Maxwell term for the gauge field b_μ. b_μ will then "Higgs" a_μ down to a Z_2 gauge field through the mutual CS term, so that when z_α condenses we obtain an ordered phase with GSM $\mathrm{SO}(3)_e$ [30]: this corresponds to the $\sqrt{3}\times\sqrt{3}$ noncollinear spin order. (3) When z_α is gapped and v_β condenses, the situation is "dual" to (2), and the system possesses the $\sqrt{12}\times\sqrt{12}$ VBS order discussed in Ref. 112, with an approximate GSM $\mathrm{SO}(3)_m$. The transition between the Z_2 spin liquid and the $\sqrt{3}\times\sqrt{3}$ spin order, and the transition between the Z_2 spin liquid and the VBS order both have an emergent O(4) symmetry [30, 112].

v_β is the vison of the spin liquid, and it carries a $\pi-$flux of a_μ due to the mutual CS term in Eq. (3.1). The $\pi-$flux of a_μ is bound with the Z_2 vortex of the $\mathrm{SO}(3)_e$ GSM of the $\sqrt{3}\times\sqrt{3}$ spin order (the homotopy group $\pi_1[\mathrm{SO}(3)] = Z_2$). Similarly z_α is also the Z_2 vortex of the $\mathrm{SO}(3)_m$ GSM of the VBS order, analogous to the vortex of the VBS order on the square lattice. This mutual "decoration" of topological defects is what we mean by "intertwinement" between the magnetic and VBS orders.

To capture the "intertwinement" of the two phases with GSM SO(3), *i.e.* to capture the mutual decoration of topological defects, we need to design a topological term for these order parameters, just like the O(5) WZW term for the dQCP on the square lattice [168]. The topological term we design is as follows:

$$\mathcal{L}_{wzw} = \int d^3x \int_0^1 du \ \frac{2\pi i}{256\pi^2}\epsilon_{\mu\nu\rho\lambda}\mathrm{tr}[\mathcal{P}\partial_\mu\mathcal{P}\partial_\nu\mathcal{P}\partial_\rho\mathcal{P}\partial_\lambda\mathcal{P}]. \tag{3.2}$$

Here $\mathcal{P}$ is a 4×4 Hermitian matrix field:

$$\mathcal{P} = \sum_{a,b=1}^{3} N_e^a N_m^b \sigma^{ab} + \sum_{a=1}^{3} M_e^a \sigma^{a0} + \sum_{b=1}^{3} M_m^b \sigma^{0b}, \tag{3.3}$$

where $\sigma^{ab} = \sigma^a \otimes \sigma^b$, and $\sigma^0 = \mathbf{1}_{2\times 2}$. All vectors $\vec{N}_e$, $\vec{N}_m$, $\vec{M}_e$ and $\vec{M}_m$ transform a vector

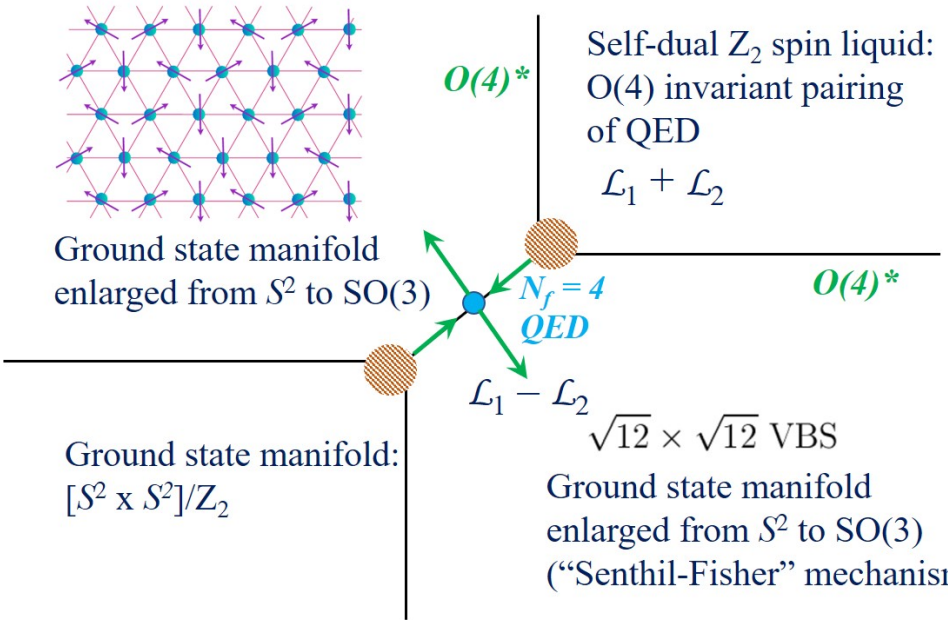

Figure 3.1: The global phase diagram of spin-1/2 systems on the triangular lattice. The intertwinement between the order parameters is captured by the WZW term Eq. (3.2). Our RG analysis concludes that there is a direct unfine-tuned SO(3)-to-SO(3) transition, which is a direct unfine-tuned transition between the noncollinear magnetic order and the VBS order. The detailed structure of the shaded areas demands further studies

under $\mathrm{SO}(3)_e$ and $\mathrm{SO}(3)_m$ depending on their subscripts. And we need to also impose some extra constraints:

$$\mathcal{P}^2 = \mathbf{1}_{4\times 4}, \qquad \vec{N}_e \cdot \vec{M}_e = \vec{N}_m \cdot \vec{M}_m = 0. \tag{3.4}$$

Then $\vec{N}_e$ and $\vec{M}_e$ together will form a tetrad, which is topologically equivalent to a SO(3) manifold, and $\vec{N}_m$ and $\vec{M}_m$ form another SO(3) manifold. With the constraints in Eq. (3.4), the matrix field $\mathcal{P}$ is embedded in the manifold

$$\mathcal{M} = \frac{U(4)}{U(2)\times U(2)}. \tag{3.5}$$

The maximal symmetry of the WZW term Eq. (3.2) is $\mathrm{PSU}(4) = \mathrm{SU}(4)/Z_4$ (which contains both $\mathrm{SO}(3)_e$ and $\mathrm{SO}(3)_m$ as subgroups), as the WZW term is invariant under a SU(4) transformation: $\mathcal{P} \to U^\dagger \mathcal{P} U$ with $U \in \mathrm{SU}(4)$, while the Z_4 center of SU(4) does not change any configuration of $\mathcal{P}$. The WZW term Eq. (3.2) is well-defined based on its homotopy group $\pi_4[\mathcal{M}] = \mathbb{Z}$.

The topological WZW term in Eq. (3.2) is precisely the boundary theory of a $3d$ symmetry protected topological (SPT) state with a PSU(4) symmetry [196]. We will discuss this further below.

Let us test that this topological term captures the correct intertwinement. To better visualize this effect, let us break $\mathrm{SO}(3)_m$ down to $\mathrm{SO}(2)_m$, which allows us to take $\vec{N}_m = (0,0,1)$, *i.e.* $N_m^1 = N_m^2 = 0$, $N_m^3 = 1$. Because $\vec{N}_m \cdot \vec{M}_m = 0$ (Eq. (3.4)), $\vec{M}_m = (M_m^1, M_m^2, 0)$. Then one allowed configuration of $\mathcal{P}$ is

$$\mathcal{P} = \sum_{a=1}^{3} N_e^a \sigma^{a3} + \sum_{b=1}^{2} M_m^b \sigma^{0b} = \vec{n} \cdot \vec{\Gamma}, \tag{3.6}$$

where $\vec{n}$ is a five component vector and $|\vec{n}| = 1$ due to the constraint $\mathcal{P}^2 = \mathbf{1}_{4\times 4}$, and $\vec{\Gamma}$ are five anticommuting Gamma matrices. Now the WZW term Eq. (3.2) reduces to the standard

O(5) WZW at level-1 in $(2+1)d$, and it becomes explicit that the vortex of (M_m^1, M_m^2) (the descendant of the Z_2 vortex of $\mathrm{SO}(3)_m$ under the assumed symmetry breaking) carries a spinor of $\mathrm{SO}(3)_e$ [51].

Eq. (3.2) is a topological term in the low energy effective field theory that describes the physics of the ordered phases. But a complete field theory which reduces to the WZW term in the infrared is still required. For example, the O(5) nonlinear sigma model with a WZW term at level-1 can be derived as the low energy effective field theory of the $N = 2$ QCD with SU(2) gauge field, with an explicit SO(5) global symmetry [179].

The WZW term in Eq. (3.2) can be derived in the same manner, by coupling the matrix field $\mathcal{P}$ to the Dirac fermions of the $N_f = 4$ QED:

$$\mathcal{L} = \sum_{j=1}^{4} \bar{\psi}_j \gamma \cdot (\partial - ia)\psi_j + m \sum_{i,j} \bar{\psi}_i \psi_j \mathcal{P}_{ij}. \tag{3.7}$$

The WZW term of $\mathcal{P}$ is generated after integrating out the fermions using the same method as Ref. 1, and the PSU(4) global symmetry becomes explicit in $N_f = 4$ QED[1].

Our goal is to demonstrate that $N_f = 4$ QED corresponds to an unfine-tuned dQCP between the noncollinear magnetic order and the VBS order, or in our notation a "SO(3)-to-SO(3)" transition (as both orders have GSM SO(3)). The PSU(4) global symmetry of $N_f = 4$ QED must be explicitly broken down to the physical symmetry. The most natural terms that beak this PSU(4) global symmetry down to $\mathrm{SO}(3)_e \times \mathrm{SO}(3)_m$ are four-fermion interaction terms, and there are *only two* such linearly independent terms [2]:

$$\mathcal{L}_1 = \left(\bar{\psi}\vec{\sigma}\psi\right) \cdot \left(\bar{\psi}\vec{\sigma}\psi\right), \qquad \mathcal{L}_2 = \left(\bar{\psi}\vec{\tau}\psi\right) \cdot \left(\bar{\psi}\vec{\tau}\psi\right), \tag{3.8}$$

where ψ carries both indices from the Pauli matrices $\vec{\sigma}$ and $\vec{\tau}$, so that ψ is a vector repre-

[1] the global symmetry of the $N_f = 4$ QED is PSU(4) instead of SU(4) because the Z_4 center of the SU(4) flavor symmetry group is also part of the U(1) gauge group.

[2] This is true under the assumption of Lorentz invariance, as Ref. 91, 198. And the SU(4) invariant mass term $\bar{\psi}\psi$ is usually forbidden by discrete space-time symmetry.

sentation $(\frac{1}{2},\frac{1}{2})$ of SO(4)∼SO(3)$_e$×SO(3)$_m$.

One can think of some other four fermion terms, for example $\mathcal{L}' = \sum_\mu \left(\bar\psi\vec\sigma\gamma_\mu\psi\right)\cdot\left(\bar\psi\vec\sigma\gamma_\mu\psi\right)$, but we can repeatedly use the Fiez identity, and reduce these terms to a linear combination of $\mathcal{L}_1$ and $\mathcal{L}_2$, as well as SU(4) invariant terms: $\mathcal{L}' = -2\mathcal{L}_2 - \mathcal{L}_1 + \cdots$. The ellipses are SU(4) invariant terms, which according to Refs. 91, 198 and 29 are irrelevant at the $N_f = 4$ QED.

The renormalization group (RG) of $\mathcal{L}_1$ and $\mathcal{L}_2$ can most conveniently be calculated by generalizing the two dimensional space of Pauli matrices $\vec\tau$ to an N-dimensional space, *i.e.* we generalize the QED$_3$ to an $N_f = 2N$ QED$_3$. And we consider the following two independent four fermion terms:

$$g\mathcal{L} = g\left(\bar\psi\vec\sigma\psi\right)\cdot\left(\bar\psi\vec\sigma\psi\right), \qquad\qquad g'\mathcal{L}' = g'\left(\bar\psi\vec\sigma\gamma_\mu\psi\right)\cdot\left(\bar\psi\vec\sigma\gamma_\mu\psi\right). \tag{3.9}$$

At the first order of $1/N$ expansion, the RG equation reads

$$\begin{aligned}\beta(g) &= \left(-1+\frac{128}{3(2N)\pi^2}\right)g + \frac{64}{(2N)\pi^2}g',\\ \beta(g') &= -g' + \frac{64}{3(2N)\pi^2}g.\end{aligned} \tag{3.10}$$

There are two RG flow eigenvectors: $(1,-1)$ with RG flow eigenvalue $-1-64/(3(2N)\pi^2)$, and $(3,1)$ with eigenvalue $-1+64/((2N)\pi^2)$ [3]. This means that when $N=2$ there is one irrelevant eigenvector with

$$\mathcal{L} - \mathcal{L}' = 2(\mathcal{L}_1 + \mathcal{L}_2) + \cdots, \tag{3.11}$$

[3]The monopoles of a_μ were ignored in this RG calculation. According to Ref. 38, monopoles of QED carry nontrivial quantum numbers. A multiple-monopole could be a singlet under the global symmetry, and hence allowed in the action. But the scaling dimension (and whether it is relevant or not under RG) of the multiple-monopole needs further study.

and a relevant eigenvector with

$$3\mathcal{L} + \mathcal{L}' = 2(\mathcal{L}_1 - \mathcal{L}_2) + \cdots . \tag{3.12}$$

Again the ellipses are SU(4) invariant terms that are irrelevant. In fact, $\mathcal{L}_1+\mathcal{L}_2$ preserves the exchange symmetry (duality) between $\mathrm{SO}(3)_e$ and $\mathrm{SO}(3)_m$, in other words $\mathcal{L}_1+\mathcal{L}_2$ preserves the O(4) symmetry that contains an extra improper rotation in addition to SO(4), while $\mathcal{L}_1 - \mathcal{L}_2$ breaks the O(4) symmetry down to SO(4). Thus $\mathcal{L}_1 + \mathcal{L}_2$ and $\mathcal{L}_1 - \mathcal{L}_2$ both *must be* eigenvectors under RG. The RG flow is sketched in Fig. 3.1.

Since $u(\mathcal{L}_1 - \mathcal{L}_2)$ is relevant, then when the coefficient $u > 0$, a simple mean field theory implies that this term leads to a nonzero expectation value for $\langle\bar{\psi}\vec{\sigma}\psi\rangle$. It appears that this order parameter is a three component vector, and so the GSM should be S^2. However, using the "Senthil-Fisher" mechanism of Ref. 168, the actual GSM is enlarged to SO(3) due to the gauge fluctuation of a_μ (see appendix A). When $u < 0$, the condensed order parameter is $\langle\bar{\psi}\vec{\tau}\psi\rangle$, and the "Senthil-Fisher" mechanism again enlarges the GSM to SO(3). Because $u(\mathcal{L}_1 - \mathcal{L}_2)$ is the only relevant perturbation allowed by symmetry, u drives a direct unfine-tuned continuous SO(3)-to-SO(3) transition, which is consistent with a transition between the $\sqrt{3}\times\sqrt{3}$ noncollinear magnetic order and the $\sqrt{12}\times\sqrt{12}$ VBS order. Further at the critical point, there is an emergent PSU(4) symmetry.

Now let us investigate the perturbation $\mathcal{L}_1 + \mathcal{L}_2$. First of all, let us think of a seemingly different term: $\mathcal{L}_3 = \sum_{a,b}\left(\bar{\psi}\sigma^a\tau^b\psi\right)\left(\bar{\psi}\sigma^a\tau^b\psi\right)$. This term also preserves the O(4) symmetry, and after some algebra we can show that $\mathcal{L}_3 = -(\mathcal{L}_1 + \mathcal{L}_2) + \cdots$. Another very useful way to rewrite $\mathcal{L}_3$ is that:

$$\mathcal{L}_3 = -\left(\bar{\psi}^t J\epsilon\bar{\psi}\right)\left(\psi^t J\epsilon\psi\right) + \cdots = -\hat{\Delta}^\dagger\hat{\Delta} + \cdots \tag{3.13}$$

where $\hat{\Delta} = \psi^t J\epsilon\psi$, $J = \sigma^2 \otimes \tau^2$. ϵ is the antisymmetric tensor acting on the Dirac indices.

Thus although the O(4) invariant deformation in our system (at low energy it corresponds

to $\mathcal{L}_1+\mathcal{L}_2$) is perturbatively irrelevant at the $N_f = 4$ QED fixed point, when it is strong and nonperturbative, the standard Hubbard-Stratonovich transformation and mean field theory suggests that, depending on its sign, it may lead to either a condensate of $\hat{\Delta}$, or condensate of $\left(\bar{\psi}\sigma^a\tau^b\psi\right)$ through extra transitions. The condensate of $\left(\bar{\psi}\sigma^a\tau^b\psi\right)$ has GSM $[S^2 \times S^2]/Z_2$, and is identical to the submanifold of $\mathcal{P}$ when $\vec{M}_e = \vec{M}_m = 0$ in Eq. (3.3). The Z_2 in the quotient is due to the fact that $\mathcal{P}$ is unaffected when both $\vec{N}_e$ and $\vec{N}_m$ change sign simultaneously. In the simplest scenario, the field theory that describes (for example) the condensation of $\hat{\Delta}$ is the similar QED-Yukawa theory discussed in Ref. 78 and Chapter 6.

Now we show that the condensate of $\hat{\Delta}$ is a self-dual Z_2 topological order described by Eq. (3.1). First of all, in the superconductor phase with $\hat{\Delta}$ condensate, there will obviously be a Bogoliubov fermion. This Bogoliubov fermion carries the $(1/2, 1/2)$ representation under $\mathrm{SO}(3)_e \times \mathrm{SO}(3)_m$. The deconfined $\pi-$flux of the gauge field a_μ is bound to a $2\pi-$vortex of the complex order parameter $\hat{\Delta}$, which then traps 4 Majorana zero modes. The 4 Majorana zero modes transform as a vector under the SO(4) action that acts on the flavor indices. The 4 Majorana zero modes define 4 different states that can be separated into two groups of states depending on their fermion parities. In fact, the two groups should be identified as the $(1/2, 0)$ doublet and the $(0, 1/2)$ doublet of $\mathrm{SO}(3)_e \times \mathrm{SO}(3)_m$. Therefore, the $\pi-$flux with two different types of doublets should be viewed as two different topological excitations. Let us denote the $(1/2, 0)$ doublet as e and the $(0, 1/2)$ doublet as m. Both e and m have bosonic topological spins. And they differ by a Bogoliubov fermion. Therefore, their mutual statistics is semionic (which rises from the braiding between the fermion and the $\pi-$flux). At this point, we can identify the topological order of the $\hat{\Delta}$ condensate as the Z_2 topological order described by Eq. (3.1).

The physics around the dQCP discussed above is equivalent to the boundary state of a $3d$ bosonic symmetry protected topological (SPT) state with $\mathrm{SO}(3)_e \times \mathrm{SO}(3)_m$ symmetry, once we view both SO(3) groups as onsite symmetries. The analogy between the dQCP on the square lattice and a $3d$ bulk SPT state with an SO(5) symmetry was discussed in

Ref. 179. We have already mentioned that the topological WZW term Eq. (3.2) is the same as the boundary theory of a $3d$ SPT state with PSU(4) symmetry [196], which comes from a $\Theta-$term in the $3d$ bulk. And by breaking the symmetry down to either $\mathrm{SO}(3)_e\times\mathrm{SO}(2)_m$ or $\mathrm{SO}(2)_e\times\mathrm{SO}(3)_m$, the bulk SPT state is reduced to a $\mathrm{SO}(3)\times\mathrm{SO}(2)$ SPT state, which can be interpreted as the decorated vortex line construction [178], namely one can decorate the SO(2) vortex line with the Haldane phase with the SO(3) symmetry, and then proliferate the vortex lines. In our case, the bulk SPT state with $\mathrm{SO}(3)_e\times\mathrm{SO}(3)_m$ symmetry can be interpreted as a similar decorated vortex line construction, *i.e.* we can decorate the Z_2 vortex line of one of the SO(3) manifolds with the Haldane phase of the other SO(3) symmetry, then proliferating the vortex lines. The Z_2 classification of the Haldane phase is perfectly compatible with the Z_2 nature of the vortex line of a SO(3) manifold. Using the method in Ref. 179, we can also see that the $(3+1)d$ bulk SPT state has a topological response action $\mathcal{S}=i\pi\int w_2[\mathcal{A}_e]\cup w_2[\mathcal{A}_m]$ in the presence of background $\mathrm{SO}(3)_e$ gauge field $\mathcal{A}_e$ and $\mathrm{SO}(3)_m$ gauge field $\mathcal{A}_m$ (w_2 represents the second Stiefel–Whitney class). This topological response theory also matches exactly with decorated vortex line construction.

Similar structure of noncollinear magnetic order and VBS orders can be found on the Kagome lattice. For example, it was shown in Ref. 68 that the vison band structure could have symmetry protected four degenerate minima just like the triangular lattice (although the emergence of O(4) symmetry in the infrared is less likely). Indeed, algebraic spin liquids with $N_f=4$ QED as their low energy description have been discussed extensively on both the triangular and the Kagome lattice [60, 61, 107, 139]. Ref. 107 also observed that the noncollinear magnetic order, the VBS order, and the Z_2 spin liquid are all nearby a $N_f=4$ QED (the so-called $\pi-$flux state from microscopic construction). The Z_2 spin liquid was shown to be equivalent to the one constructed from Schwinger boson [180], which can evolve into the $\sqrt{3}\times\sqrt{3}$ magnetic order, and the $\sqrt{12}\times\sqrt{12}$ VBS order through an $\mathrm{O}(4)^*$ transition.

In summary, we proposed a theory for a potentially direct unfine-tuned continuous quantum phase transition between the noncollinear magnetic order and VBS order on the trian-

gular lattice, and at the critical point the system has an emergent PSU(4) global symmetry. Our conclusion is based on a controlled RG calculation. The physics around the critical point has the same effective field theory as the boundary of a $3d$ SPT state [196]. The anomaly (once we view all the symmetries as onsite symmetries) of the large-N generalizations of our theory will be analyzed in the future, and a Lieb-Shultz-Mattis theorem for SU(N) and SO(N) spin systems on the triangular and Kagome lattice can potentially be developed like Ref. 77, 110.

We also note that in Ref. 89 spin nematic phases with GSM S^N/Z_2 (analogous to the spin-1/2 $\sqrt{3}\times\sqrt{3}$ state with GSM SO(3)= S^3/Z_2) and the $\sqrt{12}\times\sqrt{12}$ VBS order are found in a series of sign-problem free models on the triangular lattice. Thus it is potentially possible to design a modified version of the models discussed in Ref. 89 to access the dQCP that we are proposing.

Chapter 4

QED_3 with quenched disorder: quantum critical states with interactions and disorder

Quantum electrodynamics in 2+1-dimensions (QED_3) is a strongly coupled conformal field theory (CFT) of a U(1) gauge field coupled to $2N$ two-component massless fermions. The $N = 2$ CFT has been proposed as a ground state of the spin-1/2 kagome Heisenberg antiferromagnet. We study QED_3 in the presence of weak quenched disorder in its two spatial directions. When the disorder explicitly breaks the fermion flavor symmetry from SU($2N$)→U(1)×SU(N) but preserves time-reversal symmetry, we find that the theory flows to a non-trivial fixed line at non-zero disorder with a continuously varying dynamical critical exponent $z > 1$. We determine the zero-temperature flavor (spin) conductivity along the critical line. Our calculations are performed in the large-N limit, and the disorder is handled using the replica method.

4.1 Introduction

While our understanding of magnetic systems and spin liquids in particular has made great progress in the last two decades, most systems have been studied in the clean limit with translational symmetry present. In this paper, we explore the behavior of a critical spin liquid described by a conformal field theory (CFT) when perturbed by weak quenched disorder.

The CFT we consider is 2+1 dimensional quantum electrodynamics (QED_3), a strongly

coupled theory of a U(1) gauge field coupled to $2N$ massless two-component fermions [140, 141]. This CFT is one of the proposed ground states of the spin-1/2 kagome Heisenberg antiferromagnet, $H_{\rm H} = J\sum_{\langle ij\rangle} \boldsymbol{S}_i \cdot \boldsymbol{S}_j$, where $J > 0$ and $\langle ij\rangle$ labels nearest-neighbour sites on a kagome lattice (shown in Fig. 4.1) [58, 61, 139]. (We note that other proposed ground states are gapped $\mathbb{Z}_2$ spin liquids [153], and the choice between the CFT and the $\mathbb{Z}_2$ spin liquids remains a matter of continuing debate [60, 71, 72, 81, 102, 109].) In addition, QED$_3$ may also describe certain deconfined critical points [166, 170] between topological phases [14, 52].

The QED$_3$ action is written

$$S_{\rm qed}\left[\psi, \bar{\psi}, A\right] = -\int d^2x\, d\tau\, \bar{\psi}_\alpha \gamma^\mu \left(\partial_\mu - \frac{iA_\mu}{\sqrt{2N}}\right)\psi_\alpha + \frac{1}{4e^2(2N)}\int d^2x\, d\tau\, \left(\partial_\mu A_\nu - \partial_\nu A_\mu\right)^2 \tag{4.1}$$

where α labels the $2N$ fermion flavors, and we have denoted the Euclidean spacetime coordinates as $r = (x, \tau)$. The ψ_α's are 2-component spinors, with $\bar{\psi}_\alpha = \psi_\alpha^\dagger \tau^z$ and $\gamma^\mu = (\tau^z, \tau^y, -\tau^x)$ where the τ^a's are Pauli matrices. The dimension of the charge is $[e^2] = +1$ and so under the renormalization group (RG) flow we expect $e^2 \to \infty$; this will be discussed in greater detail in Sec. 4.2.1. This theory possesses an explicit global SU($2N$) symmetry under which the fermions flavors are rotated into one another.

The action in Eq. (4.1) specifically describes non-compact QED$_3$ *i.e.* there are no monopoles operators in the action, and flux conservation is a global symmetry: $\partial_\mu J^\mu_{\rm top} = 0$, where $J^\mu_{\rm top} = \epsilon^{\mu\nu\rho}\partial_\nu A_\rho$. Because $S_{\rm qed}$ arises in condensed matter as the low-energy description of a lattice model, monopole events must be allowed in the ultraviolet (UV). However, Berry phases from the underlying lattice spins can lead to destructive interference between monopole tunneling events [143, 144, 166, 170], and it could well be the case that monopoles carrying the smallest magnetic charge are prohibited for the clean kagome antiferromagnet; the minimal magnetic charge for allowed monopoles in the kagome antiferromagnet is unknown, and its determination remains an important open problem. In order for non-compact

QED$_3$ to be the correct low-energy description, the smallest allowed monopole operators must be irrelevant perturbations. When the number of fermion flavors is low, this is not the case and the monopoles to proliferate, confining the theory [127, 129]. As matter is added to the system, the scaling dimension of the monopoles increases and they eventually become irrelevant [19, 28, 64, 117, 132]. The number of fermion flavours required before this occurs is currently unknown, but estimates place it around $2N^c_{\text{monopole}} \lesssim 12$ for the smallest monopole charge [28]. In this paper, we work in the large-N limit, where all possible monopole operators are strongly irrelevant [117]. There is an additional critical fermion flavour number beneath which QED$_3$ spontaneously generates a chiral mass. The exact value of this number is also unknown but is expected to be $2N^c_{\text{chiral}} \approx 3$ [99, 100].

The kagome antiferromagnet corresponds to the case $N = 2$: the four flavors of fermions arise as a result of spin degrees of freedom, as well as an additional two-fold valley degeneracy. Nonetheless, when we specify to this case, we will operate under the assumption that the large N results also apply to the $N = 2$ case.

Since some degree of disorder is present in all physical systems, it is important to understand the behavior of these theories under this type of perturbation. The primary result of this paper is that when time reversal and a global U(1)×SU(N) flavour symmetry are respected microscopically, there exists a critical line with both non-zero disorder and interactions. This is obtained by coupling the theory to quenched disorder of the form

$$S_{\text{dis},z}\left[\psi,\bar{\psi}\right] = \int d^2x\, d\tau \left[M_z(x)\bar{\psi}\sigma^z\psi(x,\tau) + +i\mathcal{A}_{jz}(x)\bar{\psi}\sigma^z\gamma^j\psi(x,\tau)\right]. \tag{4.2}$$

Here, M_z and $\mathcal{A}_{jz}$ are random fields with zero mean. Both fields are independent of time: although QED$_3$ is a relativistic theory, disorder explicits breaks this symmetry. This should be contrasted with classical disordered field theories where the random fields are functions of all of the coordinates in the action. M_z and $\mathcal{A}_{jz}$ are both Gaussian and entirely determined

by their disorder averages:

$$\overline{M_z(x)M_z(x')} = \frac{g_{t,z}}{2}\delta^2(x-x'), \quad \overline{\mathcal{A}_{iz}(x)\mathcal{A}_{jz}(x')} = \delta_{ij}\frac{g_{\mathcal{A},z}}{2}\delta^2(x-x'), \quad \overline{M_z(x)\mathcal{A}_{jz}(x')} = 0. \tag{4.3}$$

The variances $g_{t,z}$ and $g_{\mathcal{A},z}$ control the strength of the disorder, and, naturally, they must be positive. Performing a diagrammatic expansion to $\mathrm{O}(g_\xi^2, g_\xi/2N)$ with $\xi = (t,z),(\mathcal{A},z)$, we find a critical line with $g_{t,z} = -8g_{\mathcal{A},z} + 64/(3\pi^2 N)$. Provided the flavor symmetry is not broken further, we expect at least a fixed point to exist at sufficiently large N: higher order corrections could convert the line to a fixed point but are not expected to lead to runaway flows to strong disorder.

In the context of the kagome antiferromagnet, the bilinear $\bar{\psi}\sigma^z\psi$ can be associated with the z-component of the Dzyaloshinskii-Moriya (DM) interaction operator:

$$\sum_{\langle ij\rangle\in\mathrm{hex}(\boldsymbol{x})} \hat{\boldsymbol{z}}\cdot(\boldsymbol{S}_i\times\boldsymbol{S}_j), \tag{4.4}$$

where hex($\boldsymbol{x}$) labels the hexagon at point $\boldsymbol{x}$ and the bonds $\langle ij\rangle$ are summed in the fashion shown in Fig. 4.1. Similarly, $i\bar{\psi}\sigma^z\gamma^{x,y}\psi$ correspond to spin currents in the microscopic theory. It follows that the fixed line could be relevant to kagome magnets with randomly varying DM fields.

We also study the RG flow when disorder couples to the more general set of operators:

$$N_s = \bar{\psi}\psi, \qquad N^a = \bar{\psi}\sigma^a\psi, \qquad J^a_\mu = i\bar{\psi}\sigma^a\gamma_\mu\psi, \qquad J_{\mathrm{top},\mu} = \epsilon_{\mu\nu\rho}\partial^\nu A^\rho \tag{4.5}$$

where $\sigma^a = (\sigma^x,\sigma^y,\sigma^z)$. We find that the U(1)×SU(N) symmetric critical line is unstable to disorder coupling to either $N^{x,y}$, $J_j^{x,y}$, and J_0^z. These theories flow to strong disorder and cannot be accessed with the perturbative methods used here. Disorder coupling to the topological current is marginal to $\mathrm{O}(1/(2N)^2)$; however, upon including higher order

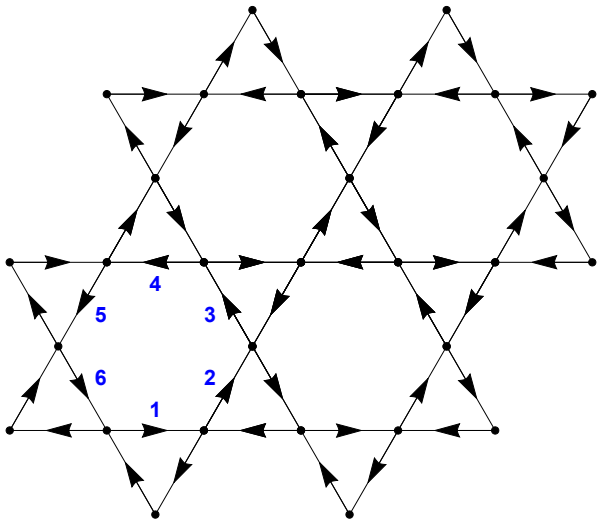

Figure 4.1: The kagome lattice. The arrows indicate the convention chosen for the bond directions of the spin chirality operator, $\boldsymbol{S}_i \times \boldsymbol{S}_j$, where i and j label nearest-neighbour sites. The order of the cross product is taken such that first spin sits at the lattice site pointing towards the site of the second spin. Later, we will use the same ordering convention to define nearest-neighbour bond operators $\boldsymbol{S}_i \cdot \boldsymbol{S}_j$.

contributions, the $J_{\text{top},0}$ disorder strength becomes relevant.

In Sec. 4.4 we will see that if the Pauli matrices in the operators of Eq. (4.5) act on the valley indices of the emergent Dirac fermions, then the mass-like terms N^a should be associated with different valence bond ordering patterns on the kagome lattice [61]. Our analysis therefore indicates that the QED$_3$ phase is unstable to random bond disorder in the kagome antiferromagnet.

There have been earlier studies of massless Dirac fermions coupled to disorder. A comprehensive analysis for free Dirac fermions was presented by Ludwig *et al.* [108]. An important ingredient in their analysis was the coupling of the disorder to components of the current operator $J^\mu(r) = i\bar{\psi}\gamma^\mu\psi(r)$. For the free theory, J^μ has scaling dimension 2 like any other globally conserved current; consequently, the disorder coupling to J^μ turns out to be marginal at the clean free fixed point, and this has important consequences for the disordered system. For the QED$_3$ case considered here, the situation is dramatically different: because of the presence of the gauge field, J^μ is no longer a globally conserved current, and its scaling di-

mension at the CFT fixed point is 3 [62]. The corresponding disorder is strongly irrelevant, and this is the reason it was not included in Eqs. (4.2) and (4.5).

Other earlier works with Dirac fermions studied the influence of disorder and the $1/r$ Coulomb interactions between the Dirac fermions [206, 207], and were motivated by the study of transitions between quantum Hall states. Today, they can be applied to graphene. As in our work, they found fixed lines at non-zero disorder and interactions.

Our paper begins in Sec. 4.2 by discussing our model in more detail. We start by reviewing some important properties of QED$_3$ in Sec. 4.2.1, before presenting the types of disorder under consideration in Sec. 4.2.2. The renormalization procedure and resulting β-functions are described in Sec. 4.3.1. The remainder of the section discusses the flows which result upon enforcing different symmetries, including the U(1)×SU(N) symmetric critical line mentioned above (Sec. 4.3.4). Sec. 4.4 focuses on applications to the kagome antiferromagnet and translates the fermion bilinears and topological current of the CFT to the microscopic observables of the spin model. Finally, in Sec. 4.5 the flavor conductivity along the critical line is calculated. We review out results and conclude in Sec. **??**.

4.2 Disordered QED$_3$

4.2.1 Pure QED$_3$

The Euclidean signature action for QED$_3$ is given in Eq. (4.1). In the IR limit, for N large enough, this theory flows to a strongly coupled CFT at $e^2 = \infty$. All loop contributions to the fermion propagator are suppressed by $1/2N$ and so we will work with the free propagator

$$G(p) = \delta_{\alpha\beta} \frac{ip_\mu \gamma^\mu}{p^2} \tag{4.6}$$

where α and β are flavor indices. The same is not true of the photon propagator. Instead, the $N = \infty$ Green's function must include a summation over the bubble diagrams shown in Fig. 4.2. The effective propagator is determined most simply by adding a non-local gauge

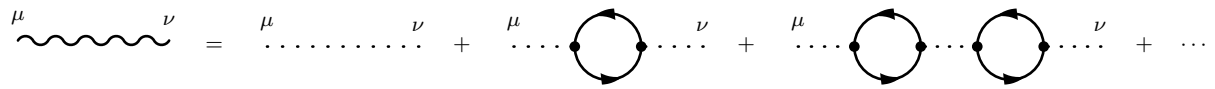

Figure 4.2: Diagrammatic expression for the effective photon propagator in the large-N limit. The dotted lines indicate the bare photon propagator, $D^0_{\mu\nu}(p)$, while the fermion bubbles are equal to $\Pi_{\mu\nu}(q)$. As indicated in the text, only the full photon propagator will be used.

fixing term to the action [29]

$$S_{\text{gauge-fixing}} = \frac{1}{32\,(\zeta-1)} \int \frac{d^3p}{(2\pi)^3} \frac{p_\mu p_\nu}{|p|} A^\mu(p) A^\nu(-p), \tag{4.7}$$

where ζ is an arbitrary parameter which cannot enter into any physical observable. The resulting free photon propagator is

$$D^0_{\mu\nu}(p) = \frac{2Ne^2}{p^2}\left(\delta_{\mu\nu} - \frac{p_\mu p_\nu}{p^2}\right) + \frac{16\,(\zeta-1)}{|p|}\frac{p_\mu p_\nu}{p^2}. \tag{4.8}$$

The polarization bubble in Fig. 4.2 can be evaluated (see Appendix C.6.1) and gives

$$\Pi^{\mu\nu}(p) = \frac{|p|}{16}\left(\delta_{\mu\nu} - \frac{p_\mu p_\nu}{p^2}\right). \tag{4.9}$$

Therefore, the $N = \infty$ propagator is

$$D^{\text{eff}}_{\mu\nu}(p) = \left(\left[D^0_{\mu\nu}(p)\right]^{-1} + \Pi_{\mu\nu}(p)\right)^{-1} = \frac{16}{|p|}\left(\delta_{\mu\nu} - \zeta\frac{p_\mu p_\nu}{p^2}\right) + \mathrm{O}\left(\frac{p^2}{e^2}\right). \tag{4.10}$$

Here, we have used the fact that, because the dimension of e^2 is 1, in the infrared limit, $p \to 0$, all terms of $\mathrm{O}(p^2/e^2)$ are suppressed. Provided we use the effective photon propagator and organize our perturbation theory such that no fermion bubbles of the type summed in Fig. 4.2 are repeated, the limit $e^2 \to \infty$ can be taken directly. We will further simplify by working in the $\zeta = 0$ gauge.

Since we will regulate the disordered theory using dimensional regularization, we write

$$S_{\rm qed}\left[\psi,\bar{\psi},A\right]=-\int d^dx\,d\tau\,\bar{\psi}_\alpha\left(\not{\partial}+\frac{i\mu^{-\epsilon/2}\not{g}}{\sqrt{2N}}\not{A}\right)\psi_\alpha, \tag{4.11}$$

where $d=2+\epsilon$, μ is an arbitrary scale, and the photon propagator is understood to be $D^{\rm eff}_{\mu\nu}(p)$. We will often write $D=d+1$ and denote spacetime coordinates by $r=(x,\tau)$. By making the coupling dimensionful, we are taking the engineering dimension of A_μ to be $d/2$. Gauge invariance guarantees that $\not{g}$ will not be renormalized, and it will be set to unity at the end of the calculation. This is discussed further in Sec. 4.3.1.

We now discuss the symmetries and operator content of the theory. QED$_3$ has a SU($2N$) symmetry under which the flavors rotate into one another:

$$\psi_\alpha\to\left[\exp\left(i\theta_{ab}\sigma^aT^b\right)\right]_{\alpha\beta}\psi_\beta\,. \tag{4.12}$$

Here, we have expressed the $(2N)^2-1$ generators of SU($2N$) as

$$\sigma^a\,T^b,\qquad\qquad \sigma^a,\qquad\qquad T^b, \tag{4.13}$$

where σ^a, $a=x,y,z$, are the 2×2 Pauli matrices and T^a, $a=1,\ldots,N^2-1$, are $N\times N$ traceless, Hermitian matrices normalized such that $\mathrm{tr}\left(T^aT^b\right)=\delta_{ab}/2$. Associated with each generator of this symmetry is a conserved current,

$$J^{ab}_\mu(r)=i\bar{\psi}\sigma^aT^b\gamma_\mu\psi(r),\qquad J^{a0}_\mu(r)=i\bar{\psi}\sigma^a\gamma_\mu\psi(r),\qquad J^{0b}_\mu(r)=i\bar{\psi}T^b\gamma_\mu\psi(r). \tag{4.14}$$

To all orders in $1/(2N)$, these operators have scaling dimension $\Delta_J=2$. When we discuss the symmetry of the theory in the remainder of the paper, we will be referring to the flavour symmetry unless explicitly stated otherwise.

As we remarked in Sec. 4.1, the irrelevance of monopoles results in an emergent U(1)$_{\rm top}$

symmetry associated with a conserved gauge flux current,

$$J^{\mu}_{\text{top}} = \epsilon^{\mu\nu\rho}\partial_{\nu}A_{\rho}. \tag{4.15}$$

Like the SU($2N$) currents, the scaling dimension of J^{μ}_{top} is exactly 2. In the limit we consider, monopole scaling dimensions are much greater than 2, though, as N descreases, this may cease to be the case.

The global U(1) transformation, $\psi \to e^{i\theta}\psi$, also has a conserved current, $J^{\mu}(r) = i\bar{\psi}\gamma^{\mu}\psi(r)$. However, because the U(1) phase rotation is also a local symmetry, its current is quite different from the SU($2N$) and U(1)$_{\text{top}}$ currents. This is evident upon considering the equations of motion:

$$J^{\mu} = \frac{1}{e^2\sqrt{2N}}\partial_{\nu}F^{\nu\mu} = \frac{1}{e^2\sqrt{2N}}\,\epsilon^{\mu\nu\rho}\partial_{\nu}J_{\text{top},\rho}. \tag{4.16}$$

Taken as an operator identity, this implies that the global U(1) current is actually a descendent of the gauge field, and, consequently, its scaling dimension is 3 instead of 2 [62].

In addition to the currents, there are $(2N)^2-1$ "mass" operators which can be constructed from the SU($2N$) generators,

$$N^{ab}(r) = \bar{\psi}\sigma^{a}T^{b}\psi(r), \qquad N^{a0}(r) = \bar{\psi}\sigma^{a}\psi(r), \qquad N^{0b}(r) = \bar{\psi}T^{b}\psi(r), \tag{4.17}$$

as well as the usual 2+1 dimensional Dirac mass term:

$$N_s(r) = \frac{1}{\sqrt{2N}}\,\bar{\psi}\psi(r). \tag{4.18}$$

Unlike the currents, at finite N these operators have nontrivial anomalous scaling dimensions [29, 62, 63]. In particular, since N_s allows for "photon decay" processes, it becomes less

relevant, with a scaling dimension of

$$\Delta_s = 2 + \frac{128}{3\pi^2(2N)} + \mathrm{O}\left(\frac{1}{N^2}\right). \tag{4.19}$$

Conversely, the SU($2N$) masses become more relevant:

$$\Delta_1 = 2 - \frac{64}{3\pi^2(2N)} + \mathrm{O}\left(\frac{1}{N^2}\right). \tag{4.20}$$

4.2.2 Disorder

We are interested in perturbing the QED$_3$ CFT with disorder. A simple scaling argument shows that there are a limited number of operators which can give interesting results upon coupling to disorder. We begin by considering disorder coupling to an arbitrary, gauge-invariant operator O with scaling dimension Δ_{O}:

$$S_{\mathrm{dis,O}}\left[\mathrm{O}\right] = \int d^d x\, d\tau\, M_{\mathrm{O}}(x)\mathrm{O}(x,\tau) \tag{4.21}$$

where $M_{\mathrm{O}}(x)$ is a Gaussian random variable with zero average and with correlations given by

$$\overline{M_{\mathrm{O}}(x)M_{\mathrm{O}}(x')} = \frac{g_{\mathrm{O}}}{2}\delta^d(x-x'). \tag{4.22}$$

g_{O} is the variance of M_{O} and controls the strength of the disorder. To allow for a well-controlled perturbative expansion, we assume that g_{O} is of the same order as $1/(2N)$; this implies that the bare disorder strength and the electromagnetic interaction are of the same magnitude.

Since S_{dis} explicitly breaks Lorentz symmetry, time and space need no longer scale in the same way. We express this by allowing time to scale as $-z$: $[\tau] = -z$. "z" is referred to as the dynamic critical exponent. While our assumption that $g_{\mathrm{O}} \sim \mathrm{O}(1/N)$ ensures that $z - 1 \sim$

$O(1/N)$ as well, the possibility that $z \neq 1$ at higher orders has several effects which will be important later. First, the dimensions of conserved currents are no longer all fixed precisely at 2. The scaling dimension of the time component remains 2, but spatial components have dimension $\Delta_{J,xy} = 1 + z$. Second, having a dynamic critical exponent different from unity also changes the dimensional analysis of the disorder strength g_{O}. Eq. (4.21) establishes that $[M_{\mathrm{O}}] = d + z - \Delta_{\mathrm{O}}$, and with Eq. (4.22), this indicates that $[g_{\mathrm{O}}] = d + 2z - 2\Delta_{\mathrm{O}}$. It follows that the critical dimension is $1 + z$. This is the quantum version of the Harris criterion [56].

At tree level, $z = 1$, so the Harris criterion indicates that in $2d$ disorder coupling to operators with $\Delta_{\mathrm{O}} > 2$ is irrelevant: at low energies, the system is described by the clean theory. Conversely, operators with scaling dimensions less than or equal to 2 are either relevant or marginal perturbations when coupled to disorder.

Referring to the previous section, to leading order in N, there are no relevant perturbations and only the global topological current, the SU($2N$) currents, and the mass terms, N_s and N_{ab}, are marginal. However, as mentioned above, at finite N, it's possible that the scaling dimension of an allowed monopole operator is less than 2, making it relevant. We will not examine this possibility in our present large N expansion. As discussed in Sec. 4.1, the global U(1) current, $J^\mu = i\bar{\psi}\gamma^\mu\psi$, is irrelevant because its scaling dimension is 3.

Keeping in mind that in order to compare with the kagome antiferromagnet we must set $N = 2$, we couple disorder to operators which break the SU($2N$) symmetry down to SU(N):

$$\begin{aligned} S_{\mathrm{dis}}[\psi, \bar{\psi}] = \int d^d x\, d\tau \Big[& M_s(x)\bar{\psi}\psi(x,\tau) + M_{t,a}(x)\bar{\psi}\sigma^a\psi(x,\tau) \\ & + i\mathcal{A}_{ja}(x)\bar{\psi}\sigma^a\gamma^j\psi(x,\tau) + V_a(x)\bar{\psi}\sigma^a\gamma^0\psi(x,\tau) \\ & + i\mathcal{E}_j(x)J^j_{\mathrm{top}}(x,\tau) + \mathcal{B}(x)J^0_{\mathrm{top}}(x,\tau)\Big] \end{aligned} \tag{4.23}$$

where M_s, $M_{t,a}$, $\mathcal{A}_{ja}$, V_a, $\mathcal{E}_j$, and $\mathcal{B}$ are Gaussian random variables with vanishing mean. Here and throughout the paper we use the convention that, when contracting vectors and γ-matrices, Roman letters i, j, ℓ, etc. indicate that the sum is only over the spatial coordinates

x, while Greek letters μ, ν, σ, etc. include time as well. We note that since the quenched disorder is classical, the random fields have been expressed in real time. That is, the time component of all classical gauge potentials picks up a factor of "i". Averaging over disorder, we have

$$\begin{aligned}
\overline{M_s(x)M_s(x')} &= \frac{g_s}{2}\delta^d(x-x'), & \overline{V_a(x)V_b(x')} &= \frac{g_{v,a}}{2}\delta_{ab}\delta^d(x-x') \\
\overline{M_{t,a}(x)M_{t,b}(x')} &= \frac{g_{t,a}}{2}\delta_{ab}\delta^d(x-x'), & \overline{\mathcal{E}_i(x)\mathcal{E}_j(x')} &= \frac{g_{\mathcal{E}}}{2}\delta_{ij}\delta^d(x-x') \\
\overline{\mathcal{A}_{ia}(x)\mathcal{A}_{jb}(x')} &= \frac{g_{\mathcal{A},a}}{2}\delta_{ab}\delta_{ij}\delta^d(x-x'), & \overline{\mathcal{B}(x)\mathcal{B}(x')} &= \frac{g_{\mathcal{B}}}{2}\delta^d(x-x')
\end{aligned} \tag{4.24}$$

with all other two-points vanishing. As in the general case considered above, we assume that the variances, $\{g_s, g_{t,a}, g_{\mathcal{A},a}, g_{v,a}, g_{\mathcal{E}}, g_{\mathcal{B}}\}$, are small and of the same order as $1/(2N)$.

When we interpret these operators in the context of the kagome antiferromagnet, the σ^a matrices will act on spin. By recalling that the Dirac mass, $\bar{\psi}\psi$, is odd under time reversal in 2+1 dimensions, we deduce that the SU(2) mass operators, $i\bar{\psi}\sigma^a\psi$, should be even. The same logic asserts that the scalar potential operators, $i\bar{\psi}\gamma^0\sigma^a\psi$, are odd under time reversal while the vector potential operators, $i\bar{\psi}\gamma^j\sigma^a\psi$, are even. Similarly, the fact that J^0_{top} and J^j_{top} are the emergent magnetic field and electric fields respectively reveals that they are odd and even under time reversal. Therefore, while the zero mean of the quenched disorder fields implies that $S_{\text{dis}}[\psi, \bar{\psi}]$ preserves time reversal on average, it is only a good symmetry everywhere within the system when M_s, V_a and $\mathcal{B}$ are not present (equivalently, $g_s = g_{v,a} = g_{\mathcal{B}} = 0$). In Sec. 4.4 we will discuss the microscopic meaning of $S_{\text{dis}}[\psi, \bar{\psi}]$ in the kagome antiferromagnet more thoroughly.

We will use dimensional regularization with $d = 2+\epsilon$ so that the dimension of the variances is shifted to $[g_\xi] = -\epsilon$, where $\xi = s$, (t,a), $(\mathcal{A},a)$, (v,a), $\mathcal{E}$, or $\mathcal{B}$. For convenience, we make the couplings dimensionless by taking $g_\xi \to \mu^{-\epsilon} g_\xi$ where μ is an arbitrary momentum scale. When we perform the renormalization group study, the couplings are restricted to non-negative values because they physically correspond to variances.

The disorder breaks translational symmetry and makes calculating quantities for a given realization of disorder completely intractable. Instead, the fundamental quantity of interest is the disorder-averaged free energy:

$$\begin{aligned}\overline{F} &= -\overline{\log Z} \\ &= -\log\Bigg[\int DM(x)\, DM_a(x)\, DM_{\mu a}(x)\, D\mathcal{A}_{\mu a}(x)\, DV_a(x)\, e^{-S_{\rm qed}-S_{\rm dis}}\, e^{-\frac{\mu^\epsilon}{2g_s^2}\int d^dx\, M_s(x)^2}\, e^{-\frac{\mu^\epsilon}{2g_{\mathcal{B}}^2}\int d^dx \mathcal{B}(x)^2} \\ &\quad\times e^{-\frac{1}{2g_{\mathcal{E}}^2}\int d^dx \mathcal{E}_j(x)\mathcal{E}^j(x)} \prod_{a=x,y,z} e^{-\frac{\mu^\epsilon}{2g_{t,a}^2}\int d^dx\, M_{t,a}(x)^2}\, e^{-\frac{\mu^\epsilon}{2g_{\mathcal{A},a}^2}\int d^dx\, \mathcal{A}_{ja}(x)A^{ja}(x)}\, e^{-\frac{\mu^\epsilon}{2g_{v,a}^2}\int d^dx\, V_a(x)^2}\Bigg].\end{aligned} \tag{4.25}$$

To solve perturbatively, we employ the replica trick. Using the identity

$$\log Z = \lim_{n\to 0}\frac{Z^n-1}{n}, \tag{4.26}$$

we instead calculate

$$Z_n \equiv \overline{Z^n} = \mathcal{N}\int \prod_{\substack{\alpha=1,\ldots,2N\\ \ell=1,\ldots,n}} D\psi_{\alpha\ell} D\bar\psi_{\alpha\ell} DA_\ell\, e^{-S_n[\psi_{\alpha\ell},\bar\psi_{\alpha\ell}]} \tag{4.27}$$

where $\mathcal{N}$ is a normalization constant and

$$\begin{aligned}S_n\left[\psi,\bar\psi,A\right] = &-\sum_\ell \int d^dx\, d\tau\, \bar\psi_\ell(x,\tau)\left(\not\partial + \frac{i\mu^{-\epsilon/2}\not g}{\sqrt{2N}}\not A_\ell\right)\psi_\ell(x,\tau) \\ &+\frac{\mu^{-\epsilon}}{2}\sum_{\ell,m}\int d^dx\, d\tau\, d\tau'\Big\{-g_s\bar\psi_\ell\psi_\ell(x,\tau)\bar\psi_m\psi_m(x,\tau') - \sum_a g_{t,a}\bar\psi_\ell\sigma^a\psi_\ell(x,\tau)\bar\psi_m\sigma_a\psi_m(x,\tau') \\ &-\sum_a g_{\mathcal{A},a}\,\bar\psi_\ell i\gamma^j\sigma^a\psi_\ell(x,\tau)\bar\psi_m i\gamma_j\sigma_a\psi_m(x,\tau') + \sum_a g_{v,a}\,\bar\psi_\ell i\gamma^0\sigma^a\psi_\ell(x,\tau)\bar\psi_m i\gamma^0\sigma_a\psi_m(x,\tau') \\ &-g_{\mathcal{B}}J^{\ell,0}_{\rm top}(x,\tau)J^{m,0}_{\rm top}(x,\tau') + g_{\mathcal{E}}\,J^{\ell,j}_{\rm top}(x,\tau)J^m_{{\rm top},j}(x,\tau')\Big\}.\end{aligned} \tag{4.28}$$

In addition to the physical flavor symmetry, the fermions and photon now carry a replica

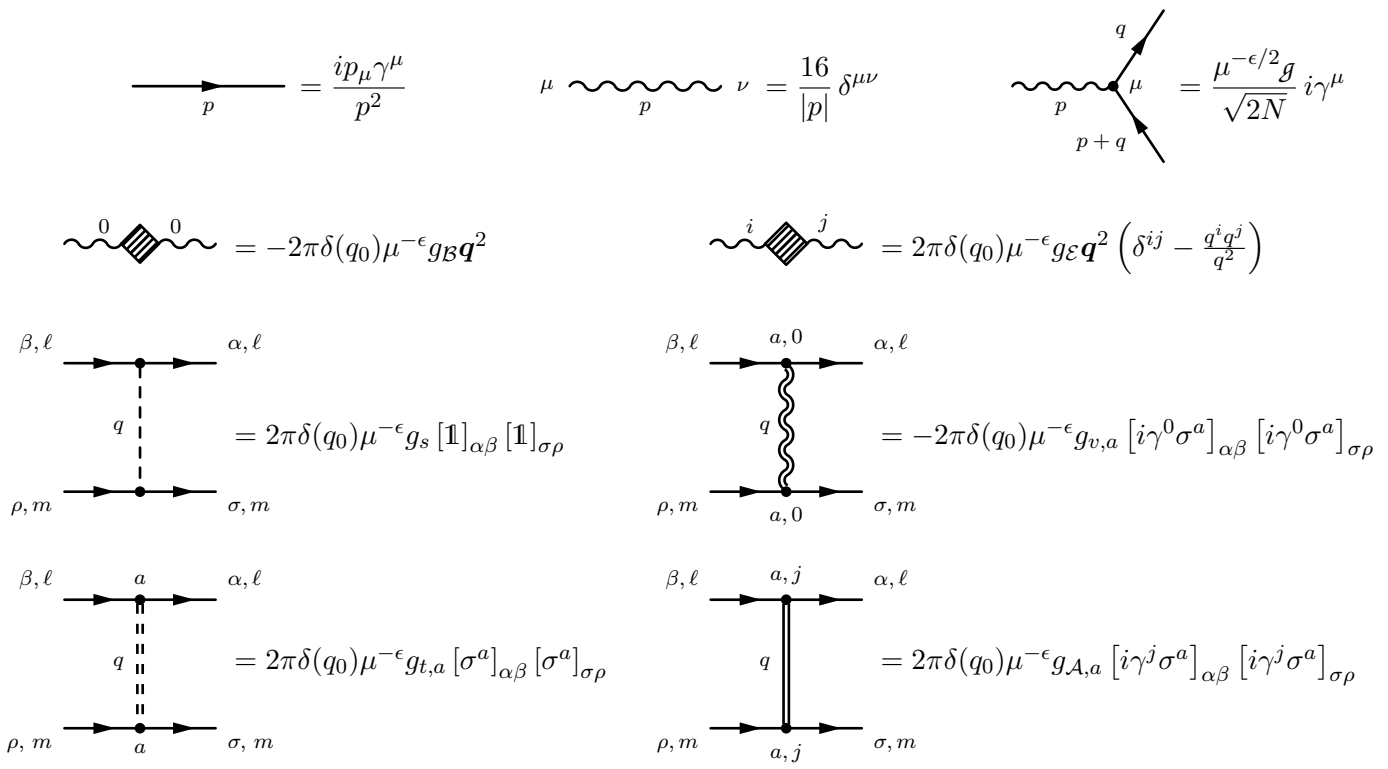

Figure 4.3: Feynman rules associated with the replicated action, $S_n\left[\psi,\bar{\psi},A\right]$. The diagrams on the first and second rows are diagonal with respect to the replica and flavor indices. In the four-point diagrams, ℓ and m are replica indices while α,β,σ,ρ label the $2N$ fermion flavors.

index denoted by ℓ and m. We have suppressed the summation over the flavour indices and will continue to do so in what follows. Likewise, the replica indices will often be left implicit. The Feynman rules corresponding to $S_n\left[\psi,\bar{\psi},A\right]$ are provided in Fig. 4.3.

4.3 Renormalization group analysis

4.3.1 Renormalized action

The low energy properties of $S_n\left[\psi,\bar{\psi},A\right]$ can be studied with the same renormalization techniques used in many-body systems provided the number of replicas, n, is taken to zero at the end of the calculation. This implies that diagrams which sum over all replicas must

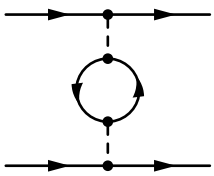

Figure 4.4: Example of a diagram which vanishes in the replica limit, $n \to 0$. The internal fermion loop involves a sum over all replica indices, and multiplies the diagram by an overall factor of n.

be neglected. For instance, Fig. 4.4 is proportional to n and should not be included.

We will use renormalized perturbation theory [6], making use of a counter term action:

$$\begin{aligned} S_n^{\mathrm{CT}}\left[\psi,\bar{\psi}\right] = &-\sum_{\ell}\int d^dx\, d\tau\, \bar{\psi}_\ell\left(i\delta_1\gamma^0\frac{\partial}{\partial\tau}+i\delta_2\gamma^j\frac{\partial}{\partial x_j}+\frac{i\mu^{-\epsilon/2}g\delta_1'}{\sqrt{2N}}A_0^\ell\gamma^0+\frac{i\mu^{-\epsilon/2}g\delta_2'}{\sqrt{2N}}A_j^\ell\gamma^j\right)\psi_\ell(x,\tau)\\ &+\frac{\mu^{-\epsilon}}{2}\sum_{\ell,m}\int d^dx\, d\tau\, d\tau'\Big\{-\delta_s\,\bar{\psi}_\ell\psi_\ell(x,\tau)\bar{\psi}_m\psi_m(x,\tau')-\sum_a\delta_{t,a}\,\bar{\psi}_\ell\sigma^a\psi_\ell(x,\tau)\bar{\psi}_m\sigma_a\psi_m(x,\tau')\\ &-\sum_a\delta_{\mathcal{A},a}\,\bar{\psi}_\ell i\gamma^j\sigma^a\psi_\ell(x,\tau)\bar{\psi}_m i\gamma_j\sigma_a\psi_m(x,\tau')+\sum_a\delta_{v,a}\,\bar{\psi}_\ell i\gamma^0\sigma^a\psi_\ell(x,\tau)\bar{\psi}_m i\gamma^0\sigma_a\psi_m(x,\tau')\\ &-\delta_{\mathcal{B}}\,J^{\ell,0}_{\mathrm{top}}(x,\tau)J^{m,0}_{\mathrm{top}}(x,\tau')+\delta_{\mathcal{E}}\,J^{\ell,j}_{\mathrm{top}}(x,\tau)J^{m}_{\mathrm{top},j}(x,\tau')\Big\}. \end{aligned} \tag{4.29}$$

The counter terms, $\{\delta_{1,2},\delta'_{1,2},\delta_s,\delta_{t,a},\delta_{v,a},\delta_{\mathcal{A},a},\delta_{\mathcal{B}},\delta_{\mathcal{E}}\}$, are determined by requiring that all physical observables are finite in a dimensional regularization scheme. While relativistic invariance is explicitly broken, there is no need track the relative flow of the fermion and photon velocities since the low-energy behaviour of the photon propagator descends entirely from its interaction with the fermions.

The bare action is the sum of S_n and $S_n^{\rm CT}$:

$$\begin{aligned} S_n^B\left[\psi,\bar\psi,A\right] = &-\sum_\ell \int d^dx_B\, d\tau_B\, \bar\psi_{\ell,B}\left(i\gamma^0\frac{\partial}{\partial\tau_B}+i\gamma^j\frac{\partial}{\partial x_{j,B}}+\frac{i\not{g}_B\gamma^0}{\sqrt{2N}}A^\ell_{0,B}+\frac{i\not{g}_B\gamma^j}{\sqrt{2N}}A^\ell_{j,B}\right)\psi_{\ell,B}(x_B,\tau_B)\\ &+\frac{1}{2}\sum_{\ell,m}\int d^dx_B\, d\tau_B\, d\tau'_B\Big\{g_s^B\,\bar\psi_{\ell,B}\psi_{\ell,B}(x_B,\tau_B)\bar\psi_{m,B}\psi_{m,B}(x_B,\tau'_B)\\ &-\sum_a g^B_{t,a}\,\bar\psi_{\ell,B}\sigma^a\psi_{\ell,B}(x_B,\tau_B)\bar\psi_{m,B}\sigma_a\psi_{m,B}(x_B,\tau'_B)\\ &-\sum_a g^B_{\mathcal{A},a}\,\bar\psi_{\ell,B}i\gamma^j\sigma^a\psi_{\ell,B}(x_B,\tau_B)\bar\psi_{m,B}i\gamma_j\sigma_a\psi_{m,B}(x_B,\tau'_B)\\ &+\sum_a g^B_{v,a}\,\bar\psi_{\ell,B}i\gamma^0\sigma^a\psi_{\ell,B}(x_B,\tau_B)\bar\psi_{m,B}i\gamma^0\sigma_a\psi_{m,B}(x_B,\tau'_B)\\ &-g^B_{\mathcal{B}}\,J^{\ell,0}_{{\rm top},B}(x_B,\tau_B)J^{m,0}_{{\rm top},B}(x_B,\tau'_B)+g^B_{\mathcal{E}}\,J^{\ell,j}_{{\rm top},B}(x_B,\tau_B)J^{m}_{{\rm top},B,j}(x_B,\tau'_B)\Big\} \end{aligned} \tag{4.30}$$

where the bare fields and coordinates are

$$\begin{aligned} \psi_B(x_B,\tau_B) &= Z_1^{1/2}\psi(x,\tau),\\ A_{0,B}(x_B,\tau_B) &= Z_{\gamma,0}^{1/2}A_0(x,\tau), \qquad & A_{jB}(x_B,\tau_B) &= Z_{\gamma,xy}^{1/2}A_j(x,\tau),\\ \tau_B &= \frac{Z_2}{Z_1}\tau, & x_B &= x. \end{aligned} \tag{4.31}$$

Here, we have written $Z_1 = 1+\delta_1$ and $Z_2 = 1+\delta_2$, and, by taking $x = x_B$, we are renormalizing relative to the spatial scale. Gauge invariance constrains the photon field strength renormalization constants to be

$$Z_{\gamma,0}^{1/2} = \frac{Z_1}{Z_2}, \qquad Z_{\gamma,xy}^{1/2} = 1, \tag{4.32}$$

and it follows that we must have $\delta_{1,2} = \delta'_{1,2}$. This has been explicitly verified. The field strength renormalization of the topological currents then follows simply from the renormal-

ization of A_μ and (x, τ):

$$J^0_{\text{top},B} = \frac{\partial A_y}{\partial x} - \frac{\partial A_x}{\partial y}, \quad J^x_{\text{top},B} = \frac{Z_1}{Z_2}\left(\frac{\partial A_0}{\partial y} - \frac{\partial A_y}{\partial \tau}\right), \quad J^y_{\text{top},B} = -\frac{Z_1}{Z_2}\left(\frac{\partial A_0}{\partial x} - \frac{\partial A_x}{\partial \tau}\right). \tag{4.33}$$

As discussed in the previous section, the dynamic critical exponent relates the scaling of time and space to one another:

$$\mu \frac{d}{d\mu}\tau = z\tau\,. \tag{4.34}$$

Since τ_B should scale like μ, taking its derivative with respect to $\log \mu$ gives

$$z = 1 - \mu \frac{d}{d\mu} \log\left(\frac{Z_2}{Z_1}\right). \tag{4.35}$$

The renormalization of the disorder strengths is determined by comparing the bare action to $S_n + S_n^{\text{CT}}$:

$$\begin{aligned} g_s^B &= \mu^{-\epsilon} Z_2^{-2}\left(g_s + \delta_s\right), & g_{t,a}^B &= \mu^{-\epsilon} Z_2^{-2}\left(g_{t,a} + \delta_{t,a}\right), \\ g_{\mathcal{A},a}^B &= \mu^{-\epsilon} Z_2^{-2}\left(g_{\mathcal{A},a} + \delta_{\mathcal{A},a}\right), & g_{v,a}^B &= \mu^{-\epsilon} Z_2^{-2}\left(g_{v,a} + \delta_{v,a}\right), \\ g_{\mathcal{E}}^B &= \mu^{-\epsilon}\left(g_{\mathcal{E}} + \delta_{\mathcal{E}}\right), & g_{\mathcal{B}}^B &= \mu^{-\epsilon} Z_1^2 Z_2^{-2}\left(g_{\mathcal{B}} + \delta_{\mathcal{B}}\right). \end{aligned} \tag{4.36}$$

The fact that the bare couplings are independent of the scale μ establishes the β-functions. For disorder coupling to fermion bilinears, we have

$$0 = -\epsilon\left(g_\xi + \delta_\xi\right) - 2\left(g_\xi + \delta_\xi\right)\mu \frac{d}{d\mu}\log Z_2 + \mu \frac{d}{d\mu}\delta_\xi + \beta_\xi, \quad \xi = s, (t,a), (\mathcal{A},a), (v,a), \tag{4.37}$$

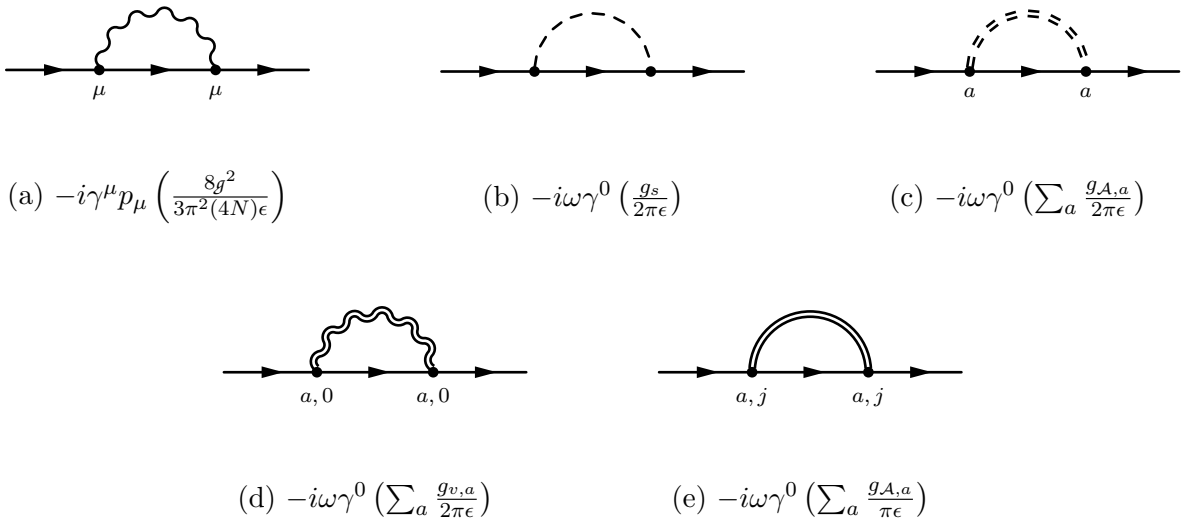

(a) $-i\gamma^\mu p_\mu \left(\frac{8g^2}{3\pi^2(4N)\epsilon}\right)$ (b) $-i\omega\gamma^0 \left(\frac{g_s}{2\pi\epsilon}\right)$ (c) $-i\omega\gamma^0 \left(\sum_a \frac{g_{\mathcal{A},a}}{2\pi\epsilon}\right)$

(d) $-i\omega\gamma^0 \left(\sum_a \frac{g_{v,a}}{2\pi\epsilon}\right)$ (e) $-i\omega\gamma^0 \left(\sum_a \frac{g_{\mathcal{A},a}}{\pi\epsilon}\right)$

Figure 4.5: Feynman diagrams which contribute to the fermion self-energy at $\mathrm{O}(g_\xi, 1/2N)$.

where $\beta_\xi = \mu d g_\xi / d\mu$ and $a = x, y, z$. Similarly, the β-functions for the flux disorder are

$$\begin{aligned} 0 &= -\epsilon\left(g_\mathcal{E} + \delta_\mathcal{E}\right) + \mu\frac{d}{d\mu}\delta_\mathcal{E} + \beta_\mathcal{E}, \\ 0 &= -\epsilon\left(g_\mathcal{B} + \delta_\mathcal{B}\right) + 2\left(g_\mathcal{B} + \delta_\mathcal{B}\right)(z-1) + \mu\frac{d}{d\mu}\delta_\mathcal{B} + \beta_\mathcal{B}. \end{aligned} \tag{4.38}$$

In the second equation, the relation $z - 1 = \mu d \log\left(Z_1/Z_2\right)/d\mu$ has been used.

The fermion self-energy diagrams which determine the counter terms δ_1 and δ_2 to leading order are shown in Fig. 4.5. These are evaluated in Appendix C.2, and the divergent pieces are listed below the corresponding diagram in the figure. Only the photon loop in Fig. 4.5(a) contributes to Z_2. In order to cancel this divergence, we must have

$$\delta_2 = \frac{8g^2}{3\pi^2(2N)\epsilon}. \tag{4.39}$$

The frequency counter term, on the other hand, receives contributions from all of the dia-

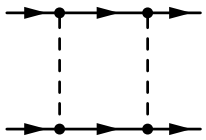

(a) $\left[\gamma^j \otimes \gamma_j\right]\left[\mathbb{1} \otimes \mathbb{1}\right]\left(-\frac{g_s^2}{4\pi\epsilon}\right)$

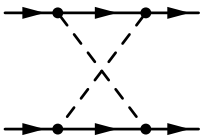

(b) $\left[\gamma^j \otimes \gamma_j\right]\left[\mathbb{1} \otimes \mathbb{1}\right]\left(\frac{g_s^2}{4\pi\epsilon}\right)$

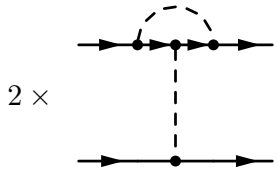

(c) $\left[\mathbb{1} \otimes \mathbb{1}\right]\left[\mathbb{1} \otimes \mathbb{1}\right]\left(\frac{g_s^2}{\pi\epsilon}\right)$

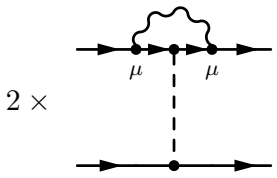

(d) $\left[\mathbb{1} \otimes \mathbb{1}\right]\left[\mathbb{1} \otimes \mathbb{1}\right]\left(-\frac{48 g_s g^2}{\pi^2(2N)\epsilon}\right)$

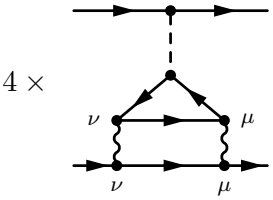

(e) $\left[\mathbb{1} \otimes \mathbb{1}\right]\left[\mathbb{1} \otimes \mathbb{1}\right]\left(\frac{64 g_s g^4}{\pi^2(2N)\epsilon}\right)$

Figure 4.6: Diagrams which contribute when only SU($2N$)-preserving, bilinear disorder is considered ($g_{t,a} = g_{\mathcal{A},a} = g_{v,a} = 0$). Both Figs. 4.6(c) and 4.6(d) are accompanied by a diagram with the interaction on the other vertex. Partner diagrams to Fig. 4.6(e) with the fermion loop direction reversed and/or the vertex switched are also present. These diagrams sum to $\left[\mathbb{1} \otimes \mathbb{1}\right]\left[\mathbb{1} \otimes \mathbb{1}\right]\left\{\frac{g_s^2}{\pi\epsilon} + \frac{64 g_s g^4}{\pi^2(2N)\epsilon} - \frac{48 g_s g^2}{\pi^2(2N)\epsilon}\right\}$

grams in Fig. 4.5:

$$\delta_1 = \frac{8g^2}{3\pi^2(2N)\epsilon} + \frac{1}{2\pi\epsilon}\left[g_s + \sum_a \left(g_{t,a} + g_{v,a} + 2g_{\mathcal{A},a}\right)\right]. \tag{4.40}$$

It follows from Eq. (4.35), the dynamic critical exponent is

$$z = 1 + \frac{1}{2\pi}\left[g_s + \sum_a \left(g_{t,a} + 2g_{\mathcal{A},a} + g_{v,a}\right)\right]. \tag{4.41}$$

The provision that all couplings be positive implies that $z \geq 1$ always.

The bilinear counter terms, δ_ξ, $\xi = s, (t,a), (\mathcal{A},a), (v,a)$, are determined by adding diagrams like those in Fig. 4.6. In particular, Fig. 4.6 shows all diagrams which renormalize disorder coupled to the SU($2N$)-symmetric mass when all other couplings have been tuned

to zero. The integrals are performed in Appendix C.3, and the remainder of the diagrams renormalizing the bilinear disorder are shown in Appendix C.4 in Tables C.1, C.2, and C.3. The resulting counter terms are

$$\begin{aligned}
\delta_s &= -\frac{1}{\pi\epsilon}\left[g_s^2 + \frac{64 g_s \mathcal{g}^4}{\pi(2N)} - \frac{48 g_s \mathcal{g}^2}{\pi(2N)} + g_s \sum_a \left(g_{t,a} + g_{v,a} - 2g_{\mathcal{A},a}\right) - 2\sum_a g_{v,a} g_{\mathcal{A},a}\right] \\
\delta_{t,a} &= -\frac{1}{\pi\epsilon}\Bigg[g_{t,a}\left(2g_{t,a} - \sum_b g_{t,b}\right) - 2g_{t,a}\left(2g_{\mathcal{A},a} - \sum_b g_{\mathcal{A},b}\right) + g_{t,a}\left(2g_{v,a} - \sum_b g_{v,b}\right) \\
&\quad + g_{t,a} g_s + 4 g_{t,a} g_{\mathcal{A},a} \mathcal{g}^2 - 4 g_{t,a} g_{v,a} \mathcal{g}^2 - 2\sum_{bc} \left|\epsilon^{abc}\right| g_{t,b} g_{\mathcal{A},c} - \frac{48 g_{t,a} \mathcal{g}^2}{\pi(2N)}\Bigg] \\
\delta_{\mathcal{A},a} &= -\frac{1}{\pi\epsilon}\left[-g_s g_{v,a} - \sum_{bc}\left|\epsilon^{abc}\right|\left(\frac{g_{t,b} g_{t,c}}{2} + 2 g_{\mathcal{A},b} g_{\mathcal{A},c} + \frac{g_{v,b} g_{v,c}}{2}\right) - \frac{16 g_{\mathcal{A},a} \mathcal{g}^2}{3\pi(2N)}\right] \\
\delta_{v,a} &= -\frac{1}{\pi\epsilon}\Bigg[-g_{v,a}\left(2g_{v,a} - \sum_b g_{v,b}\right) - g_{v,a}\left(2g_{t,a} - \sum_b g_{t,b}\right) - 2g_{v,a}\left(2g_{\mathcal{A},a} - \sum_b g_{\mathcal{A},b}\right) \\
&\quad - g_{v,a} g_s - 2 g_s g_{\mathcal{A},a} - 2\sum_{bc}\left|\epsilon^{abc}\right| g_{v,b} g_{\mathcal{A},c} - \frac{16 g_{v,a} \mathcal{g}^2}{3\pi(2N)}\Bigg].
\end{aligned} \tag{4.42}$$

The graphs which renormalize the topological disorder stengths, $g_{\mathcal{E}}$ and $g_{\mathcal{B}}$, are actually three loop diagrams at leading order. These are calculated in Appendix C.5 where we find

$$\delta_{\mathcal{E}} = \frac{g_s g_{\mathcal{B}} \mathcal{g}^4}{\pi\epsilon}, \qquad \delta_{\mathcal{B}} = \frac{g_s g_{\mathcal{E}} \mathcal{g}^4}{\pi\epsilon}. \tag{4.43}$$

Differentiating the bare couplings (Eq. (4.36)) with respect to μ, solving for the β-functions

to $\mathrm{O}(g_\xi^2, g_\xi/2N)$, and setting $\mathscr{g}^2 = 1$, we obtain

$$\begin{aligned}
\pi\beta_s &= \pi\epsilon g_s + g_s\left[g_s + \sum_a (g_{t,a} + g_{v,a} - 2g_{\mathcal{A},a}) + 2c\right] - 2\sum_a g_{v,a}g_{\mathcal{A},a} \\
\pi\beta_{t,a} &= \pi\epsilon g_{t,a} + g_{t,a}\Bigg[\left(2g_{t,a} - \sum_b g_{t,b}\right) + 2\left(2g_{\mathcal{A},a} + \sum_b g_{\mathcal{A},b}\right) - \left(6g_{v,a} + \sum_b g_{v,b}\right) \\
&\qquad + g_{t,a}g_s - 2c\Bigg] - 2\sum_{bc}\left|\epsilon^{abc}\right| g_{t,b}g_{\mathcal{A},c} \\
\pi\beta_{\mathcal{A},a} &= \pi\epsilon g_{\mathcal{A},a} - g_s g_{v,a} - \sum_{bc}\left|\epsilon^{abc}\right|\left(\frac{g_{t,b}g_{t,c}}{2} + 2g_{\mathcal{A},b}g_{\mathcal{A},c} + \frac{g_{v,b}g_{v,c}}{2}\right) \\
\pi\beta_{v,a} &= \pi\epsilon g_{v,a} - g_{v,a}\Bigg[\left(2g_{v,a} - \sum_b g_{v,b}\right) + \left(2g_{t,a} - \sum_b g_{t,b}\right) + 2g_{v,a}\left(2g_{\mathcal{A},a} - \sum_b g_{\mathcal{A},b}\right) + g_s\Bigg] \\
&\qquad - 2g_s g_{\mathcal{A},a} - 2\sum_{bc}\left|\epsilon^{abc}\right| g_{v,b}g_{\mathcal{A},c}, \\
\pi\beta_{\mathcal{E}} &= \pi\epsilon g_{\mathcal{E}} - 3g_s g_{\mathcal{B}}, \\
\pi\beta_{\mathcal{B}} &= \pi\epsilon g_{\mathcal{B}} - 3g_s g_{\mathcal{E}} - g_{\mathcal{B}}\left[g_s + \sum_a (g_{t,a} + 2g_{\mathcal{A},a} + g_{v,a})\right]. \qquad (4.44)
\end{aligned}$$

where

$$c = \frac{64}{3\pi N}. \qquad (4.45)$$

In what follows we will work in 2 spatial dimensions and set $\epsilon = 0$.

4.3.2 SU($2N$) flavour symmetry

Since disorder coupling to the U(1) gauge currents is irrelevant, the only finite couplings which preserve the SU($2N$) flavour symmetry of QED$_3$ are g_s, $g_{\mathcal{E}}$, and $g_{\mathcal{B}}$. With $g_{t,a} = g_{t,\mathcal{A}} = g_{v,a} = 0$, the only non-trivial β-functions are

$$\pi\beta_s = g_s^2 + 2cg_s, \qquad \pi\beta_{\mathcal{E}} = -3g_s g_{\mathcal{B}}, \qquad \pi\beta_{\mathcal{B}} = -g_s\left(3g_{\mathcal{E}} + g_{\mathcal{B}}\right). \qquad (4.46)$$

β_s is entirely determined by the fermion self-energy diagrams in Figs. 4.5(a) and 4.5(b) and the 4-point diagrams in Fig. 4.6. Figs. 4.6(a) and 4.6(b) cancel, and Fig. 4.6(c) contributes the second term in β_s. This is precisely the same term found in Ref. 108 for free Dirac fermions. The second term in β_s results from interactions with the photon. In fact, this is simply the anomalous dimension of $N_s(r) = \frac{1}{\sqrt{2N}}\bar{\psi}\psi(r)$ in pure QED$_3$ (Eq. (4.19)). Since $g_s > 0$, both terms in β_s are positive, and, as the energy scale is taken to zero, g_s flows to zero.

On inspecting the β-functions for the topological disorder strengths, we note an apparent inconsistency with our claim that J^μ_{top} is a conserved current. In particular, as indicated near the beginning of Sec. 4.2.2, the scaling dimensions of the spatial and time components of a conserved current are non-perturbatively protected to be $1+z$ and 2 respectively, and this should be reflected in their β-functions. However, this is not the case in the expression above for either J^j_{top} or J^0_{top} when $g_s \neq 0$. Fortunately, this result makes sense in the context of the parity anomaly: when a single species of Dirac fermions is coupled to a mass, a Chern-Simons term at level 1/2 is generated $\sim \frac{1}{2}\epsilon^{\mu\nu\rho}A_\mu\partial_\nu A_\rho/4\pi$. In the disordered system, this manifests itself through the induced coupling of the two topological currents.

Regardless, both of the β-functions for the topological disorder are directly proportional to the SU($2N$)-symmetric mass coupling and so vanish when $g_s = 0$. However, we argue that higher order effects ultimately destabilize the clean critical point in the absence of time reversal symmetry. To start, we observe that the Dirac equation has an additional discrete, anti-unitary symmetry under which both time and charge flip, leading us to refer to it as "$\mathcal{CT}$" symmetry. J^0_{top} is even under the action of $\mathcal{CT}$, while both $\bar{\psi}\psi$ and J^j_{top} are odd. Imposing this symmetry sets $g_s = g_{\mathcal{E}} = 0$ and allows only $g_{\mathcal{B}}$ to be finite. The lowest order diagram which contributes is the fermion self-energy shown in Fig. 4.7. Like the diagrams in Fig. 4.5, its divergence is cancelled by Z_1, yielding a dynamic critical exponent greater than

unity:

$$z = 1 + \frac{g_{\mathcal{B}}}{2\pi(2N)}. \tag{4.47}$$

Even though time-reversal is broken, the $\mathcal{CT}$ symmetry ensures that no diagrams mixing $g_{\mathcal{B}}$ and $g_{\mathcal{E}}$ are generated. We conclude that since flux is still conserved, the only contribution to the β-function of $g_{\mathcal{B}}$ arise from the corrections to the dynamic critical exponent given in Eq. (4.47). In Sec. 4.2.2, we showed that the dimension of disorder coupling to J^0_{top} is

$$[g_{\mathcal{B}}] = 2(1+z) - 2\left[J^0_{\text{top}}\right] = 2(z-1), \tag{4.48}$$

and, therefore, the β-function is

$$\pi\beta_{\mathcal{B}} = -\frac{g_{\mathcal{B}}^2}{2N}. \tag{4.49}$$

It follows that this theory flows to strong coupling, albeit at a higher order in g_ξ and $1/(2N)$ than what is considered in the rest of the paper: $\mathrm{O}(g_{\mathcal{B}}^2/2N) \sim \mathrm{O}(1/(2N)^3)$ instead of $\mathrm{O}(1/(2N)^2)$.

This continues to be true even upon breaking $\mathcal{CT}$ and allowing finite $g_{\mathcal{E}}$ and g_s. The g_s disorder strength will flow to zero and need not be considered further. Then, the irrelevance of monopoles ensures that $g_{\mathcal{E}}$ remains marginal and that $g_{\mathcal{B}}$ flows to strong coupling (we note $g_{\mathcal{E}}$ will give an additional contribution to z and, consequently, $\beta_{\mathcal{B}}$). In summary, the clean theory is unstable to SU($2N$) symmetric disorder when time reversal is broken.

Finally, when both the SU($2N$) flavour symmetry and time reversal are imposed, only disorder coupling to J^j_{top} is allowed, and the theory is exactly marginal to all orders in perturbation theory.

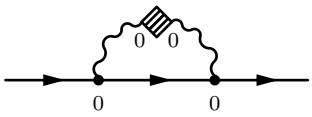

Figure 4.7: The only disorder diagram to contribute to $\mathrm{O}(g_{\mathcal{B}}/2N)$ when $\mathcal{B}(x)$ is the only random field coupled to QED$_3$. Note that it is subleading to the self-energy diagrams we consider elsewhere in the paper (Fig. 4.5). It contributes a divergence $-ip_0\gamma^0\left(\frac{g_{\mathcal{B}}}{2\pi(2N)\epsilon}\right)$.

4.3.3 SU(2)×SU(N) FLAVOUR SYMMETRY

If we instead allow disorder to break the symmetry from $\mathrm{SU}(2N) \to \mathrm{SU}(2)\times\mathrm{SU}(N)$, no non-trivial fixed point is found; the system flows to strong disorder, and out of the perturbative regime. Setting $g_{t,a} = g_t$, $g_{v,a} = g_v$, and $g_{\mathcal{A},a} = g_{\mathcal{A}}$, the resulting set of β-functions is

$$\begin{aligned}
\pi\beta_s &= g_s\left[g_s + 3g_t + 3g_v - 6g_{\mathcal{A}} + 2c\right] - 6g_v g_{\mathcal{A}},\\
\pi\beta_t &= g_t\left[-g_t + g_s - 9g_v + 6g_{\mathcal{A}} - c\right],\\
\pi\beta_{\mathcal{A}} &= -4g_{\mathcal{A}}^2 - g_t^2 - g_v^2 - g_s g_v,\\
\pi\beta_v &= g_v\left[g_v - g_s + g_t - 2g_{\mathcal{A}}\right] - 2g_s g_{\mathcal{A}},\\
\pi\beta_{\mathcal{E}} &= -3g_s g_{\mathcal{B}},\\
\pi\beta_{\mathcal{B}} &= -3g_s g_{\mathcal{E}} - g_{\mathcal{B}}\left[g_s + 3(g_t + 2g_{\mathcal{A}} + g_v)\right]\cdot
\end{aligned} \tag{4.50}$$

The third equation indicates that if either g_t, $g_{\mathcal{A}}$, or g_v is non-zero, $g_{\mathcal{A}}$ always flows to strong coupling. The four negative terms in $\beta_{\mathcal{A}}$ can be traced to the diagrams in the first, fifth, and seventh rows of Table C.1, and the second row of Table C.2 (shown in Appendix C.4). In these diagrams, the anticommutation properties of the Pauli matrices ensure that the "box" and "crossing" diagrams do not cancel as they did for the singlet mass term (Figs. 4.6(a) and (b)). In fact, it is shown in Appendix C.1 that disorder symmetric under any continuous non-abelian subgroup $\mathcal{H}$ of $\mathrm{SU}(2N)$ will have this property and, consequently, flow to strong coupling.

This may appear to contradict the argument of the previous section: since $g_{\mathcal{A}}$ couples

disorder to the spatial components of a conserved current, in the absence of a random mass $M_s(x)$, should it not be exactly marginal like $g_{\mathcal{E}}$? The key difference is that because SU(2) is non-ablelian, the SU(2)×SU(N) flavour symmetry is only present on average. The action for a specific realization of disorder, $\mathcal{A}_j^a(x)$, only has a SU(N) flavour symmetry, and, as a result, the scaling dimension of $i\bar{\psi}\gamma^j\sigma^a\psi$ is not protected.

Similarly, if $g_{\mathcal{B}}$ is non-zero and any of the other four fermion bilinears couplings are non-zero, disorder coupling to J^0_{top} also becomes strong. Again, this is because the dynamical critical exponent is greater than 1 when g_s, g_t, $g_{\mathcal{A}}$, or g_v are non-zero. We recall that the dimensional analysis of Sec. 4.2.2 indicated that when $z \neq 1$, the critical scaling dimension is no longer 2, but instead $1 + z$. Therefore, $[J^0_{\text{top}}] = 2 < 1 + z$, making it a relevant perturbation.

4.3.4 U(1)×SU(N) SYMMETRY

We turn, finally, to the case of greatest interest in the present paper. When the disorder couples to a U(1) subgroup of SU($2N$), we find a fixed line with both finite disorder and interactions.

We begin by considering an XY anisotropy where $g_{\cdot,z}$ is allowed to differ from $g_{\cdot,x} = g_{\cdot,y} =$

$g_{\cdot,\perp}$. With this restriction, the β-functions in Eq. (4.44) reduce to

$$\begin{aligned}
\pi\beta_s &= g_s\left[g_s + g_{t,z} + 2g_{t,\perp} - 2g_{\mathcal{A},z} - 4g_{\mathcal{A},\perp} + g_{v,z} + 2g_{v,\perp} + 2c\right] - 2g_{v,z}g_{\mathcal{A},z} - 4g_{v,\perp}g_{\mathcal{A},\perp},\\
\pi\beta_{t,z} &= g_{t,z}\left[g_{t,z} - 2g_{t,\perp} + 6g_{\mathcal{A},z} + 4g_{\mathcal{A},\perp} + g_s - 7g_{v,z} - 2g_{v,\perp} - c\right] - 4g_{t,\perp}g_{\mathcal{A},\perp},\\
\pi\beta_{t,\perp} &= g_{t,\perp}\left[-g_{t,z} + g_s + 8g_{\mathcal{A},\perp} - g_{v,z} - 8g_{v,\perp} - c\right] - 2g_{t,z}g_{\mathcal{A},\perp},\\
\pi\beta_{\mathcal{A},z} &= -4g_{\mathcal{A},\perp}^2 - g_{t,\perp}^2 - g_{v,\perp}^2 - g_s g_{v,z},\\
\pi\beta_{\mathcal{A},\perp} &= -4g_{\mathcal{A},\perp}g_{\mathcal{A},z} - g_{t,z}g_{t,\perp} - g_{v,z}g_{v,\perp} - g_s g_{v,\perp},\\
\pi\beta_{v,z} &= g_{v,z}\left[-g_{v,z} + 2g_{v,\perp} - g_{t,z} + 2g_{t,\perp} - 2g_{\mathcal{A},z} + 4g_{\mathcal{A},\perp} - g_s\right], -2g_s g_{\mathcal{A},z} - 4g_{v,\perp}g_{\mathcal{A},\perp}\\
\pi\beta_{v,\perp} &= g_{v\perp}\left[g_{v,z} + g_{t,z} - g_s\right] - 2g_s g_{\mathcal{A},\perp} - 2g_{v,z}g_{\mathcal{A},\perp},\\
\pi\beta_{\mathcal{E}} &= -3g_s g_{\mathcal{B}},\\
\pi\beta_{\mathcal{B}} &= -3g_s g_{\mathcal{E}} - g_{\mathcal{B}}\left[g_s + g_{t,z} + 2g_{\mathcal{A},z} + g_{v,z} + 2(g_{t,\perp} + 2g_{\mathcal{A},\perp} + g_{v,\perp})\right]\cdot
\end{aligned} \tag{4.51}$$

These results are consistent with the RG equations obtained in Ref. 44. In this paper, the authors considered Dirac cones interacting through a $3d$ Coulomb term instead of a strictly 2+1 dimension gauge field; we can compare to their results by setting the Coulomb coupling in their equations to zero and $g^2 = g_s = g_{v,z} = g_{v,\perp} = g_{\mathcal{E}} = g_{\mathcal{B}} = 0$ in Eq. (4.42).

As in the previous section, the β-functions for the vector potential couplings, $g_{\mathcal{A},z}$ and $g_{\mathcal{A},\perp}$ are all negative. In order to ensure that they do not flow to infinity, all perpendicular couplings must vanish, $g_{\mathcal{A},\perp} = g_{t,\perp} = g_{v,\perp} = 0$. This describes a situation where the U(1)×SU(N) symmetry of the underlying theory is preserved even in the presence of disorder.

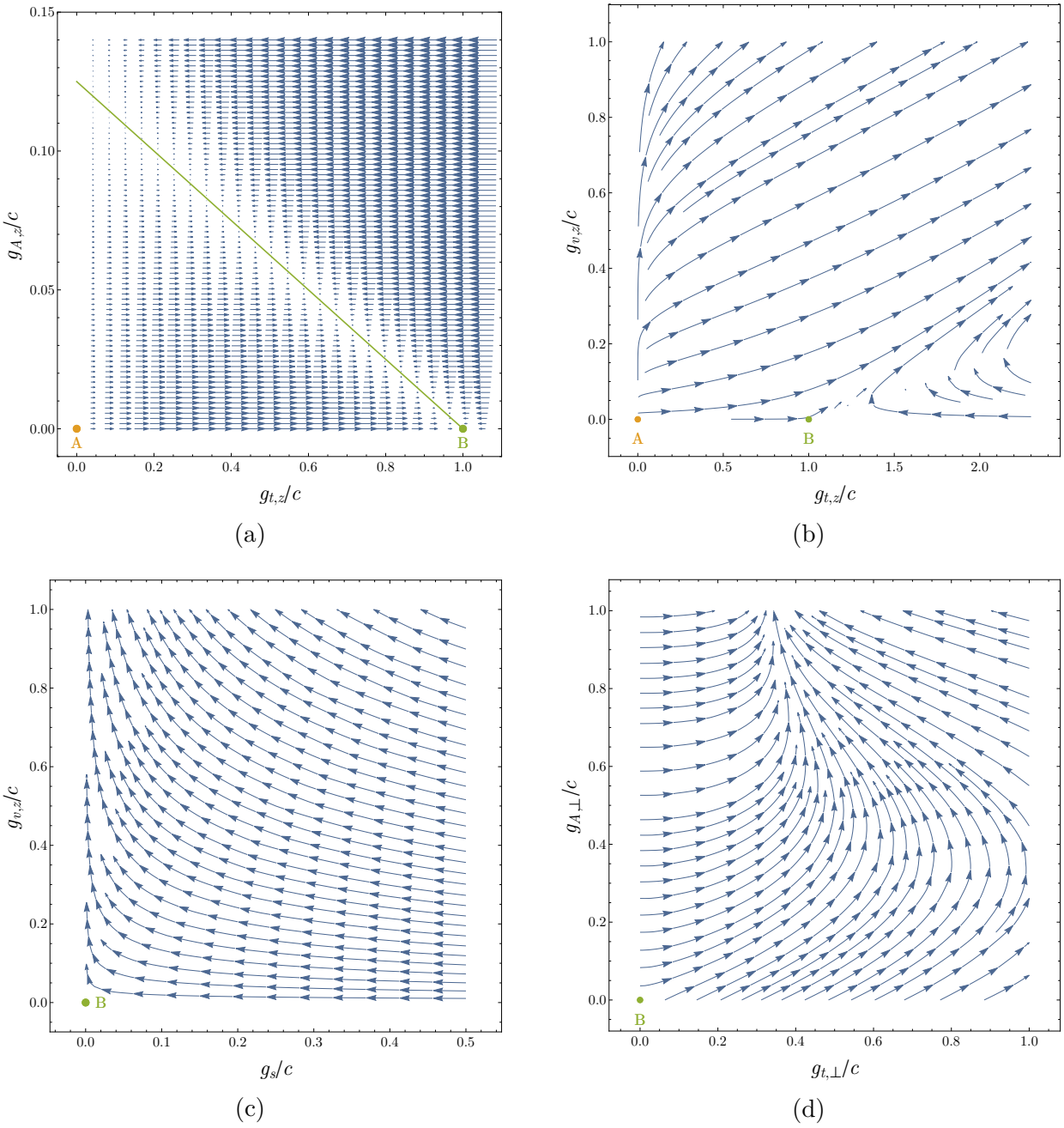

Figure 4.8: RG flow in the (a) $(g_{t,z}, g_{\mathcal{A},z})$ plane, (b) $(g_{t,z}, g_{v,z})$ plane, and (c) $(g_s, g_{v,z})$ plane with all other couplings set to zero. (d) shows the $(g_{t,\perp}, g_{\mathcal{A},\perp})$ plane with $g_{t,z} = c$ and all other couplings vanishing. The critical point with all couplings equal to zero (no disorder) is marked in orange with "A" and the critical point with $g_{t,z} = c$ is marked in green with a "B". In (a), the critical line is drawn in green. Here $c = 128/3\pi(2N)$.

The β-functions in the presence of this symmetry are

$$\begin{aligned}
\pi\beta_s &= g_s\left(g_s + g_{t,z} - 2g_{\mathcal{A},z} + 3g_{v,z} + 2c\right) - 2g_{\mathcal{A},z}g_{v,z},\\
\pi\beta_{t,z} &= g_{t,z}\left(g_{t,z} + g_s + 8g_{\mathcal{A},z} - 7g_{v,z} - c\right),\\
\pi\beta_{\mathcal{A},z} &= -g_s g_{v,z},\\
\pi\beta_{v,z} &= -g_{v,z}\left(g_{v,z} + g_s + g_{t,z} + 2g_{\mathcal{A},z}\right) - 2g_s g_{\mathcal{A},z},\\
\pi\beta_{\mathcal{E}} &= -3g_s g_{\mathcal{B}},\\
\pi\beta_{\mathcal{B}} &= -3g_s g_{\mathcal{E}} - g_{\mathcal{B}}\left(g_s + g_{t,z} + 2g_{\mathcal{A},z} + g_{v,z}\right)\cdot
\end{aligned} \tag{4.52}$$

Recalling that all couplings are positive, we find a single physical solution which breaks the SU($2N$) flavour symmetry to U(1)×SU(N). It is parametrized by the line

$$g_{t,z} = c - 8g_{\mathcal{A},z}, \qquad\qquad g_{\mathcal{A},z} \leq \frac{c}{8}, \tag{4.53}$$

with $g_{\mathcal{B}}$ and all other bilinear couplings equal to zero. Moreover, since g_s, $g_{v,z}$, and $g_{\mathcal{B}}$ are absent, each realization of disorder is invariant under time reversal and, consequently, $g_{\mathcal{E}}$ is exactly marginal (see Sec. 4.3.2). The fixed line we discuss is more correctly a fixed plane (though we will frequently refer to it only as a line). Referring to Eq. (4.41), the dynamical critical exponent on this surface is

$$z = 1 + c - 6g_{\mathcal{A},z}\cdot \tag{4.54}$$

In the presence of both time reversal and the U(1)×SU($2N$) flavor symmetry, $g_{\cdot,\perp} = 0$, the critical surface has one irrelevant and two marginal directions. It is stable to small variations in $g_{t,z}$ while perturbations in $g_{\mathcal{E}}$ and $g_{\mathcal{A},z}$ are marginal. As we saw in the previous two sections, these couplings are associated with the spatial components of a conserved current, implying that their scaling dimensions are non-perturbatively fixed at exactly two when time reversal symmetry is present. The presence of these symmetries means that we

do not expect the stability of the critical surface to change with the inclusion of higher order diagrams provided N is sufficiently large. However, it is possible that that it will be reduced to a single critical point. The RG flow in the $(g_{t,z}, g_{\mathcal{A},z})$ plane is shown in Fig. 4.8(a).

When time reversal only holds on average, g_s, $g_{v,z}$ and $g_{\mathcal{B}}$ are allowed to be finite as well. Disorder coupling to the SU($2N$)-symmetric mass term remains irrelevant, but the scalar potential-like disorder, $g_{v,z}$ and $g_{\mathcal{B}}$, take the theory into the strong coupling regime, as expected when the $z > 1$. The RG flows in the $(g_{t,z}, g_{v,z})$ and $(g_s, g_{v,z})$ planes are shown in Figs. 4.8(b) and 4.8(c).

The fixed surface is not stable to perturbations which explicitly break the U(1)×SU($2N$) flavour symmetry of the replicated theory. Fig. 4.8(d) shows the RG flow in the $(g_{t,\perp}, g_{\mathcal{A},\perp})$ plane for $g_{t,z} = c$, $g_{\mathcal{A},z} = 0$ and indicates that both parameters are relevant. This is true along the entire critical surface. Conversely, it can also be shown that along the critical line $g_{v,\perp}$ is irrelevant.

4.4 Application to the kagome antiferromagnet

The large emergent symmetry of the QED$_3$ CFT implies that the currents and the fermion bilinears which we couple to disorder can be interpreted in a number of ways. Nonetheless, it is useful to directly relate our model to the microscopic operators of the spin-1/2 kagome Heisenberg antiferromagnet ($N = 2$): $H_{\mathrm{H}} = J \sum_{\langle ij \rangle} \boldsymbol{S}_i \cdot \boldsymbol{S}_j$, where $\langle ij \rangle$ are nearest-neighbour sites on the kagome lattice (see Fig. 4.1). Special attention will be given to the fixed line found in Sec. 4.3.4. This section draws heavily from the discussion of Ref. 61, and more details can be found therein.

We begin by reviewing how the CFT is obtained as the low energy description of the kagome antiferrormagnet. We start by expressing the spin operators in terms of fermions, $\boldsymbol{S}_i = \frac{1}{2} f^\dagger_{i\tau} \boldsymbol{\sigma}_{\tau\tau'} f_{i\tau'}$, where $\boldsymbol{\sigma}$ are the three Pauli matrices. This representation reproduces the Hilbert space of the spins provided it is accompanied by the local constraint $\sum_{\tau=\uparrow,\downarrow} f^\dagger_{i\tau} f_{i\tau} = 1$. The resulting Hamiltonian, $H_{\mathrm{H}} = -\frac{J}{4} \sum_{\langle ij \rangle} f^\dagger_{i\tau} f_{j\tau} f^\dagger_{j\tau} f_{i\tau'} + \text{const.}$, can be approximated by a

mean field Hamiltonian $H_{\mathrm{MF}} = -\sum_{\langle ij \rangle} t_{ij} f^{\dagger}_{i\tau} f_{j\tau'} + H.c.$, where t_{ij} is chosen so as to minimize the ground state energy while enforcing the condition $\sum_{\tau=\uparrow,\downarrow} \langle f_{i\tau} f_{i\tau} \rangle = 1$ on average. The mean field ansatz which inserts π and zero flux through the kagome hexagon and triangle plaquettes respectively is found to have a particularly low energy [58, 61, 139]. In this case, the dispersion of H_{MF} has two Dirac cones per spin at a non-zero crystal momentum, $\pm \boldsymbol{Q}$ [58, 61]. The low energy excitations of H_{MF} are described by expanding about these two valleys, giving a free Dirac Lagrangian, $\mathcal{L}_{\mathrm{D}} = -\bar{\psi}_{\alpha} \not{\partial} \psi_{\alpha}$, where α labels both spin and valley (the relation between the continuum Dirac spinors, ψ_{α}, and the lattice fermions, $f_{i\tau}$, is given in the appendix to Ref. 61). However, since the physical spin operators, $\boldsymbol{S}_i$, are invariant under local phase rotations, $f_{i\tau} \to e^{i\phi_i} f_{i\tau}$, the fermions carry an emergent gauge charge, and, consequently, the true effective theory of H_{H} must take gauge fluctuations into account. Provided monopoles do not the confine the theory, the low energy description of the kagome antiferromagnet is QED$_3$ and not the free Dirac theory [19, 28, 64, 132]. We note that while H_{H} only had an SU(2) spin symmetry, QED$_3$ has an emergent SU(4) symmetry under which spin and valley indices are rotated into one another.

In order to calculate physical quantities, microscopic observables of the lattice theory must be associated with continuum operators of QED$_3$:

$$A_i \sim \sum_{\ell} c_{\ell} \mathrm{O}_{\ell}(\boldsymbol{r}), \tag{4.55}$$

where A_i is some function of local operators near the lattice site $\boldsymbol{r}$, and $\mathrm{O}_{\ell}(\boldsymbol{r})$ are a set of operators belonging to the CFT. At long distances, the quantities to the left and right of Eq. (4.55) must decay in the same manner. Given A_i, the set of operators O_{ℓ} for which c_{ℓ} is non-vanishing could be determined by repeating the steps used to derive QED$_3$ from the Heisenberg model on the microscopic operators O_{ℓ} [61]. However, it is easier to note that the c_{ℓ}'s can be non-zero if and only if A_i and O_{ℓ} transform in the same manner under the action of the microscopic symmetries of the theory. In particular, the action under time reversal

and space group transformations will be important. The symmetry operations relevant to the kagome antiferromagnet can be found in Ref. 61.

As discussed in Sec. 4.2.2, we only consider disorder coupling to the topological current and the fermion bilinears. That is, we restrict O_ℓ to be either the conserved currents in Eqs. (4.14) and (4.15), or the mass-like operators given in Eqs. (4.17) and (4.18). By applying our large-N results to the $N = 2$ case, we may be neglecting important types of disorder in the form of monopole operators.

With this caveat in mind, we begin by identifying the singlet mass operator $\frac{1}{\sqrt{2N}}\bar{\psi}\psi$ with the chiral mass term discussed in Ref. 58. Noting that $\frac{1}{\sqrt{2N}}\bar{\psi}\psi$ is odd under both parity and time reversal, it's not surprising that it can be associated with the scalar spin chirality,

$$\mathcal{C}_{\mathrm{SSP}}(\boldsymbol{x}_\triangle) = \sum_{(ijk)\in\triangle} \boldsymbol{S}_i \cdot (\boldsymbol{S}_j \times \boldsymbol{S}_k)\,, \tag{4.56}$$

where $\boldsymbol{x}_\triangle$ is the position of a triangle in the lattice, and (ijk) are ordered as indicated by the arrows in Fig. 4.1. Similarly, the flux disorder operator, J^0_{top}, transforms in the same way as $\frac{1}{\sqrt{2N}}\bar{\psi}\psi$, indicating that it can also be associated with $\mathcal{C}_{\mathrm{SSP}}$. We conclude that the random fields $M_s(x)$ and $\mathcal{B}(x)$ in Eq. (4.23) descend from disorder coupling to $\mathcal{C}_{\mathrm{SSP}}$. The renormalization group study of Secs. 4.3.2, 4.3.3, and 4.3.4 indicates that a randomly varying scalar spin chirality remains a marginal perturbation to leading order. However, this is not protected by any symmetry and, as discussed in Sec. 4.3.2, higher order diagrams make it relevant.

The spatial components of the topological current are time reversal invariant and transform as vectors under spatial rotations. The simplest operators invariant under time reversal are the bond operators,

$$P_{ij} = \boldsymbol{S}_i \cdot \boldsymbol{S}_j, \tag{4.57}$$

where i and j are nearest-neighbours. In order to find the simplest combination of P_{ij}'s

which rotate in the correct fashion, we calculate the irreducible representations governing the bond configurations within a unit cell. Defining

$$\mathcal{P}_x(\boldsymbol{x}) = \sum_{ij\in\mathrm{hex}(\boldsymbol{x})} e^x_{ij} P_{ij}, \qquad \mathcal{P}_y(\boldsymbol{x}) = \sum_{ij\in\mathrm{hex}(\boldsymbol{x})} e^y_{ij} P_{ij},$$
$$\left(e^x_{ij}\right)^{\mathrm{T}} = \frac{1}{2\sqrt{3}}\left(2,1,-1,-2,-1,1\right), \qquad \left(e^y_{ij}\right)^{\mathrm{T}} = \frac{1}{2}\left(0,1,1,0,-1,-1\right), \tag{4.58}$$

we identity J^x_{top} and J^y_{top} with $\mathcal{P}_x$ and $\mathcal{P}_y$ respectively; these patterns are shown in Fig. 4.9. This identification along with the results of Sec. 4.3.2 may then appear to indicate that random bond disorder, corresponding to a Hamiltonian of the form

$$H_{\mathrm{RB}} = \sum_{\mathrm{ij}} J_{ij} \boldsymbol{S}_i \cdot \boldsymbol{S}_j, \tag{4.59}$$

is an exactly marginal perturbation to the QED$_3$ fixed point when time-reversal is preserved. However, we will see shortly that this is not the case.

We next express the 15 generators of SU(4) as $\{\sigma^a, \mu^j, \sigma^a\mu^j\}$ where σ^a and μ^j are commuting sets of Pauli matrices with σ^a acting on spin and μ^j acting on valley indices. Following the notation of Ref. 61, it's useful to re-label the operators of Eqs. (4.14) and (4.17) as

$$J^{ia}_{A,\mu} = i\bar{\psi}\mu^i\sigma^a\gamma_\mu\psi, \qquad J^a_{B,\mu} = i\bar{\psi}\sigma^a\gamma_\mu\psi, \qquad J^i_{C,\mu} = i\bar{\psi}\mu^i\gamma_\mu\psi,$$
$$N^{ia}_A = \bar{\psi}\mu^i\sigma^a\psi, \qquad N^a_B = \bar{\psi}\sigma^a\psi, \qquad N^i_C = \bar{\psi}\mu^i\psi\,. \tag{4.60}$$

Each of these operators can couple to a random field to contribute to an action of the form in Eq. (4.23).

In Ref. 61, the microscopic spin operators corresponding to each of the mass operators, N^{ia}_A, N^a_B, and N^i_C are identified. We will primarily be interested in N^a_B. This is a spin triplet and is even under time reversal. The simplest microscopic operator with this property is the vector chirality operator $\boldsymbol{C}_{ij} = \boldsymbol{S}_i \times \boldsymbol{S}_j$, where i and j are nearest-neighbours. The

linear combination of $\boldsymbol{C}_{ij}$'s within a unit cell which transform in the same way as $\boldsymbol{N}_B$ can be written

$$\boldsymbol{\mathcal{C}}_s(\boldsymbol{x}) = \sum_{(ij)\in \mathrm{hex}(\boldsymbol{x})} \boldsymbol{C}_{ij}, \tag{4.61}$$

where the sum is taken around the hexagon at $\boldsymbol{x}$ following the convention in Fig. 4.1. As we indicated in Sec. 4.1, $\mathcal{C}_s$ is precisely the DM interaction term.

Similar reasoning suggests that the B-type currents, $\boldsymbol{J}_{B,\mu}(r)$, correspond to the spin operators and currents. First, the space group symmetry acts on $\boldsymbol{S}_i$ in the same way as it acts on $\boldsymbol{J}_{B,0}$; in particular, both $\boldsymbol{S}$ and $\boldsymbol{J}_{B,0}$ are invariant under spatial rotations and odd under time reversal. It's not surprising then that $\boldsymbol{J}_{B,x}$ and $\boldsymbol{J}_{B,y}$ correspond to spin currents. They are both even under time reversal and are spin triplets. As with $\boldsymbol{N}_B$, this suggests a linear combination of nearest-neighbour vector chirality operators, $\boldsymbol{C}_{ij}$, as their natural microscopic counterpart. Like J^j_{top}, they must transform as vectors under spatial rotations, implying that the C_{ij}'s should correspond to the $\boldsymbol{J}_{B,j}$ in the same way the P_{ij}'s correspond to J^j_{top}:

$$\boldsymbol{\mathcal{C}}_x(\boldsymbol{x}) = \sum_{ij\in \mathrm{hex}(\boldsymbol{x})} e^x_{ij}\boldsymbol{C}_{ij}, \qquad \boldsymbol{\mathcal{C}}_y(\boldsymbol{x}) = \sum_{ij\in \mathrm{hex}(\boldsymbol{x})} e^y_{ij}\boldsymbol{C}_{ij}, \tag{4.62}$$

where e^x_{ij} and e^y_{ij} are given in Eq. (4.58) and shown in Fig. 4.9. In fact, since we assume that fermion bilinears and topological currents are the only relevant operators of the CFT, *all* disorder coupling to the $\boldsymbol{C}_{ij}$'s is taken into account by random fields coupling to $\boldsymbol{N}_B$, $\boldsymbol{J}_{B,x}$, and $\boldsymbol{J}_{B,y}$. In particular, modulo the caveats we have already discussed, the low energy theory of the kagome AF with weak disorder of the form

$$H^{\mathrm{DM}}_{\mathrm{dis}} = \sum_{\langle ij\rangle} J^{\mathrm{DM}}_{ij}\hat{\boldsymbol{z}}\cdot \boldsymbol{S}_i \times \boldsymbol{S}_j \tag{4.63}$$

where J^{DM}_{ij} are sufficiently weak random variables, should be described by fixed line of

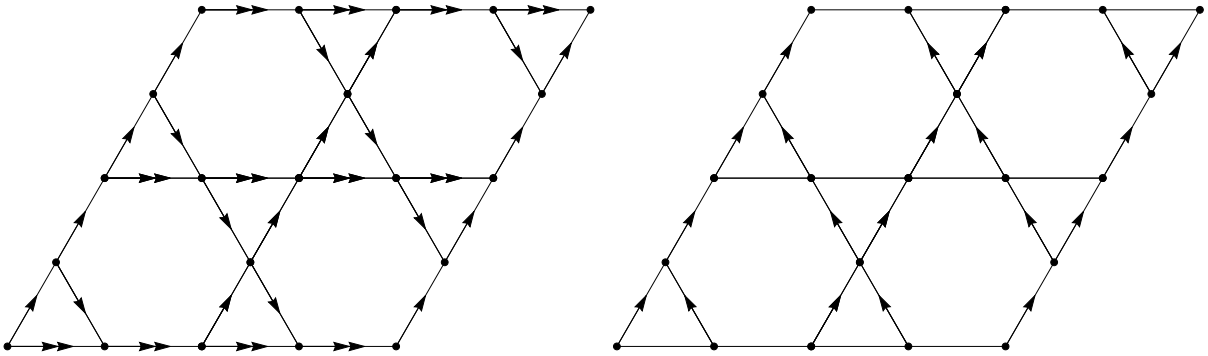

(a) Current in x-direction. (b) Current in y-direction.

Figure 4.9: Bond ordering of bond order and vector chirality operators corresponding to the topological currents, J^j_{top}, and the spin currents $J^{a,j}_B(r)$ in the x and y directions respectively. Our convention is that in $\boldsymbol{C}_{ij} = \boldsymbol{S}_i \times \boldsymbol{S}_j$, the ith site points towards the jth. The double arrows in (a) identify the bonds which are weighted twice as strongly as others, while the absence of arrows on the horizonal bonds in (b) implies that they do not contribute at all.

Sec. 4.3.4.

Unlike $\boldsymbol{N}_B$, the remaining two mass bilinears in Eq. (4.60) carry valley indices. The bilinear $\boldsymbol{N}^i_A$ represents a set of three spin triplets and is odd under time reversal. Focusing on the z component in spin space, $N^{i,z}_A$, three magnetic ordering patterns can be identified, each with a crystal momentum at a different M point in the Brillouin zone. Under rotations about the z-axis, the $N^{i,z}_A$'s transform into one another. Disorder resulting from magnetic defects could couple to bilinears of this form, but the fixed line resulting in Sec. 4.3.4 is particularly unlikely to occur. Except in cases of extreme anisotropy, we do not expect disorder to exclusively couple to a single momentum channel.

Similarly considerations hold for N^i_C. These operators are spin singlets and, like J^j_{top}, can be associated with bond ordering patterns P_{ij} [58, 61]. In this case, two 3-dimensional irreducible representations of bonds transforming in the same way as N^i_C are identified, and, again, each ordering pattern within an irreducible representation is distinguished by having a crystal momentum at one of the three M points. It follows that perturbing H_{H} by given a generic random bond Hamiltonian H_{RB} in the UV results in finite disorder strengths for N^i_C, $J^{i,a}_{C,\mu}$, as well as J^i_{top}. The appropriate form of disorder is not the the SU($2N$) symmetric

case of Sec. 4.3.2, but rather the situation discussed in Sec. 4.3.3. We therefore conclude that the kagome antiferromagnet is unstable to generic random bond disorder.

Finally, the same arguments hold for the microscopic analogues of $J^{i,a}_{A,\mu}$ and $J^{i}_{C,\mu}$.

4.5 Flavour conductivity

The flavor conductivity is a universal observable of the CFT; for the case of the kagome antiferromagnet, this conductivity is interpreted as a spin conductivity. By the usual arguments, we expect this conductivity to also be a universal observable along the fixed line with U(1)×SU(N) symmetry found in Sec. 4.3.4. Because of the presence of continuously variable critical exponents along this line, we also anticipate the flavor conductivity to be continuously variable.

The flavor conductivity is determined by the two point correlators at zero external momentum of the following currents:

$$J^x_{za}(p) = i\bar{\psi}\sigma^z T^a \gamma^x \psi(p), \quad J^x_{sa}(p) = i\bar{\psi} T^a \gamma^x \psi(p), \quad J^x_{\perp a}(p) = i\bar{\psi}\sigma^x T^a \gamma^x \psi(p) = i\bar{\psi}\sigma^y T^a \gamma^x \psi(p). \tag{4.64}$$

In particular, we calculate the *optical* conductivity, valid for frequencies greater than the temperature T, allowing us to evaluate these correlators at zero temperature. The diagrams which contribute to O($g_{t,z}, g_{\mathcal{A},z}, 1/2N$) are shown in Fig. 4.10. To this order, a non-zero $g_{\mathcal{E}}$ will not contribute.

We recall from the discussion of Sec. 4.2.2 that the dimensions of the spatial currents $J^x_{za}(x,\tau)$ and $J^x_{sa}(x,\tau)$ are fixed at $1+z$ and, therefore, their correlators contain no divergences at zero external momentum. Moreover, an inspection of the diagrams in Appendix C.4 shows that the scaling dimensions of $J^x_{a\perp}$ remain unaltered to the order we are considering. Appendix C.6 outlines how Figs. 4.10(a) to 4.10(e) are calculated, and also verifies that counter term diagrams do not contribute. The photon diagrams, Figs. 4.10(f) and 4.10(g),

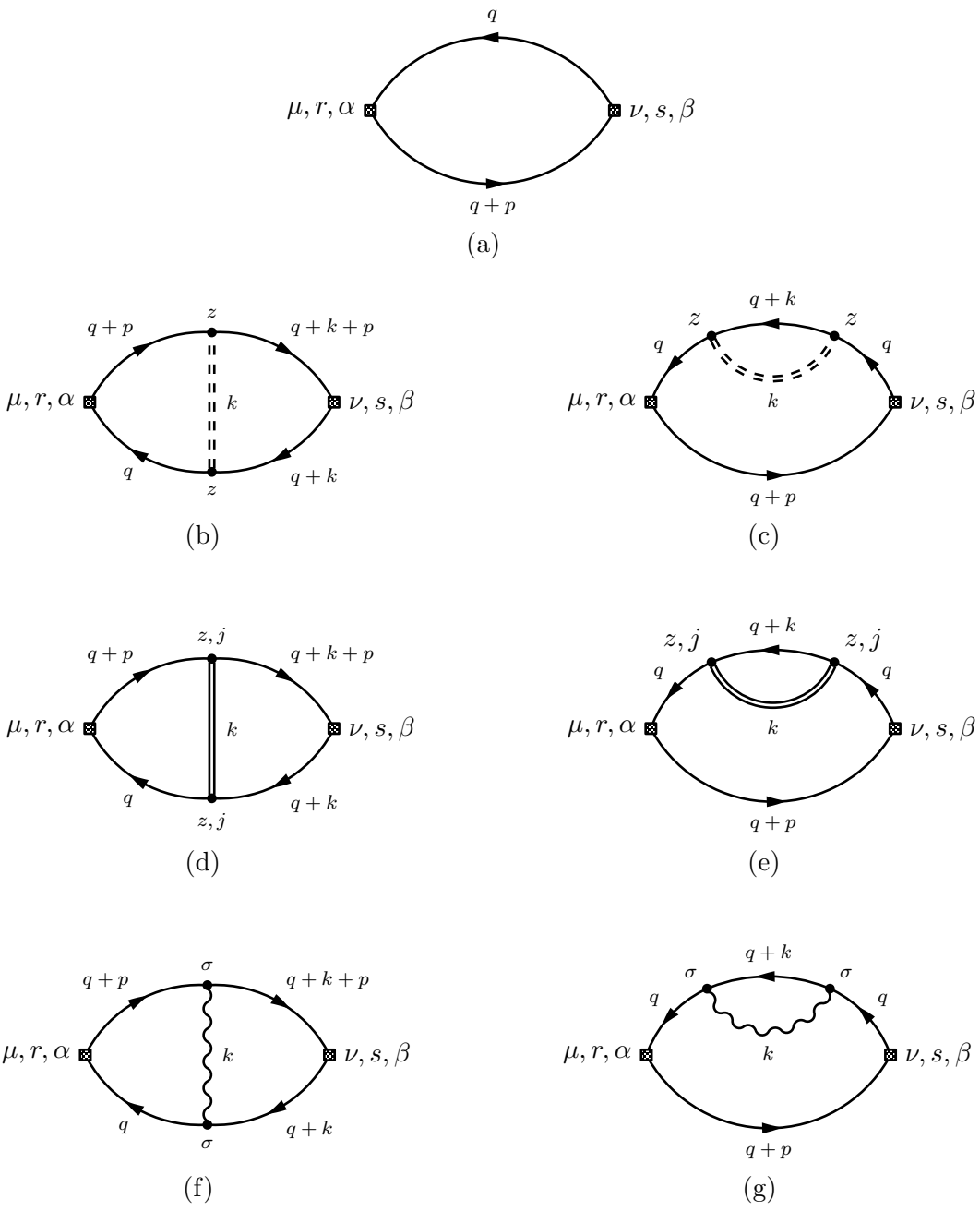

Figure 4.10: Diagrams which contribute to the current-current correlator.

are determined in Ref. 69. Combining these results, we find

$$\begin{aligned}\langle J^x_{za}(p_0)J^x_{zb}(-p_0)\rangle &= \langle J^x_{sa}(p_0)J^x_{sb}(-p_0)\rangle \\ &= \delta_{ab}\,|p_0|\left\{-\frac{1}{16}-\frac{a_\gamma}{2N}+a_{\rm V}g_{t,z}+a_\Sigma(g_{t,z}+2g_{\mathcal{A},z})\right\} \\ &= \delta_{ab}\,|p_0|\left\{-\frac{1}{16}-\frac{a_\gamma}{2N}+c(a_{\rm V}+a_\Sigma)-(8a_{\rm V}+6a_\Sigma)g_{\mathcal{A},z}\right\} \end{aligned} \tag{4.65}$$

and

$$\begin{aligned}\langle J^x_{\perp a}(p_0)J^x_{\perp b}(-p_0)\rangle &= \delta_{ab}\,|p_0|\left\{-\frac{1}{16}-\frac{a_\gamma}{2N}-a_{\rm V}g_{t,z}+a_\Sigma(g_{t,z}+2g_{\mathcal{A},z})\right\} \\ &= \delta_{ab}\,|p_0|\left\{-\frac{1}{16}-\frac{a_\gamma}{2N}+c(-a_{\rm V}+a_\Sigma)+(8a_{\rm V}-6a_\Sigma)g_{\mathcal{A},z}\right\} \end{aligned} \tag{4.66}$$

where $a_{\rm V}$, a_Σ, and a_γ are derived from Figs. 4.10(b) and (c), Figs. 4.10(d) and (e), and Figs. 4.10(f) and (g) respectively. The two disorder contributions are equal,

$$a_{\rm dis} = a_V = a_\Sigma = \frac{1}{96\pi}, \tag{4.67}$$

and the photon contribution is [69]

$$a_\gamma = \left(0.0370767 - \frac{5}{18\pi^2}\right). \tag{4.68}$$

From the Kubo formula, it follows that the conductivities are

$$\begin{aligned}\sigma_z(0) = \sigma_s(0) &= \frac{1}{16}+\frac{a_\gamma}{2N}-2a_{\rm dis}(c-7g_{\mathcal{A},z}), \\ \sigma_\perp(0) &= \frac{1}{16}+\frac{a_\gamma}{2N}-2a_{\rm dis}g_{\mathcal{A},z}. \end{aligned} \tag{4.69}$$

In both flavor channels, disorder suppresses the conductivity and, except when $g_{\mathcal{A},z} = c/8$, and $g_{t,z} = 0$, the singlet and spin-z channels are affected more strongly. This is physically

reasonable since we naturally expect transport in channels coupling directly to disorder to decrease the most.

4.6 Conclusion

This paper examined the influence of quenched disorder on the 2+1 dimensional CFT of $2N$ massless two-component Dirac fermions coupled to a U(1) field. The existence of this CFT can be established for sufficiently large N by the $1/N$ expansion, and we combined the $1/N$ expansion with a weak disorder expansion.

For generic disorder, our renormalization group analysis shows a flow to strong coupling, and so we were unable to determine the fate of the theory. However, if we restrict the disorder to obey certain global symmetries, then we were able to obtain controlled results.

For disorder respecting time reversal and the full SU($2N$) flavor symmetry of the CFT, we found in Sec. 4.3.2 that all allowed disorder perturbations were marginal to the order we considered. Such a result does *not* apply to the CFT of $2N$ free Dirac fermions: in that case, disorder coupling to a randomly varying chemical potential leads to a flow to strong coupling [108]. However, once disorder is allowed to break time reversal, we again find a runaway flow towards strong disorder, albeit at a higher order in perturbation theory.

Our main results, in Sec. 4.3.4, concerned the case in which disorder respects time-reversal and U(1) $\times$ SU(N) symmetry. In this case, to leading order in $1/N$, we found a non-trivial fixed line with both interactions and disorder. This fixed line had continuously varying exponents, in particular a dynamic critical exponent $z > 1$. It also had a continuously varying, but cutoff independent, flavor conductivity.

We also discussed the possible relevance of our results to the spin-1/2 kagome lattice antiferromagnet. In this case, the U(1) $\times$ SU(N) symmetric disorder corresponds to a randomly varying Dzyaloshinkii-Moriya field, as we described in Secs. 4.1 and 4.4.

Chapter 5

Spectrum of conformal gauge theories on a torus

Many model quantum spin systems have been proposed to realize critical points or phases described by 2+1 dimensional conformal gauge theories. On a torus of size L and modular parameter τ, the energy levels of such gauge theories equal $(1/L)$ times universal functions of τ. We compute the universal spectrum of QED_3, a U(1) gauge theory with N_f two-component massless Dirac fermions, in the large N_f limit. We also allow for a Chern-Simons term at level k, and show how the topological k-fold ground state degeneracy in the absence of fermions transforms into the universal spectrum in the presence of fermions; these computations are performed at fixed N_f/k in the large N_f limit.

5.1 Introduction

While many fractionalized states of matter have been proposed, verifying their existence is a formidable task. Not only are experimental measurements of fractional degrees of freedom difficult, but even establishing the existence of these phases in simplified lattice models can be challenging. Numerical techniques have made a great deal of progress and now provide support for some of these states of matter.

In the context of quantum spin systems, the simplest fractionalized state with an energy gap and time-reversal symmetry is the $\mathbb{Z}_2$ spin liquid. Recent work described the universal spectrum of a spin system on a torus [163, 189] across a transition between a $\mathbb{Z}_2$ spin liquid

and a conventional antiferromagnetically ordered state [189]. Such a spectrum is a unique signature of the transition between these states and goes well beyond the 4-fold topological degeneracy of the gapped $\mathbb{Z}_2$ state that is usually examined in numerical studies.

In this paper, we turn our attention to critical spin liquids with an emergent photon and gapless fractionalized excitations. Commonly referred to as an 'algebraic spin liquid' (ASL) or a 'Dirac spin liquid', it is a critical phase of matter characterized by algebraically decaying correlators, and whose long-distance properties are described by an interacting conformal field theory (CFT) called $3d$ quantum electrodynamics (QED_3) [64, 86, 87, 140, 184]. For the kagome antiferromagnet, and also for the J_1-J_2 antiferromagnet on the triangular lattice, there is an ongoing debate as to whether the ground state is a gapped $\mathbb{Z}_2$ spin liquid [35, 79, 109, 152, 203, 212] or a U(1) Dirac spin liquid [73, 74], and we hope our results here can serve as a useful diagnostic of numerical data.

In addition, although certain systems may not allow for an extended ASL phase, related CFTs could describe their phase transitions [14, 52]. These 'deconfined critical points' [166, 170] require a description beyond the standard Landau-Ginzburg paradigm and are often expressed in terms of fractionalized quasiparticles interacting through a gauge field. Our methods can be easily generalized [97] to critical points of theories with bosonic scalars coupled to gauge fields [166, 170], but we will limit our attention here to the fermionic matter cases.

A close cousin of QED_3 can be obtained by adding an abelian Chern-Simons (CS) term to the action. When a fermion mass is also present, the excitations of the resulting theory are no longer fermions, but instead obey anyonic statistics set by the coefficient, or 'level', of the CS term. The critical 'Dirac-CS' theory (with massless fermions) has been used to describe phase transitions between fractional quantum Hall plateaus in certain limits [26, 154] and transitions out of a chiral spin liquid state [14, 65, 190]

In this paper, we study the finite size spectrum of the QED_3 and Dirac-CS theories on the torus. While the state-operator correspondence often motivates theorists to put CFT's on

spheres, the torus is the most practical surface to study on a computer. The energy spectrum on the torus does not give any quantitative information regarding the operator spectrum of the theory, but it is a universal function of the torus circumference L and modular parameter τ and, therefore, can be used to compare with numerically generated data. The torus has the additional distinction of being the simplest topologically non-trivial manifold. A defining characteristic of topological order is the degeneracy of the groundstate when the theory is placed on a higher genus surface. On the torus, the pure abelian CS theory at level k has k ground states [187, 194] whose degeneracy is only split by terms which are exponentially small in L. Here, we will couple N_f massless Dirac fermions to the CS theory and find a rich spectrum of low energy states with energies which are of order $1/L$. In the limit of large N_f and k, we will present a computation which gives the k degenerate levels in the absence of Dirac fermions and a universal spectrum with energies of order $1/L$ in the presence of Dirac fermions.

Proposals for ASL phases typically begin with a parton construction of the spin-1/2 Heisenberg antiferromagnet

$$H = \sum_{\langle ij \rangle} J_{ij} \boldsymbol{S}_i \cdot \boldsymbol{S}_j \,, \tag{5.1}$$

where $\boldsymbol{S}_i$ represent the physical spin operators of the theory and i, j label points on the lattice. Slave fermions are introduced by expressing the spin operators as $\boldsymbol{S}_i = \frac{1}{2} f^\dagger_{i\alpha} \boldsymbol{\sigma}_{\alpha\beta} f_{i\beta}$, where $f_{i\alpha}$ is the fermion annihilation operator and $\boldsymbol{\sigma} = (\sigma^x, \sigma^y, \sigma^z)$ are the Pauli matrices. This is a faithful representation of the Hilbert space provided it is accompanied by the local constraint

$$\sum_\alpha f^\dagger_{i\alpha} f_{i\alpha} = 1. \tag{5.2}$$

Since the physical spin $\boldsymbol{S}_i$ is invariant under the transformation $f_{i\alpha} \to e^{i\phi_i} f_{i\alpha}$, the slave fermions necessarily carry an emergent gauge charge. Replacing spins with slave fermions,

decoupling the resulting quartic term, and enforcing $\left\langle f^\dagger_{i\alpha} f_{i\alpha} \right\rangle = 1$ on average returns an ostensibly innocuous mean field Hamiltonian $H_{\mathrm{MF}} = -\sum_{\langle ij \rangle} t_{ij} f^\dagger_{i\alpha} f_{j\alpha} + H.c.$ The mean field theory is a typical tight-binding model, but with electrons replaced by slave fermions. However, the stability of H_{MF} is by no means guaranteed, and gauge fluctuations must be taken into account. This is achieved by supplementing the mean field hopping parameter with a lattice gauge connection a_{ij}: $t_{ij} \to t_{ij} e^{i a_{ij}}$. Under the renormalization group, kinetic terms for the gauge field are generated. Since the connection a_{ij} parametrizes the phase redundancy of the $f_{i\alpha}$'s, it is a 2π-periodic quantity, and the resulting lattice gauge theory is *compact*. Determining the true fate of these theories is where numerics provide such great insight.

The mean field Hamiltonians of the models we are concerned with possess gapless Dirac cones. In the continuum they can be expressed

$$S_{\mathrm{D}}[\psi, A] = -\int d^3 r \, \bar{\psi}_\alpha i \gamma^\mu \left(\partial_\mu - i A_\mu \right) \psi_\alpha, \tag{5.3}$$

where $r = (\tau, \boldsymbol{x})$ is the Euclidean spacetime coordinate, ψ_α is a two-component complex spinor whose flavour index α is summed from 1 to N_f, and A_μ is a U(1) gauge field that is obtained from the continuum limit of the a_{ij}. The gamma matrices are taken to be $\gamma^\mu = (\sigma^z, \sigma^y, -\sigma^x)$, and $\bar{\psi}_\alpha = i \psi^\dagger_\alpha \sigma^z$. On the the kagome lattice, the mean field ansatz with a π-flux through the kagome hexagons and zero flux through the triangular plaquettes has a particularly low energy [58, 61, 139]. Its dispersion has two Dirac cones, which, accounting for spin, gives $N_f = 4$.

By writing the theory in the continuum limit in the form of Eq. (5.3), we are implicitly assuming that monopoles (singular gauge field configurations with non-zero flux) in the lattice compact U(1) gauge theory can be neglected. In their absence, the usual Maxwell

action can be added to the theory

$$S_{\rm M}[A] = \frac{1}{4e^2}\int d^3r\, F_{\mu\nu}F^{\mu\nu}, \qquad\qquad F_{\mu\nu} = \partial_\mu A_\nu - \partial_\nu A_\mu, \tag{5.4}$$

resulting in the full QED$_3$ action, $S_{\rm qed}[\psi, A] = S_{\rm D}[\psi, A] + S_{\rm M}[A]$. Importantly, when N_f is smaller than some critical value, these manipulations are no longer valid. $S_{\rm M}[A]$ is never an appropriate low-energy description of a lattice gauge theory with $N_f = 0$: for *all* values of e^2, monopoles will proliferate and confine the theory [127, 129]. In the confined phase, the slave fermions cease to be true excitations, and remain bound within the physical spins $\boldsymbol{S}_i$. However, matter content suppresses the fluctuations of the gauge field. For N_f large enough, monopoles are irrelevant operators, [19, 28, 64, 132] and $S_{\rm qed}[\psi, A]$ is a stable fixed point of the lattice theory [64]. In this limit, QED$_3$ is believed to flow to a non-trivial CFT in the infrared, and this has been shown perturbatively to all orders in $1/N_f$ [9, 75, 176, 177]. The critical theory is obtained by naïvely taking the limit $e^2 \to \infty$, and, for this reason, the Maxwell term will be largely ignored in what follows.

The Dirac fermions ψ_α represent particle or hole-like fluctuations about the Fermi level. Consequently, any single-particle state violates the local gauge constraint in Eq. (5.2) and is prohibited. Since fluctuations in A_μ are suppressed at $N_f = \infty$, we might expect this neutrality to be the only signature of the gauge field in the large N_f limit, and so the spectrum on the torus is given by the charge neutral multi-particle states of the free field theory. It is important to note that all of these multi-particle states are built out of single fermions ψ_α which obey *anti-periodic* boundary conditions around the torus: such boundary conditions (or equivalently, a background gauge flux of π and periodic boundary conditions for the fermions) minimize the ground state energy, as we show in Appendix D.3. Some of these energy levels are given in Table 5.2.

Even among the charge neutral multiparticle states, there are certain states of the free field theory which are strongly renormalized even at $N_f = \infty$. These are the SU(N_f) singlet

states which couple to the A_μ gauge field. Computation of these renormalizations is one of the main purposes of the present paper. We show that the energies of these states are instead given by the zeros of the gauge field effective action. A similar conclusion was reached in Ref. 189 for the O(N) model, where the O(N) singlet levels were given by the zeros of the effective action of a Lagrange multiplier.

In Table 5.1, we list some of the lowest frequency modes of the photon in QED_3 on a square torus, obtained in the large N_f computation just described. Because the theory on the torus is translationally invariant, we can distinguish states by their total external momentum. For each momentum considered, the left-most column gives the photon frequency with its degeneracy is shown on the right. By including multi-photon states, the actual energy levels of the photon are shown in Table 5.3 for the same set of momenta. The origin of the photon shift will be apparent when we find the free energy in Sec. 5.2.3 and explicitly calculate the energy levels in Sec. 5.3.

A similar story applies to the Dirac-CS theory with finite CS coupling k:

$$S_{\rm CS}[A] = \frac{ik}{4\pi}\int d^3r\, \epsilon^{\mu\nu\rho} A_\mu \partial_\nu A_\rho. \tag{5.5}$$

The addition of this term gives the photon a mass and attaches flux to the Dirac fermions so that they become anyons with statistical angle $\theta = 2\pi(1-1/k)$. The Dirac-CS theory applies to the chiral spin liquid which spontaneously breaks time reversal, generating a Chern-Simons term at level $k = 2$ [83]. Similarly, a CS term with odd level can be used to impose anyonic statistics on the quasiparticles of a fractional quantum Hall fluid. The Dirac-CS CFT we consider can describe the continuous transitions into and between such topological phases [14, 65, 190]. It is given by $S_{\rm DCS}[\psi, A] = S_{\rm D}[\psi, A] + S_{\rm CS}[A]$ (after taking $e^2 \to \infty$). As k becomes very large, the anyons become more fermion-like, making an expansion in $2\pi/k$ possible at large N_f [26, 154].

Once again, keeping $\lambda = N_f/k$ fixed, the critical Dirac-CS theory is both stable and

$\bar{\boldsymbol{q}} = (0,0)$		$\bar{\boldsymbol{q}} = (1,0)$		$\bar{\boldsymbol{q}} = (1,1)$	
$\bar{\omega}_\gamma$	d_γ	$\bar{\omega}_\gamma$	d_γ	$\bar{\omega}_\gamma$	d_γ
		1.437980	1		
				1.682078	1
				1.739074	1
		1.976292	1		
2.311525	2				
				2.527606	1
		2.658092	1		
				2.813224	1
		3.156341	1		
		3.407832	1		
				3.517617	1
				3.626671	1
		3.814432	1		
3.855225	2				
		4.092996	1		
				4.259784	1
				4.330137	1
		4.425387	1		
				4.523167	1
4.586816	2				
				4.657172	1
		4.685590	1		

Table 5.1: Photon modes in QED_3 (CS level $k = 0$) on a square torus of size L. Frequencies are shown for $\boldsymbol{q} = 0$, $\boldsymbol{q}_1 = 2\pi(1,0)/L$, and $\boldsymbol{q}_2 = 2\pi(1,1)/L$. The 1st, 3rd, and 5th columns list the frequencies, ω_γ, while the column immediately to the right provides the degeneracy, d_γ. The actual photon energy levels are given by these frequencies as well as integer multiples. ($\bar{\boldsymbol{q}} = L\boldsymbol{q}/2\pi$, $\bar{E} = LE/2\pi$.)

tractable in the large-N_f limit. The qualitative features of the spectrum are very similar to QED_3. Again ψ_α is not a gauge invariant quantity and cannot exist by itself in the spectrum. The Gauss law mandates that it be accompanied by k units of flux. In the large-k limit, these states have very high energies and can be neglected: only charge-neutral excitations need be considered. Likewise, the energy levels of the $\text{SU}(N_f)$ singlet states coupling to the gauge field are strongly renormalized even at large N_f, while the mixed-flavor two-particle excitations behave as free particles. As k/N_f becomes large, the Chern-Simons term will dominate and the topological degeneracy which was lost upon coupling to matter will reassert itself. The photon modes of the zero external momentum sector are shown in Table 5.4 for several values of λ.

We will calculate the energy spectrum using a path integral approach similar to that of Ref. 97. In order to ensure that the gauge redundancy is fully accounted for, it is useful to first calculate the free energy. This is done in Sec. 5.2, starting with two exactly solvable theories, pure Chern-Simons and Maxwell-Chern-Simons, before moving on to QED_3 and the Dirac-CS theory in the large-N_f limit. The structure of the free energy will allow us to identify the multi-fermion states, along with their bound states which appear in the photon contribution. In Sec. 5.3 we determine the energy levels and we conclude in Sec. 5.4.

5.2 Path integral and free energy

To understand the spectrum of the large-N_f QED_3 and Dirac-CS theory, we evaluate its path integral [97]. The path integral is

$$Z = \frac{1}{\text{Vol}(G)} \int DA\, D\psi\, e^{-S[A,\psi]} \tag{5.6}$$

where $\text{Vol}(G)$ is the volume of the gauge group. For simplicity, we work on the square torus: the modular parameter $\tau = i$ and the x- and y-cycles are equal in length: $x \sim x + L$, $y \sim y + L$. Eventually, we will specify to the zero-temperature limit, $1/T = \beta \to \infty$, but for

now we leave β finite.

The gauge field A can be split into zero and finite momentum pieces,

$$A_\mu = a_\mu + A'_\mu, \qquad\qquad A'_\mu = \frac{1}{\sqrt{\beta L^2}} \sum_p{}' A_\mu(p) e^{ipr}, \tag{5.7}$$

where p sums over $p_\mu = 2\pi n_\mu / L_\mu$, $L_\mu = (\beta, L, L)$ where $n_\mu \in \mathbb{Z}$ and the prime on the summation indicates that the $n_\mu = (0,0,0)$ mode is not included. We note that while this representation is completely sufficient for the theories we consider in the paper, it does allow for non-trivial flux sectors, and this is discussed in more detail in Appendix D.6. Overlooking this technicality, the measure of integration is $DA = Da\, DA'$. Unlike on $\mathbb{R}^3$, the zero modes a are not pure gauge configurations. Instead, the gauge transformation which shifts a,

$$U = \exp\left[2\pi i \sum_\mu \frac{n_\mu r_\mu}{L_\mu}\right], \tag{5.8}$$

is only well-defined provided $n_\mu \in \mathbb{Z}$. Under the action of U, the zero modes transform as $a_\mu \to a_\mu + 2\pi n_\mu / L_\mu$, and so they are periodic variables and should be integrated only over the intervals $[0, 2\pi/L_\mu)$. Including a Jacobian factor of $\sqrt{\beta L^2}$ for each component, we have

$$\int Da = \left(\beta L^2\right)^{3/2} \int_0^{2\pi/\beta} da_0 \int_0^{2\pi/L} d^2\boldsymbol{a}. \tag{5.9}$$

The spatially varying portion of the gauge field can be decomposed further into $A' = B + d\phi$ where ϕ parametrizes the gauge transformations of A', and B may be viewed as the gauge-fixed representative of A'. Naturally, gauge invariance implies that the action is independent of ϕ: $S[\psi, A] = S[\psi, a+B]$. Here, we work in the Lorentz gauge, $\partial^\mu B_\mu = 0$. The full measure of integration is then

$$DA = Da\, DB\, D(d\phi). \tag{5.10}$$

We begin by expressing $D(d\phi)$ directly in terms of the phases ϕ. They can be related through the distance function $\mathscr{D}(\omega, \omega + \delta\omega) = \left(\int |\delta\omega|^2\right)^{1/2}$:

$$\begin{aligned} \mathscr{D}(\phi, \phi + \delta\phi) &= \left(\int |\delta\phi|^2\right)^{1/2} \\ \mathscr{D}(d\phi, d\phi + d\delta\phi) &= \left(\int |d\delta\phi|^2\right)^{1/2} = \left(\int \delta\phi \left(-\nabla^2\right) \delta\phi\right)^{1/2}. \end{aligned} \tag{5.11}$$

Changing variables, the measure becomes

$$D(d\phi) = D'\phi \sqrt{\det{}' \left(-\nabla^2\right)} \tag{5.12}$$

where the primes indicate that constant configurations of ϕ are not included and that the zero eigenvalue of the Laplacian is omitted. This functional determinant is the familiar Faddeev-Popov (FP) contribution to the path integral. As expected for abelian gauge theories, both of these factors are independent of the gauge field B.

The volume of the gauge group can be divided in a similar fashion

$$\mathrm{Vol}(G) = \mathrm{Vol}(H) \int D'\phi, \tag{5.13}$$

where H is the group of constant gauge transformations. $\int D'\phi$ will cancel the identical factor present in the numerator from the gauge field measure in Eq. (5.12), and $\mathrm{Vol}(H)$ can be determined using the distance function defined above. A constant gauge transform has $\phi = c$, a constant, where $c \in [0, 2\pi)$. We find

$$\begin{aligned} \mathrm{Vol}(H) &= \int_0^{2\pi} dc \, \frac{\mathscr{D}(c, c + \delta c)}{\delta c} = \int_0^{2\pi} dc \, \frac{\delta c}{\delta c} \left(\int 1\right)^{1/2} \\ &= 2\pi \sqrt{\mathrm{Vol}\left(\boldsymbol{T}^2 \times \boldsymbol{S}^1\right)} = 2\pi \sqrt{\beta L^2}. \end{aligned} \tag{5.14}$$

Putting these facts together, we are left with

$$Z = \frac{\beta L^2}{2\pi}\sqrt{\det{}'\,(-\nabla^2)}\int d^3a\, DB\, D\psi\, e^{-S[a,B,\psi]}. \tag{5.15}$$

In the following two sections, we calculate the free energies and partition functions of the pure Chern-Simons and the Maxwell-Chern-Simons theories. These serve as simple examples (and verifications) of the normalization and regularization procedure, before we move on to the third section and primary purpose of this paper, large-N_f QED$_3$ and Dirac-Chern-Simons.

5.2.1 Pure Chern-Simons theory

It is well-known that pure abelian Chern-Simons theory should have $Z_{\rm CS} = k$ [194]. Since the action in Eq. (5.5) only has linear time derivatives, the Hamiltonian vanishes and it may at first be surprising that $Z_{\rm CS}$ is not simply unity: $\langle 0|0\rangle = 1$. One way to understand this is through canonical quantization. The observable operators of the theory are the two Wilson loops winding around either cycle of the torus. Their commutations relations are determined by the Chern-Simons term, and at level k, it can be shown that the resulting representation requires at least a k-dimensional Hilbert space (see e.g. [130]). The partition function is therefore $Z_{\rm CS} = \sum_{n=1}^{k} \langle n\,|\,n\rangle = k$. Within the general framework of topological field theories, the partition function on the torus should evaluate to the dimension of the corresponding quantum mechanical Hilbert space.

The pure CS partition function is

$$Z_{\rm CS} = \frac{\beta L^2}{2\pi}\sqrt{\det{}'\,(-\nabla^2)}\int da\, DB\, e^{-S_{\rm CS}[B]}. \tag{5.16}$$

We write the Chern-Simons action in momentum space as $S_{\rm CS}[B] = \frac{1}{2}\sum_q B_\mu(-q)\Pi^{\mu\nu}_{\rm CS}(q)B_\nu(q)$ where

$$\Pi^{\mu\nu}_{\rm CS}(q) = \frac{ik}{2\pi}\epsilon^{\mu\nu\rho}q_\rho, \tag{5.17}$$

with $q_\mu = 2\pi n_\mu / L_\mu$, $n_\mu \in \mathbb{Z}$. Performing the Gaussian integral, we find

$$Z_{\rm CS} = \frac{\beta L^2}{2\pi} \sqrt{\det{}' \left(-\nabla^2\right)} \sqrt{\det{}' \left(\frac{2\pi}{\Pi^{\mu\nu}_{\rm CS}}\right)} \int da. \tag{5.18}$$

It is simpler to work with the free energy and then return to the partition function at the end of the calculation:

$$F_{\rm CS} = -\frac{1}{\beta} \log Z_{\rm CS} = F_a + F_\pi + F_{\rm FP} - \frac{1}{\beta} \log \left[\frac{\beta L^2}{2\pi}\right]. \tag{5.19}$$

We proceed to treat each contribution individually. The integral over the zero modes gives

$$F_a = -\frac{1}{\beta} \log \left[\int da\right] = -\frac{1}{\beta} \log \left[\frac{(2\pi)^3}{\beta L^2}\right]. \tag{5.20}$$

This cancels the volume-dependent constant in the free energy, leaving $F_{\rm CS} = -\frac{1}{\beta} \log(2\pi)^2 + F_\pi + F_{\rm FP}$. The FP determinant's contribution is

$$F_{\rm FP} = -\frac{1}{\beta} \log \sqrt{\det{}' \left(-\nabla^2\right)} = -\frac{1}{2\beta} {\sum_q}' \log q^2 \tag{5.21}$$

where $q_\mu = 2\pi n_\mu / L_\mu$, $n_\mu \in \mathbb{Z}$. As will be the convention throughout this paper, the prime on the summation indicates that the zero momentum mode ($n_\mu = (0,0,0)$) is omitted. Finally, the piece from the Gaussian integral is

$$F_\pi = \frac{1}{2\beta} \log \det{}' \left[\frac{\Pi^{\mu\nu}_{CS}}{2\pi}\right]. \tag{5.22}$$

For each momentum q_μ, the Chern-Simons kernel has three eigenvalues, 0 and $\pm ik\left|q\right|/2\pi$, but only the non-zero values should be included. In fact, it is easy to verify that the eigenvector corresponding to the 0 eigenvalue is proportional to q_μ and consequently arises from the pure

gauge configurations $\sim \partial_\mu \phi$ which have already been accounted for. Therefore,

$$F_\pi = \frac{1}{2\beta} \sum_q{}' \log \left[\frac{1}{4\pi^2} \frac{k^2}{4\pi^2} q^2 \right]. \tag{5.23}$$

Using the zeta-function regularization identity $\sum_p{}' = -1$, we have

$$F_\pi = \frac{1}{2\beta} \sum_q{}' \log q^2 - \frac{1}{\beta} \log \left(\frac{k}{4\pi^2} \right). \tag{5.24}$$

The momentum sum in F_π cancels exactly with the sum in $F_{\rm FP}$. This is a direct consequence of the fact that the CS theory has no finite energy states and, notably, is only apparent when the Faddeev-Popov and gauge kernel determinants are considered together. All together, the total free energy is

$$F_{\rm CS} = -\frac{1}{\beta} \log k, \tag{5.25}$$

which gives $Z_{\rm CS} = k$ as claimed.

5.2.2 Maxwell-Chern-Simons theory

It is also useful to understand how the topological degeneracy emerges in the presence of finite-energy modes. This is easily accomplished by adding a Maxwell term:

$$S_{\rm MCS}[A] = S_{\rm M}[A] + S_{\rm CS}[A], \tag{5.26}$$

where $S_{\rm M}[A]$ is given in Eq. (5.4). The procedure for calculating the free energy is identical to the pure CS case except that the gauge kernel is now

$$\Pi_{\rm MCS}(q) = \frac{q^2}{e^2} \left(\delta^{\mu\nu} - \frac{q^\mu q^\nu}{q^2} \right) + \frac{ik}{2\pi} \epsilon^{\mu\nu\rho} q_\rho. \tag{5.27}$$

As above, this matrix has one vanishing eigenvalue in the pure gauge direction and two non-trivial ones in orthogonal directions:

$$\frac{q^2}{e^2} \pm \frac{ik}{2\pi} |q| \,. \tag{5.28}$$

Performing the functional integral and taking the logarithm, we find

$$F_\pi = \frac{1}{2\beta} {\sum_q}' \log \left[\frac{q^4}{e^4} + \frac{k^2 q^2}{4\pi^2} \right] . \tag{5.29}$$

As in the pure CS case, the FP determinant cancels a factor of q^2 from F_π. Now, however, this does not completely remove the momentum dependence of the sum. The total free energy is

$$F_{\rm MCS} = -\frac{1}{\beta} \log 4\pi^2 + F_\pi + F_{\rm FP} = \frac{1}{\beta} \log \left(\frac{e^2}{2\pi} \right) + \frac{1}{2\beta} {\sum_{n,\boldsymbol{q}}}' \log \left[\epsilon_n^2 + \boldsymbol{q}^2 + \frac{e^4 k^2}{4\pi^2} \right] , \tag{5.30}$$

where we've written $q^\mu = (\epsilon_n, \boldsymbol{q})$ with $\epsilon_n = 2\pi n/\beta$, $n \in \mathbb{Z}$. Analytically continuing to real time, $\epsilon_n \to -i\omega$, the argument of the logarithm is $\omega^2 - \gamma_{\boldsymbol{q}}^2$ where $\gamma_{\boldsymbol{q}} = \sqrt{\boldsymbol{q}^2 + (e^2 k/2\pi)^2}$. We recognize the $\gamma_{\boldsymbol{q}}$'s as the frequencies of a set of harmonic oscillators. As in the previous section, this is only manifest when the sum $F_\pi + F_{\rm FP}$ is considered: by itself, F_π seems to imply the existence of an extra set of oscillators whose frequencies are $\tilde{\gamma}_{\boldsymbol{q}} = |\boldsymbol{q}|$.

The presence of the oscillators is even clearer upon performing the (imaginary) frequency sum. Adding and subtracting the zero mode, we are left to evaluate an infinite sum

$$F_{\rm MCS} = -\frac{1}{\beta} \log \left(\frac{2\pi\gamma_0}{e^2} \right) + \frac{1}{2\beta} \sum_{n,\boldsymbol{q}} \log \left[n^2 + \left(\frac{\beta\gamma_{\boldsymbol{q}}}{2\pi} \right)^2 \right] . \tag{5.31}$$

By using the known analytic properties of the zeta function for complex s, we can assign a value to the otherwise obviously diverging sum. For the logarithm, this representation

results in the identification

$$\sum_n \log\left[n^2+\left(\frac{\beta\gamma_{\boldsymbol{q}}}{2\pi}\right)^2\right] = -\lim_{s\to 0}\frac{d}{ds}\sum_n\left[n^2+\left(\frac{\beta\gamma_{\boldsymbol{q}}}{2\pi}\right)^2\right]^{-s} = -\lim_{s\to 0}\frac{d}{ds}\zeta_{\mathcal{E}}\left(s;\left(\frac{\beta\gamma_{\boldsymbol{q}}}{2\pi}\right)^2\right) \tag{5.32}$$

where $\zeta_{\mathcal{E}}(s;a^2)$ is the Epstein zeta function. After some standard manipulations (given in Appendix D.2), we arrive at the expression

$$F_{\text{MCS}} = -\frac{1}{\beta}\log k - \frac{1}{\beta}\sum_{\boldsymbol{q}}\log\left[\frac{e^{-\beta\gamma_{\boldsymbol{q}}/2}}{1-e^{-\beta\gamma_{\boldsymbol{q}}}}\right]. \tag{5.33}$$

Re-exponentiating, we find

$$Z_{\text{MCS}} = k\prod_{\boldsymbol{q}} Z_{\boldsymbol{q}}, \qquad Z_{\boldsymbol{q}} = \frac{e^{-\beta\gamma_{\boldsymbol{q}}/2}}{1-e^{-\beta\gamma_{\boldsymbol{q}}}} = e^{-\beta\gamma_{\boldsymbol{q}}/2}\sum_{n=0}^{\infty} e^{-\beta n\gamma_{\boldsymbol{q}}}. \tag{5.34}$$

As observed, the partition function is a product over an infinite stack of harmonic oscillators with frequencies $\gamma_{\boldsymbol{q}}$. The topological degeneracy enters through the factor of k multiplying Z_{CS}: there are k identical sets of oscillators. We note that in the limit $e^2\to\infty$, the barrier to the first excited state becomes infinitely large, effectively projecting onto the lowest Landau level. Ignoring some constants, we arrive back at the pure Chern-Simons described above.

5.2.3 QED$_3$ and Dirac-Chern-Simons theory

When we couple the gauge field to fermions, the partition function is no longer exactly solvable. Nonetheless, when the number of fermion flavours, N_f, is large, a saddle-point approximation is valid and allows a systematic expansion in $1/N_f$. As discussed in the introduction, the QED$_3$ and Dirac-CS fixed points are obtained in the limit $e^2\to\infty$, and so we will not explicitly include the Maxwell action $S_{\text{M}}[A]$ in our calculations. In order to avoid the parity anomaly [146, 147], we take N_f to be even in all that follows. The partition

function is given in Eq. (5.15) with action

$$S_{\rm DCS}[\psi, A] = S_{\rm D}[A, \psi] + S_{\rm CS}[A]. \tag{5.35}$$

where $S_{\rm D}[A, \psi]$ and $S_{\rm CS}[A]$ are given in Eqs. (5.3) and (5.5) respectively. The Chern-Simons level k is assumed to be of the same order as N_f. We begin by integrating out the fermions,

$$Z = \frac{\beta L^2}{2\pi}\sqrt{\det{}'\left(-\nabla^2\right)}\int da\, DB\, \exp\left(-S_{\rm CS}[B] + N_f \log\det i\not{D}\right), \tag{5.36}$$

where $\not{D} = \sigma^\mu\left(\partial_\mu - ia_\mu - iB_\mu\right)$. We subsequently expand the determinant in terms of B:

$$\log\det(i\not{D}) = \mathrm{tr}\log\left(i\not{\partial} + \not{a}\right) + \mathrm{tr}\left(\frac{1}{i\not{\partial}+\not{a}}\not{B}\right) - \frac{1}{2}\mathrm{tr}\left(\frac{1}{i\not{\partial}+\not{a}}\not{B}\frac{1}{i\not{\partial}+\not{a}}\not{B}\right) + \cdots \tag{5.37}$$

By rescaling $B \to B/\sqrt{N_f}$, the subleading behaviour of the linear and quadratic terms, as well as the Chern-Simons action, is clear.

On the plane, the saddle-point value of A vanishes by symmetry and gauge invariance. However, since $A \to A + c$ for constant c is no longer a gauge transformation on the torus, the zero modes are distinct and could conceivably have a non-zero expectation value: $\langle a\rangle = \bar{a} \neq 0$. In fact, neither the pure CS nor Maxwell-CS actions depended on a_μ. The matter lifts this degeneracy by creating an effective potential for the a's, and $\bar{a}$ can be determined by minimizing the free fermion functional determinant

$$F_0(a) = -\mathrm{tr}\log\left(i\not{\partial} + \not{a}\right) = -\sum_p \log\left(p + a\right)^2. \tag{5.38}$$

The summation above is over spacetime momenta $p_\mu = 2\pi\left(n_\mu + 1/2\right)/L_\mu$, $n_\mu \in \mathbb{Z}$ as is appropriate for our choice of fermions with antiperiodic boundary conditions. This calculation is performed in Appendix D.3 where it is shown that the saddle-point value of the gauge field is $\bar{a}_\mu = 0$: this is closely linked to the choice of anti-periodic boundary conditions for

the fermions, which we have established also minimize the total energy.

The linear term in B in Eq. (5.37) vanishes, so that the subleading term in the determinant expansion is

$$S_f[B] = \frac{N_f}{2}\mathrm{tr}\left(\frac{1}{i\not{\partial}}\not{B}\frac{1}{i\not{\partial}}\not{B}\right) = \frac{N_f}{2}\sum_q B_\mu(-q)\Pi_f^{\mu\nu}(q)B_\nu(q) \tag{5.39}$$

where

$$\Pi_f^{\mu\nu}(q) = \frac{2}{\beta L^2}\sum_p \frac{p^\mu\left(p^\nu+q^\nu\right)+\left(p^\mu+q^\mu\right)p^\nu-\delta^{\mu\nu}p\cdot(p+q)}{p^2\left(p+q\right)^2}. \tag{5.40}$$

On the plane, this expression evaluates to [90]

$$\Pi_\infty^{\mu\nu} = \frac{|q|}{16}\left(\delta^{\mu\nu}-\frac{q^\mu q^\nu}{q^2}\right). \tag{5.41}$$

On the torus, a simple analytic formula is no longer available and Π_f must be calculated numerically. Expressions for the components of $\Pi_f^{\mu\nu}$ on the symmetric torus are given in Appendix D.4.

Since $k \sim \mathrm{O}(N_f)$, the CS term will contribute at the same order as Π_f. Rescaling Eq. (5.17) to bring out an overall factor of N_f, we write the momentum space kernel of the Chern-Simons term as

$$\Pi_{\mathrm{CS}}^{\mu\nu}(q) = \frac{i}{2\pi\lambda}\epsilon^{\mu\nu\rho}q_\rho, \qquad \lambda = \frac{N_f}{k}. \tag{5.42}$$

All together, the full effective potential is

$$S_{\mathrm{eff}}[B] = \frac{N_f}{2}\sum_q B_\mu(-q)\Pi^{\mu\nu}(q)B_\nu(q), \qquad \Pi^{\mu\nu}(q) = \Pi_{\mathrm{CS}}^{\mu\nu}(q)+\Pi_f^{\mu\nu}(q), \tag{5.43}$$

and the large-N_f partition function is

$$\begin{aligned} Z &\cong \frac{\beta L^2}{2\pi}\sqrt{\det{}'\,(-\nabla^2)}\,e^{-\beta N_f F_0(\bar{a})}\int DB\,\exp\left[-\frac{1}{2}\sum_q B_\mu(-q)\Pi^{\mu\nu}(q)B_\nu(q)\right] \\ &= \frac{\beta L^2}{2\pi}\sqrt{\det{}'\,(-\nabla^2)}\,e^{-\beta N_f F_0(\bar{a})}\sqrt{\det{}'\left(\frac{2\pi}{\Pi^{\mu\nu}}\right)}. \end{aligned} \tag{5.44}$$

The corresponding free energy is

$$F = -\frac{1}{\beta}\log Z \cong N_f F_0 + F_G - \frac{1}{\beta}\log\left[\frac{\beta L^2}{2\pi}\right] \tag{5.45}$$

where the full gauge field contribution is

$$\begin{aligned} &F_{\rm G} = F_{\rm FP} + F_\pi \\ &F_\pi = -\frac{1}{\beta}\log\sqrt{\det{}'\left(\frac{2\pi}{\Pi^{\mu\nu}}\right)} \qquad\qquad F_{\rm FP} = -\frac{1}{\beta}\log\sqrt{\det{}'\,(-\nabla^2)}. \end{aligned} \tag{5.46}$$

ZERO EXTERNAL MOMENTUM, $\boldsymbol{q} = 0$

We begin by considering the zero (spatial) momentum portion of the free energy. Denoting the Euclidean spacetime momenta $q^\mu = (\epsilon, \boldsymbol{q})$, we set $\boldsymbol{q} = 0$. In this case, only $\Pi^{ij}(\epsilon, 0) \neq 0$, for $i, j = x, y$:

$$\Pi^{ij}(\epsilon, 0) = \begin{pmatrix} \Pi_f^{xx} & \epsilon/2\pi\lambda \\ -\epsilon/2\pi\lambda & \Pi_f^{yy} \end{pmatrix}. \tag{5.47}$$

Expressions for Π_f^{xx} and Π_f^{yy} are given in Eqs. (D.25) and (D.26) of Appendix D.4. Taking the determinant, the free energy is

$$F_\pi^{\boldsymbol{q}=0} = \frac{1}{\beta}\log 2\pi + \frac{1}{2\beta}{\sum_n}'\log\left[\Pi_f^{xx}\,(\epsilon_n, 0)^2 + \frac{\epsilon_n^2}{4\pi^2\lambda^2}\right] \tag{5.48}$$

where $\epsilon_n = 2\pi n/\beta$, $n \in \mathbb{Z}/\{0\}$, and the symmetry of the torus has been used to set $\Pi_f^{xx} = \Pi_f^{yy}$. The FP piece is

$$F_{\rm FP}^{\boldsymbol{q}=0} = -\frac{1}{2\beta}{\sum_n}' \log \epsilon_n^2 \,. \tag{5.49}$$

Adding the two and taking the zero temperature limit, $\beta \to \infty$, the total gauge contribution is

$$F_{\rm G}^{\boldsymbol{q}=0} = \frac{1}{2}\int \frac{d\epsilon}{2\pi} \log\left[\left(\frac{\Pi_f^{xx}}{\epsilon}\right)^2 + \frac{1}{4\pi^2\lambda^2}\right]. \tag{5.50}$$

For large ϵ, the integral does not converge. Instead, Π_f^{xx} approaches its infinite volume limit in Eq. (5.41):

$$\left(\frac{\Pi_f^{xx}}{\epsilon}\right)^2 + \frac{1}{4\pi^2\lambda^2} \to \left(\frac{1}{16}\right)^2 + \frac{1}{4\pi^2\lambda^2}\,. \tag{5.51}$$

This is not a problem since an integral over a constant vanishes in the zeta regularization scheme. Adding and subtracting the large frequency limit, the free energy is a finite function

$$F_{\rm G}^{\boldsymbol{q}=0} = \frac{1}{2}\int \frac{d\epsilon}{2\pi}\left\{\log\left[\left(\frac{\Pi_f^{xx}}{\epsilon}\right)^2 + \frac{1}{4\pi^2\lambda^2}\right] - \log\left[\left(\frac{1}{16}\right)^2 + \frac{1}{4\pi^2\lambda^2}\right]\right\}. \tag{5.52}$$

Finite external momentum, $\boldsymbol{q} \neq 0$

For the finite momentum piece, we begin by restricting the polarization matrix $\Pi^{\mu\nu}(\epsilon, \boldsymbol{q})$ to the physical subspace. As required by gauge invariance, it has a vanishing eigenvalue along the $q^\mu = (\epsilon, \boldsymbol{q})$ direction: $q_\mu \Pi^{\mu\nu} = 0$. To determine the remaining two modes, we project

onto the orthogonal directions

$$v_T = \frac{1}{|\boldsymbol{q}|}\begin{pmatrix} 0 \\ q_y \\ -q_x \end{pmatrix}, \qquad v_L = \frac{1}{|\boldsymbol{q}|\sqrt{\epsilon^2+\boldsymbol{q}^2}}\begin{pmatrix} -\boldsymbol{q}^2 \\ \epsilon q_x \\ \epsilon q_y \end{pmatrix}, \tag{5.53}$$

and, after some simplifying, arrive at

$$\Pi_{\text{proj}} = \frac{1}{\boldsymbol{q}^2}\begin{pmatrix} (\epsilon^2+\boldsymbol{q}^2)\,\Pi^{00} & \sqrt{\epsilon^2+\boldsymbol{q}^2}\,(q_y\Pi^{0x}-q_x\Pi^{0y}) \\ \sqrt{\epsilon^2+\boldsymbol{q}^2}\,(q_y\Pi^{0x}-q_x\Pi^{0y}) & \boldsymbol{q}^2\,(\Pi^{xx}+\Pi^{yy})-\epsilon^2\Pi^{00} \end{pmatrix}. \tag{5.54}$$

Taking the determinant, the contribution to the free energy is

$$\begin{aligned} F_\pi^{\boldsymbol{q}\neq 0} &= -\frac{1}{\beta}\log\sqrt{\det{}'\left(\frac{2\pi}{\Pi^{\mu\nu}}\right)} = -\frac{1}{\beta}\sum_{\epsilon,\boldsymbol{q}}{}' \log 2\pi + \frac{1}{2\beta}\sum_{\epsilon,\boldsymbol{q}}{}' \log\Pi^{\mu\nu} \\ &= \frac{1}{2}\int\frac{d\epsilon}{2\pi}\sum_{\boldsymbol{q}}{}' \log\left\{\frac{(\epsilon^2+\boldsymbol{q}^2)}{\boldsymbol{q}^2}\left[\Pi^{00}\left(\Pi^{xx}+\Pi^{yy}-\frac{\epsilon^2}{\boldsymbol{q}^2}\Pi^{00}\right)-\frac{1}{\boldsymbol{q}^2}\left(q_y\Pi^{0x}-q_x\Pi^{0y}\right)^2\right]\right\} \end{aligned} \tag{5.55}$$

where the $\frac{1}{\beta}\log 2\pi$ term has vanished in the zero temperature limit. The Faddeev-Popov portion of the free energy,

$$F_{\text{FP}}^{\boldsymbol{q}\neq 0} = -\frac{1}{2}\int\frac{d\epsilon}{2\pi}\sum_{\boldsymbol{q}}\log\left(\epsilon^2+\boldsymbol{q}^2\right), \tag{5.56}$$

perfectly cancels the $\epsilon^2+\boldsymbol{q}^2$ prefactor inside the logarithm in Eq. (5.55). Had it not been included, we may have erroneously assumed the existence of a state with energy $E=|\boldsymbol{q}|$ as there is on the plane when $k=0$.

As $\epsilon^2+\boldsymbol{q}^2$ becomes large, $\Pi^{\mu\nu}$ approaches its infinite volume limit (Eq. (5.41)) like in the $\boldsymbol{q}=0$ case. Here as well, the summand becomes a constant which vanishes in our

regularization procedure. Putting this together, we have

$$F_{\mathrm{G}}^{\boldsymbol{q}\neq 0} = \frac{1}{2}\int \frac{d\epsilon}{2\pi} \sum_{\boldsymbol{q}}{}' \left\{ \log\left[\frac{\Pi^{00}}{\boldsymbol{q}^2}\left(\Pi^{xx}+\Pi^{yy}-\frac{\epsilon^2}{\boldsymbol{q}^2}\Pi^{00}\right) - \frac{1}{\boldsymbol{q}^4}\left(q_y\Pi^{0x}-q_x\Pi^{0y}\right)^2\right] - \log\left[\left(\frac{1}{16}\right)^2 + \frac{1}{4\pi^2\lambda^2}\right]\right\}. \tag{5.57}$$

The total contribution of the gauge field to the free energy is given by the sum of this expression with $F_G^{\boldsymbol{q}=0}$ in Eq. (5.52).

5.3 Spectrum

In this section we explicitly calculate the universal spectrum on the finite torus using the path integral expansion we just derived.

As the photon is the only element of the theory which differs from the free theory of N_f Dirac fermions, it is not surprising that the free theory spectrum can account for most of the states. The free Hamiltonian is

$$\mathcal{H}_{\mathrm{D}} = -i\int d^2\boldsymbol{x}\, \psi_\alpha^\dagger(\boldsymbol{x})\sigma_i\partial_i\psi_\alpha(\boldsymbol{x}), \tag{5.58}$$

and can be diagonalized by first going to Fourier space,

$$\psi_\alpha(\boldsymbol{x}) = \frac{1}{L^2}\sum_{\boldsymbol{p}} e^{i\boldsymbol{q}\cdot\boldsymbol{x}}\begin{pmatrix} c_{1\alpha}(\boldsymbol{p}) \\ c_{2\alpha}(\boldsymbol{p})\end{pmatrix}, \qquad \boldsymbol{p} = \frac{2\pi}{L}\left(n_x+\frac{1}{2}, n_y+\frac{1}{2}\right), \quad n_{x,y}\in\mathbb{Z}, \tag{5.59}$$

and then changing basis to $\chi_{\pm\alpha}(\boldsymbol{p})$:

$$\begin{pmatrix} c_{1\alpha}(\boldsymbol{p}) \\ c_{2\alpha}(\boldsymbol{p})\end{pmatrix} = \frac{1}{\sqrt{2}}\begin{pmatrix} 1 & 1 \\ P/|\boldsymbol{p}| & -P/|\boldsymbol{p}|\end{pmatrix}\begin{pmatrix}\chi_{+\alpha}(\boldsymbol{p}) \\ \chi_{-\alpha}(\boldsymbol{p})\end{pmatrix}, \tag{5.60}$$

where $P = p_x + ip_y$, $|\boldsymbol{p}| = \sqrt{p_x^2 + p_y^2}$. In this basis, the Hamiltonian is

$$\mathcal{H}_{\mathrm{D}} = \sum_{\boldsymbol{p}} |\boldsymbol{p}| \left[\chi^\dagger_{+\alpha}(\boldsymbol{p}) \chi_{+\alpha}(\boldsymbol{p}) - \chi^\dagger_{-\alpha}(\boldsymbol{p}) \chi_{-\alpha}(\boldsymbol{p}) \right]. \tag{5.61}$$

We identify the vacuum as the state having all negative energy modes filled: $\chi_{+\alpha}(\boldsymbol{p}) |0\rangle = \chi^\dagger_{-\alpha}(\boldsymbol{p}) |0\rangle = 0$. Consequently, $\chi^\dagger_{+\alpha}(\boldsymbol{p})$ is a particle creation operator carrying momentum $\boldsymbol{p}$, and $\chi_{-\alpha}(\boldsymbol{p})$ is a hole creation operator carrying momentum $-\boldsymbol{p}$. Note that all the fermionic momenta correspond to anti-periodic boundary conditions around the torus, because these minimize the ground state energy, as shown in Appendix D.3.

To determine the excitations relevant to QED_3 and the Dirac-CS theory, we recall that once the theory is gauged, neither $\chi_{+\alpha}(\boldsymbol{p})$ nor $\chi_{-\alpha}(\boldsymbol{p})$ is gauge invariant, and all single-particle states are prohibited. Similarly, only charge-neutral two-particle states are allowed. We therefore expect the lowest fermion-like energy states to be of the form

$$\chi^\dagger_{+\alpha}(\boldsymbol{p}+\boldsymbol{q}) \chi_{-\beta}(\boldsymbol{p}) |0\rangle, \qquad \chi^\dagger_{+\alpha}(-\boldsymbol{p}) \chi_{-\beta}(-\boldsymbol{p}-\boldsymbol{q}) |0\rangle. \tag{5.62}$$

Here, we have taken advantage of the translational invariance of the theory to distinguish states by their total external momentum $\boldsymbol{q}$, where $\boldsymbol{q} = 2\pi (n_x, n_y)/L$, $n_{x,y} \in \mathbb{Z}$. Provided the internal momentum $\boldsymbol{p}$ is not such that $\boldsymbol{p} + \boldsymbol{q} = -\boldsymbol{p}$, these states are distinct for each α, β, and have energy

$$E_f(\boldsymbol{q}, \boldsymbol{p}) = |\boldsymbol{p}+\boldsymbol{q}| + |\boldsymbol{p}|. \tag{5.63}$$

Naïvely counting, for every $\boldsymbol{q}$ and $\boldsymbol{p}$, the flavour symmetry gives (at least) $2N_f^2$ such states (additional degeneracies may be present depending on the lattice and internal momentum, but this will not be important for the subsequent discussion). When $\boldsymbol{p} + \boldsymbol{q} = -\boldsymbol{p}$, the two states in Eq. (5.62) are identical, and there are only N_f^2 possible states.

This story no longer holds even at $N_f = \infty$. The gauge field only couples to single

trace operators, so it is natural to expect that the corresponding states may be shifted like in the O(N) model [189]. However, QED$_3$ and the Dirac-CS theory differ from this example by having four different single-trace fermion bilinear operators: the "mass" operator $M(x) = \bar{\psi}_\alpha \psi_\alpha(x)$ and the global gauge currents, $J^\mu(x) = \bar{\psi}_\alpha \gamma^\mu \psi_\alpha(x)$. It is apparent that the current operators and the mass operator must be treated very differently when we consider the equations of motion:

$$J^\mu = \frac{k}{4\pi} J^\mu_{\text{top}} + \frac{i}{e^2} \epsilon^{\mu\nu\rho} \partial_\nu J_{\text{top},\rho}, \tag{5.64}$$

where $J^\mu_{\text{top}} = \epsilon^{\mu\nu\rho}\partial_\nu A_\rho$ is the current of the topological U(1)$_{\text{top}}$ symmetry. This symmetry is equivalent to the non-compactness of A_μ and the irrelevance of monopoles at the fixed point. At $N_f = \infty$, when $k = 0$, J_μ is more correctly understood as a descendant of the topological current and not as a composite operator. In the $e^2 \to \infty$ limit, it vanishes altogether and should not be included in the spectrum: all states corresponding the poles of $\langle J^\mu(x) J^\nu(0)\rangle$ in the free theory no longer exist in large-N_f QED$_3$. The degeneracy is reduced so that for each total momentum $\boldsymbol{q}$ and internal momentum $\boldsymbol{p}$ (where $\boldsymbol{p} + \boldsymbol{q} \neq -\boldsymbol{q}$), QED$_3$ has only $2N_f^2 - 1$ free-fermion-like states with energy $E_f(\boldsymbol{q}, \boldsymbol{p})$ (when $\boldsymbol{p} + \boldsymbol{q} = -\boldsymbol{p}$, the degeneracy is further reduced to $N_f^2 - 1$). This is discussed in more detail in Appendix D.5. For a small set of momenta, these energy levels are shown in Table 5.2 along with their respective degeneracies.

For non-vanishing k, the situation is very similar. Eq. (5.64) indicates that the CS term attaches k units of charge to each unit of magnetic flux so that the charged state with the lowest energy has k fermions accompanied by a single unit of magnetic flux. In the limit $k \to \infty$, these states have very high energies and, as in the $k = 0$ case, will not contribute to the low energy spectrum. The same free-fermion states whose energies are given in Table 5.2 also appear in the Dirac-CS theory with the same degeneracy theory regardless of the level k.

$\bar{\boldsymbol{q}} = (0,0)$		$\bar{\boldsymbol{q}} = (1,0)$		$\bar{\boldsymbol{q}} = (1,1)$	
$\bar{E}_f$	d_f	$\bar{E}_f$	d_f	$\bar{E}_f$	d_f
1.414214	$4N_f^2 - 2$	1.414214	$2N_f^2 - 1$	1.414214	$N_f^2 - 1$
		2.288246	$4N_f^2 - 2$	2.288246	$4N_f^2 - 2$
				2.828427	$2N_f^2 - 1$
3.162278	$8N_f^2 - 4$	3.162278	$2N_f^2 - 1$	3.162278	$2N_f^2 - 1$
		3.702459	$4N_f^2 - 2$		
		4.130649	$4N_f^2 - 2$	4.130649	$4N_f^2 - 2$
4.242640	$4N_f^2 - 2$				
				4.496615	$4N_f^2 - 2$
				4.670830	$4N_f^2 - 2$

Table 5.2: Energies of two-particle fermion states in QED_3 (CS level $k = 0$) on a square torus of size L. Energies are shown for $\boldsymbol{q} = 0$, $\boldsymbol{q}_1 = 2\pi(1,0)/L$ and $\boldsymbol{q}_2 = 2\pi(1,1)/L$. The 1st, 3rd, and 5th columns list the energy levels, E_f, while the column to the right, labelled d_f, shows the degeneracy of the level. The energy levels with finite external momentum, $\boldsymbol{q}_1 = 2\pi(1,0)/L$ and $\boldsymbol{q}_2 = 2\pi(1,1)/L$, have an additional 4-fold degeneracy resulting from the symmetry of the lattice. ($\bar{\boldsymbol{q}} = L\boldsymbol{q}/2\pi$, $\bar{E} = LE/2\pi$.)

For both QED_3 and Dirac-CS, the removal of J^μ is counterbalanced by the addition of A_μ. The spectrum must be supplemented by the poles of the photon propagator, $\Delta_{\mu\nu}(x) = \langle A_\mu(x) A_\nu(0)\rangle$, and, unlike for the free-fermion states, the energies of the photon states depend on the level k.

From the effective action in Eq. (5.43), the photon propagator is obtained by inverting the polarization matrix $\Pi^{\mu\nu}(q)$. However, as discussed in the previous section, gauge invariance is only fully taken into account once the FP determinant's contribution is included as well. Analogous to our identification of $\gamma_{\boldsymbol{q}}$ as the frequencies in a set of harmonic oscillators for the Maxwell-Chern-Simons theory in Eq. (5.30), the physical photon modes are actually given by the zeros of the argument of the logarithms in F_{G}. When $N_f = \infty$, each mode represents an infinite tower of states of a harmonic oscillator like in Maxwell-Chern-Simons: additional energy levels are present as integer multiples of the modes determined from F_{G}. Eqs. (5.52) and (5.57) indicate that these modes occur when the functions

$$K_0(\omega) = -\left(\frac{\Pi_f^{xx}(\omega,0)}{\omega}\right)^2 + \frac{1}{4\pi^2\lambda^2} \tag{5.65}$$

$$K_{\boldsymbol{q}}(\omega) = \frac{\Pi^{00}(\omega,\boldsymbol{q})}{\boldsymbol{q}^2}\left(\Pi^{xx}(\omega,\boldsymbol{q}) + \Pi^{yy}(\omega,\boldsymbol{q}) + \frac{\omega^2}{\boldsymbol{q}^2}\Pi^{00}(\omega,\boldsymbol{q})\right) - \frac{1}{\boldsymbol{q}^4}\left(q_y\Pi^{0x}(\omega,\boldsymbol{q}) - q_x\Pi^{0y}(\omega,\boldsymbol{q})\right)^2$$

vanish. Here, we have analytically continued to real frequencies, $\omega = i\epsilon$. In what follows ϵ will always denote an imaginary frequency, while ω will represent a real frequency; the same symbol for the polarization $\Pi^{\mu\nu}$ is used for both. For $k = 0$, some modes levels are listed in Table 5.1 while Table 5.3 shows the lowest energy levels when multi-photon states are included. Table 5.4 gives the lowest ten modes with zero external momentum for several values of $\lambda = N_f/k$.

To summarize, the $N_f = \infty$ theory does not have single-particle excitations. Instead, the lowest energy states are of the form given in Eq. (5.62) or are created by the photon, A_μ. The free fermion 2-particle energies $E_f(\boldsymbol{q},\boldsymbol{p})$ occur with either a $(2N_f^2-1)$ or a (N_f^2-1)-fold degeneracy depending on the internal momentum $\boldsymbol{p}$ (and before additional lattice symmetries

$\bar{\boldsymbol{q}} = (0,0)$		$\bar{\boldsymbol{q}} = (1,0)$		$\bar{\boldsymbol{q}} = (1,1)$	
$\bar{E}_\gamma$	d_γ^E	$\bar{E}_\gamma$	d_γ^E	$\bar{E}_\gamma$	d_γ^E
0.58413	2				
1.16826	4				
		1.43798	1		
				1.68208	1
				1.73907	1
1.75239	8				
		1.97629	1		
		2.02211	2		
				2.26621	2
2.31153	2				
				2.3232	2
2.33652	16				
				2.52761	1
		2.56042	2		
		2.60624	4		
		2.65809	1		
				2.81322	1
				2.85034	4
2.87596	2				
2.89566	4				
2.89566	4				
				2.90733	4
2.92065	32				
				3.11174	2
		3.14455	4		
		3.15634	1		
		3.19037	8		
		3.24222	2		
3.36416	2				
				3.39735	2

Table 5.3: Photon energy levels in QED_3 (CS level $k = 0$) on a square torus of size L. Energies are shown for states with total momentum $\boldsymbol{q} = 0$, $\boldsymbol{q}_1 = 2\pi(1,0)/L$ and $\boldsymbol{q}_2 = 2\pi(1,1)/L$. The 1st, 3rd, and 5th columns list the energy levels, E_γ, while the column immediately to the right provides their degeneracy, d_γ^E. ($\bar{\boldsymbol{q}} = L\boldsymbol{q}/2\pi$, $\bar{E} = LE/2\pi$.)

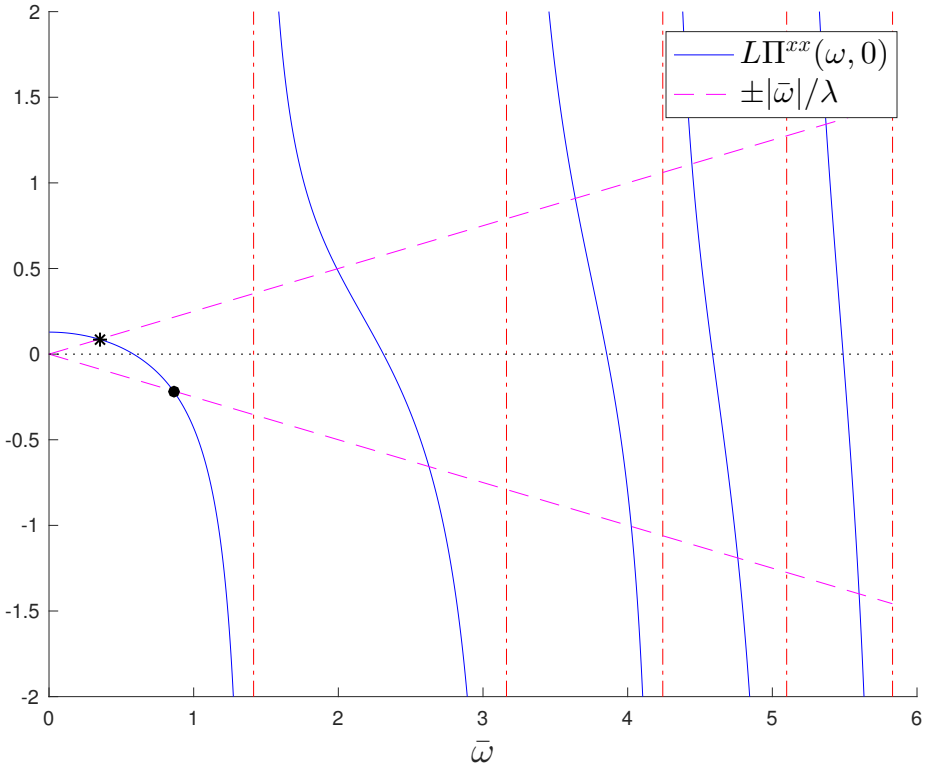

Figure 5.1: Plot of $\Pi_f^{xx}(\omega,0)$ and $|\omega|/2\pi\lambda$. When $k=0$, the modes are two-fold degenerate and occur when $\Pi_f^{xx}=0$. For $k\neq 0$, the degeneracy splits and the frequencies are given by the intersection points $\Pi_f^{xx}(\omega,0)=\pm|\omega|/(2\pi\lambda)$. For $\lambda=4$, this occurs when the solid blue and dashed magenta lines cross. The lowest and second-lowest energies are shown in black with an asterisk and a circle respectively. The vertical dash-dotted lines in red mark the poles of Π_f^{xx} at the two-particle energies of the free theory. ($\bar{\omega}=L\omega/2\pi$.)

are taken into account). The frequency modes of the photon operator are given by the gauge-fixed poles of $\Delta_{\mu\nu}$ and correspond to the zeros of the expressions in Eq. (5.65). Each mode, ω_γ, represents a harmonic oscillator so that the energies $2\omega_\gamma, 3\omega_\gamma, \omega_\gamma+\omega_{\gamma'},\ldots$ are present in the spectrum as well. We will examine Eq. (5.65) in more detail in the subsequent sections.

5.3.1 Zero external momentum, $\boldsymbol{q}=0$

When the external momentum vanishes, the zeros of Eq. (5.65) occur when

$$\Pi_f^{xx}(\omega,0)=\pm\frac{|\omega|}{2\pi\lambda}. \tag{5.66}$$

In Fig. 5.1, the left-hand side is shown with a solid blue line and the right-hand side is shown with a dashed magenta line for $\lambda = 4$.

When $k = 0$ ($\lambda \to \infty$), the energy modes are two-fold degenerate and are given by the point where Π_f^{xx} crosses the x-axis. This degeneracy may be surprising since in 2+1 dimensions we expect the photon to have a single polarization. However, if we had approached the problem by gauge fixing in the Coulomb gauge, we would immediately see that the constraint $\nabla \cdot \boldsymbol{A} = 0$ does not affect the $\boldsymbol{q} = 0$ modes, again resulting in a degeneracy. In fact, the exact degeneracy is a result of the additional symmetry of our torus, which gives $\Pi_f^{xx}(\epsilon, 0) = \Pi_f^{yy}(\epsilon, 0)$.

To understand the effect of the gauge field on the theory, it's useful to explicitly write the form $\Pi_f^{xx}(\omega, 0)$ takes:

$$\Pi_f^{xx}(\omega, 0) = \frac{y_2}{4\pi L} - \frac{\omega^2}{2L^2} \sum_{\boldsymbol{p}} \frac{1}{|\boldsymbol{p}|} \frac{1}{4\boldsymbol{p}^2 - \omega^2} \tag{5.67}$$

where $y_2 = -Y_2(1/2) \cong 1.6156$ for the function $Y_2(s)$ defined in Eq. (D.1). Schematically, we see from Fig. 5.1 that we could rewrite this as a rational function:

$$\Pi_f^{xx}(\omega, 0) \sim \frac{\prod_\gamma \left(\omega^2 - \omega_\gamma^2\right)}{\prod_{\boldsymbol{p}} \left(\omega^2 - E_f(0, \boldsymbol{p})^2\right)} \tag{5.68}$$

where ω_γ are the zeros of the polarization, $\Pi_f^{xx}(\omega_\gamma, 0) = 0$, and $E_f(0, \boldsymbol{p}) = 2\,|\boldsymbol{p}|$ are its poles. Its contribution to the partition function is therefore something like

$$Z^{\boldsymbol{q}=0} \sim \prod_{i\epsilon_n} \left\{ \frac{\prod_{\boldsymbol{p}} \left[(i\epsilon_n)^2 + 4\boldsymbol{p}^2\right]}{\prod_\gamma \left[(i\epsilon_n)^2 + (\omega_\gamma)^2\right]} \right\}^2 . \tag{5.69}$$

Not only are the interacting theory's energies present as poles, but the free theory's two-particle energies are accounted for as zeros in the numerator, thereby removing them from the spectral function. The fact that the function is squared accounts for the square symmetry of the torus.

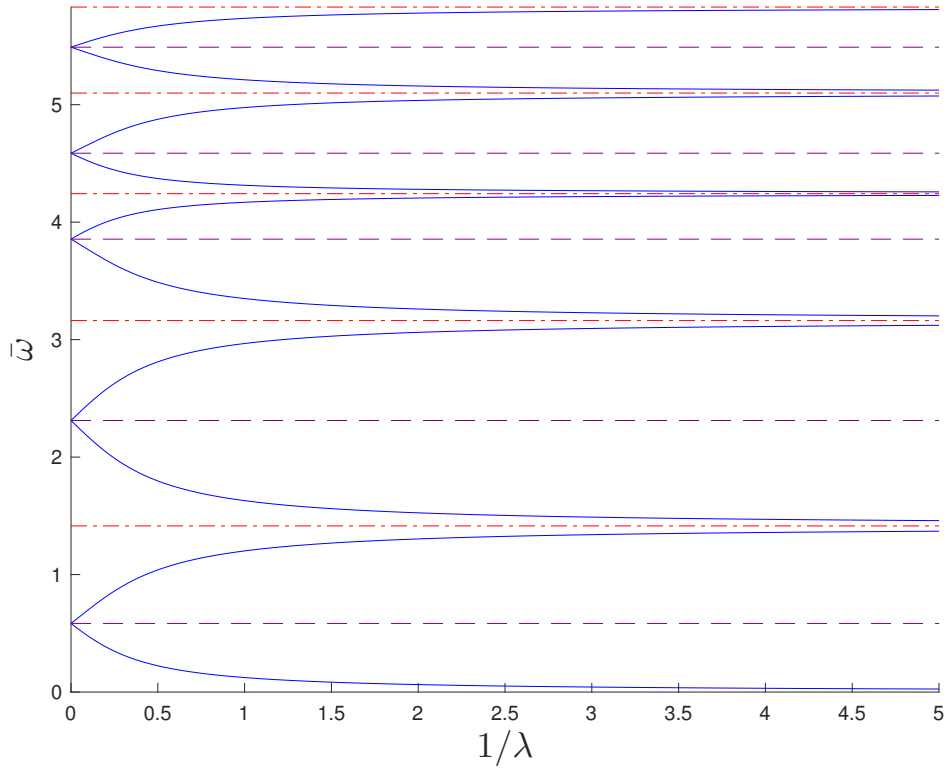

Figure 5.2: Plot of the modes of the Dirac-CS theory as a function of $1/\lambda$. When $1/\lambda \to 0$, the CS term vanishes, and the energies are two-fold degenerate, occurring when $\Pi_f^{xx} = 0$. These are marked with the dashed purple line. As $1/\lambda$ becomes large, the lowest mode approaches zero and all others approach the two-particle energies of the free theory, shown with a dash-dotted red line. ($\bar{\omega} = L\omega/2\pi$, $\lambda = N_f/k$.)

When k is non-zero, the degeneracy splits. The energies are depicted in Fig. 5.1 as the intersection points of Π_f^{xx} and $\pm|\omega|/2\pi\lambda$ for $\lambda = 4$. Fig. 5.2 plots the first few modes in blue as a function of $1/\lambda$, and for several values of λ, the first ten modes are listed in Table 5.4. When λ is very large, these modes have only a small splitting and are nearly the same as in QED_3, shown with the purple dashed line in Fig. 5.2. Conversely, as $\lambda \to 0$, the lowest mode ω_0^* approaches zero while all other levels approach one of the free theory two-particle energies, depicted with a dash-dotted red line in Fig. 5.2.

The lowest energy level, ω_0^*, can be identified as the splitting between the groundstates of the pure CS theory induced by matter. In the limit of λ and ω_0^* very small, the topological degeneracy is restored (albeit in the $k \to \infty$ limit). This aligns with out expectation that gauge fluctuations are suppressed at large k even when N_f is small [26]. In a similar fashion, when the fermions have a large mass M_f, we find $\lim_{\omega\to 0}\Pi_f^{xx}(\omega, 0) \sim e^{-M_f}$, once again implying an effective topological ground-state degeneracy.

5.3.2 Finite external momentum, $\boldsymbol{q} \neq 0$

The situation for finite external momenta is very similar. Using Eq. (5.65), along with Eqs. (D.25) and (D.26), all levels can be numerically evaluated for any value of λ.

The next-lowest energies occur when the total momentum is $\boldsymbol{q}_1 = 2\pi(1, 0)/L$, or any other of the momenta related to it by a $\pi/2$ rotation: $2\pi(0, 1)/L$, $2\pi(-1, 0)/L$, and $2\pi(0, -1)/L$. The C_4 symmetry of the square torus implies an additional four-fold degeneracy for all energy levels which would not generally be present. For these particular momenta, it turns out that the second term of $K_{\boldsymbol{q}_1}(\omega)$ in Eq. (5.65) vanishes for all ω when $k = 0$, and the zeros of the determinant can be found by separately solving for the zeros of Π_f^{00} and $\Pi_f^T = \Pi_f^{xx} + \Pi_f^{yy} + \omega^2\Pi_f^{00}/\boldsymbol{q}^2$. These functions are plotted in Fig. 5.3 and the resulting modes are given in Table 5.1 along with the results for $\boldsymbol{q}_2 = 2\pi(1, 1)/L$.

$\lambda = N_f/k$							
0	1/10	1/4	1/2	1	4	10	∞
0	0.012851	0.032056	0.063615	0.123519	0.347859	0.475391	0.584130
	1.39173	1.358213	1.303479	1.201486	0.859690	0.700684	
1.4142136	1.436722	1.470375	1.525588	1.629405	1.990723	2.171077	2.311525
	3.142113	3.111848	3.061891	2.966946	2.626458	2.450844	
3.162278	3.182355	3.212169	3.260552	3.349688	3.637930	3.765391	3.855225
	4.235129	4.223855	4.205187	4.169170	4.025093	3.935641	
4.242641	4.250129	4.261281	4.279522	4.313961	4.443737	4.761364	4.586816
	5.086480	5.067543	5.036016	4.975471	4.519975	4.660037	
5.099020	5.111437	5.129740	5.159072	5.211794	5.371116	5.439288	5.489309
	5.820132	5.804317	5.779259	5.734850	5.599761	5.537818	

Table 5.4: Dirac-Chern-Simons modes at N_f, $k = \infty$ with zero external momentum, $\boldsymbol{q} = 0$. ($\bar{\omega} = LE/2\pi$.)

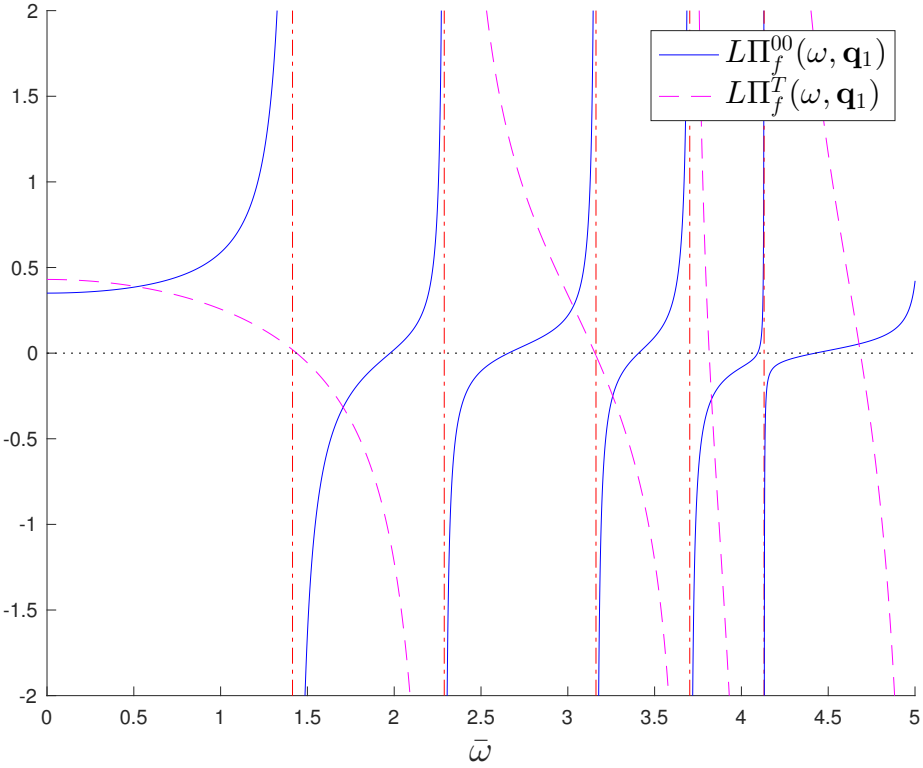

Figure 5.3: Plot of $\Pi_f^{00}(\omega, \boldsymbol{q}_1)$ and $\Pi_f^{T}(\omega, \boldsymbol{q}_1)$ for $\boldsymbol{q}_1 = 2\pi(1,0)/L$, shown in solid blue and dashed magenta respectively. The vertical dash-dotted lines in red denote the two-particle energies of the free theory, $E_f(\boldsymbol{q}_1, \boldsymbol{p})$. ($\bar{\omega} = L\omega/2\pi$.)

5.4 Conclusion

This paper has described the structure of 2+1 dimensional conformal gauge theories on the two-torus $\boldsymbol{T}^2$. We computed the partition function on $\boldsymbol{T}^2 \times \mathbb{R}$ in the limit of large fermion flavor number, N_f, using strategies similar to those employed for the computation on the three-sphere $\boldsymbol{S}^3$ in Ref. 97. We also deduced the energies of the low-lying states in the spectrum. For large N_f, most of the states are simply given by the sum of the free fermion energies with anti-periodic boundary conditions, as established in Appendix D.3. However, singlet combinations of pairs of fermions which couple to the current operator are strongly renormalized even at $N_f = \infty$: these states appear instead as bound states given by the zeros of the effective action for the gauge field. A similar phenomenon appears [189] in the O(N) Wilson-Fisher conformal theory.

These results should be useful in identifying possible realizations of non-trivial conformal field theories in exact diagonalization studies of model quantum spin systems in a manner similar to the study in Ref. 163. For instance, focusing on the $\boldsymbol{q} = (0, 0)$ sector, a comparison of Tables 5.2 and 5.3 indicates the existence of a two-fold degenerate singlet state with significantly lower energy than the $(N_f^2 - 1)$-fold generate fermion states. Although higher order effects from both the finite-N CFT and the numerics will undoubtedly split the energies of these fermion states, it is reasonable to predict that a significant gap will remain. This and similar trends between numerics and analytics could serve as a useful diagnostic tool for the state being simulated.

Chapter 6

Fermionic spinon theory of square lattice spin liquids near the Néel state

Quantum fluctuations of the Néel state of the square lattice antiferromagnet are usually described by a $\mathbb{CP}^1$ theory of bosonic spinons coupled to a U(1) gauge field, and with a global SU(2) spin rotation symmetry. Such a theory also has a confining phase with valence bond solid (VBS) order, and upon including spin-singlet charge 2 Higgs fields, deconfined phases with $\mathbb{Z}_2$ topological order possibly intertwined with discrete broken global symmetries. We present dual theories of the same phases starting from a mean-field theory of fermionic spinons moving in π-flux in each square lattice plaquette. Fluctuations about this π-flux state are described by 2+1 dimensional quantum chromodynamics (QCD_3) with a SU(2) gauge group and $N_f = 2$ flavors of massless Dirac fermions. It has recently been argued by Wang *et al.* [179] that this QCD_3 theory describes the Néel-VBS quantum phase transition. We introduce adjoint Higgs fields in QCD_3, and obtain fermionic dual descriptions of the phases with $\mathbb{Z}_2$ topological order obtained earlier using the bosonic $\mathbb{CP}^1$ theory. We also present a fermionic spinon derivation of the monopole Berry phases in the U(1) gauge theory of the VBS state. The global phase diagram of these phases contains multi-critical points, and our results imply new boson-fermion dualities between critical gauge theories of these points.

6.1 Introduction

Spin liquid states of the square lattice antiferromagnet, with global SU(2) spin rotation symmetry, have long been recognized as important ingredients in the theory of the cuprate

high temperatures superconductors [8, 16, 96, 148]. The earliest established examples of gapped states were 'chiral spin liquids,' which were constructed by analogy to the fractional quantum Hall states [83, 188]. These have a topological order which is not compatible with time-reversal symmetry. Soon after, '$\mathbb{Z}_2$ spin liquids' were proposed [12, 45, 54, 145, 157, 167, 183]: their topological order is compatible with time-reversal symmetry, and exactly solvable examples were later found in Kitaev's toric code and honeycomb lattice models [94, 95, 185]. Wen [184] used a fermionic spinon representation of the antiferromagnet to obtain a plethora of possible square lattice spin liquid states, distinguished by different realizations of 'symmetry-enriched' topological order [27, 43]. Wen's classification criterion was that the spin liquid states preserve time-reversal, SU(2) spin rotations, and all the square lattice space group symmetries. However, in the application to the cuprates, there is no fundamental reason all such symmetries should be preserved. If we also allow for breaking of time-reversal and/or point group symmetries, then many more spin liquid states are clearly possible, all of which preserve SU(2) spin rotations and the square lattice translational symmetry [15, 21, 145, 157]. This proliferation of possible spin liquids, intertwining with broken symmetries, sets up a daunting task of deciding which states, if any, are relevant for the pseudogap phase of the underdoped cuprates.

We need an energetic and physical criterion to focus on a smaller set of relevant spin liquid states, rather than relying exclusively on symmetry and topology. In recent work, Chatterjee *et al.* [23] proposed examining spin liquids which are proximate to the magnetically ordered Néel state. These proximate states are reachable by continuous (or nearly continuous) quantum phase transitions involving the long-wavelength excitations of the antiferromagnet. Specifically, they used a $\mathbb{CP}^1$ theory of quantum fluctuations of the Néel state, expressed in terms of bosonic spinons, z_α, to argue for the importance of 3 possible $\mathbb{Z}_2$ spin liquid states. These 3 states are identified here as A_b, B_b, and C_b, and appear below in Figs. 6.1(a) and 6.2(a). The state A_b preserves all symmetries [205], while B_b breaks lattice rotation symmetries and so has Ising-nematic order [145]. The state C_b breaks inversion

and time-reversal symmetries, but not their product, and was argued to possess current loop order.

A related motivation for the physical importance of these states comes from an examination of the classical phase diagram of frustrated antiferromagnets on the square lattice. By examining models with two-spin near-neighbor and four-spin ring exchange interactions, Ref. 23 found magnetically ordered states with canted, spiral, and conical spiral order near the Néel state. Quantum fluctuations about these classical ordered states can be described by extensions of the $\mathbb{CP}^1$ theory, and the 'quantum disordered' states obtained across a continous transition involving loss of magnetic order are precisely the three $\mathbb{Z}_2$ spin liquids, with the correspondence [22, 23]

$$\text{canted order} \to A_b\,, \quad \text{spiral order} \to B_b\,, \quad \text{conical spiral order} \to C_b\,. \tag{6.1}$$

One of the purposes of the present paper is to present a unified theory of the 3 $\mathbb{Z}_2$ spin liquids noted above, but using the fermionic spinon approach [2, 3, 184]. For gapped $\mathbb{Z}_2$ spin liquid states, a mapping between the fermionic and bosonic spinons approaches has been achieved for specific states on the kagome, triangular, square, and rectangular lattices [21, 43, 106, 107, 136, 204, 205, 208, 211]. This mapping relies on the fusion rules of the toric code [94]: the fusion of any two of the anyon species yields the third. In $\mathbb{Z}_2$ spin liquids, the three types of anyons are bosonic spinons, fermionic spinons, and a bosonic $\mathbb{Z}_2$-flux spinless vison. We will extend such mappings here to the states of interest on the square lattice, but using a method which allows us to treat the 3 $\mathbb{Z}_2$ spin liquids and the quantum phase transitions between them in a unified manner. We will obtain a phase diagram of the states proximate to the Néel state using the fermionic spinon approach, and propose critical theories of the phase transitions involving massless Dirac fermions. The connection to the earlier analysis [23] using the bosonic spinons of the $\mathbb{CP}^1$ model will also lead us to propose new boson-fermion dualities of the strongly-coupled, gapless, quantum field theories describing the (multi-)critical points.

Our point of departure will be a boson-fermion duality of a conformal field theory (CFT) proposed by Wang *et al.* [179]. They examined the critical theory of the Néel-valence bond solid (VBS) transition in the $\mathbb{CP}^1$ theory [143, 144, 166, 170], and proposed that it was equivalent to quantum chromodynamics (QCD) with a SU(2) gauge group and $N_f = 2$ flavors of massless, two-component Dirac fermions (note: the SU(2) gauge group is not to be confused with the global SU(2) spin rotation symmetry). The latter theory can also be obtained from the fermionic spinon approach to the square lattice antiferromagnet: it describes fluctuations about a π-flux mean-field theory [2, 3, 184], which is labeled by Wen as SU2Bn0n1.

Starting from the SU(2) QCD_3 theory, we will explore routes to condensing Higgs fields for fermionic bilinears, so that the SU(2) gauge group is ultimately broken down to $\mathbb{Z}_2$ and we obtain gapped spin liquids with $\mathbb{Z}_2$ topological order. Our main results are contained in the phase diagrams in Fig. 6.2. These phase diagrams contain the phases A_f, B_f and C_f, which are fermionic counterparts of the A_b, B_b, and C_b states obtained from the bosonic $\mathbb{CP}^1$ theory.

One important feature of the fermionic phase diagram in Fig. 6.1(b) is that it does not contain the counterparts of the magnetically ordered Néel and canted states in the bosonic phase diagram in Fig. 6.1(a). Instead Fig. 6.1(b) contains two critical phases, with massless Dirac fermions interacting with gapless SU(2) and U(1) gauge bosons. Building on the fermion-boson equivalence of Wang *et al.* [179], we argue here that these critical phases of Fig. 6.1(b) are unstable to the corresponding magnetically ordered phases in Fig. 6.1(b); the instability is assumed to be driven by relevant operators which are allowed by the symmetries of the underlying square lattice antiferromagnet. However, given the strongly-coupled nature of the critical theories, this conclusion is based upon circumstantial, rather than firm, evidence.

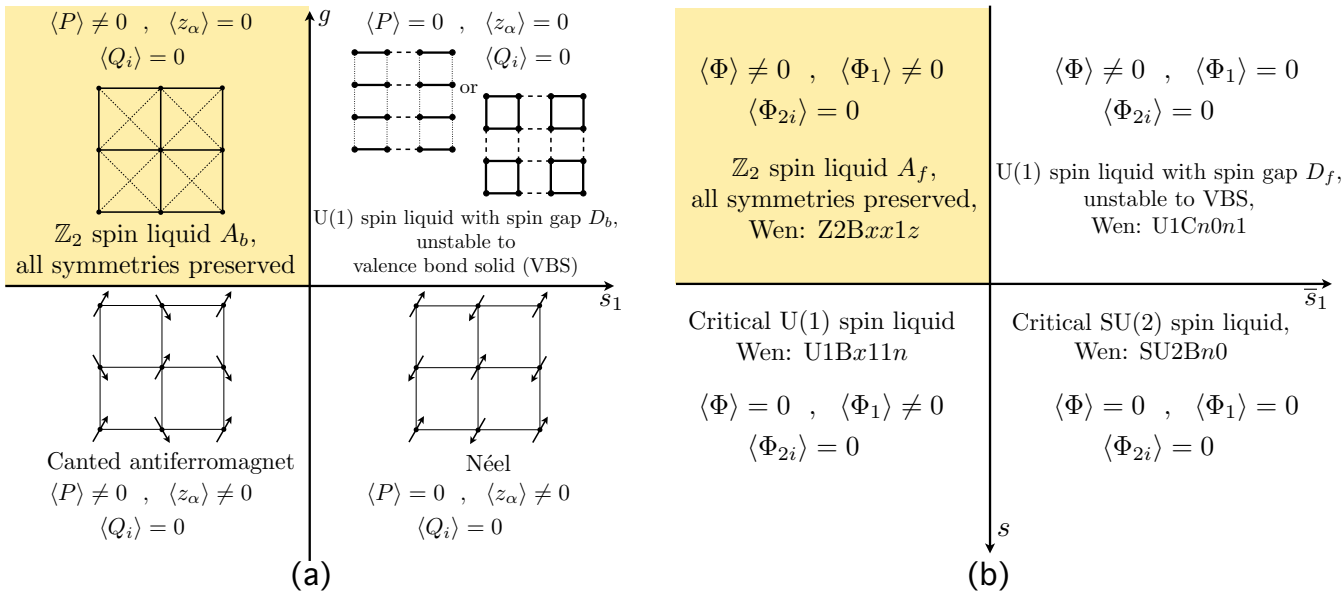

Figure 6.1: (a) Schematic phase diagram of the $\mathbb{CP}^1$ theory in Eq. (6.4) as a function of g and s_1 (s_2 in Eq. (6.7) is large and positive); Eq. (6.2) describes the deconfined critical Néel-VBS transition at a critical $g = g_c$. (b) Schematic phase diagram of the SU(2) QCD_3 theory with $N_f = 2$ flavors of massless Dirac fermions in Eq. (6.6) as a function of s and $\overline{s}_1$ ($\overline{s}_2$ in Eq. (6.8) is large and positive). The 'Wen' labels refer to the naming scheme in Ref. 184. The $\mathbb{Z}_2$ spin liquids A_b and A_f in (a) and (b) are argued to be topologically identical, as are the confining states with VBS order. The critical spin liquids in (b) to be unstable to the corresponding phases with magnetic order in (a), with the critical SU(2) spin liquid surviving only at the Néel-VBS transition. All $\mathbb{Z}_2$ spin liquids are shown shaded in all figures.

6.1.1 Summary of results

Let us first recall the bosonic spinon approach [10, 23] to the phases in Fig. 6.1(a). This is obtained by extending the Lagrangian for the theory of deconfined criticality for the Néel-VBS transition [156]

$$\mathcal{L}_{dcp} = \frac{1}{g} |(\partial_\mu - ib_\mu) z_\alpha|^2 + S_B \, . \tag{6.2}$$

The Lagrangian is in three spacetime dimensions with μ a spacetime index in Minkowski signature $(+,-,-)$, and $\alpha, \beta = \uparrow, \downarrow$ so there is global SU(2) spin rotation symmetry. The Néel order parameter is $z^*_\alpha \sigma^a_{\alpha\beta} z_\beta$, where σ^a are the Pauli matrices. The U(1) gauge field b_μ is compact, and monopole tunneling events are permitted, and associated with a Berry phase S_B [53, 144]. The spinons are represented by the bosonic complex scalar z_α which is of unit length

$$\sum_\alpha |z_\alpha|^2 = 1 \, , \tag{6.3}$$

and carries unit U(1) charge. For small g, z_α is condensed, and this yields the Néel phase with broken spin rotation symmetry. For large g, z_α is not condensed, and we appear to obtain a U(1) spin liquid (which we call D_b) with a gapless photon b_μ, and gapped z_α spinons. However, the condensation of monopoles yields the confinement of spinons and the appearance of VBS order [143, 144]. The transition from the Néel state to the VBS is described by a deconfined critical theory [166, 170] at $g = g_c$ in which monopoles are suppressed.

We will now extend $\mathcal{L}_{dcp}$ by including complex, charge 2 Higgs fields whose condensation can induce phases with $\mathbb{Z}_2$ topological order, while preserving SU(2) spin rotation symmetry. We can construct such Higgs fields by pairing spinons, but the simplest possibility, $\varepsilon_{\alpha\beta} z_\alpha z_\beta$, vanishes identically. Any such spinon pair Higgs field must involve gradients, and the simplest non-vanishing cases involve a single temporal or spatial gradient. We consider first the Higgs field, P, conjugate to a pair of spinons with a single temporal gradient, and will include the

spatial gradient Higgs field, Q_i later. The Lagrangian for z_α, b_μ, and P is

$$\mathcal{L}_b = \mathcal{L}_{dcp} + |(\partial_\mu - 2ib_\mu)P|^2 - s_1|P|^2 + \lambda_1 P^* \varepsilon_{\alpha\beta} z_\alpha \partial_0 z_\beta + \lambda_1 P \varepsilon_{\alpha\beta} z_\alpha^* \partial_0 z_\beta^* + \dots , \tag{6.4}$$

where $\varepsilon_{\alpha\beta}$ is the unit anti-symmetric tensor, and so SU(2) spin rotation symmetry is maintained. For s_1 large and positive, when there is no P condensate, we obtain the phases of $\mathcal{L}_{dcp}$ already described. For smaller s_1, when there is a P Higgs condensate, we obtain the canted antiferromagnet and the symmetric $\mathbb{Z}_2$ spin liquid A_b for small and large g respectively, as shown in Fig. 6.1(a). The $\mathbb{Z}_2$ spin liquid A_b was first obtained in Ref. 205, where it was called $\mathbb{Z}_2[0,0]$.

Now we turn to our results for the fermionic counterpart of Fig. 6.1(a), which is shown in Fig. 6.1(b). We start with fermionic equivalent of the deconfined Néel-VBS critical theory, which was identified by Wang *et al.* [179] as SU(2) QCD_3 with $N_f = 2$, described by the Lagrangian

$$\mathcal{L}_{\text{QCD}_3} = i\text{tr}\left(\bar{X}\gamma^\mu(\partial_\mu X + iXa_\mu)\right) \tag{6.5}$$

Here X represents the massless Dirac fermions, γ^μ are Dirac matrices, and the details of the index structure will be specified in Section 6.2.2. The SU(2) gauge field is represented by a_μ. The fermion kinetic term in Eq. (6.5) has a global SO(5) symmetry, which is an enlargement of the global SU(2) spin rotation and $\mathbb{Z}_4$ lattice rotation symmetries of the lattice Hamiltonian [179]. To obtain Fig. 6.1(b), we extend Eq. (6.5) in Section 6.3.2 by adding two real Higgs fields, $\Phi = \Phi^a\sigma^a$ and $\Phi_1 = \Phi_1^a\sigma^a$, both of which transform as adjoints of the gauge SU(2). So we have the Lagrangian

$$\begin{aligned}\mathcal{L}_f = \mathcal{L}_{\text{QCD}_3} \quad &+ \quad (D_\mu\Phi^a)^2 - s\left(\Phi^a\right)^2 + \lambda_2\,\Phi^a\,\text{tr}\left(\sigma^a\bar{X}\mu^y X\right) \\ &+ \quad (D_\mu\Phi_1^a)^2 - \bar{s}_1\left(\Phi_1^a\right)^2 + i\lambda_3\,\Phi_1^a\,\text{tr}\left(\sigma^a\bar{X}\partial_0 X\right) + \cdots\end{aligned} \tag{6.6}$$

Here D_μ is a covariant derivative, a is SU(2) gauge index, σ^a are Pauli matrices, while μ^y is a Pauli matrix which acts on the flavor space. We assume the higher order terms are such

that when both Higgs condensates are present, $\langle\Phi\rangle$ and $\langle\Phi_1\rangle$ will be oriented perpendicular to each other in SU(2) gauge space. For instance, the topological order would be stabilized by the presence of a term like $-\mu\left(\Phi^a\Phi_1^a\right)^2$ when $\mu > 0$. By varying s and $\overline{s}_1$ we can obtain four phases in which the two Higgs condensates are either present or absent, as shown in Fig. 6.1(b). We will show in Section 6.4.1 that the gapped $\mathbb{Z}_2$ spin liquid, A_f, so obtained is topologically identical to the $\mathbb{Z}_2$ spin liquid A_b in Fig. 6.1(a).

We will also examine the U(1) spin liquid with a spin gap, D_f, obtained when there is only a Φ condensate. We compute the monopole Berry phases in this state in Section 6.4.3, and find that they are identical to those indicated by S_B in the bosonic theory in Eq. (6.4). As monopoles are eventually expected to proliferate in this U(1) spin liquid [143], we expect VBS order to appear, just as in the corresponding phase in Fig. 6.1(a).

Now we turn our attention to the critical U(1) and SU(2) spin liquids in Fig. 6.1(b). As we noted earlier, we expect that in the absence of fine-tuning, there are relevant perturbations to $\mathcal{L}_f$ which will drive these critical phases to the corresponding magnetically ordered phases in Fig. 6.1(a). These perturbations will break the SO(5) flavor symmetry of $\mathcal{L}_{\mathrm{QCD}_3}$ down to the symmetries of the underlying lattice Hamiltonian [179].

Finally, we note that both Figs. 6.1(a) and 6.1(b) contain multicritical points accessed by tuning 2 couplings where all 4 phases meet. A natural conjecture is that these multicritical points are identical to each other. On the bosonic side, this is the theory obtained by tuning g and s_1, so that both the matter fields z_α and P are critical. On the fermionic side, this is the theory obtained by tuning s and $\overline{s}_1$, so that the bosonic matter fields Φ and Φ_1 are critical, while the fermionic matter X remains critical. A further conjecture is that the Yukawa couplings λ_1 and λ_3 renormalize to zero at the multicritical point: then both the bosonic and fermionic theories will represent CFTs.

We also extend our results to include additional Higgs fields which lead to phases with $\mathbb{Z}_2$ topological order and broken lattice rotation and/or time-reversal symmetries. On the bosonic side, we introduce the complex, charge 2 Higgs field Q_i, where $i = x, y$ is a spatial

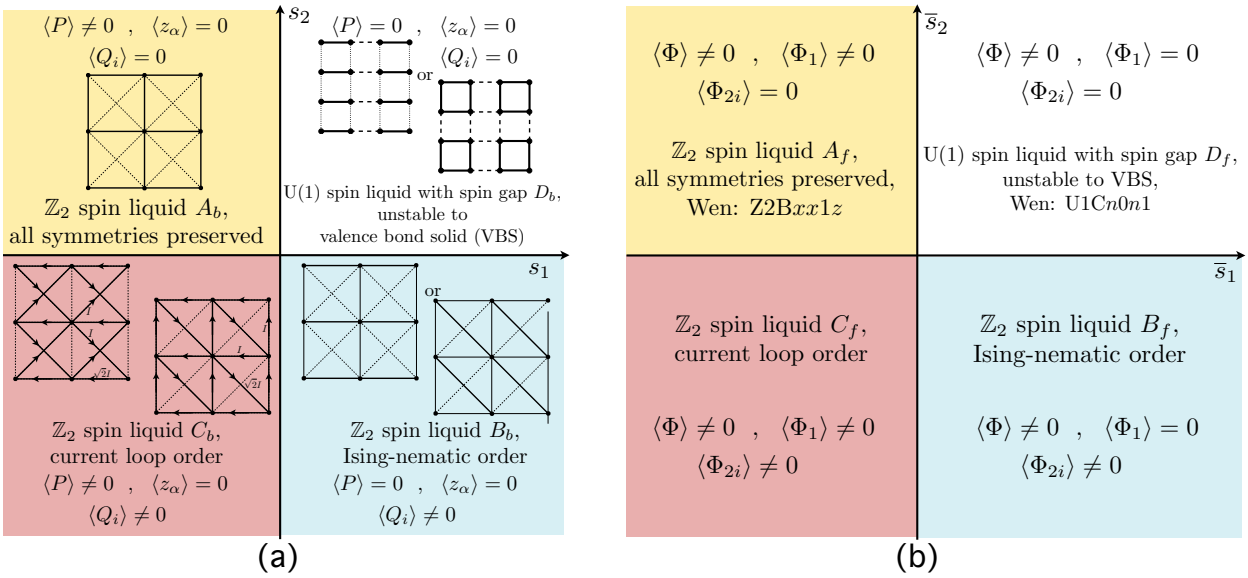

Figure 6.2: (a) Schematic phase diagram of the $\mathbb{CP}^1$ theory in Eqs. (6.4) and (6.7) as a function of s_1 and s_2 (for large g). (b) Schematic phase diagram of the SU(2) QCD$_3$ theory with $N_f = 2$ flavors of massless Dirac fermions in Eqs. (6.6) and (6.8) as a function of $\overline{s}_1$ and $\overline{s}_2$ (for $s < 0$ and $|s|$ large). All four phases in (a) and (b) are argued to be topologically identical. So for the $\mathbb{Z}_2$ spin liquids $A_b = A_f$, $B_b = B_f$, and $C_b = C_f$. Phases B_f and C_f do not appear in Wen's classification [184] because they break global symmetries.

index, leading to the Lagrangian [157]

$$\mathcal{L}_b' = \mathcal{L}_b + |(\partial_\mu - 2ib_\mu)Q_i|^2 - s_2|Q_i|^2 + \lambda_4\, Q_i^*\, \varepsilon_{\alpha\beta} z_\alpha \partial_i z_\beta + \lambda_4\, Q_i\, \varepsilon_{\alpha\beta} z_\alpha^* \partial_i z_\beta^* + \cdots \tag{6.7}$$

In the absence of magnetic order, so that g is large, the phase diagram obtained by varying s_1 and s_2, with possible condensates of P and Q_i is shown in Fig. 6.2(a). There are now 3 $\mathbb{Z}_2$ spin liquids, and these meet at a possible multicritical point with the VBS state.

On the fermionic side, in Section 6.3.3, we add another real Higgs field, Φ_{2i}, which transforms as the adjoint of SU(2). We now extend $\mathcal{L}_f$ in Eq. (6.6) to

$$\mathcal{L}_f' = \mathcal{L}_f + (D_\mu \Phi_{2i}^a)^2 - \overline{s}_2\, (\Phi_{2i}^a)^2 + i\lambda_5\, \Phi_{2i}^a\, \mathrm{tr}\left(\sigma^a \bar{X} \partial_i X\right) + \cdots \tag{6.8}$$

The phase diagram obtained by varying $\overline{s}_1$ and $\overline{s}_2$, to obtain possible Higgs condensates of Φ_1 and Φ_{2i} is shown in Fig. 6.2(b). We assume that s is negative, so that a Higgs condensate Φ is always present in Fig. 6.2(b). We obtain 3 $\mathbb{Z}_2$ spin liquids in Fig. 6.2(b), and one of our

main results is that these are topologically identical to the corresponding $\mathbb{Z}_2$ spin liquids in Fig. 6.2(a). The relative orientations of the condensates of Φ, Φ_1, and Φ_2 in gauge space are discussed in Section 6.3.4. Note that the spin liquids B_f and C_f do not appear in Wen's classification: this is because they break global symmetries associated with the appearance of Ising-nematic and current loop order respectively.

Again, the multicritical points in Figs. 6.2(a) and 6.2(b), if present, are expected to map to each other, setting up possible dualities of critical fermionic and bosonic gauge theories.

The paper is organized as follows. In Sec. 6.2, we provide the background information necessary for our analysis. We begin by discussing the relevant symmetries and reviewing the π-flux phase, showing that its low energy dynamics are described by $N_f = 2$ QCD. The section finishes with a brief summary of the boson-fermion duality proposed by Wang *et al.* [179]. Sec. 6.3 explains our procedure for finding spin liquids and how these phases are classified. Using this, we next list all gapped spin liquids accessible using our methods and which are either fully symmetric or have Ising-nematic order. We also describe how spin liquids breaking additional discrete symmetries can be realized, with particular focus given to the $\mathbb{Z}_2$ spin liquid C_f with current-loop order. These spin liquids, both symmetric and ordered, are subsequently identified in Sec. 6.4. We start by using the symmetry fractionalization technique to verify the correspondence between the $\mathbb{Z}_2$ spin liquids we study and those realized using Schwinger bosons. This allows us to verify the equivalence of A_f, B_f, and C_f with A_b, B_b, and C_b. A comparison with Wen's [184] lattice classification scheme is also provided before we turn to the unstable U(1) spin liquid D_f and demonstrate that the proliferation of monopoles necessarily results in a confined phase with VBS order. We conclude in Sec. 6.5 with some discussion.

We note a related paper [78] which appeared while our work was being completed, describing phases of antiferromagnets with only a U(1), 'easy-plane', global spin rotation symmetry.

6.2 π-FLUX PHASE AND $N_f = 2$ QCD

6.2.1 MODEL AND SYMMETRIES

We are interested in this paper in spin liquid states of the spin-1/2 Heisenberg model on the square lattice, with Hamiltonian of the form

$$H_{\mathrm{H}} = J \sum_{\langle ij \rangle} \boldsymbol{S_i} \cdot \boldsymbol{S_j} + \cdots \tag{6.9}$$

where the summation is over nearest-neighbours and the ellipsis indicates interactions over further distances or terms which comprise three or more spin operators. In the absence of these higher order terms, the ground state is known to have Néel order; nonetheless, we will operate under the assumption that the terms contained in the ellipsis provide enough frustration that the ground state loses long-range magnetic order.

It has been shown that a fully symmetric phase describing spin 1/2's on a square lattice must have topological order [59, 103]. It turns out that there are many possible such symmetric spin liquids, and a large body of work has been directed at classifying these phases. One such scheme is provided by Wen in Ref. 184. He extended the physical symmetry group to include gauge transformations, and showed that distinct spin liquids can be differentiated based on the behaviour of the gauge degrees of freedom. We take this approach and apply it it to a continuum formulation of the phases in question. However, as discussed, the true hallmark of a spin liquid is topological order, not the absence of broken symmetries, and there is no *a priori* reason to restrict to fully symmetric spin liquids. We therefore also consider phases in which certain discrete symmetries are broken.

The physical symmetries relevant to the problem are the SU(2) spin symmetry, time reversal $\mathcal{T}$, and the space group symmetries. The space group of the lattice is generated by the two translation operators, T_x and T_y, the inversion operator P_y, and the rotation

operator $R_{\pi/2}$. These act on the lattice sites as

$$\begin{aligned} T_x &: (i_x, i_y) \mapsto (i_x + 1, i_y), & T_y &: (i_x, i_y) \mapsto (i_x, i_y + 1), \\ P_y &: (i_x, i_y) \mapsto (i_x, -i_y), & R_{\pi/2} &: (i_x, i_y) \mapsto (-i_y, i_x). \end{aligned} \tag{6.10}$$

In addition, these generators imply a symmetry under inversion of the x-coordinate, $P_x = R_{\pi/2} P_y R_{\pi/2}^{-1}$, as well as reflection about the $x = y$ axis, $P_{xy} = P_y R_{\pi/2}^{-1}$. An equivalent definition of the space group is given through its commutation relations:

$$\begin{aligned} T_y^{-1} T_x T_y T_x^{-1} &= \mathbb{1}, & P_y^{-1} R_{\pi/2} P_y R_{\pi/2} &= \mathbb{1}, \\ P_y^{-1} T_x P_y T_x^{-1} &= \mathbb{1}, & R_{\pi/2}^4 &= \mathbb{1}, \\ P_y^{-1} T_y P_y T_y &= \mathbb{1}, & R_{\pi/2}^{-1} T_x R_{\pi/2} T_y &= \mathbb{1}, \\ P_y^2 &= \mathbb{1}, & R_{\pi/2}^{-1} T_y R_{\pi/2} T_x^{-1} &= \mathbb{1}. \end{aligned} \tag{6.11}$$

The generators all commute with time reversal, $G^{-1}\mathcal{T}^{-1}G\mathcal{T} = \mathbb{1}$, $G = \{T_x, T_y, P_y, R_{\pi/2}\}$. Because the fundamental degrees of freedom are bosonic spins, we have $\mathcal{T}^2 = \mathbb{1}$.

Naturally, a different set of commutation relations is required to describe the space group in a symmetry broken phase, and these will be presented as needed. To make contact with these phases, we will often describe the action of P_x independently from the other symmetries even when considering fully symmetric spin liquids.

6.2.2 Heisenberg antiferromagnet and the π-flux state

We now present a lattice derivation of the π-flux model. We begin by re-writing the spin operators in terms of so-called slave fermions [184]:

$$\boldsymbol{S_i} = \frac{1}{2} f_{\boldsymbol{i}\alpha}^\dagger \boldsymbol{\sigma}_{\alpha\beta} f_{\boldsymbol{i}\beta}, \tag{6.12}$$

where $\boldsymbol{\sigma} = (\sigma^x, \sigma^y, \sigma^z)$ are the Pauli matrices. This expression introduces additional degrees of freedom and therefore cannot reproduce the Hilbert space of the spin operators without be-

ing supplemented by a constraint. It can easily be verified that provided $\sum_\alpha f^\dagger_{\boldsymbol{i}\alpha} f_{\boldsymbol{i}\alpha} = 1$ on *every* site, the representation in Eq. (6.12) is correct. This further implies that $\sum_{\alpha,\beta} \epsilon_{\alpha\beta} f_{\boldsymbol{i}\alpha} f_{\boldsymbol{i}\beta} = \sum_{\alpha,\beta} \epsilon_{\alpha\beta} f^\dagger_{\boldsymbol{i}\alpha} f^\dagger_{\boldsymbol{i}\beta} = 0$ where $\epsilon_{\alpha\beta}$ is the fully anti-symmetric 2-index tensor. By defining a matrix

$$\mathcal{X}_{\boldsymbol{i}} = \begin{pmatrix} f_{\boldsymbol{i}\uparrow} & -f^\dagger_{\boldsymbol{i}\downarrow} \\ f_{\boldsymbol{i}\downarrow} & f^\dagger_{\boldsymbol{i}\uparrow} \end{pmatrix} \tag{6.13}$$

we see that these constraints generate an SU(2) gauge symmetry which acts on $\mathcal{X}_{\boldsymbol{i}}$ as

$$\mathrm{SU}(2)_g : \mathcal{X}_{\boldsymbol{i}} \to \mathcal{X}_{\boldsymbol{i}} U^\dagger_{g,\boldsymbol{i}}. \tag{6.14}$$

The physical spin symmetry acts on $\mathcal{X}_{\boldsymbol{i}}$ on the left:

$$\mathrm{SU}(2)_s : \mathcal{X}_{\boldsymbol{i}} \to U_s \mathcal{X}_{\boldsymbol{i}}. \tag{6.15}$$

The absence of a charge degree of freedom suggests that a more natural fermionic representation may be obtained by replacing the complex f-fermions with Majoranas:

$$f_{\boldsymbol{i}\uparrow} = \frac{1}{\sqrt{2}} \left(\chi_{\boldsymbol{i},0} + i\chi_{\boldsymbol{i},z}\right), \qquad f_{\boldsymbol{i}\downarrow} = \frac{1}{\sqrt{2}} \left(-\chi_{\boldsymbol{i},y} + i\chi_{\boldsymbol{i},x}\right), \tag{6.16}$$

where $\chi^\dagger_{\boldsymbol{i},a} = \chi_{\boldsymbol{i},a}$ and $\{\chi_{\boldsymbol{i},a}, \chi_{\boldsymbol{j},b}\} = \delta_{ab}\delta_{\boldsymbol{ij}}$. In this notation, the matrix $\mathcal{X}_{\boldsymbol{i}}$ is written $\mathcal{X}_{\boldsymbol{i}} = \frac{1}{\sqrt{2}} \left(\chi_{\boldsymbol{i},0} + i\chi_{\boldsymbol{i},a}\sigma^a\right)$ and the local constraints can be expressed as the conditions

$$\mathrm{tr}\left(\sigma^a \mathcal{X}^\dagger_{\boldsymbol{i}} \mathcal{X}_{\boldsymbol{i}}\right) = 0. \tag{6.17}$$

The first step to an approximate solution to H_{H} is to loosen the local constraint on the fermions to

$$\left\langle \mathrm{tr}\left(\sigma^a \mathcal{X}^\dagger_{\boldsymbol{i}} \mathcal{X}_{\boldsymbol{i}}\right) \right\rangle = 0. \tag{6.18}$$

Next, we decouple the 4-fermion interaction through a Hubbard-Stratonovich transformation, leaving a quadratic mean field Hamiltonian. The most general such Hamiltonian which can

be made symmetric under spin rotation symmetry is [24, 184]

$$H_{\mathrm{MF}} = \sum_{\langle \boldsymbol{ij} \rangle} \left[i\alpha_{\boldsymbol{ij}} \mathrm{tr}\left(\mathcal{X}_{\boldsymbol{i}}^{\dagger}\mathcal{X}_{\boldsymbol{j}}\right) + \beta_{\boldsymbol{ij}}^{a} \mathrm{tr}\left(\sigma^{a}\mathcal{X}_{\boldsymbol{i}}^{\dagger}\mathcal{X}_{\boldsymbol{j}}\right) + i\gamma_{\boldsymbol{ij}} \mathrm{tr}\left(\sigma^{a}\mathcal{X}_{\boldsymbol{i}}^{\dagger}\sigma^{a}\mathcal{X}_{\boldsymbol{j}}\right) \right], \tag{6.19}$$

where $\alpha_{\boldsymbol{ij}}$, $\beta_{\boldsymbol{ij}}^{a}$, and $\gamma_{\boldsymbol{ij}}$ are real numbers. In accordance with its name, the π-flux state is obtained by threading a π-flux through every plaquette: we take $\beta_{\boldsymbol{ij}}^{a} = \gamma_{\boldsymbol{ij}} = 0$ and

$$\alpha_{\boldsymbol{ij}} = -\alpha_{\boldsymbol{ji}}, \qquad \alpha_{\boldsymbol{i}+\hat{\boldsymbol{x}},\boldsymbol{i}} = \alpha, \qquad \alpha_{\boldsymbol{i}+\hat{\boldsymbol{y}},\boldsymbol{i}} = (-1)^{i_x}\alpha. \tag{6.20}$$

This gives

$$H_{\pi} = -i\alpha \sum_{\boldsymbol{i}} \left[\mathrm{tr}\left(\mathcal{X}_{\boldsymbol{i}}\mathcal{X}_{\boldsymbol{i}+\hat{\boldsymbol{x}}}\right) + (-)^{i_x} \mathrm{tr}\left(\mathcal{X}_{\boldsymbol{i}}\mathcal{X}_{\boldsymbol{i}+\hat{\boldsymbol{y}}}\right) \right]. \tag{6.21}$$

While it is clear that this ansatz preserves the full SU(2) gauge and spin symmetries, the invariance of the π-flux Hamiltonian under the space group symmetries may be less clear. In particular, translations in the x-direction do not preserve the form of H_{π}. However, the original Hamiltonian can be recovered through a gauge transformation, implying that the symmetry transformed state is (gauge) equivalent to the original. Wen [184] termed this extended symmetry group the "projective symmetry group" (PSG) and used it to show the existence of eight distinct fully-symmetric SU(2) spin liquids on the square lattice. In his scheme, the Hamiltonian H_{π} describes the SU2Bn0 state (this is shown in Appendix E.3.1). We will discuss the PSG extensively in subsequent sections, albeit in a slightly different context than originally formulated. His scheme is briefly reviewed in Appendix E.2.

The band structure of H_{π} has two Dirac cones. We expand about these cones, labelling them by a valley index $v = 1, 2$. A convenient expression for the resulting theory is achieved by defining the 4×2 matrix operator

$$X_{\alpha,v;\beta} = \frac{1}{\sqrt{2}} \left(\chi_{0,v}\delta_{\alpha\beta} + i\chi_{a,v}\sigma_{\alpha\beta}^{a} \right), \tag{6.22}$$

where α, β, and v are spin, gauge, and valley indices respectively. The low energy excitation

of H_{MF} are described by the relativistic Dirac Lagrangian

$$\mathcal{L}_{\mathrm{MF}} = i\mathrm{tr}\left(\bar{X}\gamma^{\mu}\partial_{\mu}X\right) \tag{6.23}$$

where $\bar{\chi} = \chi^{T}\gamma^{0}$, $(\gamma^{0},\gamma^{x},\gamma^{y}) = (\tau^{y}, i\tau^{z}, i\tau^{x})$. Here and in what follows, we express operators in *real* time.

While Eq. (6.18) may hold in the ground state of H_{π}, the full constraint in Eq. (6.17) does not, and gauge fluctuations must be included to take this into account. The SU(2) gauge transformation in Eq. (6.14) becomes

$$\mathrm{SU}(2)_{g}: \; X \to XU_{g}^{\dagger}, \quad a_{\mu} \to U_{g}a_{\mu}U_{g}^{\dagger} + i\partial_{\mu}U_{g}U_{g}^{\dagger}, \tag{6.24}$$

in the continuum. As before, global spin rotations act the Majorana X on the left,

$$\mathrm{SU}(2)_{s}: X \to U_{s}X. \tag{6.25}$$

Letting $D_{\mu}^{a}X = \partial_{\mu}X + iXa_{\mu}$, the inclusion of quantum fluctuations results in the following Lagrangian:

$$\mathcal{L}_{\mathrm{QCD}_3} = i\mathrm{tr}\left(\bar{X}\gamma^{\mu}D_{\mu}^{a}X\right). \tag{6.26}$$

$\mathcal{L}_{\mathrm{QCD}_3}$ can be expressed in a more familiar form by defining Dirac fermions

$$\psi_{1,v} = \frac{i}{\sqrt{2}}\left(\chi_{x,v} - i\chi_{y,v}\right), \qquad \psi_{2,v} = -\frac{1}{\sqrt{2}}\left(\chi_{0,v} + i\chi_{z,v}\right). \tag{6.27}$$

In terms of these operators, the Lagrangian becomes

$$\mathcal{L}_{\mathrm{QCD}_3} = \sum_{v=1,2} i\bar{\psi}_{v}\gamma^{\mu}\left(\partial_{\mu} - ia_{\mu}^{a}\sigma^{a}\right)\psi_{v}. \tag{6.28}$$

That is, the low energy physics of the π-flux state is described by QCD_3 with $N_f = 2$ fermions. The Dirac representation is not nearly as useful as the Majorana representation of

$\mathcal{L}_{\mathrm{QCD}_3}$: while gauge transformations act of the ψ-fermions in the usual fashion, the action of the spin symmetry is nontrivial. We will therefore primarily use the form given in Eq. (6.26).

A side-effect of the expansion about the Dirac cones is that the χ fermions transform nontrivially under time reversal and the space group symmetries:

$$\begin{aligned} T_x &: \chi \to \mu^x \chi, & R_{\pi/2} &: \chi \to e^{i\pi\tau^y/4} e^{-i\pi\mu^y/4} \chi(-y, x), \\ T_y &: \chi \to \mu^z \chi, & P_x &: \chi \to \tau^z \mu^z \chi(-x, y), \\ \mathcal{T} &: \chi \to \tau^y \mu^y \chi, \quad i \to -i, & P_y &: \chi \to -\tau^x \mu^x \chi(x, -y). \end{aligned} \tag{6.29}$$

In addition, the spin and space group symmetries of the model are significantly enlarged at this fixed point. Not only is $\mathcal{L}_{\mathrm{QCD}_3}$ Lorentz invariant, but it is symmetric under rotations mixing the spin and valley indices of X: $X \to LX$, where L is a 4×4 unitary matrix. Because X is composed of Majorana fermions, there is an important reality condition,

$$X^* = \sigma^y X \sigma^y \,, \tag{6.30}$$

and therefore only L such that $L^T \sigma^y L = \sigma^y$ are allowed. This reduces what would have been a U(4) symmetry to Sp(4). Finally, since both $\mathrm{SU}(2)_g$ and Sp(4) share the nontrivial element -1, the true global symmetry is obtained by taking the quotient: $\mathrm{Sp}(4)/\mathbb{Z}_2 \cong \mathrm{SO}(5)$.

6.2.3 Dual description

As with any mean field approach involving a continuous gauge group, the existence of $\mathcal{L}_{\mathrm{QCD}_3}$ is by no means guaranteed once gauge fluctuations have been taken into account. However, in spite of some of the terminology, in this paper we do not view the π-flux 'phase' as a stable state of matter existing over a finite region in parameter space. Instead we treat it as a parent theory with instabilities potentially leading to U(1) and $\mathbb{Z}_2$ spin liquids, as well as to ordered phases like Néel and VBS. This approach is motivated by a duality between $\mathcal{L}_{\mathrm{QCD}_3}$ and $\mathbb{CP}^1$ proposed by Wang *et al.* [179] to describe the Néel-VBS transition. We

discuss the relation between $\mathbb{CP}^1$ and QCD_3 in this context.

One of the key components to their proposal is the SO(5) symmetry we just discussed. On the QCD_3 side of the duality, an order parameter for this symmetry is

$$n^j = \text{tr}\left(\bar{X}\Gamma^j X\right), \qquad \Gamma^j = \{\mu^x, \mu^z, \mu^y\sigma^x, \mu^y\sigma^y, \mu^y\sigma^z\}. \tag{6.31}$$

The symmetry transformations in Eq. (6.29) indicate that n^1 and n^2 are the VBS order parameters, while n^3, n^4, and n^5 correspond to the Néel order parameter. Using this, Refs. 1, 168, 175 showed that taking $\mathcal{L}_{\text{QCD}_3}$ to

$$\mathcal{L}_{\text{QCD}_3,\phi} = \mathcal{L}_{\text{QCD}_3} + m\,\phi^j\,\text{tr}\left(\bar{X}\Gamma^j X\right), \tag{6.32}$$

and subsequently integrating out the fermions, yields a non-linear sigma model for ϕ with a Wess-Zumino-Witten (WZW) term. This topological term manifests itself physically by making the defects of the order parameter of one symmetry transform nontrivially under the action of the other symmetry. These nontrivial correlations prompted Tanaka and Hu [175] and Senthil and Fisher [168] to propose this non-linear sigma model as a description of the critical theory describing the Landau-forbidden continuous phase transition between Néel and VBS.

Conversely, the $\mathbb{CP}^1$ formulation of the phase transition circumvents the obstruction to continuity by eschewing the traditional notion of an order parameter. While the Néel phase is entered through the condensation of $N^a = z^\dagger\sigma^a z$, the VBS phase is described by the proliferation of monopoles, events which change the flux of the gauge field by 2π (or, equivalently, change the global skyrmion number by one). Not only do these monopoles confine the U(1) gauge field, but, because they transform nontrivially under the space group, this symmetry is necessarily broken in the condensate. In spite of the very different forms the Néel and VBS order parameters take, numerics [121] have observed an emergent SO(5) symmetry between the two, implying that SO(5) emerges as a symmetry in the IR. In this version, the VBS portion of SO(5) order parameter is given by

$(\phi_1, \phi_2) = 2\,(\mathrm{Re}\,\mathcal{M}, \mathrm{Im}\,\mathcal{M})$ where $\mathcal{M}$ denotes the monopole operator, while the remaining pieces are simply $(\phi_3, \phi_4, \phi_5) = \left(z^\dagger \sigma^x z, z^\dagger \sigma^y z, z^\dagger \sigma^z z\right)$.

Wang et. al. [179] suggest that both of these models flow to the same SO(5) symmetric CFT in the IR. An important feature of this CFT is the absence of a relevant singlet operator. The critical point is instead obtained by tuning the coupling μ of a relevant, anistropic operator to zero,

$$\mathcal{L} = \mathcal{L}_{\mathrm{SO}(5)} + \mu \mathrm{O}_{an} \qquad \mathrm{O}_{an} \sim \frac{2}{5}\left(\phi_3^2 + \phi_4^2 + \phi_5^2\right) - \frac{3}{5}\left(\phi_1^2 + \phi_2^2\right). \tag{6.33}$$

When $\mu > 0$, the system has VBS order, while when $\mu < 0$, it orders along the Néel directions. The approach we take is slightly different in spirit to this proposal, and we discuss this further in Sec. 6.4.3.

6.3 Spin liquids proximate to the π-flux phase

In this section, we describe the Higgs descendants of QCD_3 and our approach to their classification. We start by discussing which operators can couple to the Higgs field, before turning to a more complete discussion of the projective symmetry group than what was provided in the previous section. Given a set of criteria described below, we conclude that there exists a single (spin) gapped U(1) spin liquid among the Higgs descendents of QCD_3. We next list all gapped and fully symmetry $\mathbb{Z}_2$ spin liquids, as well as all gapped $\mathbb{Z}_2$ spin liquids with Ising-nematic order. Special note is taken of the spin liquids A_f and B_f, though we wait until until Sec. 6.4.1 to prove their equivalence to A_b and A_f. The section finishes with a description of the gapped $\mathbb{Z}_2$ spin liquid with current-loop order we call C_f.

6.3.1 Higgs fields

We being by examining the set of operators we will be coupling to the Higgs field. QCD_3 is strongly coupled in the IR, and so very little can be said with certainty regarding the operators and their scaling dimensions in the IR. We focus on fermion bilinears since these

are the most relevant gauge invariant bosonic operators of the UV theory. Non-perturbative operators such as monopoles are not considered.

We consider interaction terms of the form

$$\mathrm{tr}\left(\varphi \bar{X} M X\right) = \varphi^a \mathrm{tr}\left(\sigma^a \bar{X} M X\right) \tag{6.34}$$

where $\varphi = \varphi^a \sigma^a$ is a generic Higgs field transforming in the adjoint representation of $\mathrm{SU}(2)_g$ and M is a matrix acting on the sublattice, colour, and/or flavour space of the fermions and which may or may not contain derivatives. The physical properties of the various possible Higgs phases are defined primarily by the bilinear it couples to.

Restricting for the moment to bilinears without derivatives, those which are charged under the gauge group are

$$\mathrm{tr}\left(\sigma^a \bar{X} \gamma^\mu X\right), \qquad \mathrm{tr}\left(\sigma^a \bar{X} \Gamma^j \gamma^\mu X\right), \qquad \mathrm{tr}\left(\sigma^a \bar{X} T^j X\right). \tag{6.35}$$

where $\Gamma^j = \{\mu^z, -\mu^x, \mu^y \sigma^a\}$ and $T^j = \{\mu^y, \sigma^a, \mu^x \sigma^a, \mu^z \sigma^a\}$ are the vector and adjoint representations of SO(5) respectively. The first set of operators are the gauge currents $J^{a,\mu}$. These cannot couple a Higgs field since the gauge theory description of the Heisenberg model is predicated on the requirement that these currents vanish. In fact, the gauge fields can be interpreted as Lagrange multipliers which have been added to $\mathcal{L}_{\mathrm{QCD}_3}$ in order to impose the $J^{a,\mu} = 0$ constraint.

No such obstacles exist for the other two sets of bilinears. The second group of operators, $\mathrm{tr}\left(\sigma^a \bar{X} \Gamma^a \gamma^\mu X\right)$, are SO(5) and spacetime vectors in addition to gauge adjoints. The presence of the gamma matrices γ^μ indicates that the fermions will remain massless upon coupling these bilinears to a condensed φ.

On the other hand, should the Higgs field couple to one of the final operators in Eq. (6.35), $\langle\varphi\rangle \neq 0$ will act as a mass for the fermions. The only other bilinears which act as masses to the fermions are the singlet and SO(5) vector, neither of which are fully symmetric. Therefore, given the aforementioned restriction on which operators we consider, we conclude

that an operator of the form $\text{tr}\left(\sigma^a \bar{X} T^j X\right)$ must couple to a condensed Higgs field in A_f and D_f. (It can also be verified that these colour-singlet mass terms cannot provide a spin gap to the ordered spin liquids, B_f or C_f.)

We will see shortly that the operators in Eq. (6.35) are not sufficient to reproduce the phase diagram in Figs. 6.1(b) and 6.2(b). Consequently, we also allow the Higgs field to couple to bilinears which contain a single derivative:

$$\text{tr}\left(\sigma^a \bar{X} i\partial_\mu X\right), \qquad \text{tr}\left(\sigma^a \bar{X} \Gamma^j i\partial_\mu X\right), \qquad \text{tr}\left(\sigma^a \bar{X} T^j \gamma^\mu i\partial_\nu X\right). \tag{6.36}$$

We now discuss how symmetries manifest in Higgs phases. The action of the space group and time reversal on the bilinears listed above is given in Tables 6.1 and 6.2; the spin symmetry rotates operators with spin indices among themselves in the usual way. It naïvely appears that a Higgs field coupling to any of these bilinears will necessarily break one or more symmetries upon condensing. As with the π-flux Hamiltonian in Eq. (6.21), H_π, this intuition does not account for the fact that the Higgs field is not a gauge invariant operator. A symmetry is only truly broken if the original and symmetry transformed actions are *not* gauge equivalent.

For instance, in Eq. (6.6), $\text{tr}\left(\sigma^a \bar{X} \mu^y X\right)$ couples to the Higgs field Φ. Since $\text{tr}\left(\sigma^a \bar{X} \mu^y X\right)$ maps to minus itself under $\mathcal{T}$, T_x, and T_y, the naïve argument would suggest that these symmetries are broken when $\langle \Phi^a \rangle \neq 0$. However, it's not difficult to find a gauge transformation capable of "undoing" the action of these symmetries. In particular, supposing that only $\langle \Phi^x \rangle \neq 0$, we see that the gauge transformation $V = i\sigma^z$ takes $\text{tr}\left(\sigma^x \bar{X} \mu^y X\right)$ to minus itself, thereby proving the equivalence of the original and symmetry transformed actions.

This set of gauge transformations comprises the PSG and is what we use to characterize the Higgs descendants. More generally, when a group element acts on a bilinear as

$$G : \text{tr}\left(\sigma^a \bar{X} M X\right) \to \text{tr}\left(\sigma^a \bar{X} \bar{U}_G M U_G X\right) \tag{6.37}$$

T^j	$\mathcal{T}$	P_x	P_y	T_x	T_y	$R_{\pi/2}$
μ^y	$-$	$+$	$+$	$-$	$-$	μ^y
σ^a	$-$	$-$	$-$	$+$	$+$	σ^a
$\mu^x\sigma^a$	$+$	$+$	$-$	$+$	$-$	$\mu^z\sigma^a$
$\mu^z\sigma^a$	$+$	$-$	$+$	$-$	$+$	$-\mu^x\sigma^a$

Table 6.1: Transformation properties of $\mathrm{tr}\left(\sigma^a\bar{X}T^jX\right)$ under the action of the physical symmetries. $T^j = \{\mu^y, \sigma^a, \mu^x\sigma^a, \mu^z\sigma^a\}$ are the 10 generators of SO(5).

Γ^j	$\mathcal{T}$	P_x	P_y	T_x	T_y	$R_{\pi/2}$
$\mu^x\gamma^0$	$+$	$-$	$+$	$+$	$-$	$\mu^z\gamma^0$
$\mu^x\gamma^x$	$-$	$+$	$+$	$+$	$-$	$\mu^z\gamma^y$
$\mu^x\gamma^y$	$-$	$-$	$-$	$+$	$-$	$-\mu^z\gamma^x$
$\mu^z\gamma^0$	$+$	$+$	$-$	$-$	$+$	$-\mu^x\gamma^0$
$\mu^z\gamma^x$	$-$	$-$	$-$	$-$	$+$	$-\mu^x\gamma^y$
$\mu^z\gamma^y$	$-$	$+$	$+$	$-$	$+$	$\mu^x\gamma^x$
$\mu^y\sigma^a\gamma^0$	$+$	$-$	$-$	$-$	$-$	$\mu^y\sigma^a\gamma^0$
$\mu^y\sigma^a\gamma^x$	$-$	$+$	$-$	$-$	$-$	$\mu^y\sigma^a\gamma^y$
$\mu^y\sigma^a\gamma^y$	$-$	$-$	$+$	$-$	$-$	$-\mu^y\sigma^a\gamma^x$

Table 6.2: Transformation properties of $\mathrm{tr}\left(\sigma^a\bar{X}\Gamma^j\gamma^\mu X\right)$ under the action of the physical symmetries. $\Gamma^j = \{\mu^x, \mu^z, \mu^y\sigma^a\}$ transform under the vector representation of the emergent SO(5).

where $\bar{U}_G = \gamma^0 U^\dagger \gamma^0$, the projective symmetry group is defined as

$$\mathscr{P}G : \mathrm{tr}\left(\sigma^a\bar{X}MX\right) \to \mathrm{tr}\left(V_G^\dagger\sigma^a V_G\bar{X}\bar{U}_G M U_G X\right) \tag{6.38}$$

where

$$\mathrm{tr}\left(V_G^\dagger\sigma^a V_G\bar{X}\bar{U}_G M U_G X\right) = \mathrm{tr}\left(\sigma^a\bar{X}MX\right). \tag{6.39}$$

We will see that requiring the existence of a V_G for every U_G places stringent conditions on which operators can couple to a Higgs field while preserving certain symmetries in the condensed phase.

$\mu^y\gamma^\mu i\partial_\nu$	$\mathcal{T}$	P_x	P_y	T_x	T_y	$R_{\pi/2}$
$\mu^y\gamma^0 i\partial_0$	$+$	$-$	$-$	$-$	$-$	$\mu^y\gamma^0 i\partial_0$
$\mu^y\gamma^0 i\partial_x$	$-$	$+$	$-$	$-$	$-$	$\mu^y\gamma^0 i\partial_y$
$\mu^y\gamma^0 i\partial_y$	$-$	$-$	$+$	$-$	$-$	$-\mu^y\gamma^0 i\partial_x$
$\mu^y\gamma^x i\partial_0$	$-$	$+$	$-$	$-$	$-$	$\mu^y\gamma^y\mu_0^\partial$
$\mu^y\gamma^x i\partial_x$	$+$	$-$	$-$	$-$	$-$	$\mu^y\gamma^y i\partial_y$
$\mu^y\gamma^x i\partial_y$	$+$	$+$	$+$	$-$	$-$	$-\mu^y\gamma^y i\partial_x$
$\mu^y\gamma^y i\partial_0$	$-$	$-$	$+$	$-$	$-$	$-\mu^y\gamma^x i\partial_0$
$\mu^y\gamma^y i\partial_x$	$+$	$+$	$+$	$-$	$-$	$-\mu^y\gamma^x i\partial_y$
$\mu^y\gamma^y i\partial_y$	$+$	$-$	$-$	$-$	$-$	$\mu^y\gamma^x i\partial_x$

$\mu^{0,x,y} i\partial_\mu$	$\mathcal{T}$	P_x	P_y	T_x	T_y	$R_{\pi/2}$
$i\partial_0$	$+$	$-$	$-$	$+$	$+$	$i\partial_0$
$i\partial_x$	$-$	$+$	$-$	$+$	$+$	$i\partial_y$
$i\partial_y$	$-$	$-$	$+$	$+$	$+$	$-i\partial_x$
$\mu^x i\partial_0$	$-$	$+$	$-$	$+$	$-$	$\mu^z i\partial_0$
$\mu^x i\partial_x$	$+$	$-$	$-$	$+$	$-$	$\mu^z i\partial_y$
$\mu^x i\partial_y$	$+$	$+$	$+$	$+$	$-$	$-\mu^z i\partial_x$
$\mu^z i\partial_0$	$-$	$-$	$+$	$-$	$+$	$-\mu^x i\partial_0$
$\mu^z i\partial_x$	$+$	$+$	$+$	$-$	$+$	$-\mu^x i\partial_y$
$\mu^z i\partial_y$	$+$	$-$	$-$	$-$	$+$	$\mu^x i\partial_x$

Table 6.3: Symmetry transformation properties of bilinears of the form $\mathrm{tr}\left(\sigma^a \bar{X} i\partial_\mu X\right)$, $\mathrm{tr}\left(\sigma^a \bar{X}\Gamma^j i\partial_\mu X\right)$, and $\mathrm{tr}\left(\sigma^a \bar{X} T^j \gamma^\mu i\partial_\nu X\right)$ which do *not* transform under spin. The operators which can couple to a Higgs fields in a gapped symmetric spin $\mathbb{Z}_2$ spin liquid are coloured; entries with the same colour transform into one another under $R_{\pi/2}$.

6.3.2 Symmetric spin liquids

In this section, we focus on fully symmetric and gapped spin liquids (by 'gapped,' we are referring specifically to the matter content). As mentioned, in order to simultaneously gap the fermions and Higgs the gauge boson, an operator of the form $\mathrm{tr}\left(\sigma^a \bar{X} T^j X\right)$ where T^j is a generator of SO(5) must couple to a Higgs field. These are listed in Table 6.1. Of the ten generators of SO(5), nine transform as vectors under the spin symmetry, and we show in Appendix E.1 that a fully symmetry spin liquid cannot be formed by coupling a Higgs field to any of these bilinears. Roughly, the argument relies on the fact that in order to preserve the spin symmetry, a linear combination of the form $\sim \sum_a \mathrm{tr}\left(\sigma^a \bar{X} M \sigma^a X\right)$ for $M = \mathbb{1}, \mu^x, \mu^z$ must couple to the Higgs, which then makes it impossible preserve all of the discrete symmetries.

This observation establishes $\mathrm{tr}\left(\sigma^a \bar{X} \mu^y X\right)$ as the only fermion bilinear capable of both giving the fermions a mass and coupling to a Higgs field. As indicated in Eq. (6.6) and Section 6.3.1, we denote the Higgs field coupling to this bilinear as Φ^a. Since the action remains invariant under all gauge transformations about the direction of the condensate, Φ^a cannot fully Higgs the SU(2) gauge symmetry down to $\mathbb{Z}_2$. For instance, if we will assume

that only $\langle \Phi^x \rangle \neq 0$, U(1) operations of the form $X \to X e^{-i\theta\sigma^x}$ remain a gauge symmetry. We label this U(1) spin liquid D_f.

It is well-known [64] that without gapless degrees of freedom, a U(1) gauge theory is unstable to the proliferation of monopoles and confinement [126]. We will ignore the ultimate fate of D_f until Sec. 6.4.3 where we show that the true ground state is a VBS.

With this caveat in mind, we deduce the projective symmetry group of the gapped U(1) spin liquid from Table 6.1:

$$\begin{aligned} V_t &= e^{i\theta_t\sigma^x} i\sigma^z, & V_{tx} &= e^{i\theta_{tx}\sigma^x} i\sigma^z, \\ V_{py} &= e^{i\theta_{py}\sigma^x}, & V_{ty} &= e^{i\theta_{ty}\sigma^x} i\sigma^z, \\ V_{px} &= e^{i\theta_{py}\sigma^x}, & V_r &= e^{i\theta_r\sigma^x}, \end{aligned} \tag{6.40}$$

where the θ_G are arbitrary angles parametrizing the residual U(1) gauge degree of freedom. Here, the subscripts t, px, py, tx, ty and r indicate that these gauge transformation accompany the action of $\mathcal{T}, P_x, P_y, T_x, T_y$, and $R_{\pi/2}$ respectively.

We note that while the physical symmetries are all preserved in D_f, the emergent SO(5) symmetry of QCD_3 has been broken. Of the SO(5) generators, $T^j = \{\mu^y, \sigma^a, \mu^x\sigma^a, \mu^z\sigma^a\}$, the U(1) gauge theory is only invariant under $\{\mu^y\} \times \{\sigma^a\}$, indicating that the SO(5) is broken to U(1)×SU(2). From the perspective of the SO(5) order parameter, $n^j = \text{tr}\left(\bar{X}\Gamma^j X\right)$, $\Gamma^j = \{\mu^x, \mu^z, \mu^y\sigma^a\}$, the VBS order parameters, n^1 and n^2 can no longer be rotated into the Néel order parameters, n^3, n^4, and n^5.

To break the gauge group down to $\mathbb{Z}_2$, an additional Higgs field Φ_1 is needed. However, there are strict constraints on which bilinears can couple to Φ_1 in order for the resultant $\mathbb{Z}_2$ spin liquid to preserve all physical symmetries. We approach this problem from a vector representation by associating an SO(3) matrix Q to each $\text{SU}(2)_g$ gauge transformation V. That is, instead of looking at V such that $\text{tr}\left(\varphi\bar{X}MX\right) \to \text{tr}\left(V^\dagger\varphi V\bar{X}MX\right)$, we consider Q such that $\varphi^a\text{tr}\left(\sigma^a\bar{X}MX\right) \to (Q\varphi)^a\text{tr}\left(\sigma^a\bar{X}MX\right)$. In this notation, when $\langle\Phi^x\rangle \neq 0$, we must

have

$$Q_G = \begin{pmatrix} 1 & \mathbf{0} \\ \mathbf{0} & R_G \end{pmatrix}, \qquad G = px, py, r, \tag{6.41}$$

and

$$Q_G = \begin{pmatrix} -1 & \mathbf{0} \\ \mathbf{0} & \tilde{R}_G \end{pmatrix}, \qquad G = t, tx, ty, \tag{6.42}$$

where R_G and $\tilde{R}_G$ are determined by the bilinear coupling to Φ_1. The constraints on this bilinear arise from the fact that Q_G must be special orthogonal, therefore implying that R_G and $\tilde{R}_G$ must be 2×2 orthogonal matrices with determinants $+1$ and -1 respectively.

We now argue that none of the operators in Table 6.2 satisfy these requirements. First, all bilinears with spin indices can be excluded by the same reasoning given above and in Appendix E.1. Next, we note that all remaining operators still transform differently than $\mathrm{tr}\left(\sigma^a \bar{X} \mu^y X\right)$ under at least one of the symmetries, and therefore the Φ_1 condensate *must* be perpendicular to x in colour space. For the remaining six operators, the obstruction to forming a spin liquid may be understood by studying the action of a 90^0 rotation. The last column of the table indicates that $R_{\pi/2}$ maps each bilinear to plus or minus another bilinear in the table, eg. $R_{\pi/2} : \mathrm{tr}\left(\sigma^a \bar{X} \mu^x \gamma^0 X\right) \to \mathrm{tr}\left(\sigma^a \bar{X} \mu^z \gamma^0 X\right)$. In order for this to describe a rotationally symmetric phase, both bilinears must couple to a Higgs field. We might imagine that Φ_1 couples to both operators in a pair, but this is not a viable option because the other discrete symmetries do not act on the members of each pair in the same way. For instance, no gauge transformation can preserve the form of $\langle \Phi_1^a \rangle \ \mathrm{tr}\left(\sigma^a \bar{X} \gamma^0 \left[\mu^x \pm \mu^z\right] X\right)$ under P_x, P_y, T_x, and T_y since $\mathrm{tr}\left(\sigma^a \bar{X} \gamma^0 \mu^x X\right)$ and $\mathrm{tr}\left(\sigma^a \bar{X} \gamma^0 \mu^z X\right)$ behave differently under these symmetries. We might try coupling each of these operators to *different* Higgs fields, Φ_1 and Φ_1', and require that they condense in mutually perpendicular channels, eg. $\langle \Phi_1^y \rangle \neq 0$ and $\langle {\Phi_1'}^z \rangle \neq 0$. However, the matrix required to undo the action of the time reversal symmetry is then

sPSG	M	Q_t/V_t	$Q_{px,py}/V_{px,py}$	$Q_{tx,ty}/V_{tx,ty}$	Q_r/V_r
1	$\mu^y\gamma^0 i\partial_0,\ \mu^y\left(\gamma^x i\partial_x+\gamma^y i\partial_y\right)$	$\mathrm{diag}(-1,1,1)$ $i\sigma^y$	$\mathrm{diag}(1,-1,-1)$ $i\sigma^x$	$\mathrm{diag}(-1,-1,1)$ $i\sigma^z$	$\mathbb{1}$ $\mathbb{1}$
2	$\mu^y\left(\gamma^x i\partial_x-\gamma^y i\partial_y\right)$	$\mathrm{diag}(-1,1,1)$ $i\sigma^y$	$\mathrm{diag}(1,-1,-1)$ $i\sigma^x$	$\mathrm{diag}(-1,-1,1)$ $i\sigma^z$	$\mathrm{diag}(1,-1,-1)$ $i\sigma^x$
3	$\mu^y\left(\gamma^x i\partial_y+\gamma^y i\partial_x\right)$	$\mathrm{diag}(-1,1,1)$ $i\sigma^y$	$\mathbb{1}$ $\mathbb{1}$	$\mathrm{diag}(-1,-1,1)$ $i\sigma^z$	$\mathrm{diag}(1,-1,-1)$ $i\sigma^x$
4	$\mu^y\left(\gamma^x i\partial_y-\gamma^y i\partial_x\right)$	$\mathrm{diag}(-1,1,1)$ $i\sigma^y$	$\mathbb{1}$ $\mathbb{1}$	$\mathrm{diag}(-1,-1,1)$ $i\sigma^z$	$\mathbb{1}$ $\mathbb{1}$
5	$i\partial_0$	$\mathrm{diag}(-1,1,1)$ $i\sigma^y$	$\mathrm{diag}(1,-1,-1)$ $i\sigma^x$	$\mathrm{diag}(-1,1,-1)$ $i\sigma^y$	$\mathbb{1}$ $\mathbb{1}$

Table 6.4: All symmetric PSG's associated with symmetric $\mathbb{Z}_2$ spin liquids in which $\langle\Phi^x\rangle\neq 0$ where Φ couples to $\mathrm{tr}\left(\sigma^a\bar{X}\mu^y X\right)$. These are listed as a function of the operator $\mathrm{tr}\left(\sigma^a\bar{X}MX\right)$ which Φ_1 couples to. We assume that only $\langle\Phi_1^y\rangle\neq 0$.

$Q_t=\mathrm{diag}(-1,1,1)$ which is not an element of SO(3). We conclude that this does not work either.

We next perform the same analysis on bilinears containing a single derivative. Once again, the arguments in Appendix E.1 are valid, and we immediately exclude all operators in Eq. (6.36) which transform nontrivially under spin rotations. The action of the space group and time reversal symmetries on the remaining operators is provided in Table 6.3. Again, $R_{\pi/2}$ maps many of the operators to plus or minus a different operator in the table. As discussed in the previous paragraph, only bilinears which transform in the same way under $\mathcal{T}, P_x, P_y, T_x$, and T_y as their partner under $R_{\pi/2}$ are suitable candidates, and these have been highlighted in different colours. In Table 6.4 we list the PSG's of all gapped and symmetric $\mathbb{Z}_2$ spin liquids which can be formed using this set of operators.

In Sec. 6.4.1 we determine which (if any) bosonic ansatz these PSG's correspond to. We find that sPSG5 corresponds to the fully symmetric spin liquid A_b, and for this reason, we denote it A_f.

6.3.3 $\mathbb{Z}_2$ spin liquids with Ising-nematic order

As emphasized in Section 6.1, it is not necessary to restrict to fully symmetric spin liquids. We therefore also study gapped, nematic $\mathbb{Z}_2$ spin liquids proximate to the gapped U(1) spin liquid D_f. In particular, we investigate spin liquids which are obtained by coupling a third Higgs field, Φ_{2i}, to the operators in Tables 6.1, 6.2, and 6.3, and which preserve the continuous spin symmetry, $\mathcal{T}$, P_x, P_y, T_x, and T_y, but break the 90^0 rotation symmetry, $R_{\pi/2}$. The absence of rotation symmetry makes it possible to couple any of the operators in Tables 6.1 and 6.2 to the Higgs field, and the ten candidates we find are listed in Table 6.5.

We note that nPSG5 and nPSG6 are continuously connected to sPSG1-2 and sPSG3-4 respectively. For instance, in the case of nPSG5, if the Higgs field couples as $\sum_{i=x,y} \Phi^a_{2i} \mathrm{tr}\left(\sigma^z \bar{X} \gamma^i i\partial_i X\right)$, then phases where the condensate satisfies $\langle \Phi^a_{2x} \rangle = \pm \langle \Phi^a_{2y} \rangle$ do not break $R_{\pi/2}$ and are precisely sPSG1 and sPSG2. The same considerations hold for nPSG6 in relation to sPSG3 and sPSG4.

In all cases, the phase with $\langle \Phi \rangle = 0$ and $\langle \Phi_1 \rangle \neq 0$ is a fully symmetric U(1) spin liquid. However, unlike D_f, the matter sector is gapless.

In the next section we find that nPSG7 is the fermionic version of the bosonic phase B_b, leading us to label it B_f.

6.3.4 $\mathbb{Z}_2$ spin liquid with current-loop order

So far, we have defined three separate Higgs fields. To ensure that the condensed phases had a spin gap, Φ and $\mathrm{tr}\left(\sigma^a \bar{X} \mu^y X\right)$ were required to couple. We then identified which bilinears could couple to a second Higgs field, Φ_1, such that the phase with $\langle \Phi \rangle \neq 0$, $\langle \Phi_1 \rangle \neq 0$, and $\langle \Phi \rangle \perp \langle \Phi_1 \rangle$ was a fully symmetric spin $\mathbb{Z}_2$ liquid. Similarly, we determined in the previous section which bilinears could couple to a Higgs field Φ_{2i} such that the phase with $\langle \Phi \rangle \neq 0$ and $\langle \Phi_{2i} \rangle \neq 0$ was a $\mathbb{Z}_2$ spin liquid with Ising-nematic order, again provided $\langle \Phi \rangle \perp \langle \Phi_{2i} \rangle$.

A natural extension is to ask which phases result when all three Higgs fields have con-

nPSG		M_i	V_t	V_{px}	V_{py}	V_{tx}	V_{ty}
1	x	$\mu^x\gamma^0$	$i\sigma^y$	$i\sigma^x$	$\mathbb{1}$	$i\sigma^y$	$i\sigma^z$
	y	$\mu^z\gamma^0$	$i\sigma^y$	$\mathbb{1}$	$i\sigma^x$	$i\sigma^z$	$i\sigma^y$
2	x	$\mu^z\gamma^y$	$i\sigma^z$	$\mathbb{1}$	$\mathbb{1}$	$i\sigma^z$	$i\sigma^y$
	y	$\mu^x\gamma^x$	$i\sigma^z$	$\mathbb{1}$	$\mathbb{1}$	$i\sigma^y$	$i\sigma^z$
3	x	$\mu^x\gamma^y$,	$i\sigma^z$	$i\sigma^x$	$i\sigma^x$	$i\sigma^y$	$i\sigma^z$
	y	$\mu^z\gamma^x$	$i\sigma^z$	$i\sigma^x$	$i\sigma^x$	$i\sigma^z$	$i\sigma^y$
4	x	$\mu^y\gamma^0 i\partial_x$, $\mu^y\gamma^x i\partial_0$	$i\sigma^z$	$\mathbb{1}$	$i\sigma^x$	$i\sigma^z$	$i\sigma^z$
	y	$\mu^y\gamma^0 i\partial_y$, $\mu^y\gamma^y i\partial_0$	$i\sigma^z$	$i\sigma^x$	$\mathbb{1}$	$i\sigma^z$	$i\sigma^z$
5	x	$\mu^y\gamma^x i\partial_x$	$i\sigma^y$	$i\sigma^x$	$i\sigma^x$	$i\sigma^z$	$i\sigma^z$
	y	$\mu^y\gamma^y i\partial_y$	$i\sigma^y$	$i\sigma^x$	$i\sigma^x$	$i\sigma^z$	$i\sigma^z$
6	x	$\mu^y\gamma^x i\partial_y$	$i\sigma^y$	$\mathbb{1}$	$\mathbb{1}$	$i\sigma^z$	$i\sigma^z$
	y	$\mu^y\gamma^y i\partial_x$	$i\sigma^y$	$\mathbb{1}$	$\mathbb{1}$	$i\sigma^z$	$i\sigma^z$
7	x	$i\partial_x$	$i\sigma^z$	$\mathbb{1}$	$i\sigma^x$	$i\sigma^y$	$i\sigma^y$
	y	$i\partial_y$	$i\sigma^z$	$i\sigma^x$	$\mathbb{1}$	$i\sigma^y$	$i\sigma^y$
8	x	$\mu^x i\partial_0$	$i\sigma^z$	$\mathbb{1}$	$i\sigma^x$	$i\sigma^y$	$i\sigma^z$
	y	$\mu^z i\partial_0$	$i\sigma^z$	$i\sigma^x$	$\mathbb{1}$	$i\sigma^z$	$i\sigma^y$
9	x	$\mu^z i\partial_x$	$i\sigma^y$	$\mathbb{1}$	$\mathbb{1}$	$i\sigma^z$	$i\sigma^y$
	y	$\mu^x i\partial_y$	$i\sigma^y$	$\mathbb{1}$	$\mathbb{1}$	$i\sigma^y$	$i\sigma^z$
10	x	$\mu^x i\partial_x$	$i\sigma^y$	$i\sigma^x$	$i\sigma^x$	$i\sigma^y$	$i\sigma^z$
	y	$\mu^z i\partial_y$	$i\sigma^y$	$i\sigma^x$	$i\sigma^x$	$i\sigma^z$	$i\sigma^y$

Table 6.5: Nematic PSG's associated with order parameters of the form $\Phi^a \mathrm{tr}\left(\sigma^a \bar{X} \mu^y X\right) + \Phi^a_{2i} \mathrm{tr}\left(\sigma^a \bar{X} M^i X\right)$. We have not included $\mathrm{tr}\left(\sigma^a \bar{X} \partial_0 X\right)$ since this operator is invariant under the action of $R_{\pi/2}$ and already accounted for as sPSG5. The labels x, y are simply a convenient notation and do not necessarily signify a physical direction.

densed: $\langle\Phi\rangle \neq 0$, $\langle\Phi_1\rangle \neq 0$, and $\langle\Phi_{2i}\rangle \neq 0$. However, there are clearly a large number of possibilities. Not only have we identified many candidate s- and nPSG's, but different symmetries will be broken depending on the relative orientation of the Higgs fields. Therefore, we focus on producing the phase diagram in Fig. 6.2(b) and restrict our study to the situation where the symmetric and nematic spin liquids are A_f and B_f, the phases described by sPSG5 and nPSG7.

This scenario describes four different patterns of symmetry breaking:

1. $\langle\Phi\rangle \perp \langle\Phi_1\rangle$, $\langle\Phi\rangle \perp \langle\Phi_{2i}\rangle$, & $\langle\Phi_1\rangle \parallel \langle\Phi_{2i}\rangle$
2. $\langle\Phi\rangle \perp \langle\Phi_1\rangle$, $\langle\Phi_1\rangle \perp \langle\Phi_{2i}\rangle$, & $\langle\Phi\rangle \parallel \langle\Phi_{2i}\rangle$
3. $\langle\Phi_{2i}\rangle \perp \langle\Phi\rangle$, $\langle\Phi_{2i}\rangle \perp \langle\Phi_1\rangle$, & $\langle\Phi\rangle \parallel \langle\Phi_1\rangle$
4. $\langle\Phi\rangle \perp \langle\Phi_1\rangle \perp \langle\Phi_{2i}\rangle$

In Table 6.6 we list which symmetries are broken for each of these cases.

Referring to the phase diagram in Fig. 6.1(b), it is natural to restrict to the case where A_f and B_f are accessible by taking $\langle\Phi_{2i}\rangle$ or $\langle\Phi_1\rangle$ to zero. Since both the second and third cases have $\langle\Phi\rangle$ parallel to either $\langle\Phi_1\rangle$ or $\langle\Phi_{2i}\rangle$, we eliminate these options. Of the remaining two phases, the resulting spin liquid only possesses current-loop order when $\langle\Phi_1\rangle \parallel \langle\Phi_{2i}\rangle$. This situation is further distinguished by breaking the fewest symmetries. We refer to this phase as C_f and later equate it and the bosonic phase C_b.

6.4 Spin liquid identification

We now identify the phases examined above with previously studied spin liquids. On the lattice, Wen [184] showed that 58 distinct $\mathbb{Z}_2$ PSG's can be accessed from the π-flux state (SU2Bn0). However, his PSG classification gives no indication of the physical properties of these phases and, moreover, as we will see, it includes certain "anomalous" PSG's which cannot be obtained from a mean field ansatz. We therefore begin by discussing the "symmetry

	Direction			Broken
	$\langle\Phi\rangle$	$\langle\Phi_1\rangle$	$\langle\Phi_{2x}\rangle$	Symmetries
1	x	y	y	$\mathcal{T}$, P_x
2	x	y	x	P_y, T_x, T_y
3	x	x	y	$\mathcal{T}$, P_x, P_y, T_x, T_y
4	x	y	z	P_x, T_x, T_y

Table 6.6: Symmetries broken depending on the orientation in gauge space taken by the Higgs condensates. The fields couple to the bilinears as $\mathrm{tr}\left(\Phi\bar{X}\mu^y X\right) + \mathrm{tr}\left(\Phi_1\bar{X}i\partial_0 X\right) + \mathrm{tr}\left(\Phi_{2x}\bar{X}i\partial_x X\right)$.

fractionalization" approach to spin liquid classification, and relate it to Wen's scheme. This will significantly simplify the process of relating the symmetric U(1) spin liquids and the phases in Table 6.4 to the spin liquids studied by Wen. Its greatest power, however, will be to treat fermionic and bosonic mean field ansatze on the same footing, allowing us relate our results to phases described using Schwinger bosons, and prove our earlier claim that A_f, B_f, and C_f are fermionic versions of A_b, B_b, and C_b.

We next show that the gapped U(1) spin liquid D_f corresponds to D_b. The gapless gauge degrees of freedom invalidate the symmetry fractionalizaton approach to comparing spin liquids represented with bosons and fermions. Instead, we show through linear response that the proliferation of monopoles induces the condensation of the VBS order parameters given by the first two components of the vector in Eq. (6.31). We provide additional verification by demonstrating that the Berry phase of the monopole matches the calculation performed by Haldane [53] and Read and Sachdev [144].

6.4.1 Symmetry fractionalization and $\mathbb{Z}_2$ spin liquid identification

In this section, we relate the gapped $\mathbb{Z}_2$ spin liquids determined in the previous section to spin liquids obtained using Schwinger bosons by Yang and Wang [205] and Chatterjee *et al.* [21]. Since these phases are gapped, they are completely defined via their "symmetry fractionalization" [43]. Of the PSGs listed in Tables 6.4 and 6.5, we find that precisely

	Group relations	sPSG1	sPSG2	sPSG3	sPSG4	sPSG5	vison	twist	$\mathbb{Z}_2[0,0]$	$\mathbb{Z}_2[0,\pi]$
1	$T_y^{-1}T_xT_yT_x^{-1}$	-1	-1	-1	-1	-1	-1	1	1	1
2	$P_y^{-1}T_xP_yT_x^{-1}$	-1	-1	1	1	-1	-1	1	1	1
3	$P_y^{-1}T_yP_yT_y$	-1	-1	1	1	-1	1	1	-1	-1
4	P_y^2	-1	-1	1	1	-1	1	-1	1	1
5	$P_y^{-1}R_{\pi/2}P_yR_{\pi/2}$	1	-1	-1	1	1	1	1	1	-1
6	$R_{\pi/2}^4$	1	1	1	1	1	-1	-1	1	1
7	$R_{\pi/2}^{-1}T_xR_{\pi/2}T_y$	-1	-1	-1	-1	-1	-1	1	1	1
8	$R_{\pi/2}^{-1}T_yR_{\pi/2}T_x^{-1}$	-1	-1	-1	-1	-1	1	1	-1	-1
9	$R_{\pi/2}^{-1}\mathcal{T}^{-1}R_{\pi/2}\mathcal{T}$	1	-1	-1	1	1	1	1	1	-1
10	$P_y^{-1}\mathcal{T}^{-1}P_y\mathcal{T}$	-1	-1	1	1	-1	1	-1	1	1
11	$T_x^{-1}\mathcal{T}^{-1}T_x\mathcal{T}$	1	1	1	1	-1	1	1	-1	-1
12	$T_y^{-1}\mathcal{T}^{-1}T_y\mathcal{T}$	1	1	1	1	-1	1	1	-1	-1
13	$\mathcal{T}^2$	-1	-1	-1	-1	-1	1	1	-1	-1

Table 6.7: The columns labeled "sPSG1-5," list the symmetry fractionalizations of the gapped, symmetric $\mathbb{Z}_2$ spin liquids given in Table 6.4. The corresponding bosonic symmetry fractionalization numbers are obtained by multiplying the sPSG numbers with the those given in the 'vison' and 'twist' columns. We see that sPSG5 corresponds to the $\mathbb{Z}_2[0,0]$ state of Ref. 205. No bosonic counterparts to sPSG1-4 are present in Ref. 205.

one matches onto the spin liquid A_b, and one onto B_b of Fig. 6.2(a). We begin by briefly reviewing this classification scheme in the context of $\mathbb{Z}_2$ topological order. The reader is referred to Ref. 43 for more details.

One of the defining characteristics of topological order is the presence of anyonic excitations. For the $\mathbb{Z}_2$ case we consider here, there are two bosonic particles, typically denoted e and m, which are mutually semionic: the wavefunction picks up a minus sign upon the adiabatic motion of an e particle travelling around an m particle. A bound state of an e and m is a fermionic excitation, $\varepsilon \sim em$, and it also satisfies mutual semionic statistics with e and m. We will frequently refer to the m particle as the 'vison' and the e and ε particles as the bosonic and fermionic 'spinon' respectively. These excitations carry $\mathbb{Z}_2$ gauge charge and therefore must appear in pairs. Nonetheless, the $\mathbb{Z}_2$ gauge field is gapped and these phases are deconfined, meaning that e, m, and ε particles may be very far from one another.

A comparison of these particles with the excitations in the Higgs phases implies that the fermionic spinons ε should be identified with the excitations of the field operator X. In

addition, in 2+1d the Abrikosov vortices of the condensate are pointlike, and we associate these with the vison excitations m. The remaining particle, the bosonic spinon e, is therefore described by a bound state of X and the vortex. In contrast, $\mathbb{CP}^1$ is formulated in terms of the bosonic spinons. The vison is present as a vortex in the condensate as before, but now it is the fermionic spinon that is expressed as a bound state.

This representation of the degrees of freedom of a gapped $\mathbb{Z}_2$ spin liquid provides a means to compare phases described using fermionic and bosonic ansatze. In a manner analogous to the classification of symmetries in terms of quantum numbers, these symmetry enriched topological phases can be classified by what is known as symmetry fractionalization numbers. Independent of any formalism, suppose we create from the groundstate two ε (or e or m) excitations and separate them so that they lie at very distant points $\boldsymbol{r}$ and $\boldsymbol{r}'$: $|\boldsymbol{r}, \boldsymbol{r}'\rangle$. Since the rest of the system is indistinguishable from the groundstate, the action of an unbroken symmetry G will exclusively affect these regions:

$$G\,|\boldsymbol{r}, \boldsymbol{r}'\rangle = \mathscr{G}_\varepsilon(\boldsymbol{r})\mathscr{G}_\varepsilon(\boldsymbol{r}')\,|\boldsymbol{r}, \boldsymbol{r}'\rangle\,, \tag{6.43}$$

where $\mathscr{G}_\varepsilon(\boldsymbol{r})$ only has support in the region immediately surrounding $\boldsymbol{r}$. As discussed in Sec. 6.2.1, the generators of a symmetry group satisfy certain commutation relations, and for the space group of the square lattice (plus time reversal), these relations are given in Eq. (6.11) and below. It follows that the action of any of these operations on *all* wavefunctions must be equivalent to the identity. For example, since $T_y^{-1}T_xT_yT_x^{-1} = \mathbb{1}$, it must map $|\boldsymbol{r}, \boldsymbol{r}'\rangle$ to itself:

$$|\boldsymbol{r}, \boldsymbol{r}'\rangle = T_y^{-1}T_xT_yT_x^{-1}\,|\boldsymbol{r}, \boldsymbol{r}'\rangle\,. \tag{6.44}$$

In terms of the local symmetry operations, this becomes

$$|\boldsymbol{r}, \boldsymbol{r}'\rangle = \mathscr{T}_{\varepsilon,y}^{-1}(\boldsymbol{r})\mathscr{T}_{\varepsilon,x}(\boldsymbol{r})\mathscr{T}_{\varepsilon,y}(\boldsymbol{r})\mathscr{T}_{\varepsilon,x}^{-1}(\boldsymbol{r})\cdot \tag{6.45}$$

Since the transformations are localized at either $\boldsymbol{r}$ and $\boldsymbol{r}'$, they must be independent from one another and therefore constant. However, because of the $\mathbb{Z}_2$ gauge degree of freedom, $\zeta^{\varepsilon}_{txty} = \mathscr{T}^{-1}_{\varepsilon,y}(\boldsymbol{r})\mathscr{T}_{\varepsilon,x}(\boldsymbol{r})\mathscr{T}_{\varepsilon,y}(\boldsymbol{r})\mathscr{T}^{-1}_{\varepsilon,x}(\boldsymbol{r})$ need not necessarily equal unity: the symmetry can be *fractionalized* such that $\zeta^{\varepsilon}_{txty} = -1$. The value of $\zeta^{\varepsilon}_{txty}$ will be consistent for every excitation of that species within a phase

It is not difficult to connect this to the PSG classification of the previous section. The PSG is the set gauge transformations required to preserve the form of the action following a symmetry transformation, as shown in Eq. (6.39). Now, however, we present the PSG action solely in terms of operator which creates fermionic spinons, X:

$$\mathscr{P}G : X \to U_G X V_G^{\dagger}. \tag{6.46}$$

The same argument given above then requires that under the action of $T_y^{-1}T_xT_yT_x^{-1}$, X is mapped to plus or minus itself:

$$T_y^{-1}T_xT_yT_x^{-1}[X] = U_{tx}^{\dagger}U_{ty}U_{xy}U_{ty}^{\dagger}\, X\, V_{ty}V_{tx}^{\dagger}V_{ty}^{\dagger}V_{tx} = \pm X. \tag{6.47}$$

This factor is precisely the fractionalization number of ε. When time reversal is involved, this is modified to

$$\begin{aligned} G^{-1}\mathcal{T}^{-1}G\mathcal{T}[X] &= U_t^*\sigma^y U_G^*\sigma^y U_t^T U_G^{\dagger}\, X\, V_G V_t^*\sigma^y V_G^T\sigma^y V_t^T, \\ \mathcal{T}^2[X] &= U_t^*\sigma^y U_t\sigma^y\, X\, \sigma^y V_t^{\dagger}\sigma^y V_t^T, \end{aligned} \tag{6.48}$$

where the reality condition in Eq. (6.30) has been used. Table 6.1 lists the numbers corresponding to each of the *s*PSG's in Table 6.7. (We note that the 7th group relation, $R_{\pi/2}^{-1}T_xR_{\pi/2}T_y = \mathbb{1}$, can be fixed by a gauge transformation on the relative sign of V_{tx} and V_{ty}. In keeping with the convention of Ref. 205, we require that the symmetry fractionalization number be -1 for the fermionic spinons.)

The argument also demonstrates a shortcoming of the PSG classification. While it im-

mediately returns the symmetry fractionalization of the fermionic spinons, it provides no information regarding the symmetry fractionalization of the vison and bosonic spinon. However, it fortunately turns out that the vison's fractionalization numbers are independent of the precise $\mathbb{Z}_2$ spin liquid under study and can be obtained by examining a fully frustrated transverse-field Ising model [76, 158, 197, 205]. We quote these results in the column labeled "vison" in Table 6.7.

Correspondence between fermionic and bosonic ansatze

Comparing fermionic and bosonic ansatze may appear straightforward from this point: since $e \sim \varepsilon\, m$, it seems reasonable to assume that the symmetry fractionalization of the bosonic spinon is obtained through a simple multiplication of the symmetry fractionalization numbers of the fermionic spinon and the vison. However, the mutual statistics of ε and m occasionally change this relation. For instance, upon rotating e by 360^0, $R^4_{\pi/2}$, either the vison will encircle the fermionic spinon or vice versa. In either case, an extra factor of -1 must be taken into account. These additional multiplication factors were worked out in Ref. 205, and we quote them under the column labeled "twist" in Table 6.7.

The comparison with the bosonic symmetry fractionalization allows us to identify sPSG5 with $\mathbb{Z}_2[0,0]$, showing that $A_f = A_b$ as promised. We do not find fermionic counterparts to the remaining four spin liquids in Ref. 205.

Using a slightly altered set of commutation relations to account for the symmetry breaking, the exact same analysis can be performed for the nematic spin liquids. These symmtery fractionalization numbers are shown in Table 6.5, and, as claimed, by comparing with the analysis of Ref. [21] we positively identify B_f (nPSG7) with the Ising-nematic $\mathbb{Z}_2$ spin liquid B_b.

Finally, the equivalence of A_f and B_f with A_b and B_b indicates the equivalence of C_f and C_b. In Appendix E.4, we provide additional verification of this result using the symmetry fractionalization technique.

6.4.2 Lattice classification of fermionic PSG's

The data compiled in Table 6.7 can also be used to compare the phases we find against fermionic spin liquids described on the lattice. In Appendix E.2, we review Wen's classification scheme [184] and identify the lattice PSG's corresponding to the two U(1) spin liquids as well as the five symmetric $\mathbb{Z}_2$ spin liquids. This classification is useful since it allows us to express the phases we've studied on the lattice without having to reverse engineer the bilinears.

We identify the gapped U(1) spin liquid, D_f, with U1C$n0n1$ and the gapless U(1) spin liquid ($\langle\Phi_1\rangle \neq 0$) with U1B$x11n$. The lattice PSG's corresponding to the five symmetric $\mathbb{Z}_2$ spin liquids we obtained are shown in Table 6.8.

Both sPSG1 and sPSG5 seemingly correspond to multiple lattice PSG's. However, in Appendix E.2.4, we prove that while the spin liquids have the same symmetry fractionalizations, of the two shown, only one of each pair actually corresponds to the spin liquids we consider. In the case of sPSG5, it is not difficult to show that Z2B$xx2z$ is always gapless, immediately ruling it out as a description of the gapped phase A_f. Further, we show that Z2B$xx2z$ is not proximate to either the gapped or gapless U(1) spin liquids U1C$n0n1$ and U1B$x11n$. Similarly, we find that Z2B$xx23$ is not proximate to U1C$n0n1$, leaving Z2B$xx13$ as the sole realizable lattice PSG capable of reproducing sPSG1.

These statements can be verified explicitly by comparing our continuum theory with mean field Hamiltonians on the lattice which have been constructed using only information provided by the lattice PSG. In Appendix E.3 we study the lattice Hamilonians for the gapped and gapless U(1) spin liquids, as well as A_f. We find that a low-energy expansion of the mean field Hamiltonian describing U1C$n0n1$ corresponds to adding $\mathrm{tr}\left(\sigma^x \bar{X} \mu^y X\right)$ to the π-flux Hamiltonian as expected, but that no analogous statement can be made for either U1B$x11n$ or Z2B$xx1z$. In particular, we demonstrate that no mean field ansatz on the lattice can realize the U(1) spin liquid U1B$x11n$. This should not be too surprising as the continuum realization of this phase is the product of condensing Φ_1 when coupled to

	*s*PSG1	*s*PSG2	*s*PSG3	*s*PSG4	*s*PSG5 (A_f)
Lattice PSG	Z2Bxx13 *Z2Bxx23*	Z2Bxx03	Z2B0013	Z2B0001	Z2B$xx1z$ *Z2Bxx2z*

Table 6.8: Spin liquids according to the labeling scheme given in Ref. 184 and reviewed in Appendix E.2.4. All of the spin liquids listed are found to be proximate to the π-flux phase SU2n0 though not necessarily U1Cn0n1. While the symmetry fractionalization of *s*PSG1 and *s*PSG5 corresponds to multiple fermionic PSG's, the two which have been italicized (Z2Bxx23 and Z2B$xx2z$) are not proximate to U1Cn0n1 and therefore cannot represent the Higgs phases we obtain (see Appendix E.2.4).

$\text{tr}\left(\sigma^a \bar{X} \partial_0 X\right)$, the time component of a vector. This description is manifestly dependent on the presence of temporal fluctuations in contrast to the purely static mean field analysis.

Conversely, a lattice Hamiltonian describing the $\mathbb{Z}_2$ phase A_f does exist. However, upon expanding the resulting Hamiltonian about its Dirac cones, the hopping term which breaks the U(1) symmetry down to $\mathbb{Z}_2$ appears to arise from coupling $\text{tr}\left(\sigma^a \bar{X} \mu^y \partial_x \partial_y \left[\partial_x^2 - \partial_y^2\right] X\right)$ to a condensed Higgs field. We can see why this may be the case by observing how symmetries act on $\Xi = \text{tr}\left(\sigma^a \bar{X} \mu^y \partial_x \partial_y \left[\partial_x^2 - \partial_y^2\right] X\right)$:

$$\mathcal{T}[\Xi] = -\Xi, \qquad P_{x,y}[\Xi] = -\Xi, \qquad T_{x,y}[\Xi] = -\Xi, \qquad R_{\pi/2}[\Xi] = \Xi. \tag{6.49}$$

It follows that a Higgs field Φ_1' which couples to Ξ may have a non-zero expectation value in the A_f phase provided it is perpendicular in colour space to both Φ and Φ_1. That is, supposing $\langle \Phi^x \rangle \neq 0$ and $\langle \Phi_1^z \rangle \neq 0$, having $\langle {\Phi_1'}^z \rangle \neq 0$ will not break any of the symmetries.

It can also be shown that the Ising-nematic spin liquid, B_f, is not 'anomalous' in the manner just discussed.

6.4.3 Identification of U(1) spin liquid

The arguments which allowed us to compare $\mathbb{Z}_2$ spin liquids expressed using bosonic and fermionic spinons breaks down in the presence of gapless degrees of freedom. In both cases, these phases are unstable to the proliferation of monopoles, and their true ground states

	Group relations	vison	twist	nPSGx									
				1	2	3	4	5	6	7	8	9	10
1	$T_y^{-1}T_xT_yT_x^{-1}$	-1	1	1	1	1	-1	-1	-1	-1	1	1	1
2	$P_x^{-1}T_xP_xT_x$	1	1	-1	1	-1	1	-1	1	1	1	1	-1
3	$P_y^{-1}T_xP_yT_x^{-1}$	-1	1	1	1	-1	-1	-1	1	-1	-1	1	-1
4	$P_x^{-1}T_yP_xT_y^{-1}$	-1	1	-1	1	-1	1	-1	1	1	1	1	-1
5	$P_y^{-1}T_yP_yT_y$	1	1	1	1	-1	-1	-1	1	-1	-1	1	-1
6	P_x^2	1	-1	-1	1	-1	1	-1	1	1	1	1	-1
7	P_y^2	1	-1	1	1	-1	-1	-1	1	-1	-1	1	-1
8	$P_x^{-1}P_y^{-1}P_xP_y$	-1	-1	1	1	1	1	1	1	1	1	1	1
9	$T_x^{-1}\mathcal{T}^{-1}T_x\mathcal{T}$	1	1	-1	-1	1	-1	1	1	1	1	1	-1
10	$T_y^{-1}\mathcal{T}^{-1}T_y\mathcal{T}$	1	1	1	1	-1	-1	1	1	1	-1	-1	1
11	$P_x^{-1}\mathcal{T}^{-1}P_x\mathcal{T}$	1	-1	-1	1	-1	1	-1	1	1	1	1	-1
12	$P_y^{-1}\mathcal{T}^{-1}P_y\mathcal{T}$	1	-1	1	1	-1	-1	-1	1	-1	-1	1	-1
13	$\mathcal{T}^2$	1	1	-1	-1	-1	-1	-1	-1	-1	-1	-1	-1

Table 6.9: Symmetry fractionalization of nematic PSG's (nPSG's) for spin liquids listed in Table 6.5. nPSG7x (highlighted in blue) corresponds to the fermionic PSG determined in [21]. The columns labelled 'v' and 't' list the vison fractionalization numbers and the twist factors respectively.

will break any symmetries under which the monopoles transform nontrivially. In order to ensure that D_f actually corresponds to the massive phase of the $\mathbb{CP}^1$ theory, D_b, we verify that the two spin liquids share the same fate and ultimately realize a VBS. We approach this problem from two perspectives. We first follow the method outlined in Ref. 48 and determine which bilinear operators *respond* to a weakly varying flux and, consequently, the monopoles' presence. We complement this analysis by calculating the Berry phase of the monopole in a certain limit and show that it agrees with the analogous calculation performed using Schwinger bosons in Ref. 144.

Flux Response

The effective Lagrangian describing D_f is

$$\mathcal{L}_{\mathrm{U}(1)} = i\mathrm{tr}\left(\bar{X}\gamma^\mu\left[\partial_\mu X + iX\sigma^x a_\mu^x\right]\right) + \lambda_2\left\langle\Phi^x\right\rangle \mathrm{tr}\left(\sigma^x\bar{X}\mu^y X\right). \tag{6.50}$$

Because both a_μ^y and a_μ^z are gapped, only a_μ^x is included in $\mathcal{L}_{\mathrm{U}(1)}$. In what follows, we drop the 'x' index, taking $a_\mu^x \to a_\mu$ (this a_μ should not be confused with the gauge field of the original SU(2) gauge field). Finally, at this point in the discussion, it is more convenient to express the Lagrangian in terms of Dirac spinors. Using Eq. (6.27), we find

$$\mathcal{L}_{\mathrm{U}(1)} = \bar{\psi} i\gamma^\mu \left(\partial_\mu - i a_\mu \sigma^x\right) \psi + m\bar{\psi}\sigma^x \mu^y \psi \tag{6.51}$$

where $m = \lambda_2 \langle \Phi^x \rangle$.

In the context of a U(1) gauge theory, a monopole is a topologically nontrivial field configuration of a_μ. In imaginary time, this configuration corresponds exactly to a (stationary) Dirac monopole in 3+1d electromagnetism. However, instead of behaving as a particle, in 2+1d the monopole is actually an instanton: it describes tunneling between different vacua or topological sectors labeled by their total flux, $\int dS_\mu \epsilon^{\mu\nu\lambda}\partial_\nu a_\lambda = 2\pi n$ where n is an integer. This number is zero in the deconfined phase of the gauge theory whereas it fluctuates and ceases to take a definite value once the monopoles proliferate.

A complete treatment of the monopole proceeds by first expanding the gauge field into a classical background piece A_μ and a quantum fluctuation piece $\tilde{a}_\mu$, $a_\mu = A_\mu + \tilde{a}_\mu$, and quantizing the theory about this background. Because the monopole background breaks translational symmetry, this is quite an involved calculation which we will not perform. Instead, we investigate the impact a non-zero flux has on the other operators of the theory. That is, we assume that the classical monopole configuration described by A_μ varies very slowly and, through linear response, determine which operators, O, the flux couples to at leading order: $\langle \mathrm{O}(x) \rangle = \int d^3x' \, \chi_{\mathrm{O}}^\mu(x, x') A_\mu(x')$ where $\chi_{\mathrm{O}}^\mu = \left\langle \mathrm{O}(x) \bar{\psi}\gamma^\mu \sigma^x \psi(x') \right\rangle$. This calculation is outlined in Appendix E.5 and at low energies yields

$$\left\langle \bar{\psi}\gamma^\mu \mu^y \psi \right\rangle = \frac{1}{\pi} \epsilon^{\mu\alpha\beta} \partial_\alpha A_\beta. \tag{6.52}$$

Consequently, whenever there is a net flux, $\int d^2x \left(\partial_x A_y - \partial_y A_x\right) \neq 0$, we expect $\left\langle \bar{\psi}\gamma^0 \mu^y \psi \right\rangle \neq 0$ as well. This allows us to identify $\bar{\psi}\gamma^\mu \mu^y \psi$ with the topological current. The topological

charge is then obtained by integrating the zeroth component of the current over space:

$$Q = \frac{1}{2}\int d^2r\, \bar{\psi}\gamma^0\mu^y\psi. \tag{6.53}$$

The factor of $1/2$ is chosen to ensure that Q is always an integer, as follows from Eq. (6.52).

A conserved charge is the generator of the associated symmetry, meaning that Q generates the flux conservation symmetry. However, this operator should be familiar from Sec. 6.3.1 where it was observed to be the generator of the U(1) VBS symmetry. This can be confirmed by checking that

$$[Q, V_x] = iV_y, \qquad [Q, V_y] = -iV_x. \tag{6.54}$$

where $V_x = \frac{1}{2}\bar{\psi}\mu^x\psi$, $V_y = \frac{1}{2}\bar{\psi}\mu^z\psi$. It follows that Q is conjugate to the VBS order parameters.

When the gapped U(1) gauge theory confines, the monopole proliferation induces large fluctuations in Q. This in turn suppresses the fluctuations of the operators conjugate to Q, ultimately resulting in long range order. We conclude from the analysis above that the proliferation of monopoles triggers the condensation of one of the VBS order parameters, proving that D_f is unstable to a VBS and therefore equivalent to D_b. This mechanism should be contrasted with the scenario outlined in Sec. 6.2.3 where VBS order was achieved by tuning $\mu > 0$ in Eq. (6.33).

Berry phase

A separate argument for the identification of the U(1) spin liquid proceeds by a computation of the monopole Berry phase, along the lines of the original arguments using the semiclassical quantization of the antiferromagnet [53], or the Schwinger boson theory of the U(1) spin liquid [144]. Here, this argument starts from a lattice Hamiltonian for the U1Cn0n1 U(1)

spin liquid, which we obtain from Eq. (E.46) for a generic direction of the Higgs field Φ

$$H = -\sum_{\boldsymbol{i}} \Big\{ i\alpha \left(\psi^\dagger_{\boldsymbol{i}} \psi_{\boldsymbol{i}+\hat{\boldsymbol{x}}} + (-)^{i_x} \psi^\dagger_{\boldsymbol{i}} \psi_{\boldsymbol{i}+\hat{\boldsymbol{y}}} + h.c. \right) + \Phi^a (-)^{i_x+i_y} \beta \left(\psi^\dagger_{\boldsymbol{i}} \tau^a \psi_{\boldsymbol{i}+2\hat{\boldsymbol{x}}} + \psi^\dagger_{\boldsymbol{i}} \tau^a \psi_{\boldsymbol{i}+2\hat{\boldsymbol{y}}} + h.c. \right) - \Phi^a a_0 (-)^{i_x+i_y} \psi^\dagger_{\boldsymbol{i}} \tau^a \psi_{\boldsymbol{i}} \Big\}. \tag{6.55}$$

We are interested in saddle-points of the associated action where the Φ^a Higgs field, and the associated SU(2) gauge field (not written explicitly in Eq. (6.55)) take the configuration of 't Hooft-Polyakov monopoles [66, 128] in 2+1 dimensional spacetime. After obtaining such saddle points, we have to compute the fermion determinant in such a background, and the phase of this determinant will yield the needed monopole Berry phase. This is clearly a demanding computation, and we will not attempt to carry it out in any generality. However, assuming the topological invariance of the needed quantized phase, we can compute it by distorting the saddle point Lagrangian, without closing the fermion gap, to a regime where the phase is easily computable. Specifically, consider the limit where the parameter a_0 in Eq. (6.55) is much larger than all other parameters, including α and β. For the 't Hooft-Polyakov monopole at the origin of spacetime, $\Phi^a \sim \hat{r}^a$, where $\hat{r}^a$ is a unit radial vector in spacetime. Ignoring all but the a_0 term in Eq. (6.55), we then have to compute the Berry phases of single fermions, each localized on a single site, in the presence of a staggered field $\propto \Phi^a$. However, this Berry phase is precisely that computed by Haldane [53]; in his case the staggered field was the antiferromagnetic order parameter which acts in the spin SU(2) space (in contrast to the staggered field in the gauge SU(2) space in our case), and the Berry phase arose from that of a quantized $S = 1/2$ spin. As the Berry phase of a spin 1/2 localized fermion is equal to the spin Berry phase, we conclude that the 't Hooft-Polyakov monopole Berry phase is equal to that obtained by Haldane [53] for $S = 1/2$. Therefore, the monopole Berry phases in the fermionic spinon U(1) spin liquid U1C$n0n1$ are equal to those of the U(1) spin liquid of the bosonic $\mathbb{CP}^1$ theory of the square lattice antiferromagnet [10, 156].

6.5 Conclusions

Two distinct classes of $2+1$ dimensional fermion-boson dualities have recently seen much discussion in the literature.

One class concerns gapped $\mathbb{Z}_2$ spin liquids which have both bosonic and fermionic spinon excitations. Binding with a vison transmutes a spinon from a boson to a fermion, or vice versa [142], and this allows one to map between $\mathbb{Z}_2$ spin liquids obtained in mean-field theory using fermionic or bosonic ansatze. Specific examples of such dualities have been described on a variety of lattices [21, 43, 106, 107, 136, 204, 205, 208, 211], and our results for such dualities appear in Figs. 6.1 and 6.2. We described the dualities between the bosonic $\mathbb{Z}_2$ spin liquids A_b, B_b, C_b and the fermionic spin liquids A_f, B_f, C_f respectively. The first two of these dualities have been obtained earlier [21, 205], but we obtained all three in a unified manner with reference to continuum theories.

The second class of dualities concern conformal gauge theories with fermionic and bosonic matter [25, 82, 85, 111, 118, 164]. Most relevant to our considerations is the proposed duality [179] between the critical bosonic $\mathbb{CP}^1$ U(1) gauge theory, and fermionic SU(2) QCD_3 with $N_f = 2$ flavors of Dirac fermions.

Among our results was a demonstration of the compatibility between these two classes of dualities. We Higgsed the critical bosonic $\mathbb{CP}^1$ and fermionic QCD_3 theories, and found nontrivial consistency between the gapped $\mathbb{Z}_2$ spin liquids so obtained. We also obtained a fermionic counterpart to the U(1) spin liquid with gapped bosonic spinons on the square lattice originally obtained by Arovas and Auerbach [10] (which is equivalent to the gapped z_α phase of the $\mathbb{CP}^1$ theory [143, 144]): the U(1) spin liquid with gapped fermionic spinons was identified as U1Cn0n1 (in Wen's notation). Both the bosonic and fermionic U(1) spin liquids are eventually unstable to monopole proliferation, confinement, and VBS order, and have identical monopole Berry phases (as shown in Section 6.4.3).

Our analysis also led us to propose new fermion-boson dualities between multi-critical

theories. One example is the duality between (*i*) the U(1) gauge theory in Eq. (6.4) with two unit charge bosons z_α, a doubly charged Higgs field P, and the masses of both fields tuned to criticality; and (*ii*) the SU(2) gauge theory in Eq. (6.6) with $N_f = 2$ massless fundamental Dirac fermions ψ, and two adjoint Higgs fields Φ, Φ_1, and the masses of both Higgs field tuned to criticality.

The fermionic approach to square lattice spin liquids [2, 3, 184] yields a variety of critical spin liquids coupled to U(1) and SU(2) gauge fields. Two examples are in Fig. 6.1(b), the states labeled by Wen as U1Bx11n and SU2Bn0. The results of Wang *et al.* [179] indicate that the SU(2) critical state SU2Bn0 cannot appear as an extended critical phase in a square lattice antiferromagnet, and it is only realized as a critical point between the Néel and VBS states. From our comparison of Fig. 6.1(b) and Fig. 6.1(a), we obtain evidence that the critical U(1) spin liquid U1Bx11n also cannot be realized as an extended phase on the square lattice: it is unstable to the appearance of canted antiferromagnetic order.

Appendix A

Appendix to Chapter 2

A.1 Mean field theory with boundary

In this appendix, we consider the mean field equations in the presence of a boundary. We define the lattice to be finite in the x-direction, $x_i = 1, \ldots, N$, and infinite in the y-direction (to remove factors of i, we actually switch the x- and y-directions compared to Eq. (2.6)). We rewrite the Fourier transform, which is now only valid in the y-direction:

$$\begin{aligned} c_{ij\sigma} &= \int \frac{dk}{2\pi} e^{iky_j} c_{ik\sigma}, \qquad d_{ij\alpha} = \int \frac{dk}{2\pi} e^{iky_j} \left[2\alpha \sin k\, c_{ik\alpha} + (c_{j+1,k\alpha} - c_{i-1,k\alpha})\right], \\ f_{ij\sigma} &= \int \frac{dk}{2\pi} e^{iky_j} f_{ik\sigma}. \end{aligned} \tag{A.1}$$

Translational invariance in the y-direction implies that the mean field parameters will depend only on the distance from the boundary – the roman indices i, j, etc. label the x-coordinate only. We express the Hamiltonian in block form as

$$\begin{aligned} \hat{H}_{MF} &= \sum_k \Psi^\dagger_{k\sigma} \mathcal{H}_\sigma(k) \Psi_{k\sigma}, \qquad \Psi^\dagger_{k\sigma} = \left(c^\dagger_{1k\sigma}, c^\dagger_{2k\sigma}, \ldots, f^\dagger_{1k\sigma}, f^\dagger_{2k\sigma}, \ldots\right) \\ &\qquad\qquad = \left(\psi^\dagger_{1k\sigma}, \psi^\dagger_{2k\sigma}, \ldots, \psi^\dagger_{1+N,k\sigma}, \psi^\dagger_{2+N,k\sigma}, \ldots\right) \\ \mathcal{H}_\uparrow(k) &= \begin{pmatrix} h_c(k) & h_{cf}(k) \\ h^\dagger_{cf}(k) & h_f(k) \end{pmatrix} \qquad \mathcal{H}_\downarrow(k) = \mathcal{H}_\uparrow(-k)^* \end{aligned} \tag{A.2}$$

with blocks given by

$$h_c(k) = -\frac{t_1}{2}\begin{pmatrix} 2\cos k & 1 & 0 & \cdots \\ 1 & 2\cos k & 1 & \cdots \\ 0 & 1 & 2\cos k & \cdots \\ \vdots & \vdots & \vdots & \ddots \end{pmatrix} - t_2\cos k \begin{pmatrix} 0 & 1 & 0 & \cdots \\ 1 & 0 & 1 & \cdots \\ 0 & 1 & 0 & \cdots \\ \vdots & \vdots & \vdots & \ddots \end{pmatrix} - \begin{pmatrix} \mu_1 & 0 & 0 & \cdots \\ 0 & \mu_2 & 0 & \cdots \\ 0 & 0 & \mu_3 & \cdots \\ \vdots & \vdots & \vdots & \ddots \end{pmatrix} \tag{A.3}$$

$$\begin{aligned} h_f(k) = -\frac{1}{2}&\begin{pmatrix} 2\chi_{1y}\cos k & \chi_{1x} & 0 & 0 & \cdots & \cdots & \cdots \\ \chi_{1x} & 2\chi_{2y}\cos k & \chi_{2x} & 0 & \cdots & \cdots & \cdots \\ 0 & \chi_{2x} & 2\chi_{3y}\cos k & \chi_{3x} & \cdots & \cdots & \cdots \\ \vdots & \vdots & \vdots & \vdots & \ddots & \cdots & \cdots \\ \vdots & \vdots & \vdots & \vdots & \vdots & 2\chi_{N-1,y}\cos k & \chi_{N-1,x} \\ \vdots & \vdots & \vdots & \vdots & \vdots & \chi_{N-1,x} & 2\chi_{Ny}\cos k \end{pmatrix} \\ &+ \begin{pmatrix} \lambda_1 & 0 & 0 & 0 & \cdots & \cdots & \cdots \\ 0 & \lambda_2 & 0 & 0 & \cdots & \cdots & \cdots \\ 0 & 0 & \lambda_3 & 0 & \cdots & \cdots & \cdots \\ \vdots & \vdots & \vdots & \vdots & \ddots & \cdots & \cdots \\ \vdots & \vdots & \vdots & \vdots & \vdots & \lambda_{N-1} & 0 \\ \vdots & \vdots & \vdots & \vdots & \vdots & 0 & \lambda_N \end{pmatrix} \end{aligned} \tag{A.4}$$

$$h_{cf}(k) = \frac{1}{2}\begin{pmatrix} 2V_1\sin k & -V_2 & 0 & \cdots \\ V_1 & 2V_2\sin k & -V_3 & \cdots \\ 0 & V_2 & 2V_3\sin k & \cdots \\ \vdots & \vdots & \vdots & \ddots \end{pmatrix}. \tag{A.5}$$

To determine correlation functions, we diagonalize the Hamiltonian numerically. For each

k, we find the matrices $U(k)$ such that

$$U^\dagger \mathcal{H}(k) U(k) = \Lambda(k), \qquad \Lambda_{ij}(k) = \delta_{ij} E_j(k)\,. \tag{A.6}$$

Then, the mean field equations of Eqs. (2.9) – (2.11) may be expressed as

$$1 = \sum_\alpha \int \frac{dk}{2\pi} \left\langle f^\dagger_{kj\alpha} f_{kj\alpha} \right\rangle = \sum_\alpha \int \frac{dk}{2\pi} \left\langle \psi^\dagger_{k,j+N,\alpha} \psi_{k,j+N,\alpha} \right\rangle = 2 \int \frac{dk}{2\pi} \sum_{l=1}^{2N} n(E_l(k)) U_{j+N,l}(k) U^\dagger_{l,j+N}(k) \tag{A.7}$$

$$1 = \sum_\alpha \int \frac{dk}{2\pi} \left\langle c^\dagger_{kj\alpha} c_{kj\alpha} \right\rangle = \sum_\alpha \int \frac{dk}{2\pi} \left\langle \psi^\dagger_{kj\alpha} \psi_{kj\alpha} \right\rangle = 2 \int \frac{dk}{2\pi} \sum_{l=1}^{2N} n(E_l(k)) U_{jl}(k) U^\dagger_{lj}(k) \tag{A.8}$$

$$\begin{aligned} V_i &= -\frac{J_K}{2} \sum_\alpha \int \frac{dk}{2\pi} \left\langle d^\dagger_{ik\alpha} f_{ik\alpha} \right\rangle = -\frac{J_K}{2} \sum_\alpha \int \frac{dk}{2\pi} \left[2\alpha \sin k \left\langle c^\dagger_{ik\alpha} f_{ik\alpha} \right\rangle + \left\langle c^\dagger_{i+1,k\alpha} f_{ik\alpha} \right\rangle - \left\langle c^\dagger_{i-1,k\alpha} f_{ik\alpha} \right\rangle \right] \\ &= -\frac{J_K}{2} \sum_\alpha \int \frac{dk}{2\pi} \left[2\alpha \sin k \left\langle \psi^\dagger_{ik\alpha} \psi_{i+N,k\alpha} \right\rangle + \left\langle \psi^\dagger_{i+1,k\alpha} \psi_{i+N,k\alpha} \right\rangle - \left\langle \psi^\dagger_{i-1,k\alpha} \psi_{i+N,k\alpha} \right\rangle \right] \\ &= -J_K \int \frac{dk}{2\pi} \sum_{l=1}^{2N} n(E_l(k)) \left[2 \sin k \; U_{i+N,l}(k) U^\dagger_{l,i}(k) + U_{i+N,l}(k) U^\dagger_{l,i+1}(k) - U_{i+N,l}(k) U^\dagger_{l,i-1}(k) \right] \end{aligned} \tag{A.9}$$

$$\begin{aligned} \chi_{ix} &= \frac{J_H}{2} \sum_\alpha \int \frac{dk}{2\pi} \left[\left\langle f^\dagger_{i+1,k\alpha} f_{ik} \right\rangle + \left\langle f^\dagger_{ik\alpha} f_{i+1,k\alpha} \right\rangle \right] \\ &= \frac{J_H}{2} \sum_\alpha \int \frac{dk}{2\pi} \left[\left\langle \psi^\dagger_{i+N+1,k\alpha} \psi_{i+N,k\alpha} \right\rangle + \left\langle \psi^\dagger_{i+N,k\alpha} \psi_{i+N+1,k\alpha} \right\rangle \right] \\ &= J_H \int \frac{dk}{2\pi} \sum_{l=1}^{2N} n(E_l(k)) \left[U_{i+N,l}(k) U^\dagger_{l,i+N+1}(k) + U_{i+N,1,l}(k) U^\dagger_{l,i+N+1}(k) \right] \end{aligned} \tag{A.10}$$

$$\begin{aligned} \chi_{iy} &= \frac{J_H}{2} \sum_\alpha \int \frac{dk}{2\pi} 2 \cos k \left\langle f^\dagger_{ik\alpha} f_{ik\alpha} \right\rangle = J_H \sum_\alpha \int \frac{dk}{2\pi} \cos k \left\langle \psi^\dagger_{i+N,k\alpha} \psi_{i+N,k\alpha} \right\rangle \\ &= 2\, J_H \int \frac{dk}{2\pi} \sum_{l=1}^{2N} n(E_l(k)) \cos k \; U_{i+N,l}(k) U^\dagger_{l,i+N}(k) \end{aligned} \tag{A.11}$$

Appendix B

Appendix to Chapter 3

B.1 The "Senthil-Fisher" mechanism

Here we reproduce the discussion in Ref. 168, and demonstrate how the GSM of the order of $\bar{\psi}\vec{\sigma}\psi$ (and similarly $\bar{\psi}\vec{\tau}\psi$) is enlarged from S^2 to SO(3). First we couple the $N_f = 4$ QED to a three component dynamical unit vector field $\boldsymbol{N}(x,\tau)$:

$$\mathcal{L} \;=\; \bar{\psi}\gamma_\mu(\partial_\mu - ia_\mu)\psi + m\bar{\psi}\boldsymbol{\sigma}\psi\cdot\boldsymbol{N}. \tag{B.1}$$

The flavor indices are hidden in the equation above for simplicity. Now following the standard $1/m$ expansion of Ref. 1, we obtain the following action after integrating out the fermion ψ_j:

$$\mathcal{L}_{eff} = \frac{1}{g}(\partial_\mu \boldsymbol{N})^2 + i2\pi\mathrm{Hopf}[\boldsymbol{N}] + i2a_\mu J^T_\mu + \frac{1}{e^2}f^2_{\mu\nu}, \tag{B.2}$$

where $1/g \sim m$. $J^T_0 = \frac{1}{4\pi}\epsilon_{abc}N^a\partial_x N^b\partial_y N^c$ is the Skyrmion density of $\boldsymbol{N}$, thus J^T_μ is the Skyrmion current. The second term of Eq. (B.2) is the Hopf term of $\boldsymbol{N}$ which comes from the fact that $\pi_3[S^2] = \mathbb{Z}$.

Now if we introduce the CP^1 field $z_\alpha = (z_1, z_2)^t = (n_1 + in_2, n_3 + in_4)^t$ for $\boldsymbol{N}$ as $\boldsymbol{N} = z^\dagger\boldsymbol{\sigma}z$, the Hopf term becomes precisely the $\Theta-$term for the O(4) *unit* vector $\boldsymbol{n}$ with $\Theta = 2\pi$:

$$i2\pi\mathrm{Hopf}[\boldsymbol{N}] = \frac{i2\pi}{2\pi^2}\epsilon_{abcd}n^a\partial_x n^b\partial_y n^c\partial_\tau n^d. \tag{B.3}$$

In the CP^1 formalism, the Skyrmion current $J^T_\mu = \frac{1}{2\pi}\epsilon_{\mu\nu\rho}\partial_\nu\alpha_\rho$, where α_μ is the gauge field that the CP^1 field z_α couples to. The coupling between a_μ and α_μ

$$2ia_\mu J^T_\mu = \frac{i2}{2\pi}\epsilon_{\mu\nu\rho}a_\mu\partial_\nu\alpha_\mu \tag{B.4}$$

takes precisely the form of the mutual CS theory of a Z_2 topological order, and it implies that the gauge charge z_α is an anyon of a Z_2 topological order, and the condensate of z_α (equivalently the order of $\boldsymbol{N}$) has a GSM $= \mathrm{SO}(3) = S^3/Z_2$, where S^3 is the manifold of the unit vector $\vec{n}$.

B.2 Deriving the WZW term

Let us consider a theory of QED_3 with $N_f = 4$ flavors of Dirac fermions coupled to a matrix order parameter field $\mathcal{P}$:

$$\mathcal{L} = \sum_{i,j}\bar{\psi}_i(\gamma_\mu(\partial_\mu - ia_\mu)\delta_{ij} + m\mathcal{P}_{ij})\psi_j. \tag{B.5}$$

$\mathcal{P}$ takes values in the target manifold $\mathcal{P} \in \mathcal{M} = \frac{U(4)}{U(2)\times U(2)}$. We can parametrize the matrix field $\mathcal{P} = U^\dagger\Omega U$, where $U \in SU(4)$ and $\Omega = \sigma^z \otimes \mathbf{1}_{2\times 2}$. $\mathcal{P}$ satisfies $\mathcal{P}^2 = \mathbf{1}_{4\times 4}$ and $\mathrm{tr}\mathcal{P} = 0$.

The effective action after integrating over the fermion fields formally reads

$$\begin{aligned}\mathcal{S}_{eff}[a_\mu, \mathcal{P}] &= -\ln\int D\bar{\psi}D\psi\exp\left[-\int d^3x\mathcal{L}(\psi, a_\mu, \mathcal{P})\right] \\ &= -\ln\det[\mathcal{D}(a_\mu, \mathcal{P})] = -\mathrm{Tr}\ln[\mathcal{D}(a_\mu, \mathcal{P})].\end{aligned} \tag{B.6}$$

The expansion of $\mathcal{S}_{eff}$ has the following structure

$$\mathcal{S}_{eff}[a_\mu, \mathcal{P}] = \mathcal{S}_{eff}[a_\mu = 0, \mathcal{P}] + O(a) \tag{B.7}$$

and we will look at the first term in the expansion. In general, all terms that respect the

symmetry of the original action will appear in the expansion of the fermion determinant. Here we want to derive the topological term of $\mathcal{P}$. One way to obtain the effective action is the perturbative method developed in Ref. 1. Let us vary the action over the matrix field $\mathcal{P}$

$$\delta\mathcal{S}_{eff} = -\mathrm{Tr}(m\delta\mathcal{P}(\mathcal{D}^\dagger\mathcal{D})^{-1}\mathcal{D}^\dagger) \tag{B.8}$$

and then expand $(\mathcal{D}^\dagger\mathcal{D})^{-1}$ in gradients of $\mathcal{P}$:

$$\begin{aligned}(\mathcal{D}^\dagger\mathcal{D})^{-1} &= (-\partial^2 + m^2 - m\gamma_\mu\partial_\mu\mathcal{P})^{-1} \\ &= (-\partial^2+m^2)^{-1}\sum_{n=0}^{\infty}\left[(-\partial^2+m^2)^{-1}m\gamma_\mu\partial_\mu\mathcal{P}\right]^n\end{aligned} \tag{B.9}$$

Since the coefficient of the WZW term is dimensionless, we will look at the following term in the expansion

$$\begin{aligned}\delta W(\mathcal{P}) &= -\mathrm{Tr}\left[m^2\delta\mathcal{P}\frac{1}{-\partial^2+m^2}\left[(-\partial^2+m^2)^{-1}m\gamma_\mu\partial_\mu\mathcal{P}\right]^3\mathcal{P}\right] \\ &= -K\int d^3x\ \mathrm{Tr}[\delta\mathcal{P}(\gamma_\mu\partial_\mu\mathcal{P})^3\mathcal{P}]\end{aligned} \tag{B.10}$$

where

$$K = \int\frac{d^3p}{(2\pi)^3}\frac{m^5}{(p^2+m^2)^4} = \frac{1}{64\pi} \tag{B.11}$$

is a dimensionless number, and "Tr" is the trace over both the Dirac and flavour indices. After tracing over the Dirac indices,

$$\mathrm{Tr}(\gamma_\mu\gamma_\nu\gamma_\rho) = 2i\epsilon_{\mu\nu\rho} \tag{B.12}$$

we obtain the following term for the variation

$$\delta W(\mathcal{P}) = -\frac{2\pi i}{64\pi^2}\epsilon_{\mu\nu\rho}\int d^3x\ \mathrm{tr}[\delta\mathcal{P}\partial_\mu\mathcal{P}\partial_\nu\mathcal{P}\partial_\rho\mathcal{P}\mathcal{P}], \tag{B.13}$$

where "tr" now refers to a trace over the flavour indices only.

We can restore the topological term of the nonlinear σ-model by the standard method of introducing an auxiliary coordinate u. The field $\tilde{\mathcal{P}}(x,u)$ interpolates between $\tilde{\mathcal{P}}(x,u=0)=\Omega$ and $\tilde{\mathcal{P}}(x,u=1)=\mathcal{P}(x)$. The topological term reads

$$W(\tilde{\mathcal{P}})=-\frac{2\pi i}{256\pi^2}\epsilon_{\mu\nu\rho\delta}\int_0^1 du\int d^3x\,\mathrm{tr}[\tilde{\mathcal{P}}\partial_\mu\tilde{\mathcal{P}}\partial_\nu\tilde{\mathcal{P}}\partial_\rho\tilde{\mathcal{P}}\partial_\delta\tilde{\mathcal{P}}]. \tag{B.14}$$

The extra factor of $1/4$ comes from the anti-symmetrization of the u coordinate with other indices.

Appendix C

Appendix to Chapter 4

C.1 General non-abelian subgroup of SU($2N$)

In this appendix, we briefly discuss the RG flow which results upon breaking the flavor symmetry from SU($2N$)$\to \mathcal{G}\times$SU($2N$)/$\mathcal{G}$, where $\mathcal{G}$ is a continuous non-abelian subgroup of SU($2N$). The most general form the disorder could take is

$$S^{\mathcal{G}}_{\rm dis}[\psi,\bar\psi] = \int d^dx\, d\tau \left[M^{\mathcal{G}}_a(x)\bar\psi \mathcal{T}^a\psi(x,\tau) + i\mathcal{A}^{\mathcal{G}}_{ja}(x)\mathcal{T}^a\gamma^j\psi(x,\tau) + V^{\mathcal{G}}_a(x)\mathcal{T}^a\gamma^0\psi(x,\tau)\right] \tag{C.1}$$

where $\mathcal{T}^a$ are the generators of $\mathcal{G}$. Averaging over disorder, we assume

$$\begin{aligned}
\overline{M^{\mathcal{G}}_a(x)M^{\mathcal{G}}_b(x')} &= \frac{\mu^{-\epsilon}\lambda_t}{2}\delta_{ab}\delta^d(x-x'), & \overline{M^{\mathcal{G}}_a(x)\mathcal{A}^{\mathcal{G}}_{jb}(x')} &= 0,\\
\overline{\mathcal{A}^{\mathcal{G}}_{ia}(x)\mathcal{A}^{\mathcal{G}}_{jb}(x')} &= \frac{\mu^{-\epsilon}\lambda_{\mathcal{A}}}{2}\delta_{ab}\delta_{ij}\delta^d(x-x'), & \overline{M^{\mathcal{G}}_a(x)V^{\mathcal{G}}_b(x')} &= 0,\\
\overline{V^{\mathcal{G}}_a(x)V^{\mathcal{G}}_b(x')} &= \frac{\mu^{-\epsilon}\lambda_v}{2}\delta_{ab}\delta^d(x-x'), & \overline{\mathcal{A}^{\mathcal{G}}_{ja}(x)V^{\mathcal{G}}_b(x')} &= 0.
\end{aligned} \tag{C.2}$$

We can study this theory in the same way we did in Secs. 4.2.2 and 4.3.1. The Feynman rules will be analogous to those shown in Fig. 4.3.

From the calculations in Appendix C.3, we see that only the diagrams in Figs. C.2(a) and (b), and Figs. C.3(a) and (b) contribute to the renormalization of $\lambda_{\mathcal{A}}$. In particular,

letting $\Gamma_{\mathcal{A}}$ be the vertex function whose spinor indices are proportional to $i\gamma^j \otimes i\gamma_j$, we find

$$\begin{aligned}\Gamma_a\, i\gamma^j \otimes i\gamma_j &= -\frac{1}{4\pi\epsilon}\left(\lambda_t^2 + 4\lambda_{\mathcal{A}}^2 + \lambda_v^2\right)\gamma^j \otimes \gamma_j \sum_{ab}\left[\mathcal{T}^a\mathcal{T}^b \otimes \mathcal{T}^a\mathcal{T}^b - \mathcal{T}^a\mathcal{T}^b \otimes \mathcal{T}^b\mathcal{T}^a\right] \\ &= +\frac{1}{8\pi\epsilon}\left(\lambda_t^2 + 4\lambda_{\mathcal{A}}^2 + \lambda_v^2\right) i\gamma^j \otimes i\gamma_j \sum_{ab}\left[\mathcal{T}^a, \mathcal{T}^b\right] \otimes \left[\mathcal{T}^a, \mathcal{T}^b\right] \\ &= -\frac{1}{8\pi\epsilon}\left(\lambda_t^2 + 4\lambda_{\mathcal{A}}^2 + \lambda_v^2\right) i\gamma^j \otimes i\gamma_j \sum_{a}\mathcal{T}^a \otimes \mathcal{T}^a \end{aligned} \tag{C.3}$$

where we've used the fact that

$$\sum_{ab}\left[\mathcal{T}^a, \mathcal{T}^b\right] \otimes \left[\mathcal{T}^a, \mathcal{T}^b\right] = \sum_{abcd} if^{abc}\, if^{abd}\mathcal{T}^c \otimes \mathcal{T}^d = -\sum_{cd}\delta_{cd}\mathcal{T}^c \otimes \mathcal{T}^d = -\sum_{a}\mathcal{T}^a \otimes \mathcal{T}^a, \tag{C.4}$$

where f^{abc} are the structure constants of the algebra. It follows that

$$\pi\beta_{\mathcal{A}} = -\left(\lambda_t^2 + 4\lambda_{\mathcal{A}}^2 + \lambda_v^2\right). \tag{C.5}$$

C.2 Fermion self-energy

In this section, we calculate the fermion self-energy diagrams given in Fig. 4.5.

Self-energy contribution from photon: Fig. 4.5(a)

$$\text{Fig. 4.5(a)} = \frac{16}{2N}\mu^{-\epsilon}g^2 \int \frac{d^Dq}{(2\pi)^D}\, i\gamma^\mu \frac{i(p+q)_\alpha\gamma^\alpha}{(p+q)^2} i\gamma^\nu \frac{\delta_{\mu\nu}}{|q|}. \tag{C.6}$$

Using the identity

$$\frac{1}{AB^n} = \int_0^1 dx\, \frac{n(1-x)^{n-1}}{[A + x(B-A)]^{n+1}} \tag{C.7}$$

and the fact that $\gamma^\mu\gamma^\alpha\gamma_\mu = (2\delta^{\alpha\mu} - \gamma^\alpha\gamma^\mu)\,\gamma_\mu = -(D-2)\gamma^\alpha$, we write

$$\begin{aligned}\text{Fig. 4.5(a)} &= \frac{i(D-2)16\mu^{-\epsilon}g^2}{2N}\gamma^\mu \int \frac{d^Dq}{(2\pi)^D}\int_0^1 dx\,\frac{1}{2\sqrt{1-x}}\frac{q_\mu + (1-x)p_\mu}{[q^2+x(1-x)p^2]^{3/2}} \\ &= -i\gamma^\mu p_\mu\left(\frac{8g^2}{3\pi^2(2N)\epsilon}\right) + \text{finite.}\end{aligned} \tag{C.8}$$

Self-energy contribution from singlet mass disorder: Fig. 4.5(b)

$$\begin{aligned}\text{Fig. 4.5(b)} &= g_s\int\frac{d^Dq}{(2\pi)^D}\,2\pi\delta(q_0)\frac{i(q+p)_\mu\gamma^\mu}{(q+p)^2} \\ &= ig_s\int\frac{d^dq}{(2\pi)^d}\,\frac{i\left[(q+p)_i\gamma^i + p_0\gamma^0\right]}{(q+p)^2+p_0^2} = -ip_0\gamma^0\left(\frac{g_s}{2\pi\epsilon}\right) + \text{finite.}\end{aligned} \tag{C.9}$$

Self-energy contribution from SU(2) mass disorder: Fig. 4.5(c)

The contribution from the SU(2) mass disorder is the same, since the Pauli matrices square to the identity:

$$\text{Fig. 4.5(c)} = g_{t,a}\sigma^a\sigma^a\int\frac{d^Dq}{(2\pi)^D}\,2\pi\delta(q_0)\frac{i(q+p)_\mu\gamma^\mu}{(q+p)^2} = -ip_0\gamma^0\left(\frac{g_{t,a}}{2\pi\epsilon}\right) + \text{finite.} \tag{C.10}$$

Self-energy contribution from scalar potential disorder: Fig. 4.5(d)

$$\text{Fig. 4.5(d)} = -g_{v,a}\int\frac{d^Dq}{(2\pi)^D}2\pi\delta(q_0)i\gamma^0\frac{i(q+p)_\alpha\gamma^\alpha}{(q+p)^2}i\gamma^0 = -ip_0\gamma^0\left(\frac{g_{v,a}}{2\pi\epsilon}\right) + \text{finite.} \tag{C.11}$$

Self-energy contribution from vector potential disorder: Fig. 4.5(e)

$$\text{Fig. 4.5(e)} = g_{\mathcal{A},a}\int\frac{d^Dq}{(2\pi)^D}2\pi\delta(q_0)i\gamma^j\frac{i(q+p)_\alpha\gamma^\alpha}{(q+p)^2}i\gamma_j = -ip_0\gamma^0\left(\frac{g_{\mathcal{A},a}}{\pi\epsilon}\right) + \text{finite.} \tag{C.12}$$

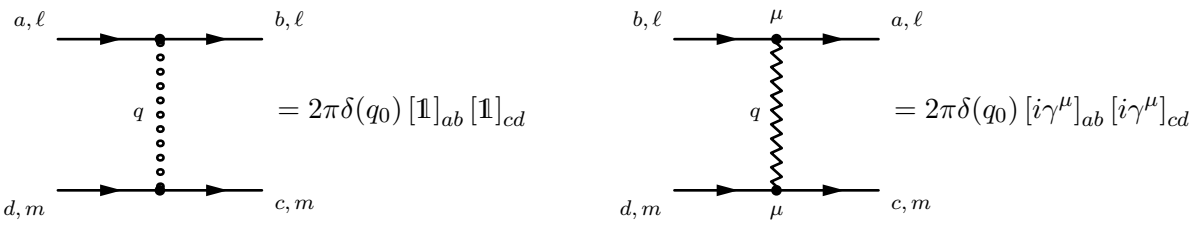

Figure C.1: Feynman rules for diagrams without flavor indices. a, b, c, d on the graphs label the spinor indices, and ℓ and m label the replica indices. The vertex on the left describes mass-like disorders, such as $M_s(r)$ and $M_{t,a}(r)$, and the diagram on the right corresponds to the SU(2) scalar and vector potential disorder, $V_a(r)$, and $\mathcal{A}_{j,a}(r)$.

C.3 Diagrams without flavor indices

Since the spinor and flavor structure of the interactions factor, it's convenient to first calculate the diagrams which correct the four-point interaction without reference to the fermion flavor indices. We denote these generalized vertices with the Feynman graphs shown in Fig. C.1. The set of diagrams with only internal mass-like disorder and photon lines is shown in Fig. C.2, while diagrams with only gauge-like disorder and photon lines are shown in Fig. C.3. Finally, Fig. C.4 lists those diagrams which have contributions from both mass and gauge-like disorder. While there are many repetitions, all integrals have been included for completeness.

C.3.1 Diagrams with mass-type disorder and photon lines: Fig: C.2

In this section, we evaluate the diagrams with only internal mass disorder and photon lines. These are listed in Fig. C.2.

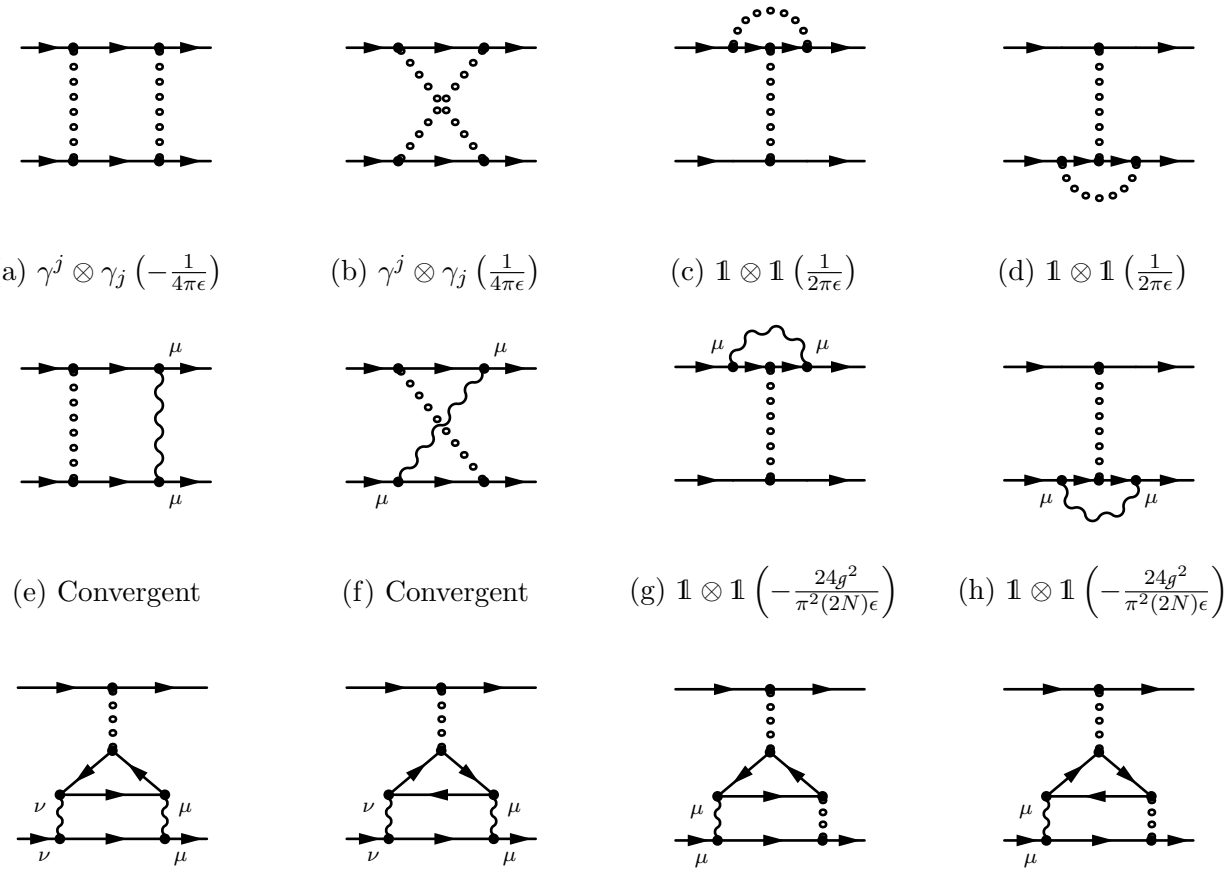

(a) $\gamma^j \otimes \gamma_j \left(-\frac{1}{4\pi\epsilon}\right)$ (b) $\gamma^j \otimes \gamma_j \left(\frac{1}{4\pi\epsilon}\right)$ (c) $\mathbb{1} \otimes \mathbb{1} \left(\frac{1}{2\pi\epsilon}\right)$ (d) $\mathbb{1} \otimes \mathbb{1} \left(\frac{1}{2\pi\epsilon}\right)$

(e) Convergent (f) Convergent (g) $\mathbb{1} \otimes \mathbb{1} \left(-\frac{24g^2}{\pi^2(2N)\epsilon}\right)$ (h) $\mathbb{1} \otimes \mathbb{1} \left(-\frac{24g^2}{\pi^2(2N)\epsilon}\right)$

(i) $\mathbb{1} \otimes \mathbb{1} \left(\frac{16g^4}{\pi^2(2N)\epsilon}\right)$ (j) $\mathbb{1} \otimes \mathbb{1} \left(\frac{16g^4}{\pi^2(2N)\epsilon}\right)$ (k) Cancels Fig. 12l (l) Cancels Fig. 12k

Figure C.2: 4-point diagrams with photon and mass-like disorder internal lines. Below each diagram, the divergent piece, if present, is given. (The factor of $2\pi\delta(q_0)$ has been been suppressed for simplicity.)

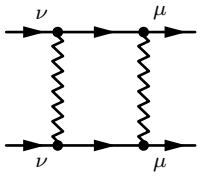

(a) $\left(\frac{1}{4\pi\epsilon}\right)\begin{cases} -\sum_j \gamma^j \otimes \gamma_j, & (\mu,\nu) = (0,0),(k,\ell) \\ \mathbb{1}\otimes\mathbb{1} - \gamma^0\otimes\gamma^0, & (\mu,\nu) = (0,\ell),(\ell,0) \end{cases}$

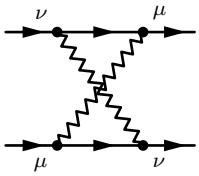

(b) $\left(\frac{1}{4\pi\epsilon}\right)\begin{cases} \sum_j \gamma^j \otimes \gamma_j, & (\mu,\nu) = (0,0),(k,\ell) \\ \mathbb{1}\otimes\mathbb{1} + \gamma^0\otimes\gamma^0, & (\mu,\nu) = (0,\ell),(\ell,0) \end{cases}$

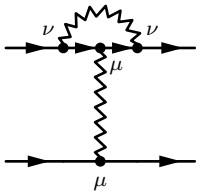

(c) $2\pi(p_0)\gamma^0\otimes\gamma^0\left(\frac{1}{2\pi\epsilon}\right)$
$\times\delta^{\mu 0}\left[-\delta^{\nu 0} + \sum_j \delta^{\nu j}\right]$

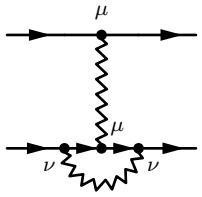

(d) $2\pi(p_0)\gamma^0\otimes\gamma^0\left(\frac{1}{2\pi\epsilon}\right)$
$\times\delta^{\nu 0}\left[-\delta^{\mu 0} + \sum_j \delta^{\mu j}\right]$

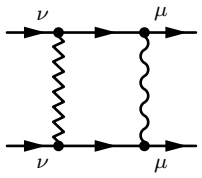

(e) Convergent

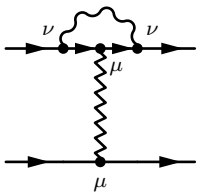

(f) $2\pi\delta(p_0)\gamma^\mu\otimes\gamma^\mu\left(-\frac{8g^2}{3\pi^2(2N)\epsilon}\right)$

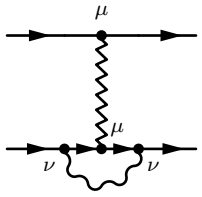

(g) $2\pi\delta(p_0)\gamma^\mu\otimes\gamma^\mu\left(-\frac{8g^2}{3\pi^2(2N)\epsilon}\right)$

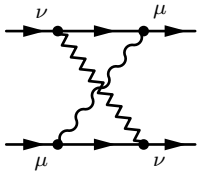

(h) Convergent

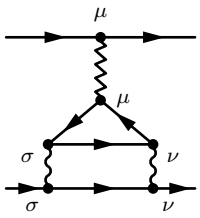

(i) Vanishes

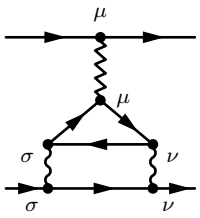

(j) Vanishes

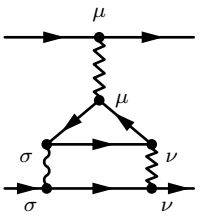

(k) Cancels Fig. 13l

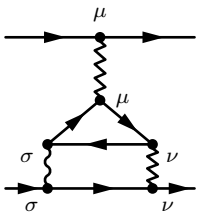

(l) Cancels Fig. 13k

Figure C.3: 4-point diagrams with photon and gauge-like disorder internal lines. Below each diagram, the divergent piece, if present, is given. (The factor of $2\pi\delta(q_0)$ has been been suppressed for simplicity.)

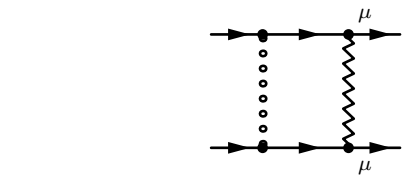

(a) $\left(\frac{1}{4\pi\epsilon}\right)\begin{cases} -\sum_j \gamma^j \otimes \gamma_j, & \mu = 0, \\ \mathbb{1} \otimes \mathbb{1} - \gamma^0 \otimes \gamma^0, & \mu = x, y \end{cases}$

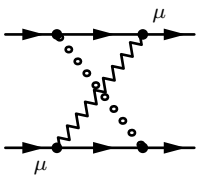

(b) $\left(\frac{1}{4\pi\epsilon}\right)\begin{cases} -\sum_j \gamma^j \otimes \gamma_j, & \mu = 0, \\ -\mathbb{1} \otimes \mathbb{1} - \gamma^0 \otimes \gamma^0, & \mu = x, y \end{cases}$

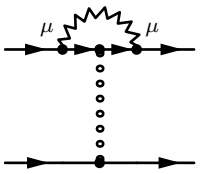

(c) $\mathbb{1} \otimes \mathbb{1}\left(-\frac{1}{2\pi\epsilon}\right)$

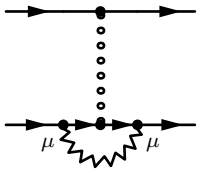

(d) $\mathbb{1} \otimes \mathbb{1}\left(-\frac{1}{2\pi\epsilon}\right)$

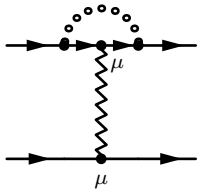

(e) $\delta^{\mu 0}\gamma^0 \otimes \gamma^0\left(\frac{1}{2\pi\epsilon}\right)$

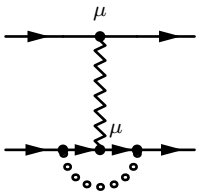

(f) $\delta^{\mu 0}\gamma^0 \otimes \gamma^0\left(\frac{1}{2\pi\epsilon}\right)$

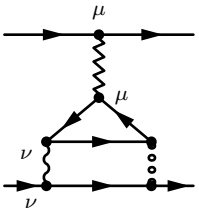

(g) Cancels Fig. 14h

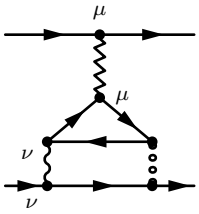

(h) Cancels Fig. 14g

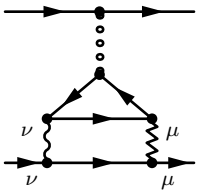

(i) $\mathrm{tr}\left[\mathcal{O}_{fl}\right]\frac{g^2}{2N}\left(\frac{1}{4\pi\epsilon}\right) \times (2 - \delta_{\mu j})\,\mathbb{1} \otimes \mathbb{1}$

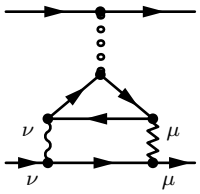

(j) $\mathrm{tr}\left[\mathcal{O}_{fl}\right]\frac{g^2}{2N}\left(\frac{1}{4\pi\epsilon}\right) \times (2 - \delta_{\mu j})\,\mathbb{1} \otimes \mathbb{1}$

Figure C.4: 4-point diagrams with both mass-like and gauge-like disorder internal lines. Below each diagram, the divergent piece, if present, is given. (The factor of $2\pi\delta(q_0)$ has been been suppressed for simplicity.) The $\mathrm{tr}\left[\mathrm{O}_{fl}\right]$ term in Figs. C.4(i) and (j) indicates that once the action on the flavour indices has been specified, a trace over this operator should be taken.

TWO INTERNAL MASS LINES, NO CROSSING: FIG. C.2(A)

$$\begin{aligned}\text{Fig. C.2(a)} &= \mu^{-\epsilon}\int \frac{d^Dq}{(2\pi)^D}2\pi\delta(q_0)2\pi\delta(q_0+p_0)\frac{i\left[-q-p\right)_\alpha\gamma^\alpha}{(q+p)^2}\otimes\frac{i(q+p)_\beta\gamma^\beta}{(q+p)^2}\\ &= 2\pi(p_0)\mu^{-\epsilon}\int\frac{d^dq}{(2\pi)^d}\int_0^1 dx\,\gamma^j\otimes\gamma_j\frac{q^2/2}{\left[q^2+x(1-x)p^2\right]^2}\\ &= 2\pi(p_0)\gamma^j\otimes\gamma_j\left(-\frac{1}{4\pi\epsilon}\right)+\text{finite.}\end{aligned}\tag{C.13}$$

TWO INTERNAL MASS LINES, WITH CROSSING: FIG. C.2(B)

$$\begin{aligned}\text{Fig. C.2(b)} &= \mu^{-\epsilon}\int \frac{d^Dq}{(2\pi)^D}2\pi\delta(q_0)2\pi\delta(q_0+p_0)\frac{iq_\alpha\gamma^\alpha}{q^2}\otimes\frac{i(q+p)_\beta\gamma^\beta}{(q+p)^2}\\ &= 2\pi(p_0)\gamma^i\otimes\gamma_i\left(\frac{1}{4\pi\epsilon}\right)+\text{finite.}\end{aligned}\tag{C.14}$$

VERTEX CORRECTION FROM DISORDER: FIGS. C.2(C) AND (D)

$$\begin{aligned}\text{Fig. C.2(c)} &= \mu^{-\epsilon}\int \frac{d^Dq}{(2\pi)^D}2\pi\delta(q_0)2\pi\delta(p_0)\frac{iq_\alpha\gamma^\alpha}{q^2}\frac{i\left(q-p\right)_\beta\gamma^\beta}{(q-p)^2}\otimes\mathbb{1}\\ &= 2\pi(p_0)\,\mu^{-\epsilon}\left[-\frac{\gamma^j\otimes\gamma_j}{2}\int\frac{d^dq}{(2\pi)^d}\int_0^1 dx\,\frac{q^2}{\left[q^2+x(1-x)p^2\right]^2}\right]\otimes\mathbb{1}+\text{finite}\\ &= 2\pi(p_0)\,\mathbb{1}\otimes\mathbb{1}\left(\frac{1}{2\pi\epsilon}\right)+\text{finite.}\end{aligned}\tag{C.15}$$

The other vertex gives the same correction:

$$\text{Fig. C.2(d)} = 2\pi(p_0)\,\mathbb{1}\otimes\mathbb{1}\left(\frac{1}{2\pi\epsilon}\right)+\text{finite.}\tag{C.16}$$

One internal gauge-like disorder line and one photon line: Figs. C.2(e) and (f)

The diagrams are both convergent. We see this by writing

$$\begin{aligned}\text{Fig. C.2(e)} &= \frac{\mu^{-\epsilon}g^2}{2N}\int\frac{d^Dk}{(2\pi)^D}\,2\pi\delta(k_0)\,\frac{1}{|k|}i\gamma^\mu\frac{(-ik_\alpha\gamma^\alpha)}{k^2}\otimes i\gamma^\mu\frac{i(k+q)_\beta\gamma^\beta}{(k+q)^2}\\ &= \frac{\mu^{-\epsilon}g^2}{2N}\int\frac{d^dk}{(2\pi)^d}\gamma^\mu\gamma^\alpha\otimes\gamma_\mu\gamma_\alpha\cdot\frac{1}{|k|\,(q_0^2+k^2)}\\ &= \text{finite},\end{aligned}\tag{C.17}$$

where we have assumed that $q = (q_0, 0)$. The same reasoning shows that Fig. C.2(f) is convergent as well.

Vertex correction from photon: Figs. C.2(g) and (h)

$$\begin{aligned}\text{Fig. C.2(g)} &= 2\pi\delta(p_0)\frac{16\mu^{-\epsilon}g^2}{2N}\int\frac{d^Dq}{(2\pi)^D}i\gamma^\mu\frac{iq_\alpha\gamma^\alpha}{q^2}\frac{i(q+p)_\beta\gamma^\beta}{(q+p)^2}i\gamma_\mu\frac{1}{|q|}\otimes\mathbb{1}\\ &= 2\pi\delta(p_0)\frac{16\mu^{-\epsilon}g^2}{2N}\gamma^\mu\gamma^\alpha\gamma^\beta\gamma_\mu\otimes\mathbb{1}\int\frac{d^Dq}{(2\pi)^D}\int_0^1dx\,\frac{3}{2}\sqrt{1-x}\,\frac{q_\alpha q_\beta - x(1-x)p_\alpha p_\beta}{[q^2+x(1-x)p^2]^{5/2}}\\ &= 2\pi\delta(p_0)\mathbb{1}\otimes\mathbb{1}\left(-\frac{24g^2}{\pi^2(2N)\epsilon}\right)+\text{finite}.\end{aligned}\tag{C.18}$$

Similarly,

$$\text{Fig. C.2(h)} = 2\pi\delta(p_0)\mathbb{1}\otimes\mathbb{1}\left(-\frac{24g^2}{\pi^2(2N)\epsilon}\right)+\text{finite}.\tag{C.19}$$

Internal fermion loop with two photon legs: Figs. C.2(i) and (j)

Because of the sum over N in the internal fermion loop, several two-loop diagrams contribute to the order in perturbation theory we are considering. Since the frequency δ-function which renormalizes disorder must come entirely from the single disorder leg in Figs. C.2(i) and (j), we can determine the divergence by sending zero (spatial) momentum through this diagram.

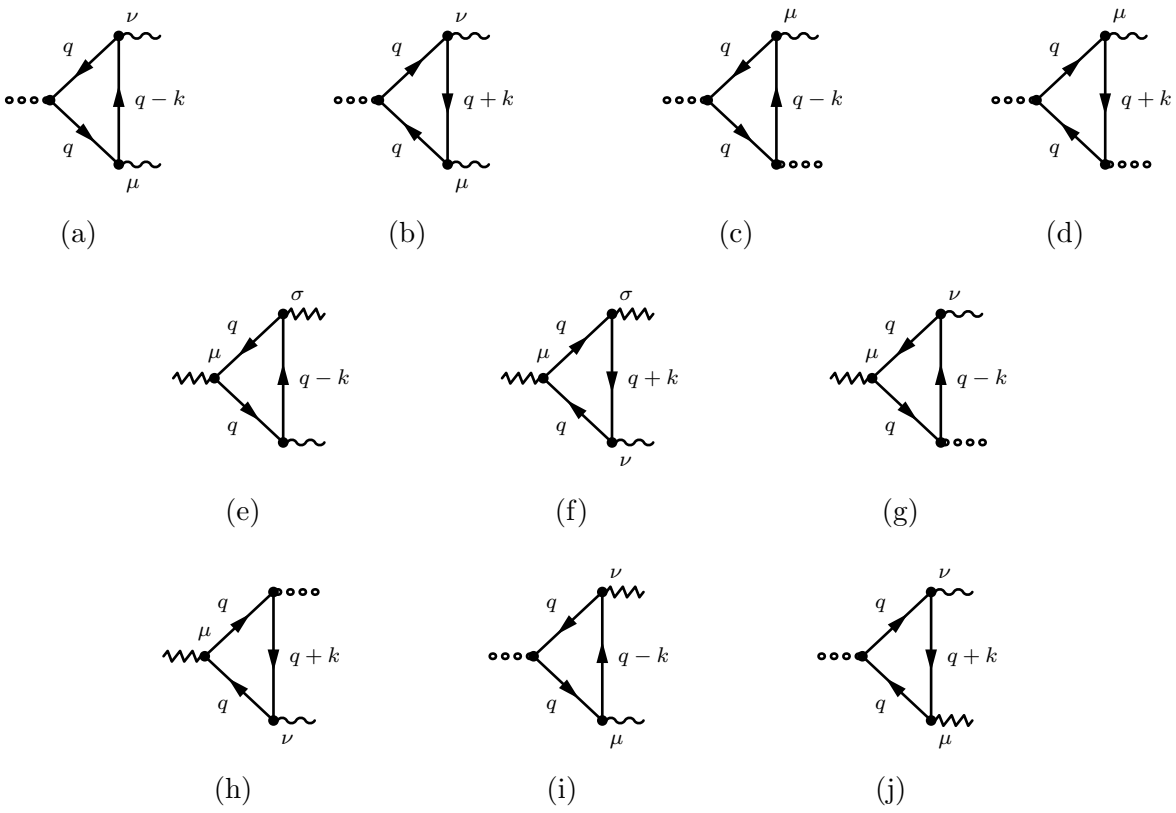

Figure C.5: Fermion loop subdiagrams which appear in the $\mathrm{O}(g_\xi^2, g_\xi/2N)$ bilinear counter terms.

Therefore, it becomes easier to first calculate the vertices shown in Fig. C.5.

We have

$$\begin{aligned}\text{Fig. C.5(a)} &= -\frac{\mu^{-\epsilon}g^2}{2N}2N\int\frac{d^Dq}{(2\pi)^D}\text{tr}\left[\frac{iq_\alpha\gamma^\alpha}{q^2}\frac{iq_\beta\gamma^\beta}{q^2}i\gamma^\nu\frac{i(q-k)_\gamma\gamma^\rho}{(q-k)^2}\gamma^\mu\right]\\ &= -i\mu^{-\epsilon}g^2\int\frac{d^Dq}{(2\pi)^D}\text{tr}\left[\gamma^\nu\gamma^\rho\gamma^\mu\right]\frac{q_\alpha q_\beta(q-k)_\rho}{(q^2)^2(q-k)^2}\\ &= 2\mu^{-\epsilon}g^2\epsilon^{\mu\nu\rho}\int\frac{d^Dq}{(2\pi)^D}\frac{(q-k)_\rho}{q^2(q-k)^2} = -\mu^{-\epsilon}g^2\int\frac{d^Dq}{(2\pi)^D}\int_0^1dx\,\frac{2\epsilon^{\mu\nu\rho}(1-x)k_\rho}{\left[q^2+x(1-x)k^2\right]^2}\end{aligned} \tag{C.20}$$

We note that since the photons are diagonal in flavour space, the mass disorder in the loop must also be diagonal. It follows that this diagram will only contribute to disorder coupling to the singlet mass operator, $\bar\psi\psi$, and, for this reason, we have taken the flavour trace to be $2N$. The full diagram is then

$$\text{Fig. C.2(i)} = -2\pi\delta(p_0)\mathbb{1}\otimes\mu^{-2\epsilon}\frac{g^4}{2N}\int\frac{d^Dk}{(2\pi)^D}i\gamma^\nu\frac{i(k+p)_\sigma\gamma^\sigma}{(k+p)^2}i\gamma^\mu\frac{(16)^2}{|k|^2}\cdot\int\frac{d^Dq}{(2\pi)^D}\int_0^1dx\,\frac{2\epsilon^{\mu\nu\rho}(1-x)k_\rho}{\left[q^2+x(1-x)k^2\right]^2} \tag{C.21}$$

We set $p=0$ and use an IR cutoff. Then, we can take $k_\sigma k_\rho\to\delta_{\sigma\rho}k^2/d$ and

$$-\frac{i}{d}\gamma^\nu\gamma^\sigma\gamma^\mu\epsilon_{\mu\nu\sigma} = \frac{1}{d}\gamma^\nu\gamma_\lambda\epsilon^{\sigma\mu\lambda}\epsilon_{\sigma\mu\nu} = \mathbb{1}. \tag{C.22}$$

Inserting this into the expression above, we find

$$\begin{aligned}\text{Fig. C.2(i)} &= -2\pi\delta(p_0)\mathbb{1}\otimes\mathbb{1}\cdot2(16)^2\mu^{-2\epsilon}\frac{g^4}{2N}\int_0^1dx\int\frac{d^Dk}{(2\pi)^D}\frac{d^Dq}{(2\pi)^D}\,\frac{1-x}{k^2\left[q^2+x(1-x)k^2\right]^2}\\ &= 2\pi\delta(p_0)\mathbb{1}\otimes\mathbb{1}\left(\frac{16g^4}{\pi^2(2N)\epsilon}\right)+\text{finite}\cdot\end{aligned} \tag{C.23}$$

For the second diagram, we calculate the vertex in Fig. C.5(b).

$$\text{Fig. C.5(b)} = -\frac{\mu^{-\epsilon}g^2}{2N}2N\int\frac{d^Dq}{(2\pi)^D}\text{tr}\left[\frac{iq_\alpha\gamma^\alpha}{q^2}\frac{iq_\beta\gamma^\beta}{q^2}i\gamma^\mu\frac{i(q+k)_\gamma\gamma^\rho}{(q+k)^2}i\gamma^\nu\right] \tag{C.24}$$

This is identical to Eq. (C.20) except with $k \to -k$ and $\mu \leftrightarrow \nu$:

$$\text{Fig. C.5(b)} = \mu^{-\epsilon} g^2 \int \frac{d^D q}{(2\pi)^D} \int_0^1 dx \, \frac{2\epsilon^{\nu\mu\rho}(1-x)k_\rho}{\left[q^2 + x(1-x)k^2\right]^2} = \text{Fig. C.5(a)}. \tag{C.25}$$

It follows that

$$\text{Fig. C.2(j)} = \text{Fig. C.2(i)} = 2\pi\delta(p_0)\mathbb{1} \otimes \mathbb{1} \left(\frac{16 g^4}{\pi^2 (2N)\epsilon} \right) + \text{finite}\cdot \tag{C.26}$$

Internal fermion loop with one photon and one disorder line: Figs. C.2(k) and (l)

As above, we approach the two-loop diagrams by first calculating the relevant fermion loop vertices, shown in Figs. C.5(c) and (d). We have

$$\text{Fig. C.5(c)} = -\frac{\mu^{-\epsilon/2} g^2}{\sqrt{2N}} \text{tr}\left[\mathrm{O}_{fl}\right] \int \frac{d^D q}{(2\pi)^D} \text{tr}\left[\frac{i q_\alpha \gamma^\alpha}{q^2} \frac{i q_\beta \gamma^\beta}{q^2} i\gamma^\mu \frac{i(q-k)_\sigma \gamma^\sigma}{(q-k)^2} \right] \tag{C.27}$$

Here, we leave the flavour index behaviour of the vertices arbitrary by letting O_{fl} be a general $2N \times 2N$ Hermitian matrix. Similarly

$$\text{Fig. C.5(d)} = -\frac{\mu^{-\epsilon/2} g^2}{\sqrt{2N}} \text{tr}\left[\mathrm{O}_{fl}\right] \int \frac{d^D q}{(2\pi)^D} \text{tr}\left[\frac{i(q+k)_\sigma \gamma^\sigma}{(q+k)^2} i\gamma^\mu \frac{i q_\beta \gamma^\beta}{q^2} \frac{i q_\alpha \gamma^\alpha}{q^2} \right] \tag{C.28}$$

Taking $q \to -q$ and noting that $\text{tr}[\gamma^\sigma \gamma^\mu \gamma^\beta \gamma^\alpha] = \text{tr}[\gamma^\alpha \gamma^\beta \gamma^\mu \gamma^\sigma]$, this becomes

$$\text{Fig. C.5(d)} = \frac{\mu^{-\epsilon/2} g^2}{\sqrt{2N}} \text{tr}\left[\mathrm{O}_{fl}\right] \int \frac{d^D q}{(2\pi)^D} \text{tr}\left[\frac{i q_\alpha \gamma^\alpha}{q^2} \frac{i q_\beta \gamma^\beta}{q^2} i\gamma^\mu \frac{i(q-k)_\sigma \gamma^\sigma}{(q-k)^2} \right] = -\text{Fig. C.5(c)}. \tag{C.29}$$

It follows that the divergences in Figs. C.2(k) and (l) cancel.

C.3.2 Diagrams with gauge-like disorder and photon lines: Fig. C.3

Two internal gauge-like disorder lines, no crossing: Fig. C.3(a)

$$\text{Fig. C.3(a)} = 2\pi(p_0)\frac{1}{2}\sum_j \gamma^\mu\gamma^j\gamma^\nu \otimes \gamma^\mu\gamma_j\gamma^\nu \left(-\frac{1}{2\pi\epsilon}\right) + \text{finite}$$
$$= 2\pi(p_0)\left(\frac{1}{4\pi\epsilon}\right)\begin{cases} -\sum_j \gamma^j \otimes \gamma_j, & (\mu,\nu) = (0,0) \\ \mathbb{1}\otimes\mathbb{1} - \gamma^0\otimes\gamma^0, & (\mu,\nu) = (0,\ell)\,,(\ell,0) \\ -\sum_j \gamma^j \otimes \gamma_j, & (\mu,\nu) = (\ell,k) \end{cases} + \text{finite} \tag{C.30}$$

Two internal gauge-like disorder lines, with crossing: Fig. C.3(b)

$$\text{Fig. C.3(b)} = 2\pi(p_0)\frac{1}{2}\sum_j \gamma^\mu\gamma^j\gamma^\nu \otimes \gamma^\nu\gamma_j\gamma^\mu \left(\frac{1}{2\pi\epsilon}\right) + \text{finite}$$
$$= 2\pi(p_0)\left(\frac{1}{4\pi\epsilon}\right)\begin{cases} \sum_j \gamma^j \otimes \gamma_j, & (\mu,\nu) = (0,0) \\ \mathbb{1}\otimes\mathbb{1} + \gamma^0\otimes\gamma^0, & (\mu,\nu) = (0,\ell)\,,(\ell,0) \\ \sum_j \gamma^j \otimes \gamma_j, & (\mu,\nu) = (k,\ell) \end{cases} + \text{finite} \tag{C.31}$$

Vertex correction from gauge-like disorder: Figs. C.3(c) and (d)

$$\begin{aligned}
\text{Fig. C.3(c)} &= \int \frac{d^D q}{(2\pi)^D} 2\pi\delta(q_0) 2\pi\delta(p_0) i\gamma^\nu \frac{i q_\alpha \gamma^\alpha}{q^2} i\gamma^\mu \frac{i\,[q-p]_\beta\,\gamma^\beta}{(q-p)^2} i\gamma_\nu \otimes i\gamma_\mu \\
&= 2\pi(p_0) \left[-\frac{1}{2} \int \frac{d^d q}{(2\pi)^d} \int_0^1 dx\, \frac{q^2}{\left[q^2 + x(1-x)p^2\right]^2} \right] \gamma^\nu \gamma^j \gamma^\mu \gamma_j \gamma_\nu \otimes \gamma^\nu + \text{finite} \\
&= 2\pi(p_0) \left(\frac{1}{2\pi\epsilon} \right) \times \begin{cases} 0 & (\mu,\nu) = (\ell,0)\,,(\ell,k) \\ -\gamma^0 \otimes \gamma^0 & (\mu,\nu) = (0,0) \\ \gamma^0 \otimes \gamma^0 & (\mu,\nu) = (0,\ell) \end{cases} + \text{finite} \\
&= 2\pi(p_0) \gamma^0 \otimes \gamma^0 \left(\frac{1}{2\pi\epsilon} \right) \delta^{\mu 0} \left[-\delta^{\nu 0} + \sum_j \delta^{\nu j} \right]
\end{aligned} \tag{C.32}$$

The other vertex gives the same correction:

$$\text{Fig. C.3(d)} = 2\pi(p_0) \gamma^0 \otimes \gamma^0 \left(\frac{1}{2\pi\epsilon} \right) \delta^{\nu 0} \left[-\delta^{\mu 0} + \sum_j \delta^{\mu j} \right] + \text{finite} \tag{C.33}$$

One internal gauge-like disorder line and one photon line: Figs. C.3(e) and (h)

This situation is identical to the one in Eq. (C.17) except for some γ matrices: both Fig. C.3(e) and Fig. C.3(h) are finite.

Vertex correction from photon: Figs. C.3(f) and (g)

$$\begin{aligned}
\text{Fig. C.3(f)} &= 2\pi\delta(p_0) \frac{16\mu^{-\epsilon} g^2}{2N} \sum_\nu \int \frac{d^D q}{(2\pi)^D} i\gamma^\nu \frac{i q_\alpha \gamma^\alpha}{q^2} i\gamma^\mu \frac{i(q+p)_\beta \gamma^\beta}{(q+p)^2} i\gamma_\nu \frac{1}{|q|} \otimes \gamma^\mu \\
&= 2\pi\delta(p_0) \frac{16\mu^{-\epsilon} g^2}{2N} i \sum_\nu \gamma^\nu \gamma^\alpha \gamma^\mu \gamma^\beta \gamma_\nu \otimes \gamma^\mu \int \frac{d^D q}{(2\pi)^D} \int_0^1 dx\, \frac{3}{2} \sqrt{1-x}\, \frac{q_\alpha q_\beta - x(1-x) p_\alpha p_\beta}{\left[q^2 + x(1-x)p^2\right]^{5/2}} \\
&= 2\pi\delta(p_0) \gamma^\mu \otimes \gamma^\mu \left(-\frac{8 g^2}{3\pi^2 (2N)\epsilon} \right) + \text{finite.}
\end{aligned} \tag{C.34}$$

Similarly,

$$\text{Fig. C.3(g)} = 2\pi\delta(p_0)\gamma^\mu \otimes \gamma^\mu \left(-\frac{8g^2}{3\pi^2(2N)\epsilon}\right) + \text{finite}. \tag{C.35}$$

Internal fermion loop with one disorder and two photon legs: Figs. C.3(i) and (j)

None of the gauge-like disorder terms are diagonal in the flavour indices. As we remarked above, this is because the global U(1) current has scaling dimension 3, making it extremely irrelevant. Therefore, the gauge-like disorder in Figs. C.3(i) and (j) inserts an $2N \times 2N$ traceless Hermitian matrix into the fermion loop. Upon taking the trace, both vanish.

Internal fermion loops with two disorder and one photon leg: Figs. C.3(k) and (l)

As we did for the two loop diagrams with mass-like disorder above, we first calculate the fermion loop vertices. The vertices relevant to our diagrams are shown in Figs. C.5(e) and (f). We have

$$\begin{aligned}\text{Fig. C.5(e)} &= -\frac{\mu^{-\epsilon/2}g}{\sqrt{2N}}\text{tr}\left[\text{O}_{fl}\right]\int\frac{d^Dq}{(2\pi)^D}\text{tr}\left[\frac{iq_\beta\gamma^\beta}{q^2}i\gamma^\mu\frac{iq_\alpha\gamma^\alpha}{q^2}i\gamma^\nu\frac{i(q-k)_\rho\gamma^\rho}{(q-k)^2}i\gamma^\sigma\right] \\ &= \frac{\mu^{-\epsilon/2}g}{\sqrt{2N}}\text{tr}\left[\text{O}_{fl}\right]\int\frac{d^Dq}{(2\pi)^D}\text{tr}\left[\gamma^\nu\gamma^\rho\gamma^\sigma\gamma^\beta\gamma^\mu\gamma^\alpha\right]\frac{q_\alpha q_\beta(q-k)_\sigma}{(q^2)^2(q-k)^2},\end{aligned} \tag{C.36}$$

where O_{fl} is the matrix in flavour space coming from disorder vertices. Similarly, reversing the direction of the fermion loop, we have

$$\begin{aligned}\text{Fig. C.5(f)} &= -\frac{\mu^{-\epsilon/2}g}{\sqrt{2N}}\text{tr}\left[\text{O}_{fl}\right]\int\frac{d^Dq}{(2\pi)^D}\text{tr}\left[\frac{iq_\alpha\gamma^\alpha}{q^2}i\gamma^\mu\frac{iq_\beta\gamma^\beta}{q^2}i\gamma^\sigma\frac{i(q+k)_\rho\gamma^\rho}{(q+k)^2}i\gamma^\nu\right] \\ &= \frac{\mu^{-\epsilon/2}g}{\sqrt{2N}}\text{tr}\left[\text{O}_{fl}\right]\int\frac{d^Dq}{(2\pi)^D}\text{tr}\left[\gamma^\alpha\gamma^\mu\gamma^\beta\gamma^\sigma\gamma^\rho\gamma^\nu\right]\frac{q_\alpha q_\beta(q+k)_\sigma}{(q^2)^2(q+k)^2}.\end{aligned} \tag{C.37}$$

Noting that

$$\text{tr}\left[\gamma^{\mu_1}\gamma^{\mu_2}\cdots\gamma^{\mu_n}\right] = (-1)^n\text{tr}\left[\gamma^{\mu_n}\gamma^{\mu_{n-1}}\cdots\gamma^{\mu_1}\right] \tag{C.38}$$

and taking $q \to -q$, we have

$$\text{Fig. C.5(f)} = -\frac{\mu^{-\epsilon/2}\mathcal{g}}{\sqrt{2N}}\text{tr}\left[\text{O}_{fl}\right]\int\frac{d^Dq}{(2\pi)^D}\text{tr}\left[\gamma^\nu\gamma^\rho\gamma^\sigma\gamma^\beta\gamma^\mu\gamma^\alpha\right]\frac{q_\alpha q_\beta(q-k)_\sigma}{(q^2)^2(q-k)^2} = -\text{Fig. C.5(e)}. \tag{C.39}$$

We conclude that Figs. C.3(k) and (l) cancel one another.

C.3.3 Both potential and mass disorder diagrams

One internal mass-like and gauge-like disorder lines, no crossing: Fig. C.4(a)

$$\begin{aligned}
\text{Fig. C.4(a)} &= \int\frac{d^Dq}{(2\pi)^D}2\pi\delta(q_0)2\pi\delta\left(q+p\right)\,i\gamma^\mu\,\frac{i\left[-q\right]_\alpha\gamma^a}{q^2}\otimes\,i\gamma^\mu\frac{i(q+p)_\beta\gamma^\beta}{(q+p)^2}\\
&= -2\pi\delta(p_0)\gamma^\mu\gamma^i\otimes\gamma^\mu\gamma^j\cdot\frac{\delta_{ij}}{2}\int\frac{d^dq}{(2\pi)^2}\int_0^1dx\,\frac{q^2}{\left[q+x(1-x)p^2\right]^2}+\text{finite}\\
&= 2\pi\delta(p_0)\sum_j\gamma^\mu\gamma^j\otimes\gamma^\mu\gamma_j\left(\frac{1}{4\pi\epsilon}\right)+\text{finite}\\
&= 2\pi\delta(p_0)\left(\frac{1}{4\pi\epsilon}\right)\begin{cases}-\sum_j\gamma^j\otimes\gamma_j, & \mu=0,\\ \mathbb{1}\otimes\mathbb{1}-\gamma^0\otimes\gamma^0, & \mu=\ell\end{cases}
\end{aligned} \tag{C.40}$$

One internal mass-like and gauge-like disorder lines, with crossing: Fig. C.4(b)

$$\begin{aligned}
\text{Fig. C.4(b)} &= -2\pi\delta(p_0)\sum_j\gamma^\mu\gamma^j\otimes\gamma^j\gamma_\mu\left(\frac{1}{4\pi\epsilon}\right)+\text{finite}\\
&= 2\pi\delta(p_0)\left(\frac{1}{4\pi\epsilon}\right)\begin{cases}-\sum_j\gamma^j\otimes\gamma_j, & \mu=0,\\ -\mathbb{1}\otimes\mathbb{1}-\gamma^0\otimes\gamma^0, & \mu=\ell\end{cases}
\end{aligned} \tag{C.41}$$

MASS DISORDER VERTEX CORRECTION FROM POTENTIAL DISORDER: FIGS. C.4(C) AND (D)

$$\text{Fig. C.4(c)} = 2\pi(p_0)\,\mathbb{1}\otimes\mathbb{1}\left(-\frac{1}{2\pi\epsilon}\right) + \text{finite} \tag{C.42}$$

and

$$\text{Fig. C.4(d)} = 2\pi(p_0)\,\mathbb{1}\otimes\mathbb{1}\left(-\frac{1}{2\pi\epsilon}\right) + \text{finite} \tag{C.43}$$

POTENTIAL DISORDER VERTEX CORRECTION FROM MASS DISORDER: FIGS. C.4(E) AND (F)

$$\begin{aligned}\text{Fig. C.4(e)} &= \int \frac{d^Dq}{(2\pi)^D}2\pi\delta(q_0)2\pi\delta(p_0)\frac{iq_\alpha\gamma^\alpha}{q^2}i\gamma^\mu\frac{i\left[q-p\right]_\beta\gamma^\beta}{(q-p)^2}\otimes i\gamma_\mu \\ &= 2\pi(p_0)\left[\frac{1}{2}\int\frac{d^dq}{(2\pi)^d}\int_0^1 dx\,\frac{q^2}{\left[q^2+x(1-x)p^2\right]^2}\right]\gamma^j\gamma^\mu\gamma_j\otimes\gamma^\mu + \text{finite} \\ &= 2\pi(p_0)\delta^{\mu0}\gamma^0\otimes\gamma^0\left(\frac{1}{2\pi\epsilon}\right) + \text{finite}\end{aligned} \tag{C.44}$$

Similarly,

$$\text{Fig. C.4(f)} = 2\pi\delta(p_0)\delta^{\mu0}\gamma^0\otimes\gamma^0\left(\frac{1}{2\pi\epsilon}\right) + \text{finite} \tag{C.45}$$

INTERNAL FERMION LOOP WITH INTERNAL GAUGE AND PHOTON LEGS: FIGS. C.4(G) AND (H)

In order to calculate Figs. C.4(g) and (h), we being by determining the subdiagrams in Figs. C.5(g) and (h):

$$\text{Fig. C.5(g)} = -\frac{\mu^{-\epsilon/2}g}{\sqrt{2N}}\text{tr}\left[\text{O}_{fl}\right]\int\frac{d^Dq}{(2\pi)^D}\text{tr}\left[\frac{iq_\alpha\gamma^\alpha}{q^2}i\gamma^\mu\frac{iq_\beta\gamma^\beta}{q^2}i\gamma^\nu\frac{i(q-k)_\sigma\gamma^\sigma}{(q-k)^2}\right] \tag{C.46}$$

where O_{fl} is the matrix in flavour space resulting from disorder vertices. Similarly, the other diagram gives

$$\begin{aligned}\text{Fig. C.5(h)} &= -\frac{\mu^{-\epsilon/2}\mathcal{g}}{\sqrt{2N}}\mathrm{tr}\left[\mathrm{O}_{fl}\right]\int\frac{d^Dq}{(2\pi)^D}\mathrm{tr}\left[\frac{iq_\alpha\gamma^\alpha}{q^2}i\gamma^\mu\frac{iq_\beta\gamma^\beta}{q^2}i\gamma^\nu\frac{i(q+k)_\sigma\gamma^\sigma}{(q+k)^2}\right]\\ &= \frac{\mu^{-\epsilon/2}\mathcal{g}}{\sqrt{2N}}\mathrm{tr}\left[\mathrm{O}_{fl}\right]\int\frac{d^Dq}{(2\pi)^D}\mathrm{tr}\left[\frac{iq_\alpha\gamma^\alpha}{q^2}i\gamma^\mu\frac{iq_\beta\gamma^\beta}{q^2}i\gamma^\nu\frac{i(q-k)_\sigma\gamma^\sigma}{(q-k)^2}\right] = -\text{Fig. C.5(g)}\end{aligned} \tag{C.47}$$

where in the last line we took $q\to -q$. It follows that these diagrams cancel with each other.

Internal fermion loop with internal mass and gauge disorder and photon lines: Figs. C.4(i) and (j)

We start by evaluating the fermion loop vertices in Figs. C.5(j) and (j). Actually, it's not difficult to see that up to the photon vertex coupling, $\mu^{-\epsilon/2}\mathcal{g}/\sqrt{2N}$, these diagrams are identical to the vertices in Figs. C.5(a) and (b), determined in Eqs. (C.20) and (C.25):

$$\begin{aligned}\text{Fig. C.5(i)} &= \text{Fig. C.5(j)}\\ &= -\frac{\mu^{-\epsilon/2}\mathcal{g}}{\sqrt{2N}}\mathrm{tr}\left[\mathrm{O}_{fl}\right]\int\frac{d^Dq}{(2\pi)^D}\int_0^1 dx\,\frac{2\epsilon^{\mu\nu\rho}(1-x)k_\rho}{\left[q^2+x(1-x)k^2\right]^2}.\end{aligned} \tag{C.48}$$

Proceeding as we did for this case, we have

$$\begin{aligned}\text{Fig. C.4(i)} &= \text{Fig. C.4(j)}\\ &= -2\pi\delta(p_0)\mathbb{1}\otimes\frac{\mu^{-\epsilon}g^2}{2N}\mathrm{tr}\left[\mathrm{O}_{fl}\right]\\ &\quad\times\int\frac{d^Dk}{(2\pi)^D}2\pi\delta(k_0)i\gamma^\nu\frac{ik_\sigma\gamma^\sigma}{k^2}i\gamma^\mu\frac{16}{|k|}\int\frac{d^Dq}{(2\pi)^D}\int_0^1 dx\,\frac{2\epsilon^{\mu\nu\rho}(1-x)k_\rho}{\left[q^2+x(1-x)k^2\right]^2}\\ &= -2\pi\delta(p_0)\mathbb{1}\otimes\frac{32\mu^{-\epsilon}g^2}{2N}\mathrm{tr}\left[\mathrm{O}_{fl}\right]\\ &\quad\times\int\frac{d^dk}{(2\pi)^d}\int\frac{d^Dq}{(2\pi)^D}\int_0^1 dx\,(-i)\gamma^\nu\gamma^\sigma\gamma^\mu\epsilon_{\mu\nu\rho}\frac{\delta_\sigma^{\,j}\delta_j^\rho}{d}\frac{1}{|k|}\frac{1-x}{\left[q^2+x(1-x)k^2\right]^2}\end{aligned} \tag{C.49}$$

where $\mathrm{tr}\left[\mathrm{O}_{fl}\right]$ indicates that, in order to allow disorder vertices which are off-diagonal in the flavour indices, we have not yet explicitly taken the trace over the flavours. Moreover, we

sum over ν, σ, and ρ but *not* μ. With this in mind, we note

$$-\frac{i}{d}\sum_{\sigma\rho\nu j}\gamma^{\nu}\gamma^{\sigma}\gamma^{\mu}\epsilon_{\mu\nu\rho}\delta^{j}_{\sigma}\delta^{\rho}_{j}=\frac{1}{d}\sum_{\nu\lambda j}\epsilon^{\nu j\lambda}\epsilon_{\mu\nu j}\gamma_{\lambda}\gamma^{\mu}=\frac{1}{d}\left(d-\delta^{j}_{\mu}\right)\mathbb{1}. \tag{C.50}$$

Performing the q, k, and x integrals, we obtain,

$$\begin{aligned}\text{Fig. C.4(i)} &= \text{Fig. C.4(j)}\\ &= 2\pi\delta(p_0)\mathbb{1}\otimes\mathbb{1}\mathrm{tr}\left[\mathrm{O}_{fl}\right]\frac{g^2}{2N}\left(\frac{1}{4\pi\epsilon}\right)(2-\delta_{\mu j})+\text{finite}\\ &= \begin{cases}2\pi\delta(p_0)\mathrm{tr}\left[\mathrm{O}_{fl}\right]\frac{g^2}{2N}\left(\frac{1}{2\pi\epsilon}\right)\mathbb{1}\otimes\mathbb{1}, & \mu=0,\\ 2\pi\delta(p_0)\mathrm{tr}\left[\mathrm{O}_{fl}\right]\frac{g^2}{2N}\left(\frac{1}{4\pi\epsilon}\right)\mathbb{1}\otimes\mathbb{1}, & \mu=x,y\end{cases}\end{aligned} \tag{C.51}$$

C.4 4-POINT DIAGRAMS CONTRIBUTING TO FERMION BILINEAR COUNTER TERMS

The diagrams which contribute to the β-functions at $\mathrm{O}(g_\xi^2, g_\xi/N)$ are shown in Fig. 4.6 and in Tables. C.1 through C.3. The divergences are based on the integrals determined in Sec. C.3 and only diagrams which do not vanish are shown. The label "n_d" indicates the degeneracy of the diagram or else the existence of a diagram with a nearly identical form.

Some of the diagrams result in divergences proportional to $[\gamma^\mu\otimes\gamma^\mu][\mathbb{1}\otimes\mathbb{1}]$ and would appear to imply that disorder coupling to the U(1) gauge current J^μ is generated. While counter terms are technically required to render the theory finite, we emphasize that it is not necessary to consider them since J^μ already has a large scaling dimension at the QED_3 fixed point.

diagram	n_d	divergence	diagram	n_d	divergence
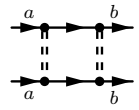	1	$\sum_{ab}\left(\frac{g_{t,a}g_{t,b}}{4\pi\epsilon}\right)\Big\{-\delta^{ab}\left[\gamma^j\otimes\gamma_j\right]\left[\mathbb{1}\otimes\mathbb{1}\right]$ $+\sum_c\left\|\epsilon^{abc}\right\|\left[\gamma^j\otimes\gamma_j\right]\left[\sigma_c\otimes\sigma_c\right]\Big\}$	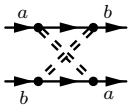	1	$\sum_{ab}\left(\frac{g_{t,a}g_{t,b}}{4\pi\epsilon}\right)\Big\{\delta^{ab}\left[\gamma^j\otimes\gamma_j\right]\left[\mathbb{1}\otimes\mathbb{1}\right]$ $+\sum_c\left\|\epsilon^{abc}\right\|\left[\gamma^j\otimes\gamma_j\right]\left[\sigma_c\otimes\sigma_c\right]\Big\}$
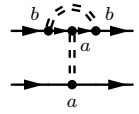	2	$\sum_a\frac{g_{t,a}}{\pi\epsilon}\left(2g_{t,a}-\sum_b g_{t,b}\right)\left[\mathbb{1}\otimes\mathbb{1}\right]\left[\sigma^a\otimes\sigma_a\right]$	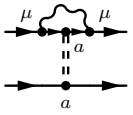	2	$\sum_a\left(-\frac{48g_{t,a}g^2}{\pi^2(4N)\epsilon}\right)\left[\mathbb{1}\otimes\mathbb{1}\right]\left[\sigma^a\otimes\sigma_a\right]$
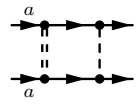	2	$\sum_a\left(-\frac{g_s g_{t,a}}{2\pi\epsilon}\right)\left[\gamma^j\otimes\gamma_j\right]\left[\sigma^a\otimes\sigma_a\right]$	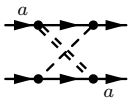	2	$\sum_a\left(\frac{g_s g_{t,a}}{2\pi\epsilon}\right)\left[\gamma^j\otimes\gamma_j\right]\left[\sigma^a\otimes\sigma_a\right]$
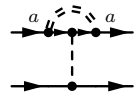	2	$\sum_a\left(\frac{g_s g_{t,a}}{\pi\epsilon}\right)\left[\mathbb{1}\otimes\mathbb{1}\right]\left[\mathbb{1}\otimes\mathbb{1}\right]$	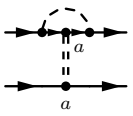	2	$\sum_a\left(\frac{g_s g_{t,a}}{\pi\epsilon}\right)\left[\mathbb{1}\otimes\mathbb{1}\right]\left[\sigma^a\otimes\sigma_a\right]$
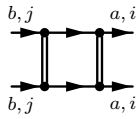	1	$\sum_{ab}\left(\frac{g_{\mathcal{A},a}g_{\mathcal{A},b}}{\pi\epsilon}\right)\sum_c\left\|\epsilon^{abc}\right\|\left[\gamma^j\otimes\gamma_j\right]\left[\sigma_c\otimes\sigma_c\right]$ $+\sum_a\left(-\frac{g^2_{\mathcal{A},a}}{\pi\epsilon}\right)\left[\gamma^j\otimes\gamma_j\right]\left[\mathbb{1}\otimes\mathbb{1}\right]$	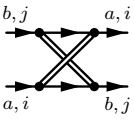	1	$\sum_{ab}\left(\frac{g_{\mathcal{A},a}g_{\mathcal{A},b}}{\pi\epsilon}\right)\sum_c\left\|\epsilon^{abc}\right\|\left[\gamma^j\otimes\gamma_j\right]\left[\sigma_c\otimes\sigma_c\right]$ $+\sum_a\left(\frac{g^2_{\mathcal{A},a}}{\pi\epsilon}\right)\left[\gamma^j\otimes\gamma_j\right]\left[\mathbb{1}\otimes\mathbb{1}\right]$
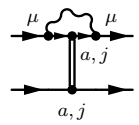	1	$\sum_a\left(\frac{16g_{\mathcal{A},a}g^2}{3\pi^2(2N)\epsilon}\right)\left[\gamma^j\otimes\gamma_j\right]\left[\sigma^a\otimes\sigma_a\right]$	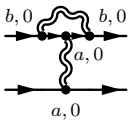	2	$\sum_a\left(-\frac{g_{v,a}}{\pi\epsilon}\right)\left(2g_{v,a}-\sum_b g_{v,b}\right)$ $\times\left[\gamma^0\otimes\gamma^0\right]\left[\sigma^a\otimes\sigma_a\right]$
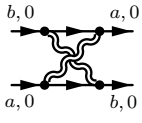	1	$\sum_{ab}\frac{g_{v,a}g_{v,b}}{4\pi\epsilon}\sum_c\left\|\epsilon^{abc}\right\|\left[\gamma^j\otimes\gamma_j\right]\left[\sigma_c\otimes\sigma_c\right]$ $+\sum_a\left(\frac{g^2_{v,a}}{4\pi\epsilon}\right)\left[\gamma^j\otimes\gamma_j\right]\left[\mathbb{1}\otimes\mathbb{1}\right]$	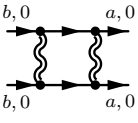	1	$\sum_{ab}\frac{g_{v,a}g_{v,b}}{4\pi\epsilon}\sum_c\left\|\epsilon^{abc}\right\|\left[\gamma^j\otimes\gamma_j\right]\left[\sigma_c\otimes\sigma_c\right]$ $+\sum_a\left(-\frac{g^2_{v,a}}{4\pi\epsilon}\right)\left[\gamma^j\otimes\gamma_j\right]\left[\mathbb{1}\otimes\mathbb{1}\right]$
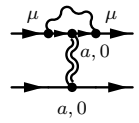	2	$\sum_a\left(-\frac{16g_{v,a}g^2}{3\pi^2(2N)\epsilon}\right)\left[\gamma^0\otimes\gamma^0\right]\left[\sigma^a\otimes\sigma_a\right]$	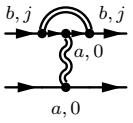	2	$\sum_a\left(-\frac{2g_{v,a}}{\pi\epsilon}\right)\left(2g_{\mathcal{A},a}-\sum_b g_{\mathcal{A},b}\right)$ $\times\left[\gamma^0\otimes\gamma^0\right]\left[\sigma^a\otimes\sigma_a\right]$

Table C.1: Feynman diagrams which determine the bilinear counter terms.

diagram	n_d	divergence	diagram	n_d	divergence
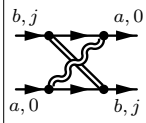	2	$\sum_a \frac{g_{v,a} g_{\mathcal{A},a}}{\pi\epsilon} \Big\{ - [\mathbb{1}\otimes\mathbb{1}]\,[\mathbb{1}\otimes\mathbb{1}]$ $- [\gamma^0\otimes\gamma^0]\,[\mathbb{1}\otimes\mathbb{1}] \Big\}$ $+ \sum_{ab} \frac{g_{v,a} g_{\mathcal{A},b}}{\pi\epsilon} \sum_c \lvert\epsilon^{abc}\rvert \Big\{ - [\mathbb{1}\otimes\mathbb{1}]\,[\sigma_c\otimes\sigma_c]$ $- [\gamma^0\otimes\gamma^0]\,[\sigma_c\otimes\sigma_c] \Big\}$	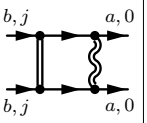	2	$\sum_a \frac{g_{v,a} g_{\mathcal{A},a}}{\pi\epsilon} \Big\{ - [\mathbb{1}\otimes\mathbb{1}]\,[\mathbb{1}\otimes\mathbb{1}]$ $+ [\gamma^0\otimes\gamma^0]\,[\mathbb{1}\otimes\mathbb{1}] \Big\}$ $+ \sum_{ab} \frac{g_{v,a} g_{\mathcal{A},b}}{\pi\epsilon} \sum_c \lvert\epsilon^{abc}\rvert \Big\{ [\mathbb{1}\otimes\mathbb{1}]\,[\sigma_c\otimes\sigma_c]$ $- [\gamma^0\otimes\gamma^0]\,[\sigma_c\otimes\sigma_c] \Big\}$
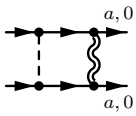	2	$\sum_a \left(\frac{g_s g_{v,a}}{2\pi\epsilon}\right) [\gamma^j\otimes\gamma_j]\,[\sigma^a\otimes\sigma_a]$	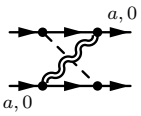	2	$\sum_a \left(\frac{g_s g_{v,a}}{2\pi\epsilon}\right) [\gamma^j\otimes\gamma_j]\,[\sigma^a\otimes\sigma_a]$
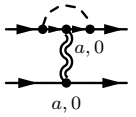	2	$\sum_a \left(-\frac{g_s g_{v,a}}{\pi\epsilon}\right) [\gamma^0\otimes\gamma^0]\,[\sigma^a\otimes\sigma_a]$	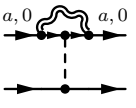	2	$[\mathbb{1}\otimes\mathbb{1}]\,[\mathbb{1}\otimes\mathbb{1}]\,\left(\frac{g_s}{\pi\epsilon}\sum_a g_{v,a}\right)$
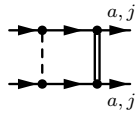	2	$\sum_a \left(\frac{g_s g_{\mathcal{A},a}}{\pi\epsilon}\right) [\mathbb{1}\otimes\mathbb{1}]\,[\sigma^a\otimes\sigma_a]$ $+ \sum_a \left(-\frac{g_s g_{\mathcal{A},a}}{\pi\epsilon}\right) [\gamma^0\otimes\gamma^0]\,[\sigma^a\otimes\sigma_a]$	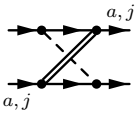	2	$\sum_a \left(-\frac{g_s g_{\mathcal{A},a}}{\pi\epsilon}\right) [\mathbb{1}\otimes\mathbb{1}]\,[\sigma^a\otimes\sigma_a]$ $+ \sum_a \left(-\frac{g_s g_{\mathcal{A},a}}{\pi\epsilon}\right) [\gamma^0\otimes\gamma^0]\,[\sigma^a\otimes\sigma_a]$
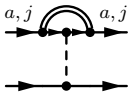	2	$\left(-\frac{2g_s}{\pi\epsilon}\sum_a g_{\mathcal{A},a}\right) [\mathbb{1}\otimes\mathbb{1}]\,[\mathbb{1}\otimes\mathbb{1}]$	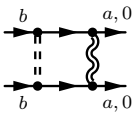	2	$\sum_a \left(\frac{g_{v,a} g_{t,a}}{2\pi\epsilon}\right) [\gamma^j\otimes\gamma_j]\,[\mathbb{1}\otimes\mathbb{1}]$ $- \sum_{ab} \left(\frac{g_{v,a} g_{t,b}}{2\pi\epsilon}\right) \sum_c \lvert\epsilon^{abc}\rvert\,[\gamma^j\otimes\gamma_j]\,[\sigma_c\otimes\sigma_c]$
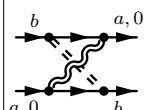	2	$\sum_a \left(\frac{g_{v,a} g_{t,a}}{2\pi\epsilon}\right) [\gamma^j\otimes\gamma_j]\,[\mathbb{1}\otimes\mathbb{1}]$ $+ \sum_{ab} \left(\frac{g_{v,a} g_{t,b}}{2\pi\epsilon}\right) \sum_c \lvert\epsilon^{abc}\rvert\,[\gamma^j\otimes\gamma_j]\,[\sigma_c\otimes\sigma_c]$	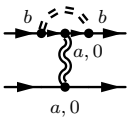	2	$\sum_a \left(-\frac{g_{v,a}}{\pi\epsilon}\right) \left(2g_{t,a} - \sum_b g_{t,b}\right)$ $\times [\gamma^0\otimes\gamma^0]\,[\sigma^a\otimes\sigma_a]$
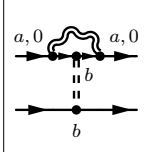	2	$\sum_a \left(\frac{g_{t,a}}{\pi\epsilon}\right) \left(2g_{v,a} - \sum_b g_{v,b}\right) [\mathbb{1}\otimes\mathbb{1}]\,[\sigma^a\otimes\sigma_a]$	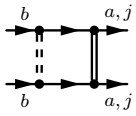	2	$\sum_a \frac{g_{t,a} g_{\mathcal{A},a}}{\pi\epsilon} \Big\{ [\mathbb{1}\otimes\mathbb{1}]\,[\mathbb{1}\otimes\mathbb{1}]$ $- [\gamma^0\otimes\gamma^0]\,[\mathbb{1}\otimes\mathbb{1}] \Big\}$ $+ \sum_{ab} \frac{g_{t,a} g_{\mathcal{A},b}}{\pi\epsilon} \sum_c \lvert\epsilon^{abc}\rvert \Big\{ - [\mathbb{1}\otimes\mathbb{1}]\,[\sigma^c\otimes\sigma_c]$ $+ [\gamma^0\otimes\gamma^0]\,[\sigma^a\otimes\sigma_a] \Big\}$

Table C.2: Feynman diagrams which determine the bilinear counter terms.

diagram	n_d	divergence	diagram	n_d	divergence
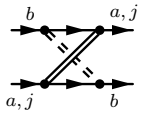	2	$\sum_a \frac{g_{t,a} g_{\mathcal{A},a}}{\pi\epsilon} \Big\{ -[\mathbb{1}\otimes\mathbb{1}][\mathbb{1}\otimes\mathbb{1}] - [\gamma^0\otimes\gamma^0][\mathbb{1}\otimes\mathbb{1}] \Big\}$ $+\sum_{ab} \frac{g_{t,a} g_{\mathcal{A},b}}{\pi\epsilon} \sum_c \lvert\epsilon^{abc}\rvert \Big\{ -[\mathbb{1}\otimes\mathbb{1}][\sigma^c\otimes\sigma_c] - [\gamma^0\otimes\gamma^0][\sigma^a\otimes\sigma_a] \Big\}$	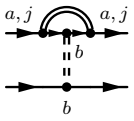	2	$\sum_a \left(-\frac{2g_{t,a}}{\pi\epsilon}\right)(2g_{\mathcal{A},a} - \sum_b g_{\mathcal{A},b})$ $\times [\mathbb{1}\otimes\mathbb{1}][\sigma^a\otimes\sigma_a]$
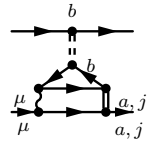	8	$\sum_a \frac{4 g_{t,a} g_{\mathcal{A},a} g^2}{\pi\epsilon} [\mathbb{1}\otimes\mathbb{1}][\sigma^a\otimes\sigma_a]$	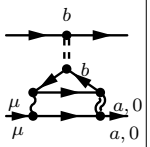	8	$\sum_a \left(-\frac{4 g_{t,a} g_{v,a} g^2}{\pi\epsilon}\right)[\mathbb{1}\otimes\mathbb{1}][\sigma^a\otimes\sigma_a]$

Table C.3: Feynman diagrams which determine the bilinear counter terms.

C.5 Diagrams renormalizing flux disorder, $g_{\mathcal{E}}$ and $g_{\mathcal{B}}$

The renormalization of $g_{\mathcal{E}}$ and $g_{\mathcal{B}}$ result from terms in the photon self-energy which are proportional to $2\pi\delta(p_0)$. It follows that the usual $1/2N$ corrections to the photon propagator, like shown in Fig. C.6(a), do not renormalize the flux disorder.

In order to renormalize $g_{\mathcal{E}}$ and $g_{\mathcal{B}}$ we must have a disorder line going through the middle. This would allow a diagram like that shown in Fig. C.6(b). The trace over fermion flavours means that the only disorder we could place between the two loops is the singlet mass-like disorder, with coupling g_s. This diagram is $\mathrm{O}(2Ng_s) \sim \mathrm{O}(1)$ and so thankfully it vanishes:

$$\text{Fig. C.6(b)} = 2\pi\delta(p_0) 2N \mu^{-2\epsilon} g^2 g_s \underbrace{\int \frac{d^D q}{(2\pi)^D} \mathrm{tr}\left[\frac{i q_\alpha \gamma^\alpha}{q^2} \frac{i(q+p)_\beta \gamma^\beta}{(q+p)^2} i\gamma^\mu\right]}_{\mathcal{I}^\mu(p)} \underbrace{\int \frac{d^D k}{(2\pi)^D} \mathrm{tr}\left[\frac{i k_\sigma \gamma^\sigma}{k^2} \frac{i(k+p)_\rho \gamma^\rho}{(k+p)^2} i\gamma^\nu\right]}_{\mathcal{I}^\nu(p)} \tag{C.52}$$

where

$$\mathcal{I}^\mu(p) = -i\mathrm{tr}\left[\gamma^\alpha \gamma^\beta \gamma^\mu\right] \int \frac{d^D q}{(2\pi)^D} \int_0^1 dx \frac{q_\alpha q_\beta - x(1-x) p_\alpha p_b}{\left[q^2 + x(1-x)p^2\right]^2} = 0. \tag{C.53}$$

We next consider the situation with two internal disorder lines. These lines must go

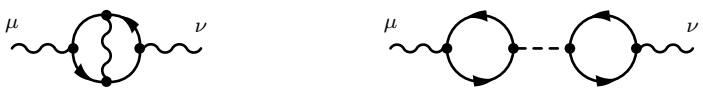

(a) (b)

Figure C.6: Diagrams which enter into the photon self-energy at leading order. (a) will not renormalize the disorder and (b) vanishes.

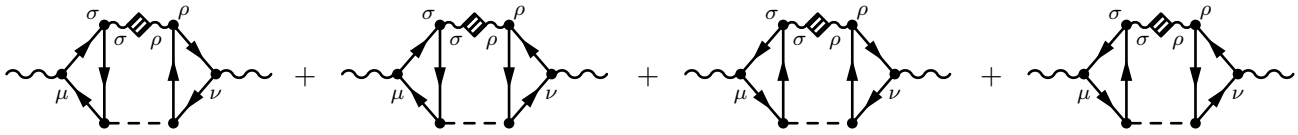

Figure C.7: Diagrams which renormalizes the flux disorder at $\mathrm{O}(g_\xi, g_\xi/2N)$. Depending on whether the internal indices are $(\sigma, \rho) = (0, 0)$ or (i, j), the coupling constant are $-g_{\mathcal{B}}$ or $g_{\mathcal{E}}$ respectively.

between the two bubbles otherwise they will be cancelled by a vertex or a field strength renormalization and will not lead to a renormalization of the flux disorder. Furthermore, one of the internal lines must correspond to a flux disorder interaction since otherwise the divergence will be cancelled by one of the bilinear disorder counter terms we determined in the previous two sections. This leaves the diagrams with one internal disorder line coupling to the topological current and one to the mass since all other bilinear disorder types will vanish upon tracing over the flavour indices. These diagrams are shown in Fig. C.7. Depending on whether the internal indices (σ, ρ) are $(0, 0)$ or (i, j) the diagrams are proportional to $-g^4 g_s g_\beta$ or $g^4 g_s g_{\mathcal{E}}$ respectively. They therefore contribute at the same order as the diagrams in the previous two sections. We note that diagrams which two internal flux disorder lines appear at a order in g_ξ and $1/2N$.

Ignoring coupling constants for the moment, for any give μ, ν, σ, and ρ, it's easy to check that the four diagrams being added in Fig. C.7 all have the same value. Therefore, their

sum is equal to

$$\text{Fig. C.7} = 4(-1)^2(16)^2 \int \frac{d^Dk}{(2\pi)^D} \int \frac{d^Dq}{(2\pi)^D} \frac{d^D\ell}{(2\pi)^D} 2\pi\delta(k_0) 2\pi\delta(-k_0+p_0) \left(\delta_{\sigma\rho} - \frac{k_\sigma k_\rho}{k^2}\right) \times \text{tr}\left[i\gamma^\mu \frac{iq_\alpha\gamma^\alpha}{q^2} i\gamma^\sigma \frac{i(q+k)_\beta}{(q+k)^2} \frac{i(q+p)_\lambda\gamma^\lambda}{(q+p)^2}\right] \text{tr}\left[\frac{i(\ell+p)_{\lambda'}\gamma^{\lambda'}}{(q+p)^2} \frac{i(\ell+k)_{\beta'}}{(\ell+k)^2} i\gamma^\rho \frac{i\ell_{\alpha'}\gamma^{\alpha'}}{\ell^2} i\gamma^\nu\right] \tag{C.54}$$

Noting that

$$\text{tr}\left[\frac{i(\ell+p)_{\lambda'}\gamma^{\lambda'}}{(q+p)^2} \frac{i(\ell+k)_{\beta'}}{(\ell+k)^2} i\gamma^\rho \frac{i\ell_{\alpha'}\gamma^{\alpha'}}{\ell^2} i\gamma^\nu\right] = -\text{tr}\left[i\gamma^\nu \frac{i\ell_{\alpha'}\gamma^{\alpha'}}{\ell^2} i\gamma^\rho \frac{i(\ell+k)_{\beta'}}{(\ell+k)^2} \frac{i(\ell+p)_{\lambda'}\gamma^{\lambda'}}{(q+p)^2}\right], \tag{C.55}$$

we define a function

$$\mathcal{F}^{\mu\sigma}(k,p) = \int \frac{d^Dq}{(2\pi)^D} \text{tr}\left[\gamma^\mu\gamma^\alpha\gamma^\sigma\gamma^\beta\gamma^\lambda\right] \frac{q_\alpha(q+k)_\beta(q+p)_\lambda}{q^2(q+k)^2(q+p)^2}. \tag{C.56}$$

It follows that

$$\text{Fig. C.7} = 4(16)^2 \cdot 2\pi\delta(p_0) \int \frac{d^dk}{(2\pi)^d} \mathcal{F}^{\mu\sigma}(k,p)\mathcal{F}^{\nu\rho}(k,p) \left(\delta_{\sigma\rho} - \frac{k_\sigma k_\rho}{k^2}\right). \tag{C.57}$$

By dimensional analysis and gauge invariance, we know that any divergence arising from the sum of these diagrams must take the form

$$\text{Fig. C.7} = C^{\mu\nu,\sigma\rho} \times 2\pi\delta(p_0)p^2 \left(\delta_{\mu\nu} - \frac{p_\mu p_\nu}{p^2}\right) + \text{finite} \tag{C.58}$$

where $C^{\mu\nu,\sigma\rho}$ is a constant proportional to $1/\epsilon$. It follows that our problem can be significantly simplified by differentiating twice with respect to p, setting it to zero, and using a cuttoff μ_{IR} to regulate the IR divergence. That is

$$C^{\mu\nu,\sigma\rho} = 4(16)^2 \int \frac{d^dk}{(2\pi)^d} \left(\delta_{\sigma\rho} - \frac{k_\sigma k_\rho}{k^2}\right) \frac{\partial}{\partial p^2} \left[\mathcal{F}^{\mu\sigma}(k,0)\mathcal{F}^{\nu\rho}(k,0)\right], \tag{C.59}$$

up to finite pieces. Noting that we should only differentiate with respect to $p^2 = p_x^2 + p_y^2$,

since $p_0 = 0$, we have

$$\frac{\partial^2}{\partial p^2}\left[\mathcal{F}^{\mu\sigma}(k,0)\mathcal{F}^{\nu\rho}(k,0)\right] = \frac{1}{2d}\sum_j \left[\partial_j\partial^j\mathcal{F}^{\mu\sigma}\mathcal{F}^{\nu\rho} + \mathcal{F}^{\mu\sigma}\partial^j\partial_j\mathcal{F}^{\nu\rho} + 2\partial_j\mathcal{F}^{\mu\sigma}\partial^j\mathcal{F}^{\nu\rho}\right]. \quad \text{(C.60)}$$

where $\partial_j = \partial/\partial p_j$.

We start by finding $\mathcal{F}^{\mu\sigma}(k,0)$:

$$\begin{aligned}
\mathcal{F}^{\mu\sigma}(k,0) &= \mathrm{tr}\left[\gamma^\mu\gamma^\alpha\gamma^\sigma\gamma^\beta\gamma^\lambda\right]\int\frac{d^Dq}{(2\pi)^D}\frac{q_\alpha(q+k)_\beta q_\lambda}{(q^2)^2(q+k)^2} \\
&= \mathrm{tr}\left[\gamma^\mu\gamma^\alpha\gamma^\sigma\gamma^\beta\gamma^\lambda\right]\int\frac{d^Dq}{(2\pi)^D}\int_0^1 dx\frac{2(1-x)}{\left[q^2+x(1-x)k^2\right]^3} \\
&\quad\times\left(\frac{q^2}{D}\left[-x\delta_{\alpha\beta}k_\lambda - x\delta_{\beta\lambda k_\alpha} + (1-x)\delta_{\alpha\lambda}k_\beta\right] + x^2(1-x)k_\alpha k_\beta k_\lambda\right) \\
&= \frac{\mathrm{tr}\left[\gamma^\mu\gamma^\alpha\gamma^\sigma\gamma^\beta\gamma^\lambda\right]}{128\,|k|}\left(3\delta_{\alpha\lambda}k_\beta - \delta_{\alpha\beta}k_\lambda - \delta_{\beta\lambda}k_\alpha + \frac{k_\alpha k_\beta k_\lambda}{k^2}\right) \\
&= 0. \qquad \text{(C.61)}
\end{aligned}$$

Here, we have set $D = 3$ since the integral is finite; we will continue to do so below. So the first two terms in the derivative of $\mathcal{F}^{\mu\sigma}\mathcal{F}^{\nu\rho}$ vanish, leaving only the third. We are left to find

$$\partial_j\mathcal{F}^{\mu\sigma}(k,0) = \delta_{j\eta}\mathrm{tr}\left[\gamma^\mu\gamma^\alpha\gamma^\sigma\gamma^\beta\gamma^\lambda\right]\int\frac{d^Dq}{(2\pi)}\frac{q_\alpha(q+k)_\beta}{(q^2)^2(q+k)^2}\left(\delta_{\eta\lambda} - \frac{2q_\lambda q_\eta}{q^2}\right). \quad \text{(C.62)}$$

We separate this into two terms:

$$\begin{aligned}
\left[\partial_j\mathcal{F}^{\mu\sigma}(k,0)\right]_A &= \delta_{j\eta}\mathrm{tr}\left[\gamma^\mu\gamma^\alpha\gamma^\sigma\gamma^\beta\gamma^\eta\right]\int\frac{d^Dq}{(2\pi)}\frac{q_\alpha(q+k)_\beta}{(q^2)^2(q+k)^2}, \\
\left[\partial_j\mathcal{F}^{\mu\sigma}(k,0)\right]_B &= -2\delta_{j\eta}\,\mathrm{tr}\left[\gamma^\mu\gamma^\alpha\gamma^\sigma\gamma^\beta\gamma^\lambda\right]\int\frac{d^Dq}{(2\pi)}\frac{q_\alpha(q+k)_\beta q_\lambda q_\eta}{(q^2)^3(q+k)^2}. \qquad \text{(C.63)}
\end{aligned}$$

The "A" contribution is

$$\begin{aligned}
\left[\partial_j \mathcal{F}^{\mu\sigma}(k,0)\right]_A &= \delta_{j\eta}\mathrm{tr}\left[\gamma^\mu\gamma^\alpha\gamma^\sigma\gamma^\beta\gamma^\eta\right]\int\frac{d^Dq}{(2\pi)^D}\frac{2(1-x)}{[q^2+x(1-x)k^2]^3}\left(\frac{q^2}{D}\delta_{\alpha\beta}-x(1-x)k_\alpha k_\beta\right)\\
&= \delta_{j\eta}\,\frac{\mathrm{tr}\left[\gamma^\mu\gamma^\alpha\gamma^\sigma\gamma^\beta\gamma^\eta\right]}{32\,|k|}\left(\delta_{\alpha\beta}-\frac{k_\alpha k_\beta}{k^2}\right)\\
&= \delta_{j\eta}\,\frac{2i}{32\,|k|}\left(-\epsilon^{\mu\sigma\eta}+\frac{1}{k^2}\left[\epsilon^{\sigma\eta\alpha}k_\alpha k^\mu+\epsilon^{\mu\sigma\alpha}k_\alpha k^\eta+\epsilon^{\mu\eta\alpha}k_\alpha k^\sigma\right]\right).
\end{aligned}\tag{C.64}$$

The "B" part is slightly more complicated,

$$\begin{aligned}
\left[\partial_j \mathcal{F}^{\mu\sigma}(k,0)\right]_B = -6\,\delta_{j\eta}\;\mathrm{tr}\left[\gamma^\mu\gamma^\alpha\gamma^\sigma\gamma^\beta\gamma^\lambda\right]\int\frac{d^Dq}{(2\pi)^D}\int_0^1 dx\frac{(1-x)^2}{[q^2+x(1-x)k^2]^4}\Bigg(&q_\alpha q_\beta q_\lambda q_\eta\\
&+\frac{q^2}{D}\Big[x^2\left(\delta_{\alpha\beta}k_\lambda k_\eta+\delta_{\beta\lambda}k_\alpha k_\eta+\delta_{\beta\eta}k_\alpha k_\lambda\right)-x(1-x)\left(\delta_{\alpha\lambda}k_\beta k_\eta-\delta_{\alpha\eta}k_\beta k_\lambda-\delta_{\lambda\eta}k_\alpha k_\beta\right)\Big]\\
&-x^3(1-x)k_\alpha k_\beta k_\lambda k_\eta\Bigg),
\end{aligned}\tag{C.65}$$

and so we further separate this into three pieces:

$$\left[\partial_j \mathcal{F}^{\mu\sigma}(k,0)\right]_B^n = -6\,\delta_{j\eta}\;\mathrm{tr}\left[\gamma^\mu\gamma^\alpha\gamma^\sigma\gamma^\beta\gamma^\lambda\right]\int\frac{d^Dq}{(2\pi)^D}\int_0^1 dx\frac{(1-x)^2}{[q^2+x(1-x)k^2]^4}f^n_{\alpha\beta\lambda\eta}(q,k),\tag{C.66}$$

where

$$\begin{aligned}
f^1_{\alpha\beta\lambda\eta}(q,k) &= q_\alpha q_\beta q_\lambda q_\eta,\\
f^2_{\alpha\beta\lambda\eta}(q,k) &= \frac{q^2}{D}\Big[x^2\left(\delta_{\alpha\beta}k_\lambda k_\eta+\delta_{\beta\lambda}k_\alpha k_\eta+\delta_{\beta\eta}k_\alpha k_\lambda\right)-x(1-x)\left(\delta_{\alpha\lambda}k_\beta k_\eta-\delta_{\alpha\eta}k_\beta k_\lambda-\delta_{\lambda\eta}k_\alpha k_\beta\right)\Big],\\
f^3_{\alpha\beta\lambda\eta}(q,k) &= -x^3(1-x)k_\alpha k_\beta k_\lambda k_\eta.
\end{aligned}\tag{C.67}$$

For the first part of $\left[\partial_j \mathcal{F}^{\mu\sigma}(k,0)\right]_B$ we replace the four q's with

$$q_\alpha q_\beta q_\lambda q_\eta \to \frac{(q^2)^2}{D(D+2)}\left(\delta_{\alpha\beta}\delta_{\lambda\eta}+\delta_{\alpha\lambda}\delta_{\beta\eta}+\delta_{\alpha\eta}\delta_{\beta\lambda}\right)\tag{C.68}$$

which gives

$$[\partial_j \mathcal{F}^{\mu\sigma}(k,0)]_B^1 = -\delta_{j\eta}\frac{3}{256\,|k|}\mathrm{tr}\left[\gamma^\mu\gamma^\alpha\gamma^\sigma\gamma^\beta\gamma^\lambda\right](\delta_{\alpha\beta}\delta_{\lambda\eta}+\delta_{\alpha\lambda}\delta_{\beta\eta}+\delta_{\alpha\eta}\delta_{\beta\lambda})$$
$$= \delta_{j\eta}\frac{2i}{256\,|k|}\cdot 15\epsilon^{\mu\sigma\eta}. \tag{C.69}$$

The second piece evaluates to

$$[\partial_j \mathcal{F}^{\mu\sigma}(k,0)]_B^2 = \delta_{j\eta}\,\mathrm{tr}\left[\gamma^\mu\gamma^\alpha\gamma^\sigma\gamma^\beta\gamma^\lambda\right]\left(-\frac{1}{256\,|k|^3}\left[\delta_{\alpha\beta}k_\lambda k_\eta+\delta_{\beta\lambda}k_\alpha k_\eta+\delta_{\beta\eta}k_\alpha k_\lambda\right]\right.$$
$$\left.+\frac{3}{256\,|k|^3}\left[\delta_{\alpha\lambda}k_\beta k_\eta-\delta_{\alpha\eta}k_\beta k_\lambda-\delta_{\lambda\eta}k_\alpha k_\beta\right]\right)$$
$$= -\delta_{j\eta}\frac{2i}{256\,|k|^3}\left(\epsilon^{\mu\sigma\alpha}k_\alpha k^\eta+4\epsilon^{\sigma\eta\alpha}k_\alpha k^\mu+4\epsilon^{\mu\eta\alpha}k_\alpha k^\sigma+3\epsilon^{\mu\sigma\eta}k^2\right). \tag{C.70}$$

Finally, the third part is

$$[\partial_j \mathcal{F}^{\mu\sigma}(k,0)]_B^3 = \delta_{j\eta}\frac{3}{256\,|k|^5}\mathrm{tr}\left[\gamma^\mu\gamma^\alpha\gamma^\sigma\gamma^\beta\gamma^\lambda\right]k_\alpha k_\beta k_\lambda k_\eta = -\frac{2i}{256\,|k|^3}\cdot 3\epsilon^{\mu\sigma\alpha}k_\alpha k^\eta. \tag{C.71}$$

Adding the three contributions, we find

$$[\partial_j \mathcal{F}^{\mu\sigma}(k,0)]_B = \delta_{j\eta}\frac{2i}{64\,|k|}\left(3\epsilon^{\mu\sigma\eta}-\frac{1}{k^2}\left[\epsilon^{\mu\sigma\alpha}k_\alpha k^\eta+\epsilon^{\sigma\eta\alpha}k_\alpha k^\mu+\epsilon^{\mu\eta\alpha}k_\alpha k^\sigma\right]\right), \tag{C.72}$$

and, upon including $[\partial_j \mathcal{F}^{\mu\sigma}(k,0)]_A$, we obtain

$$\partial_j \mathcal{F}^{\mu\sigma}(k,0) = \delta_{j\eta}\frac{i}{32\,|k|}\left(\epsilon^{\mu\sigma\eta}+\frac{1}{k^2}\left[\epsilon^{\mu\sigma\alpha}k_\alpha k^\eta+\epsilon^{\sigma\eta\alpha}k_\alpha k^\mu+\epsilon^{\mu\eta\alpha}k_\alpha k^\sigma\right]\right). \tag{C.73}$$

We can now extract the divergence. When we only consider the magnetic disorder, the internal indices in Eq. (C.59) are fixed at $(\sigma,\rho)=(0,0)$. In this case, we have

$$C^{\mu\nu,00} = 4(16)^2\int\frac{d^dk}{(2\pi)^d}\frac{1}{k^2}\frac{2}{2d}\sum_{j=x,y}\partial^j\mathcal{F}^{\mu\sigma}(k,0)\partial_j\mathcal{F}^{\nu\rho}(k,0) = -\delta^{\mu i}\delta^{\nu j}\delta_{ij}2(16)^2\frac{4}{4(16)^2}\int\frac{d^dk}{(2\pi)^d}\frac{1}{k^2}$$
$$= \delta^{\mu i}\delta^{\nu j}\delta_{ij}\left(\frac{1}{\pi\epsilon}\right). \tag{C.74}$$

When we have $(\sigma,\rho)=(i,j)$ we find

$$\begin{aligned}\sum_{i,j=x,y} C^{\mu\nu,ij} &= 4(16)^2 \int \frac{d^dk}{(2\pi)^d}\frac{1}{k^2}\frac{2}{2d}\sum_{\ell,i,j=x,y}\partial^\ell\mathcal{F}^{\mu i}(k,0)\partial_\ell\mathcal{F}^{\nu j}(k,0)\left(\delta_{ij}-\frac{k_ik_j}{k^2}\right)\\ &= \delta^{\mu 0}\delta^{\nu 0}\left(\frac{1}{\pi\epsilon}\right).\end{aligned} \tag{C.75}$$

Multiplying by the corresponding coupling constants, we obtain the counter terms cited in Eq. (4.43):

$$\delta_{\mathcal{E}} = \mathcal{g}^4 g_s g_{\mathcal{B}}\left(\frac{1}{\pi\epsilon}\right), \qquad \delta_{\mathcal{B}} = \mathcal{g}^4 g_s g_{\mathcal{E}}\left(\frac{1}{\pi\epsilon}\right). \tag{C.76}$$

C.6 Current-current correlators

In this appendix we review our calculation of the Feynman diagrams shown in Figs. 4.10(a) to (e). Since no divergences are present in these diagrams, no counter-terms will be necessary.

C.6.1 Bare loop

The leading term is shown in Fig. 4.10(a). It is simply

$$\begin{aligned}\text{Fig. 4.10(a)} &= (-1)\mathrm{tr}\left[T^rT^s\right]\mathrm{tr}\left[\sigma^a\sigma^b\right]\int\frac{d^Dq}{(2\pi)^D}\mathrm{tr}\left[i\gamma^\mu\frac{iq_\alpha\gamma^\alpha}{q^2}i\gamma^\nu\frac{i(q+p)_\beta\gamma^\beta}{(q+p)^2}\right]\\ &= -\delta^{rs}\delta^{ab}\frac{|p|}{16}\left(\delta^{\mu\nu}-\frac{p^\mu p^\nu}{p^2}\right)\end{aligned} \tag{C.77}$$

where we used $\mathrm{tr}\left[T^rT^s\right]=\frac{\delta^{rs}}{2}$. Setting $\boldsymbol{p}=0$ and $\mu=\nu=x$,we have

$$\text{Fig. 4.10(a)} = -\frac{|p_0|}{16}. \tag{C.78}$$

(a) (b) (c) (d)

Figure C.8: Subdiagrams which contribute to the flavour conductivity.

C.6.2 Vertex diagrams

Contribution proportional to $g_{t,z}$

We begin by calculating the 1-loop vertex contribution shown in Fig. C.8(a):

$$\begin{aligned}\text{Fig. C.8(a)} &= g_{t,z}T^r \otimes \sigma^z\sigma^a\sigma^z \int \frac{d^Dk}{(2\pi)^d} 2\pi\delta(k_0) \frac{i(q+p)_\alpha\gamma^\alpha}{(q+p)^2} \frac{i(q+k+p)_\beta\gamma^\beta}{(q+k+p)^2} i\gamma^\mu \frac{i(q+k)_\sigma\gamma^\sigma}{q^2} \frac{iq_\rho\gamma^\rho}{q^2} \\ &= ig_{t,z}T^r \otimes \sigma^z\sigma^a\sigma^z \otimes \gamma^a\gamma^\rho\gamma^\mu\gamma^\sigma\gamma^\rho \frac{(q+p)_a q_\rho}{(q+p)^2q^2} I_{\beta\sigma}(q_0,p_0) \end{aligned} \tag{C.79}$$

where

$$I_{\beta\sigma}(q_0,p_0) = \delta_{\beta 0}\delta_{\sigma 0} \underbrace{\int \frac{d^dk}{(2\pi)^d} \frac{q_0(q_0+p_0)}{[(q_0+p_0)^2+\boldsymbol{k}^2]\,[q_0^2+\boldsymbol{k}^2]}}_{I_0(q_0,p_0)} + \frac{\delta_{\beta j}\delta_{\sigma i}\delta^{ij}}{d} \underbrace{\int \frac{d^dk}{(2\pi)^d} \frac{\boldsymbol{k}^2}{[(q_0+p_0)^2+\boldsymbol{k}^2]\,[q_0^2+\boldsymbol{k}^2]}}_{I_d(q_0,p_0)}. \tag{C.80}$$

The full diagram in Fig. 4.10(b) is then

$$\begin{aligned}\text{Fig. 4.10(b)} &= -1\times 2\times g_{t,z}\mathrm{tr}[T^rT^s]\mathrm{tr}[\sigma^z\sigma^a\sigma^z\sigma^b]\mathrm{tr}\left[\gamma^\alpha\gamma^\beta\gamma^x\gamma^\sigma\gamma^\rho\gamma^x\right](i)^2 \int \frac{d^3q}{(2\pi)^3} \frac{(q+p)_a q_\rho}{(q+p)^2q^2} I_{\beta\sigma}(q_0,p_0) \\ &= -2\eta_a\delta^{rs}\delta^{ab} \int \frac{d^3q}{(2\pi)^3} \mathrm{tr}\left[\gamma^\rho\gamma^x\gamma^\alpha\gamma^x\right] \left(I_{\mathrm{V},0}(q_0,p_0) + \frac{(d-2)}{2} I_{\mathrm{V},d}(q_0,p_0)\right) \frac{(q+p)_a q_\rho}{(q+p)^2q^2} \\ &= 4\eta_a\delta^{rs}\delta^{ab} \int \frac{d^3q}{(2\pi)^3} \left(I_{\mathrm{V},0}(q_0,p_0) + \frac{(d-2)}{2} I_{\mathrm{V},d}(q_0,p_0)\right) \frac{q_0(q_0+p_0)}{[(q_0+p_0)^2+\boldsymbol{q}^2]\,[q_0^2+\boldsymbol{q}^2]} \end{aligned} \tag{C.81}$$

where $\eta_z = +1$ and $\eta_{x,y} = -1$.

We perform the integral over $\boldsymbol{k}$ in $I_{\mathrm{V},0}$ and $I_{\mathrm{V},d}$ and analytically continuing to $d = 2 + \epsilon$ spatial dimensions:

$$I^{\mathrm{V}}_{\mathrm{tot}}(q_0, p_0) = I_{\mathrm{V},0}(q_0, p_0) + \frac{(d-2)}{2} I_{\mathrm{V},d}(q_0, p_0) = -\frac{1}{4\pi}\left\{1 + \frac{q_0(q_0+p_0)}{p_0(p_0+2q_0)} \log\left[\frac{q_0^2}{(q_0+p_0)^2}\right]\right\}. \tag{C.82}$$

Performing the $\boldsymbol{q}$ integral, we have

$$\int \frac{d^2q}{(2\pi)^2} \frac{q_0(q_0+p_0)}{[(q_0+p_0)^2 + \boldsymbol{q}^2]\,[q_0^2 + \boldsymbol{q}^2]} = -\frac{1}{4\pi} \frac{q_0(q_0+p_0)}{p_0(p_0+2q_0)} \log\left[\frac{q_0^2}{(q_0+p_0)^2}\right]. \tag{C.83}$$

Plugging these into Eq. C.81 and integrating over q_0 we find,

$$\text{Fig. 4.10(b)} = \eta_a \delta^{rs} \delta^{ab} \cdot g_{t,z} \frac{|p_0|}{96\pi}. \tag{C.84}$$

Contribution proportional to $g_{\mathcal{A},z}$

The diagram in Fig. 4.10(d) vanishes. We can see this by noting that

$$\begin{aligned}\text{Fig. C.8(b)} &= g_{\mathcal{A},z} T^r \otimes \sigma^z \sigma^a \sigma^z \int \frac{d^D k}{(2\pi)^d} 2\pi\delta(k_0) \frac{i(q+p)_\alpha \gamma^\alpha}{(q+p)^2} i\gamma^j \frac{i(q+k+p)_\beta \gamma^\beta}{(q+k+p)^2} i\gamma^\mu \frac{i(q+k)_\sigma \gamma^\sigma}{q^2} \gamma_j \frac{iq_\rho \gamma^\rho}{q^2} \\ &= -i g_{\mathcal{A},z} T^r \otimes \sigma^z \sigma^a \sigma^z \otimes \gamma^\alpha \gamma^j \gamma^\rho \gamma^\mu \gamma^\sigma \gamma_j \gamma^\rho \frac{(q+p)_\alpha q_\rho}{(q+p)^2 q^2} I_{\beta\sigma}(q_0, p_0)\end{aligned} \tag{C.85}$$

where $I_{\beta\sigma}(q_0, p_0)$ is defined in Eq. C.80. The full diagram is therefore

$$\begin{aligned}\text{Fig. 4.10(d)} &= (-1)^2 \times 2 \times g_{\mathcal{A},z} \mathrm{tr}[T^r T^s] \mathrm{tr}[\sigma^z \sigma^a \sigma^z \sigma^b] \mathrm{tr}\left[\gamma^\alpha \gamma^j \gamma^\beta \gamma^x \gamma^\sigma \gamma_j \gamma^\rho \gamma^x\right] (i)^2 \int \frac{d^3q}{(2\pi)^3} \frac{(q+p)_a q_\rho}{(q+p)^2 q^2} I_{\beta\sigma}(q_0, p_0) \\ &= 2\eta_a g_{\mathcal{A},z} \delta^{rs} \delta^{ab} \int \frac{d^3q}{(2\pi)^3} \mathrm{tr}\left[\gamma^\rho \gamma^x \gamma^\alpha \gamma^x\right] (2-d) \left(I_{\mathrm{V},0}(q_0, p_0) + \frac{(d-2)}{2} I_{\mathrm{V},d}(q_0, p_0)\right) \frac{(q+p)_a q_\rho}{(q+p)^2 q^2} \\ &= (d-2) g_{\mathcal{A},z} \times \left(\frac{1}{g_{t,z}} \text{Fig. 4.10(b)}\right).\end{aligned} \tag{C.86}$$

Noting that Fig. 4.10(b) has no epsilon pole, when $\epsilon \to 0$, this diagram vanishes: Fig. 4.10(d)=0.

C.6.3 Self-energy diagram

Contribution proportional to $g_{t,z}$

The self-energy subdiagram is

$$\begin{aligned}\text{Fig. C.8(c)} &= g_{t,z}\sigma^z\sigma^z \otimes \int \frac{d^Dk}{(2\pi)^D} 2\pi\delta^(k_0)\frac{i(q+k)_\beta\gamma^\beta}{(q+k)^2} = g_{t,z}i\gamma^0\int\frac{d^dk}{(2\pi)^d}\frac{q_0}{q_0^2+\boldsymbol{k}^2}\\ &= g_{t,z}i\gamma^0 q_0 \underbrace{\left[-\frac{1}{2\pi\epsilon}+\frac{1}{4\pi}\log\left[4\pi e^{-\gamma_E}\right]-\frac{1}{4\pi}\log q_0^2\right]}_{I_\Sigma(q_0)}.\end{aligned} \tag{C.87}$$

The full diagram is therefore

$$\begin{aligned}\text{Fig. 4.10(c)} &= -1\times 2\times g_{t,z}\mathrm{tr}[T^rT^s]\mathrm{tr}\left[\sigma^a\sigma^b\right]\int\frac{d^3q}{(2\pi)^3}\mathrm{tr}\left[\frac{iq_\alpha\gamma^\alpha}{q^2}i\gamma^0\frac{iq_\beta\gamma^\beta}{q^2}i\gamma^x\frac{i(q+p)_\rho\gamma^\rho}{(q+p)^2}i\gamma^x\right]q_0I_\Sigma(q_0)\\ &= 4g_{t,z}\delta^{rs}\delta^{ab}\int\frac{d^3q}{(2\pi)^3}\frac{q_0(q_0+p_0)(\boldsymbol{q}^2-q_0^2)}{\left[q_0^2+\boldsymbol{q}^2\right]^2\left[(q_0+p_0)^2+\boldsymbol{q}^2\right]}I_\Sigma(q_0)\\ &= -g_{t,z}\delta^{rs}\delta^{ab}\frac{2}{\pi}\int\frac{dq_0}{2\pi}\frac{q_0(q_0+p_0)I_\Sigma(q_0)}{p_0(p_0+2q_0)}\left(1+\frac{q_0^2+(q_0+p_0)^2}{2p_0(p_0+2q_0)}\log\left[\frac{q_0^2}{(q_0+p_0)^2}\right]\right)\end{aligned} \tag{C.88}$$

We see that the constant (and divergent) portion of $I_\Sigma(p_0)$ integrate to zero since it is odd.

The term proportional to the log on the other hand, can be rewritten and solved:

$$\begin{aligned}\text{Fig. 4.10(c)} &= g_{t,z}\delta^{rs}\delta^{ab}\frac{1}{4\pi^2}\int\frac{dq_0}{2\pi}\left(1+\frac{q_0^2+(q_0+p_0)^2}{2p_0(p_0+2q_0)}\log\left[\frac{q_0^2}{(q_0+p_0)^2}\right]\right)\frac{q_0(q_0+p_0)}{p_0(p_0+2q_0)}\log\left[\frac{q_0^2}{(q_0+p_0)^2}\right]\\ &= \delta^{rs}\delta^{ab}\cdot g_{t,z}\frac{|p_0|}{96\pi}\end{aligned} \tag{C.89}$$

Contribution proportional to $g_{\mathcal{A},z}$

This diagram is nearly identical to the previous one:

$$\begin{aligned}\text{Fig. 4.10(e)} &= -1\times 2\times g_{\mathcal{A},z}\mathrm{tr}[T^rT^s]\mathrm{tr}\left[\sigma^a\sigma^b\right]\int\frac{d^3q}{(2\pi)^3}\mathrm{tr}\left[\frac{iq_\alpha\gamma^\alpha}{q^2}i\gamma^j i\gamma^0 i\gamma_j\frac{iq_\beta\gamma^\beta}{q^2}i\gamma^x\frac{i(q+p)_\rho\gamma^\rho}{(q+p)^2}i\gamma^x\right]q_0I_\Sigma(q_0)\\ &= 2\times 4g_{\mathcal{A},z}\delta^{rs}\delta^{ab}\int\frac{d^3q}{(2\pi)^3}\frac{q_0(q_0+p_0)(\boldsymbol{q}^2-q_0^2)}{\left[q_0^2+\boldsymbol{q}^2\right]^2\left[(q_0+p_0)^2+\boldsymbol{q}^2\right]}I_\Sigma(q_0)\\ &= \delta^{rs}\delta^{ab}\cdot 2g_{\mathcal{A},z}\frac{|p_0|}{96\pi}.\end{aligned} \tag{C.90}$$

where $I_\Sigma(q_0)$ is given in Eq. C.87.

Appendix D

Appendix to Chapter 5

D.1 Generalized Epstein zeta function

We define the function $Y_2(s)$ to be

$$Y_2(s) = \sum_{n_1,n_2=-\infty}^{\infty} \left[\left(n_1 + \frac{1}{2}\right)^2 + \left(n_2 + \frac{1}{2}\right)^2 \right]^{-s}. \tag{D.1}$$

It is only convergent for $\mathrm{Re}\, s > 1/2$, but can be defined by analytically continuing outside of this domain. Specifically, it can be expressed in terms of the special functions λ and β [213]:

$$Y_2(s) = 4 \cdot 2^s \, \lambda(s)\beta(s), \tag{D.2}$$

where

$$\beta(s) = \sum_{n=0}^{\infty} (-1)^n \, (2n+1)^{-s}, \qquad \lambda(s) = \sum_{n=0}^{\infty} (2n+1)^{-s} = (1 - 2^{-s})\zeta(s) \tag{D.3}$$

with $\zeta(s) = \sum_{n=1}^{\infty} n^{-s}$, the Riemann zeta function.

D.2 Analytic continuation of Maxwell-Chern-Simons free energy

In Eq. (5.32) we expressed the summation over imaginary frequencies in terms of the Epstein zeta function

$$\zeta_{\mathcal{E}}(s;a^2)=\sum_{n=-\infty}^{\infty}\left[n^2+a^2\right]^{-s}, \tag{D.4}$$

where $a=\beta\gamma_{\boldsymbol{q}}/2\pi$. This expression is only valid for $\operatorname{Re}s>1/2$, but can be analytically continued onto the entire complex plane. To see this, we use the identity

$$\frac{1}{A^s}=\frac{\pi^s}{\Gamma(s)}\int_0^\infty dt\,t^{s-1}e^{-\pi tA}, \tag{D.5}$$

to write

$$\zeta_{\mathcal{E}}(s;a^2)=\sum_n\frac{\pi^s}{\Gamma(s)}\int_0^\infty dt\,t^{s-1}e^{-\pi t\left(n^2+a^2\right)}. \tag{D.6}$$

For sufficiently large values of s, we can exchange the summation and the integral, and, subsequently, use the Poisson summation formula:

$$\zeta_{\mathcal{E}}(s;a^2)=\frac{\pi^s}{\Gamma(s)}\int_0^\infty dt\,t^{s-1}e^{-\pi ta^2}\sum_n e^{-\pi tn^2}=\frac{\pi^s}{\Gamma(s)}\int_0^\infty dt\,t^{s-1}e^{-\pi ta^2}\frac{1}{\sqrt{t}}\sum_\ell e^{-\pi\ell^2/t}. \tag{D.7}$$

We see that divergence for $\operatorname{Re}s\leq 1/2$ is due to the $\ell=0$ term in the sum. Separating this term out and evaluating the integral, we have

$$\zeta_{\mathcal{E}}(s;a^2)=a^{1-2s}\frac{\sqrt{\pi}\Gamma(s-1/2)}{\Gamma(s)}+\frac{2\pi^s}{\Gamma(s)}\sum_{\ell=1}^{\infty}\int_0^\infty dt\,t^{s-3/2}e^{-\pi a^2t}e^{-\pi\ell^2/t}. \tag{D.8}$$

We can now extend s all the way to zero. Taking the derivative and limit, we have

$$-\lim_{s\to 0}\frac{d}{ds}\zeta_{\mathcal{E}}(s;a^2)=2\pi a-2\sum_{\ell=1}^{\infty}\frac{e^{-2\pi a\ell}}{\ell}=2\pi a+2\log\left(1-e^{-2\pi a}\right). \tag{D.9}$$

Plugging this result into Eq. (5.31), we obtain

$$F_{\mathrm{MCS}} = -\frac{1}{\beta}\log k - \frac{1}{\beta}\sum_{\boldsymbol{q}} \log\left[\frac{e^{-\beta\gamma_{\boldsymbol{q}}/2}}{1-e^{-\beta\gamma_{\boldsymbol{q}}}}\right]. \tag{D.10}$$

D.3 Leading order contribution

The leading order contribution in the zero temperature limit is

$$\begin{aligned} F_0(\boldsymbol{a}) &= -\frac{1}{\beta}\sum_{p}\log\left(p+a\right)^2 = -\sum_{\boldsymbol{p}}\int\frac{d\omega}{2\pi}\log\left(\omega^2+(\boldsymbol{p}+\boldsymbol{a})^2\right) \\ &= -\sum_{\boldsymbol{p}}\int\frac{d\omega}{2\pi}\log\omega^2 - \sum_{\boldsymbol{p}}\left|\boldsymbol{p}+\boldsymbol{a}\right|, \end{aligned} \tag{D.11}$$

where $p=(\omega,\boldsymbol{p})$, $\boldsymbol{p}=2\pi(n_x+1/2,n_y+1/2)/L$, $(n_x,n_y)\in\mathbb{Z}^2$. The first term vanishes using zeta-reg and the second one can be evaluating by analytically continuing to arbitrary s:

$$F_0(\boldsymbol{a}) = -\sum_{\boldsymbol{p}}\left(\boldsymbol{p}+\boldsymbol{a}\right)^{-2s} = -N_f\left(\frac{2\pi}{L}\right)^{-2s}\sum_{\boldsymbol{n}}\left(\boldsymbol{n}+\frac{1}{2}+\boldsymbol{\alpha}\right)^{-2s} \tag{D.12}$$

where

$$\alpha_\mu = \frac{L}{2\pi}a_\mu. \tag{D.13}$$

We can write this as

$$F_0(\boldsymbol{a}) = -\left(\frac{2\pi}{L}\right)^{-2s}\frac{\pi^s}{\Gamma(s)}\left[\frac{1}{s-1}+\int_1^\infty dt\, t^{s-1}\Theta\begin{bmatrix}\boldsymbol{\alpha}\\0\end{bmatrix}(it)+\int_1^\infty dt\, t^{-s}\left(\Theta\begin{bmatrix}0\\\boldsymbol{\alpha}\end{bmatrix}(it)-1\right)\right] \tag{D.14}$$

where Θ is shorthand for a product of Jacobi theta functions

$$\Theta\begin{bmatrix}\boldsymbol{\alpha}\\0\end{bmatrix}(it) = \prod_{j=1,2}\vartheta\begin{bmatrix}\alpha_j+1/2\\0\end{bmatrix}(0|it), \quad \Theta\begin{bmatrix}0\\\boldsymbol{\alpha}\end{bmatrix}(it) = \prod_{j=1,2}\vartheta\begin{bmatrix}0\\-\alpha_j-1/2\end{bmatrix}(0|it). \tag{D.15}$$

and we've used the following definition for the Jacobi theta functions with characteristics:

$$\begin{aligned}\vartheta\begin{bmatrix}a\\b\end{bmatrix}(\nu|\tau) &= \exp\left[\pi i a^2\tau + 2\pi i a(\nu+b)\right]\vartheta(\nu+a\tau+b|\tau)\\ &= \sum_{n=-\infty}^{\infty}\exp\left[\pi i(n+a)^2\tau + 2\pi i(n+a)(\nu+b)\right].\end{aligned} \tag{D.16}$$

For $s=-1/2$, we have

$$F_0(\boldsymbol{a}) = \frac{1}{L}\left[-\frac{2}{3}+\int_1^\infty dt\, t^{-3/2}\Theta\begin{bmatrix}\boldsymbol{\alpha}\\0\end{bmatrix}(it)+\int_1^\infty dt\,\sqrt{t}\left(\Theta\begin{bmatrix}0\\-\boldsymbol{\alpha}\end{bmatrix}(it)-1\right)\right]. \tag{D.17}$$

This function is plotted in Fig. D.1 and clearly has a minimum at $\boldsymbol{\alpha}=(0,0)$. In terms of the function Y_2 defined in Appendix D.1 in Eq. (D.1), this

$$F_0(0) = -\frac{2\pi}{L}Y_2\left(-\frac{1}{2}\right). \tag{D.18}$$

D.4 Polarization diagram

Here we calculate the leading $1/N_f$ contribution to the gauge kernel from the fermions. It is given by the polarization diagram:

$$\begin{aligned}S_f[B] &= \frac{1}{2}\mathrm{tr}\left(\frac{1}{i\not{\partial}}\not{B}\frac{1}{i\not{\partial}}\not{B}\right)\\ &= \frac{1}{2}\frac{1}{\beta V}\sum_{p,q}\mathrm{tr}\left(\frac{\not{p}}{p^2}\not{B}(-q)\frac{(\not{p}+\not{q})}{(p+q)^2}\not{B}(q)\right)\\ &= \frac{1}{2}\frac{1}{\beta V}\sum_{p,q}\mathrm{tr}\left(\sigma^\rho\sigma^\mu\sigma^\lambda\sigma^\nu\right)B_\mu(-q)B_\nu(q)\frac{p_\rho\,(p+q)_\lambda}{p^2\,(p+q)^2}\end{aligned} \tag{D.19}$$

where we have dropped all explicit references to $\bar{a}=0$. The internal momentum, p, corresponds to a fermionic field, $p^\mu = 2\pi(n^\mu+1/2)/L_\mu$, $n_\mu\in\mathbb{Z}$, whereas the external momentum

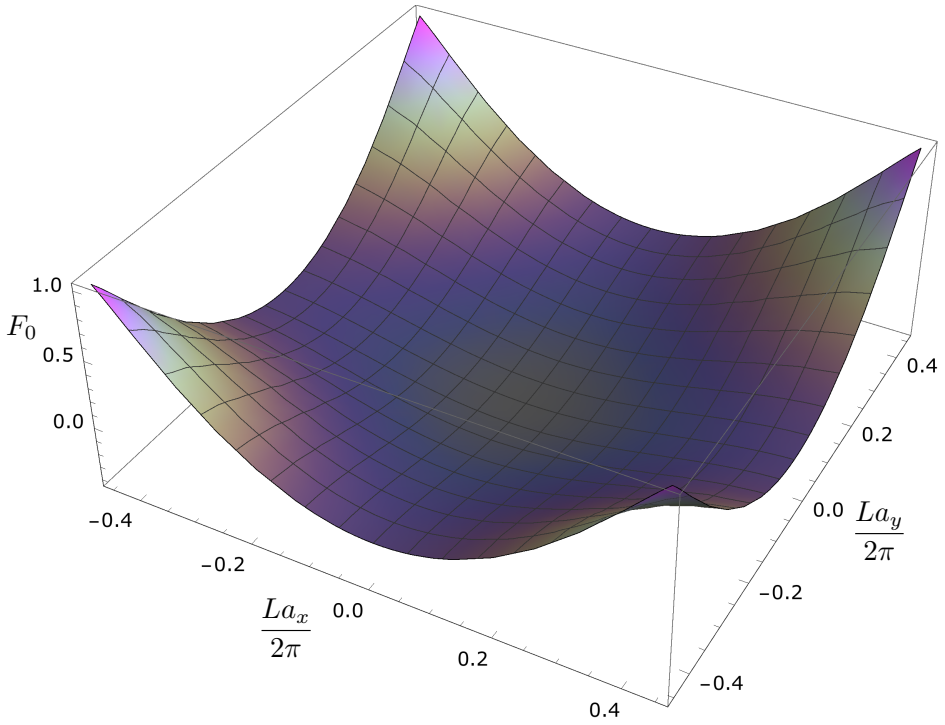

Figure D.1: Plot on the free energy of a free Dirac fermion on the torus as a function of its boundary conditions, a_x, a_y.

is appropriate for a bosonic field, $q^\mu = 2\pi n^\mu / L_\mu$, $n^\mu \in \mathbb{Z}$. This can be written as

$$S_f[B] = \frac{1}{2} \sum_q B_\nu(-q) \Pi_f^{\mu\nu}(q) B_\nu(q) \tag{D.20}$$

with

$$\begin{aligned} \Pi_f^{\mu\nu}(q) &= \frac{1}{\beta V} \sum_p \mathrm{tr}\left(\sigma^\rho \sigma^\mu \sigma^\lambda \sigma^\nu\right) \frac{p_\rho \left(p+q\right)_\lambda}{p^2 \left(p+q\right)^2} \\ &= \frac{2}{\beta L^2} \sum_p \frac{p^\mu \left(p^\nu + q^\nu\right) + \left(p^\mu + q^\mu\right) p^\nu - \delta^{\mu\nu} p \cdot \left(p+q\right)}{p^2 \left(p+q\right)^2}. \end{aligned} \tag{D.21}$$

In what follows, we will consider the zero temperature limit, $\beta \to \infty$.

We begin by calculating the the xx component:

$$\begin{aligned}\Pi_f^{xx}(\epsilon,\boldsymbol{q}) &= \frac{2}{L^2}\sum_{\boldsymbol{p}}\int\frac{d\omega}{2\pi}\frac{p_x(p_x+q_x)-p_y(p_y+q_y)-\omega(\omega+\epsilon)}{(\omega^2+\boldsymbol{p}^2)\left((\omega+\epsilon)^2+(\boldsymbol{p}+\boldsymbol{q})^2\right)}\\ &= \frac{1}{L^2}\sum_{\boldsymbol{p}}\left[\frac{p_x(p_x+q_x)-p_y(p_y+q_y)}{(|\boldsymbol{p}|+|\boldsymbol{p}+\boldsymbol{q}|)^2+\epsilon^2}\left(\frac{1}{|\boldsymbol{p}|}+\frac{1}{|\boldsymbol{p}+\boldsymbol{q}|}\right)-\frac{|\boldsymbol{p}|+|\boldsymbol{p}+\boldsymbol{q}|}{(|\boldsymbol{p}|+|\boldsymbol{p}+\boldsymbol{q}|)^2+\epsilon^2}\right]\end{aligned} \tag{D.22}$$

This is formally divergent but can be regulated by adding and subtracting the divergent piece and analytically continuing using zeta functions:

$$\begin{aligned}\Pi_f^{xx}(\epsilon,\boldsymbol{q}) = -\frac{1}{L^2}\Bigg\{&\sum_{\boldsymbol{p}}\frac{p_x(p_x+q_x)-p_y(p_y+q_y)}{(|\boldsymbol{p}|+|\boldsymbol{p}+\boldsymbol{q}|)^2+\epsilon^2}\left(\frac{1}{|\boldsymbol{p}|}+\frac{1}{|\boldsymbol{p}+\boldsymbol{q}|}\right)\\ &-\sum_{\boldsymbol{p}}\left[\frac{|\boldsymbol{p}|+|\boldsymbol{p}+\boldsymbol{q}|}{(|\boldsymbol{p}|+|\boldsymbol{p}+\boldsymbol{q}|)^2+\epsilon^2}-\frac{1}{2|\boldsymbol{p}|}\right]+\sum_{\boldsymbol{p}}\frac{1}{2|\boldsymbol{p}|}\Bigg\}.\end{aligned} \tag{D.23}$$

The divergent term is

$$\sum_{\boldsymbol{p}}\frac{1}{2|\boldsymbol{p}|} = \frac{1}{2}\frac{L}{2\pi}\sum_{\boldsymbol{n}}\frac{1}{\sqrt{(\boldsymbol{n}+1/2)^2}} = \frac{L}{4\pi}Y_2(1/2), \tag{D.24}$$

where $Y_2(s)$ is defined for all s in Appendix D.1. The finite expression is therefore

$$\begin{aligned}\Pi_f^{xx}(\epsilon,\boldsymbol{q}) = &-\frac{1}{4\pi L}Y_2(1/2)-\frac{1}{L^2}\sum_{\boldsymbol{p}}\left[\frac{|\boldsymbol{p}|+|\boldsymbol{p}+\boldsymbol{q}|}{(|\boldsymbol{p}|+|\boldsymbol{p}+\boldsymbol{q}|)^2+\epsilon^2}-\frac{1}{2|\boldsymbol{p}|}\right]\\ &+\frac{1}{L^2}\Bigg\{\sum_{\boldsymbol{p}}\frac{p_x(p_x+q_x)-p_y(p_y+q_y)}{(|\boldsymbol{p}|+|\boldsymbol{p}+\boldsymbol{q}|)^2+\epsilon^2}\left(\frac{1}{|\boldsymbol{p}|}+\frac{1}{|\boldsymbol{p}+\boldsymbol{q}|}\right).\end{aligned} \tag{D.25}$$

Similarly, we find

$$\begin{aligned}
\Pi_f^{yy}(\epsilon,\boldsymbol{q}) &= -\frac{1}{4\pi L}Y_2(1/2) - \frac{1}{L^2}\sum_{\boldsymbol{p}}\left[\frac{|\boldsymbol{p}|+|\boldsymbol{p}+\boldsymbol{q}|}{(|\boldsymbol{p}|+|\boldsymbol{p}+\boldsymbol{q}|)^2+\epsilon^2} - \frac{1}{2\,|\boldsymbol{p}|}\right] \\
&\quad - \frac{1}{L^2}\left\{\sum_{\boldsymbol{p}}\frac{p_x(p_x+q_x)-p_y(p_y+q_y)}{(|\boldsymbol{p}|+|\boldsymbol{p}+\boldsymbol{q}|)^2+\epsilon^2}\left(\frac{1}{|\boldsymbol{p}|}+\frac{1}{|\boldsymbol{p}+\boldsymbol{q}|}\right),\right. \\
\Pi_f^{xy}(\epsilon,\boldsymbol{q}) &= \frac{1}{L^2}\sum_{\boldsymbol{p}}\frac{p_x(p_y+q_y)+p_y(p_x+q_x)}{(|\boldsymbol{p}|+|\boldsymbol{p}+\boldsymbol{q}|)^2+\epsilon^2}\left(\frac{1}{|\boldsymbol{p}|}+\frac{1}{|\boldsymbol{p}+\boldsymbol{q}|}\right), \\
\Pi_f^{00}(\epsilon,\boldsymbol{q}) &= \frac{1}{L^2}\sum_{\boldsymbol{p}}\frac{|\boldsymbol{p}|\,|\boldsymbol{p}+\boldsymbol{q}|-\boldsymbol{p}\cdot(\boldsymbol{p}+\boldsymbol{q})}{(|\boldsymbol{p}|+|\boldsymbol{p}+\boldsymbol{q}|)^2+\epsilon^2}\left(\frac{1}{|\boldsymbol{p}|}+\frac{1}{|\boldsymbol{p}+\boldsymbol{q}|}\right), \\
\Pi_f^{0i}(\epsilon,\boldsymbol{q}) &= \frac{1}{L^2}\sum_{\boldsymbol{p}}\frac{\epsilon}{(|\boldsymbol{p}|+|\boldsymbol{p}+\boldsymbol{q}|)^2+\epsilon^2}\left(\frac{p_i}{|\boldsymbol{p}|}-\frac{p_i+q_i}{|\boldsymbol{p}+\boldsymbol{q}|}\right).
\end{aligned} \tag{D.26}$$

D.5 Operator contributions to the spectrum

In Sec. 5.3 we stated that in addition to imposing charge-neutrality, the gauge field alters the spectrum in two ways at $N_f = \infty$. First, its presence enforces the constraint $J^\mu(x) = 0$, removing one state from the spectrum for every choice of external momentum $\boldsymbol{q}$ and internal momentum $\boldsymbol{p}$, thereby decreasing the degeneracy of the free theory spectrum. Further, the photon creates states which contribute to the spectrum as well; their energies coincide with the poles of the photon propagator, $\Delta_{\mu\nu}(x) = \langle A_\mu(x)A_\nu(0)\rangle$.

We can understand how this comes about by translating the field theoretic operators to the quantum mechanical language of the free theory. We write

$$\begin{aligned}
J^\mu(x) &= \frac{1}{L^2}\sum_{\boldsymbol{q},E} e^{-i\boldsymbol{x}\cdot\boldsymbol{q}}J_E^\mu(\boldsymbol{q}), & J_E^\mu(\boldsymbol{q}) &= \sum_{\substack{\boldsymbol{p}\\ E_f(\boldsymbol{q},\boldsymbol{p})=E}} \bar\psi_\alpha(\boldsymbol{p}+\boldsymbol{q})\gamma^\mu\psi_\alpha(\boldsymbol{p}), \\
M(x) &= \frac{1}{L^2}\sum_{\boldsymbol{q},E} e^{-i\boldsymbol{x}\cdot\boldsymbol{q}}M_E(\boldsymbol{q}), & M_E(\boldsymbol{q}) &= \sum_{\substack{\boldsymbol{p}\\ E_f(\boldsymbol{q},\boldsymbol{p})=E}} \bar\psi_\alpha(\boldsymbol{p}+\boldsymbol{q})\psi_\alpha(\boldsymbol{p}).
\end{aligned} \tag{D.27}$$

For the moment, we specify to the case where $\boldsymbol{p}+\boldsymbol{q} \neq -\boldsymbol{p}$. Eq. (5.62) shows the two distinct states which exist for each energy $E_f(\boldsymbol{q},\boldsymbol{p})$ (additional degeneracies may be present due to the symmetry of the lattice, but this does not alter any of the following discussion). It

follows that $J^\mu_E(\boldsymbol{q})$ and $M_E(\boldsymbol{q})$ create states of the form

$$\begin{aligned} J^\mu_E(\boldsymbol{q})\,|0\rangle &= \left[v^\mu_1(\boldsymbol{p})\chi^\dagger_{+\alpha}(\boldsymbol{p}+\boldsymbol{q})\chi_{-\alpha}(\boldsymbol{p}) + v^\mu_2(\boldsymbol{p})\chi^\dagger_{+\alpha}(-\boldsymbol{p})\chi_{-\alpha}(-\boldsymbol{p}-\boldsymbol{q})\right]|0\rangle\,, \\ M_E(\boldsymbol{q})\,|0\rangle &= \left[v^M_1(\boldsymbol{p})\chi^\dagger_{+\alpha}(\boldsymbol{p}+\boldsymbol{q})\chi_{-\alpha}(\boldsymbol{p}) + v^M_2(\boldsymbol{p})\chi^\dagger_{+\alpha}(-\boldsymbol{p})\chi_{-\alpha}(-\boldsymbol{p}-\boldsymbol{q})\right]|0\rangle\,, \end{aligned} \tag{D.28}$$

where the "E" subscript on $v^\mu_i(\boldsymbol{p})$ and $v^M_i(\boldsymbol{p})$ has been dropped for notational ease. These coefficients are easily computed, and are found to be

$$\begin{aligned} \boldsymbol{v}^0 &= \frac{i}{2}\begin{pmatrix} 1 - \frac{P}{|\boldsymbol{p}|}\frac{\overline{P+Q}}{|\boldsymbol{p}+\boldsymbol{q}|} \\ 1 - \frac{\overline{P}}{|\boldsymbol{p}|}\frac{P+Q}{|\boldsymbol{p}+\boldsymbol{q}|} \end{pmatrix}, \qquad \boldsymbol{v}^x = \frac{1}{2}\begin{pmatrix} -\frac{P}{|\boldsymbol{p}|} + \frac{\overline{P+Q}}{|\boldsymbol{p}+\boldsymbol{q}|} \\ -\frac{\overline{P}}{|\boldsymbol{p}|} + \frac{P+Q}{|\boldsymbol{p}+\boldsymbol{q}|} \end{pmatrix}, \qquad \boldsymbol{v}^y = \frac{i}{2}\begin{pmatrix} \frac{P}{|\boldsymbol{p}|} + \frac{\overline{P+Q}}{|\boldsymbol{p}+\boldsymbol{q}|} \\ -\frac{\overline{P}}{|\boldsymbol{p}|} - \frac{P+Q}{|\boldsymbol{p}+\boldsymbol{q}|} \end{pmatrix}, \\ \boldsymbol{v}^M &= \frac{i}{2}\begin{pmatrix} 1 + \frac{P}{|\boldsymbol{p}|}\frac{\overline{P+Q}}{|\boldsymbol{p}+\boldsymbol{q}|} \\ 1 + \frac{\overline{P}}{|\boldsymbol{p}|}\frac{P+Q}{|\boldsymbol{p}+\boldsymbol{q}|} \end{pmatrix}, \end{aligned} \tag{D.29}$$

where $P = p_x + ip_y$, $Q = q_x + iq_y$. While it may not be obvious, it can be verified that the state created by the mass operator is orthogonal to the three states created by the current operators, and that these states are all proportional to one another.

The linear dependence of the current states actually follows directly from the conservation law $\partial_\mu J^\mu = 0$. In terms of the states, this reads

$$\left[-i\left(|\boldsymbol{p}+\boldsymbol{q}| + |\boldsymbol{p}|\right)J^0_E(\boldsymbol{q}) + q_x J^x_E(\boldsymbol{q}) + q_y J^y_E(\boldsymbol{q})\right]|0\rangle = 0. \tag{D.30}$$

The space spanned by $\chi^\dagger_{+\alpha}(\boldsymbol{p}+\boldsymbol{q})\chi_{-\alpha}(\boldsymbol{p})\,|0\rangle$ and $\chi^\dagger_{+\alpha}(-\boldsymbol{p})\chi_{-\alpha}(-\boldsymbol{p}-\boldsymbol{q})\,|0\rangle$ is a 2-dimensional complex vector space, equivalent to a $4d$ *real* vector space. Eq. (D.30) shows that the three $J^\mu_E(\boldsymbol{q})\,|0\rangle$ states actually only span a $2d$ real subspace, *ie.* a $1d$ *complex* vector space. As claimed, the currents only create a single state. The orthogonality of $M_E(\boldsymbol{q})\,|0\rangle$ to this state is then obvious since Eq. (D.29) implies that

$$(\boldsymbol{v}^\mu)^\dagger \boldsymbol{v}^M = 0. \tag{D.31}$$

Returning to the large-N_f theory, the gauge current states cease to exist, but the mass state

remains, resulting in (at least) a $2N_f^2 - 1$ degeneracy.

In the special case $\boldsymbol{p} + \boldsymbol{q} = -\boldsymbol{p}$, there is only a single state for each α, β pair, and so only a N_f^2 degeneracy in the free theory. Eq. (D.29) shows that only the current operators create states of this form, and, as above, this state is removed at $N_f = \infty$, resulting in a $N_f^2 - 1$ degeneracy.

D.6 Flux sectors

In this appendix we review the role of non-trivial flux sectors in the theories we considered in Sec. 5.2. When we defined the gauge field in Eq. (5.7), we did not consider its ability to carry non-trivial flux. This is possible because the photon is only defined modulo $2\pi/L$ and so can wind around either cycle of the torus so that

$$2\pi n = \frac{1}{\beta} \int d^3r \; (\partial_x A_y - \partial_x A_y) \neq 0. \tag{D.32}$$

Gauge field configurations with non-zero flux cannot be defined on the entire space with a single function: multiple functions defined on different patches are necessary. However, in regions intersecting one or more patches, the descriptions of A must differ only by a gauge transformation. Analogous to the quantization of electric charge through the existence of magnetic monopoles, this forces n to be an integer. Furthermore, at finite temperature, the photon can also wind around the time direction, introducing the possibility of F_{0x} or F_{y0} integrating to a non-zero value. For simplicity, we will only focus on the flux through the spatial torus though our arguments generalize easily to this case.

One way to represent a non-trivial flux state is to write

$$A_x = a_x + A'_x + \frac{2\pi n y}{L^2}. \tag{D.33}$$

The Chern-Simons partition function in Eq. (5.16) is modified by replacing $S_{\rm CS}$ with

$$S^{(n)}_{\rm CS,fl}[A] = S_{\rm CS}[B] + \frac{ik}{2\pi}\int d^3r\, a_0 \frac{2\pi n}{L^2} = S_{\rm CS}[A] + i\beta k\, n\, a_0. \tag{D.34}$$

The path integral must sum over the flux sectors separately; it becomes

$$Z_{\rm CS} = \frac{\beta L^2}{2\pi}\sqrt{\det{}'(-\nabla^2)}\sum_{n=-\infty}^{\infty}\int da\, e^{-i\beta k\, n\, a_0}\int dB\, e^{-S_{\rm CS}[B]}. \tag{D.35}$$

Upon integrating over a_0, n is restricted to be zero, and we get the partition function we determined in the main body of the paper. Similarly, when a Maxwell term is present, the action in the presence of flux is modified to

$$S^{(n)}_{\rm MCS}[A] = S_{\rm MCS}[B] + i\beta k\, n\, a_0 + \frac{\beta}{4e^2}\left(\frac{2\pi n}{L}\right)^2. \tag{D.36}$$

Integrating over a_0 from 1 to $2\pi/\beta$ again sets n to zero.

In the presence of matter, the flux sector no longer completely vanishes. However, Dirac fermions in the presence of flux have a higher energy than without. The saddle-point approximation we employ in Sec. 5.2.3 only expands about the ground state of free fermion theory; it does not take possible winding of A into account. Provided N is large enough, this is a good approximation.

Appendix E

Appendix to Chapter 6

E.1 Spin liquids with projective spin symmetry

We expand upon our assertion in Sec. 6.3.2 that a fully symmetric, gapped spin liquid cannot be obtained through the condensation of a Higgs field Φ coupling to a bilinear which transforms in a nontrivial manner under the SU(2) spin symmetry. As discussed, in order for the resulting spin liquid to have a spin gap, Φ must couple to one of the operators in Tab. 6.1. We start by studying $N^{ab} = \mathrm{tr}\left(\sigma^a \bar{X} \sigma^b X\right)$ and couple it to a Higgs field as $\sum_{a,b} \Phi^{ab} N^{ba} = \tilde{\mathrm{tr}}\left(\Phi N\right)$, where '$\tilde{\mathrm{tr}}$' refers to a trace over the spin and colour *vector* labels (as opposed to the usual trace 'tr' over spin and colour *spinor* indices). In the Higgs phase, we write $\bar{\Phi} = \langle \Phi \rangle \neq 0$.

Naturally, having the Higgs couple to N^{ab} implies that spin symmetry is realized projectively in the condensed phase, if at all. We associate SO(3) matrices to both the SU(2) gauge and spin transformations. That is, instead of studying the action of gauge and spin transformations U_g and U_s, we consider matrices $Q, R \in \mathrm{SO}(3)$ such that

$$\begin{aligned} \mathrm{SU}(2)_s : N^{ab} &\to \mathrm{tr}\left(\sigma^a \bar{X} U_s^\dagger \sigma^b U_s X\right) = N^{ac} \left(R^T\right)^{cb}, \\ \mathrm{SU}(2)_g : N^{ab} &\to \mathrm{tr}\left(U_g \sigma^a U_g^\dagger \bar{X} \sigma^b X\right) = Q^{ac} N^{cb}. \end{aligned} \tag{E.1}$$

Under a projective spin transformation,

$$\mathscr{P}\mathrm{SU}(2)_s : \tilde{\mathrm{tr}}\left(\bar{\Phi}N\right) \to \tilde{\mathrm{tr}}\left(\bar{\Phi}QNR^T\right) = \tilde{\mathrm{tr}}\left(\bar{\Phi}N\right), \tag{E.2}$$

implying that $Q = \bar{\Phi}^{-1}R$. The requirement that $Q \in \mathrm{SO}(3)$ implies that $\bar{\Phi} \in \mathrm{SO}(3)$ as well, for example $\bar{\Phi}^{ab} = |\Phi|\,\delta^{ab}$.

The obstruction to forming a fully symmetric spin liquid is then apparent. Since $N^{ab} \to -N^{ab}$ under $\mathcal{T}$, P_x and P_y, the equivalence of the original and symmetry transformed states requires that $\bar{\Phi}$ be gauge equivalent to $-\bar{\Phi}$. This in only possible if $Q_{t,px,py} = -\mathbb{1} \notin \mathrm{SO}(3)$.

These considerations apply equally to $\mathrm{tr}\left(\sigma^a \bar{X} \mu^{x,z} \sigma^b X\right)$ as indicated in Section 6.3.2.

E.2 Wen's Lattice PSG Classification Scheme

In this appendix, we relate our results to the spin liquid classification scheme proposed in Ref. 184 by Wen. We begin by reviewing his conventions and formalism before explaining what it means for two spin liquids to be "proximate" in this language. We then discuss how we determined that the gapped and gapless U(1) spin liquids in Fig. 6.1b correspond to U1Cn0n1 and U1Bx11n respectively. We subsequently consider the $\mathbb{Z}_2$ sPSG's and explain how the identification in Table 6.8 was obtained.

We note that frequent reference will be made to information that is only present in the arXiv version of Ref. 184.

E.2.1 Conventions and formalism

Here, we briefly review the spin liquid classification scheme proposed in Ref. 184; for a complete discussion the reader is referred to the original paper. In keeping with these conventions, we express the mean field Hamiltonian of Eq. (6.19) in terms of fermions $\psi =$

$(\psi_1, \psi_2)^T = \left(f_\uparrow, f_\downarrow^\dagger\right)^T$. The mean field ansatz is written in terms of the matrix

$$u_{\boldsymbol{ij}} = \frac{3}{8} J \begin{pmatrix} \alpha_{\boldsymbol{ij}}^\dagger & \beta_{\boldsymbol{ij}} \\ \beta_{\boldsymbol{ij}} & -\alpha_{\boldsymbol{ij}} \end{pmatrix} = u_{\boldsymbol{ji}}^\dagger. \tag{E.3}$$

The average constraint in Eq. (6.18) become s

$$\left\langle \psi_{\boldsymbol{i}}^\dagger \tau^\ell \psi_{\boldsymbol{i}} \right\rangle = 0 \tag{E.4}$$

where τ^ℓ are Pauli matrices (with $\tau^0 = \mathbb{1}$) and the mean field Hamiltonian can then be written

$$H_{\text{MF}} = \sum_{\langle ij \rangle} \left[\frac{4}{3J_{\boldsymbol{ij}}} \text{tr}\left(u_{\boldsymbol{ij}}^\dagger u_{\boldsymbol{ij}}\right) - \left(\psi_{\boldsymbol{i}}^\dagger u_{\boldsymbol{ij}} \psi_{\boldsymbol{j}} + h.c.\right) \right] + \sum_{\boldsymbol{i}} a_0^\ell \psi_{\boldsymbol{i}}^\dagger \tau^\ell \psi_{\boldsymbol{i}}. \tag{E.5}$$

Here, $u_{\boldsymbol{ij}}$ is the analogue to $\alpha_{\boldsymbol{ij}}, \beta_{\boldsymbol{ij}}^a$ (when $\gamma_{\boldsymbol{ij}} \neq 0$ the spin symmetry is realized projectively, a possibility this formalism does not take into account [24]). a_0^ℓ are Lagrange multipliers enforcing the constraint in Eq. (E.4). In order for H_{MF} to preserve spin, we must choose $iu_{\boldsymbol{ij}} \in \text{SU}(2)$. Finally, the SU(2) gauge symmetry acts on the ψ fermions and ansatz as

$$\psi_{\boldsymbol{i}} \to W(\boldsymbol{i}) \psi_{\boldsymbol{i}}, \qquad\qquad u_{\boldsymbol{ij}} \to W(\boldsymbol{i}) u_{\boldsymbol{ij}} W^\dagger(\boldsymbol{j}). \tag{E.6}$$

The projective symmetry group in this context is expressed as the invariance of the ansatz $u_{\boldsymbol{ij}}$ under the joint action of a symmetry transformation G and a gauge transformation W_G: Eq.

$$W_G G\left[u_{\boldsymbol{ij}}\right] = u_{\boldsymbol{ij}} \tag{E.7}$$

where

$$G[u_{\boldsymbol{ij}}] = u_{G(\boldsymbol{i}),G(\boldsymbol{j})} \qquad W_G\left[u_{\boldsymbol{ij}}\right] = W_G(\boldsymbol{i}) u_{\boldsymbol{ij}} W_G^\dagger(\boldsymbol{j}), \qquad W_G(\boldsymbol{i}) \in \text{SU}(2). \tag{E.8}$$

Here, we have assumed that G is a space group operation; for time reversal, we have $\mathcal{T}[u_{\boldsymbol{ij}}] = -u_{\boldsymbol{ij}}$. The invariant gauge group (IGG) is the set of gauge transformations which do not alter the ansatz,

$$\mathfrak{W} = \{W(\boldsymbol{i}) \,|\, W(\boldsymbol{i}) u_{\boldsymbol{ij}} W(\boldsymbol{j})^\dagger, W(\boldsymbol{i}) \in \mathrm{SU}(2)\}, \tag{E.9}$$

and, therefore, $\mathfrak{W}$ can either be SU(2), U(1), or $\mathbb{Z}_2$. In the main body of the text, this is what we simply refer to as the gauge group or, sometimes in a Higgs phase, the "residual gauge group."

In order to make use of the symmetry fractionalization technique, we translate the commutation relations in Eq. (6.11) and below to the lattice case:

$$\begin{aligned}
&1. && W_{ty}^{-1}(i_x, i_y+1) W_{tx}(i_x, i_y+1) W_{ty}(i_x-1, i_y+1) W_{tx}^{-1}(i_x, i_y) \in \mathfrak{W} \\
&2. && W_{py}^{-1}(i_x, -i_y) W_{tx}(i_x, -i_y) W_{py}(i_x-1, -i_y) W_{tx}^{-1}(i_x, i_y) \in \mathfrak{W} \\
&3. && W_{py}^{-1}(i_x, -i_y) W_{ty}(i_x, -i_y) W_{py}(i_x, -i_y-1) W_{ty}(i_x, i_y+1) \in \mathfrak{W} \\
&4. && W_{py}(i_x, i_y) W_{py}(i_x, -i_y) \in \mathfrak{W} \\
&5. && W_{py}^{-1}(i_x, -i_y) W_r(i_x, -i_y) W_{py}(-i_y, -i_x) W_r(-i_y, i_x) \in \mathfrak{W} \\
&6. && W_r(i_x, i_y) W_r(i_y, -i_x) W_r(-i_x, i_y) W_r(-i_y, i_x) \in \mathfrak{W} \\
&7. && W_r^{-1}(-i_y, i_x) W_{tx}(-i_y, i_x) W_r(-i_y-1, i_x) W_{ty}(i_x, i_y+1) \in \mathfrak{W} \\
&8. && W_r^{-1}(-i_y, i_x) W_{ty}(-i_y, i_x) W_r(-i_y, i_x-1) W_{tx}^{-1}(i_x, i_y) \in \mathfrak{W} \\
&9. && W_t^{-1}(i_x, i_y) W_r^{-1}(-i_y, i_x) W_t(-i_y, i_x) W_r(-i_y, i_x) \in \mathfrak{W} \\
&10. && W_t^{-1}(i_x, i_y) W_{py}^{-1}(i_x, -i_y) W_t(i_x, -i_y) W_{py}(i_x, -i_y) \in \mathfrak{W} \\
&11. && W_t^{-1}(i_x, i_y) W_{tx}^{-1}(i_x+1, i_y) W_t(i_x+1, i_y) W_{tx}(i_x+1, i_y) \in \mathfrak{W} \\
&12. && W_t^{-1}(i_x, i_y) W_{ty}^{-1}(i_x, i_y+1) W_t(i_x, i_y+1) W_{ty}(i_x, i_y+1) \in \mathfrak{W} \\
&13. && W_t(i_x, i_y) W_t(i_x, i_y) \in \mathfrak{W}
\end{aligned} \tag{E.10}$$

	Group relations	Gapped (D_f)	Gapless
1	$T_y^{-1}T_xT_yT_x^{-1}$	$-e^{-2i(\theta_{tx}-\theta_{ty})\sigma^z}$	$-\mathbb{1}$
2	$P_y^{-1}T_xP_yT_x^{-1}$	$e^{2i\theta_{py}\sigma^z}$	$-e^{2i\theta_{tx}\sigma^z}$
3	$P_y^{-1}T_yP_yT_y$	$e^{2i\theta_{py}\sigma^z}$	$-\mathbb{1}$
4	P_y^2	$e^{-2i\theta_{py}\sigma^z}$	$-\mathbb{1}$
5	$P_y^{-1}R_{\pi/2}P_yR_{\pi/2}$	$e^{-2i\theta_r\sigma^z}$	$\mathbb{1}$
6	$R_{\pi/2}^4$	$e^{-4i\theta_r\sigma^z}$	$e^{-4i\theta_r\sigma^z}$
7	$R_{\pi/2}^{-1}T_xR_{\pi/2}T_y$	$e^{2i\theta_r\sigma^z+i(\theta_{tx}-\theta_{ty})\sigma^z}$	$-e^{-i(\theta_{tx}+\theta_{ty})\sigma^z}$
8	$R_{\pi/2}^{-1}T_yR_{\pi/2}T_x^{-1}$	$e^{2i\theta_r\sigma^z-i(\theta_{tx}-\theta_{ty})\sigma^z}$	$e^{i(\theta_{tx}-\theta_{ty})\sigma^z}$
9	$R_{\pi/2}^{-1}\mathcal{T}^{-1}R_{\pi/2}\mathcal{T}$	$e^{2i\theta_r\sigma^z}$	$\mathbb{1}$
10	$P_y^{-1}\mathcal{T}^{-1}P_y\mathcal{T}$	$e^{2i\theta_{py}\sigma^z}$	$e^{2i\theta_t\sigma^z}$
11	$T_x^{-1}\mathcal{T}^{-1}T_x\mathcal{T}$	$-e^{2i(\theta_t+\theta_{tx})\sigma^z}$	$-\mathbb{1}$
12	$T_y^{-1}\mathcal{T}^{-1}T_y\mathcal{T}$	$-e^{2i(\theta_t+\theta_{ty})\sigma^z}$	$-\mathbb{1}$
13	$\mathcal{T}^2$	$-\mathbb{1}$	$e^{2i\theta_t\sigma^z}$

Table E.1: Symmetry fractionalization of U(1) spin liquids.

E.2.2 SU(2) spin liquid classification

We presented the mean field ansatz of the π-flux phase in Sec. 6.2.2. In Wen's notation, it corresponds to the spin liquid SU2Bn0, and consequently has the following PSG:

$$W_{tx}(\boldsymbol{i}) = (-)^{i_y} g_{tx}, \qquad W_{px}(\boldsymbol{i}) = (-)^{i_x} g_{px}, \qquad W_{pxy}(\boldsymbol{i}) = (-)^{i_x i_y} g_{pxy},$$
$$W_{ty}(\boldsymbol{i}) = g_{py}, \qquad W_{py}(\boldsymbol{i}) = (-)^{i_y} g_{py}, \qquad W_t(\boldsymbol{i}) = (-)^{i_x+i_y} g_t, \tag{E.11}$$

where $g_\xi \in \mathrm{SU}(2)$, $\xi = tx, ty, px, py, pxy, t$. All PSG's proximate to SU2Bn0 can be obtained by fixing the values of the g_ξ to a specific element in SU(2) (the PSG's are only defined modulo the IGG). In Appendix B of Ref. 184, Wen enumerates which U(1) and $\mathbb{Z}_2$ PSG's are proximate to SU2Bn0. All of the phases we consider must be identified with one of these options.

E.2.3 U(1) spin liquid classification

Wen [184] finds that the following U(1) phases are proximate to SU2Bn0:

U1B000n	U1Bn10n	U1Cn0nn	U1C11nn
U1B0001	U1Bx10x	U1Cn0n1	U1C11nx
U1B001n	U1Bx11n	U1Cn0x1	U1C11xn
U1B0011	U1Bx11x	U1Cn01n	U1C11xx

In this section we determine which of these lattice PSG's corresponds to the gapped and gapless U(1) spin liquids obtained by condensing Φ and Φ_1 respectively.

Gapped U(1) spin liquid (D_f)

To compare with Wen's classification, we condense the Higgs' fields in the z component. Therefore, for the gapped U(1) spin liquid D_f, only $\langle \Phi^z \rangle \neq 0$ and the PSG in Eq. (6.40) should be rewritten:

$$\begin{aligned} V_{tx} &= e^{i\theta_{tx}\sigma^z} i\sigma^x, & V_{px} &= e^{i\theta_{py}\sigma^z}, & V_r &= e^{i\theta_r\sigma^z}, \\ V_{ty} &= e^{i\theta_{ty}\sigma^z} i\sigma^x, & V_{py} &= e^{i\theta_{py}\sigma^z}, & V_t &= e^{i\theta_t\sigma^z} i\sigma^x, \end{aligned} \tag{E.12}$$

The resulting symmetry fractionalization is shown in Table E.1.

We identify this phase in several steps. We note that independent from θ_t, $(W_t U_t)^2 = -\mathbb{1}$, and therefore, of the spin liquids proximate to SU2Bn0, only those with $W_t(\boldsymbol{i}) \not\propto \tau^0$ are possible candidates. Moreover, the U1B spin liquids all have $W_{tx} = (-)^{i_y} g_3(\theta_{tx})$, $W_{ty}(\boldsymbol{i}) = g_3(\theta_{ty})$ where $g_\ell(\theta) = e^{i\theta\tau^\ell}$. Inserting these into group relation #1 in Eq. (E.10) returns $-\mathbb{1}$, again independent of the angles θ_{tx} and θ_{ty}, invalidating these options. This leaves four candidates: U1Cn0n1, U1Cn0x1, U1C11nx, and U1C11xx. We have computed the symmetry fractionalization of each of these phases and determined that D_f corresponds to

U1C$n0n1$ whose lattice PSG is

$$\begin{aligned}
&\text{U1C}n0n1: \\
&W_{tx}(\boldsymbol{i}) = (-)^{i_y} g_3(\theta_{tx}) i\tau^1, && W_{ty}(\boldsymbol{i}) = g_3(\theta_{ty}) i\tau^1, \\
&W_{px}(\boldsymbol{i}) = (-)^{i_x} g_3(\theta_{px}), && W_{py}(\boldsymbol{i}) = (-)^{i_y} g_3(\theta_{py}), \\
&W_{pxy}(\boldsymbol{i}) = (-)^{i_x i_y} g_3\left(\theta_{pxy}\right), && W_r(\boldsymbol{i}) = (-)^{i_x i_y + i_x} g_3\left(\theta_r\right) \\
&W_t(\boldsymbol{i}) = (-)^{i_x + i_y} g_3(\theta_t) i\tau^1. &&
\end{aligned} \tag{E.13}$$

Gapless U(1) spin liquid

The (continuum) PSG of the gapless spin liquid with $\langle \Phi_1^z \rangle \neq 0$ is

$$\begin{aligned}
&V_{tx} = e^{i\theta_{tx}\sigma^z}, && V_{px} = e^{i\theta_{py}\sigma^z}, && V_r = e^{i\theta_r\sigma^z}, \\
&V_{ty} = e^{i\theta_{ty}\sigma^z} i\sigma^x, && V_{py} = e^{i\theta_{py}\sigma^z} i\sigma^x, && V_t = e^{i\theta_t\sigma^z}.
\end{aligned} \tag{E.14}$$

From the symmetry fractionalization in Table E.1 and the arguments in the previous section, we conclude that only U1B spin liquids with $W_t \propto \tau^0$ are possible candidates: U1B000n, U1Bn10n, U1B001n, U1Bx11n. Computing the symmetry fractionalization of these four spin liquid identifies U1Bx11n as the correct lattice analogue:

$$\begin{aligned}
&\text{U1B}x11n: \\
&W_{tx}(\boldsymbol{i}) = (-)^{i_y} g_3(\theta_{tx}) \tau^0, && W_{ty}(\boldsymbol{i}) = g_3(\theta_{ty}) \tau^0, \\
&W_{px}(\boldsymbol{i}) = (-)^{i_x} g_3(\theta_{px}) i\tau^1, && W_{py}(\boldsymbol{i}) = (-)^{i_y} g_3(\theta_{py}) i\tau^1, \\
&W_{pxy}(\boldsymbol{i}) = (-)^{i_x i_y} g_3(\theta_{pxy}) i\tau^1, && W_r(\boldsymbol{i}) = (-)^{i_x i_y + i_x} g_3\left(\theta_r\right) \\
&W_t(\boldsymbol{i}) = (-)^{i_x + i_y} g_3(\theta_t) \tau^0. &&
\end{aligned} \tag{E.15}$$

In Appendix E.3.3 we show that this PSG has no lattice realization.

E.2.4 $\mathbb{Z}_2$ SPIN LIQUIDS

Wen divides the $\mathbb{Z}_2$ spin liquids into two classes. Their PSG's are

$$\begin{aligned} W_{tx}(\boldsymbol{i}) &= \tilde{\eta}^{i_y}\tau^0, & W_{px}(\boldsymbol{i}) &= \eta_{xpx}^{i_x}\eta_{xpy}^{i_y}g_{py}, & W_{pxy}(\boldsymbol{i}) &= (-)^{i_x i_y}g_{pxy}, \\ W_{ty}(\boldsymbol{i}) &= \tau^0, & W_{py}(\boldsymbol{i}) &= \eta_{xpy}^{i_x}\eta_{xpx}^{i_y}g_{py}, & W_t(\boldsymbol{i}) &= \eta_t^{i_x+i_y}g_t, \end{aligned} \tag{E.16}$$

where A spin liquids have $\tilde{\eta} = +1$ and B spin liquids have $\tilde{\eta} = -1$. Unlike for the SU(2) case, each of the group elements g_ξ takes only a single value. He labels these spin liquids by Z2A $(g_{px})_{\eta_{xpx}}(g_{py})_{\eta_{xpy}}g_{pxy}(g_t)_{\eta_t}$ and Z2B $(g_{px})_{\eta_{xpx}}(g_{py})_{\eta_{xpy}}g_{pxy}(g_t)_{\eta_t}$. An equivalent shorthand notation replaces $(\tau^0,\tau^1,\tau^2,\tau^3)$ and $(\tau_+^0,\tau_+^1,\tau_+^2,\tau_+^3)$ by $(0,1,2,3)$ and $(\tau_-^0,\tau_-^1,\tau_-^2,\tau_-^3)$ by (n,x,y,z) (this is the notation used in the majority of the paper). There are 272 distinct such PSG's; however, though at least 72 of these are anomalous and cannot be described with a mean field Hamiltonian on the lattice.

We can determine the symmetry fractionalization of each of these PSG's using Eq. (E.10), forming a table similar to Table 6.7, and this information is what leads to the identification in Table 6.8. It is clear that the symmetry fractionalization does not completely determine the PSG since both *s*PSG1 and *s*PSG5 have the same symmetry fractionalization as two different spin liquids. We will show that in both cases, a single lattice PSG can be associated with each of our continuum versions.

Our primary strategy will be to check that which PSG's in Table 6.8 are proximate to U1Cn0n1. By studying Table E.1, we determine which values of θ_ξ give the $\mathbb{Z}_2$ symmetry fractionalization of the phases we're interested in. In both cases we find only a single possibility. We also verify that *s*PSG5 is proximate to U1Bx11n.

We note that the symmetry transformations in Table E.1 depend on only five generators: $T_x, T_y, P_y, R_{\pi/2}, \mathcal{T}$. To make contact with Wen's conventions, we also display the gauge transformations corresponding to $P_x = R_{\pi/2}P_yR_{\pi/2}^{-1}$ and $P_{xy} = R_{\pi/2}P_y^{-1}$; their forms are also determined by the angles $\theta_{tx}, \theta_{ty}, \theta_{py}, \theta_r$, and θ_t.

Lattice PSG of A_f phase (sPSG5)

We begin by determining which choice of angles of the gapped U(1) spin liquid returns the symmetry fractionalization of sPSG5. Setting $\theta_{tx} = 0$ fixes the remaining angles to be

$$\theta_{ty} = \pi, \qquad \theta_{py} = \pm\frac{\pi}{2}, \qquad \theta_r = 0, \pi, \qquad \theta_t = 0, \pi. \tag{E.17}$$

The choices only result in gauge transformations differing by a minus sign and, except for W_{ty}, do not affect the symmetry fractionalization. In what follows we choose positive prefactors for all of the gauge transformations below. Modulo these considerations, this is the *only* PSG proximate to U1Cn0n1 with the same symmetry fractionalization as sPSG1. This gives

$$\begin{aligned} W_{tx} &= (-)^{i_y} i\tau^1, & W_{ty} &= -i\tau^1, \\ W_{px} &= (-)^{i_x} i\tau^3, & W_{py} &= (-)^{i_y} i\tau^3, \\ W_{pxy} &= (-)^{i_x i_y} i\tau^3, & W_r &= (-)^{i_x i_y + i_x} \tau^0, \\ W_t &= (-)^{i_x + i_y} i\tau^1. \end{aligned} \tag{E.18}$$

We can bring it into the form of Eq. (E.16) by performing the gauge transformation

$$W(\boldsymbol{i}) = \begin{cases} (-)^{(i_x+i_y)/2} i\tau^2, & i_x + i_y = even, \\ (-)^{(i_x+i_y-1)/2} i\tau^3 & i_x + i_y = odd. \end{cases} \tag{E.19}$$

Under this transformation, the PSG in Eq. (E.18) becomes

$$\begin{aligned} W_{tx} &= (-)^{i_y} \tau^0, & W_{ty} &= -\tau^0, \\ W_{px} &= (-)^{i_x + i_y} i\tau^3, & W_{py} &= (-)^{i_x + i_y} i\tau^3, \\ W_{pxy} &= (-)^{i_x(i_y+1)} i\tau^3, & W_r &= (-)^{i_x(i_y+1)} \tau^0, \\ W_t &= (-)^{i_x + i_y} i\tau^1. \end{aligned} \tag{E.20}$$

Upon shifting $i_y \to i_y + 1$, we recognize this PSG as Z2B$zz3x$, and, rotating by 90^0 about the y-axis this becomes Z2B$xx1z$. This identifies Z2B$xx1z$ as the unique lattice PSG capable of describing the phase A_f.

Another way we could have reached this conclusion is by studying the mean field ansatz allowed by either of these PSG's. It turns out that the mean field Hamiltonian corresponding to the other candidate PSG, Z2B$xx2z$, cannot be gapped, whereas no such restrictions exist for Z2B$xx1z$.

We also show that Z2B$xx1z$ is proximate to the gapless spin liquid U1B$x11n$. In order to reproduce the symmetry fractionalization of sPSG5, the angles in Eq. (E.15) must be

$$\theta_{tx} = \pm\frac{\pi}{2} \qquad \theta_{ty} = \mp\frac{\pi}{2}, \qquad \theta_r = 0, \pi, \qquad \theta_t = \pm\frac{\pi}{2}. \tag{E.21}$$

θ_{py} is un-determined, and therefore, unlike in the previous case, proximity to U1B$x11n$ does not fully determine the lattice PSG corresponding to sPSG5. The angles which are restricted indicate that

$$\begin{aligned} W_{tx} &= (-)^{i_y} i\tau^3, & W_{ty} &= -i\tau^3, \\ W_r &= (-)^{i_x(i_y+1)}\tau^0, & W_t &= (-)^{i_x+i_y} i\tau^3. \end{aligned} \tag{E.22}$$

Rotating by 90^0 about the y-axis take $\tau^3 \to \tau^1$. We then observe that all of the gauge transformations shown above are equal to the corresponding gauge transformation in Eq. (E.18). It can be shown that θ_{py} can be chosen to obtain Z2B$xx1z$ but not Z2B$xx2z$. Therefore, only Z2B$xx1z$ is proximate to U1B$x11n$. .

sPSG1

Performing the same analysis as above, we find that the only way for the symmetry fractionalization of U1C$n0n1$ to return the symmetry fractionalization of sPSG1 is if the angles

in Eq. (E.13) are

$$\theta_{ty} = \pi, \qquad \theta_{py} = \pm\frac{\pi}{2}, \qquad \theta_r = 0, \pi, \qquad \theta_t = \pm\frac{\pi}{2}, \tag{E.23}$$

where, again, we've set $\theta_{tx} = 0$. The gauge transformations associated with the symmetry generators are then

$$\begin{aligned} W_{tx} &= (-)^{i_y} i\tau^1, & W_{ty} &= -i\tau^1, \\ W_{px} &= (-)^{i_x} i\tau^3, & W_{py} &= (-)^{i_y} i\tau^3, \\ W_{pxy} &= (-)^{i_x i_y} i\tau^3, & W_r &= (-)^{i_x(i_y+1)}\tau^0, \\ W_t &= (-)^{i_x+i_y} i\tau^2. \end{aligned} \tag{E.24}$$

Performing the gauge transformation in Eq. (E.19), these become,

$$\begin{aligned} W_{tx} &= (-)^{i_y}\tau^0, & W_{ty} &= -\tau^0, \\ W_{px} &= i(-)^{i_x+i_y} i\tau^3, & W_{py} &= i(-)^{i_x+i_y} i\tau^3, \\ W_{pxy} &= (-)^{i_x(i_y+1)} i\tau^3, & W_r &= (-)^{i_x(i_y+1)}\tau^0, \\ W_t &= i\tau^2. \end{aligned} \tag{E.25}$$

It is not difficult to see that this corresponds to Z2Bzz32, which is equivalent to Z2Bxx13.

E.3 Lattice realizations of spin liquids

In this appendix, we use the lattice PSG's determined in Appendix E.2 for the π-flux phase and A_f, B_f, and D_f to write down the corresponding lattice Hamiltonian. Doing so will serve as further verification of the symmetry fractionalization used in the main text. Further, the calculation of the Berry phase in Sec. 6.4.3 requires the lattice description of the gapped U(1) spin liquid corresponding to U1Cn0n1.

E.3.1 SUBn0 MEAN FIELD HAMILTONIAN

The ansatz for the π-flux state is given in Eq. (E.11). Gauge invariance and the form of the translational symmetry operations compels the mean field parameters to take the following form:

$$u_{\boldsymbol{i},\boldsymbol{i}+\boldsymbol{m}} = (-)^{i_x m_y} i u^0_{\boldsymbol{m}}. \tag{E.26}$$

In order for the mean field Hamiltonian to be Hermition, $u^\dagger_{\boldsymbol{ij}}$ must equal $u_{\boldsymbol{ji}}$. This can be used to show that

$$(-)^{i_x m_y} i u^0_{\boldsymbol{m}} = -(-)^{i_x m_y}(-)^{m_x m_y} i u^0_{\boldsymbol{m}}, \tag{E.27}$$

which indicates

$$u^0_{-\boldsymbol{m}} = -(-)^{m_x m_y} u^0_{\boldsymbol{m}}. \tag{E.28}$$

Next, Eq. (E.7) states that $u_{\boldsymbol{ij}}$ must be invariant under the action of all (projective) symmetry operations. In particular, acting $P_x P_y$ and using Eq. (E.28), we find

$$u_{\boldsymbol{i},\boldsymbol{i}+\boldsymbol{m}} = W_{px} P_x W_{py} P_y [u_{\boldsymbol{i},\boldsymbol{i}+\boldsymbol{m}}] = -(-)^{i_x m_y}(-)^{m_x m_y}(-)^{m_x+m_y} i u^0_{\boldsymbol{m}} \tau^0. \tag{E.29}$$

Similarly, the action of time reversal requires

$$u_{\boldsymbol{i},\boldsymbol{i}+\boldsymbol{m}} = W_t \mathcal{T}[u_{\boldsymbol{i},\boldsymbol{i}+\boldsymbol{m}}] = (-)^{i_x m_y}(-)^{m_x+m_y} i u^0_{\boldsymbol{m}} \tau^0. \tag{E.30}$$

Between these two equations, we conclude that $u^0_{\boldsymbol{m}} \neq 0$ only when $m_x + m_y = odd$. Finally, we relate mean field parameters for different $\boldsymbol{m}$'s through the action of P_x, P_y, and P_{xy}:

$$u^0_{(-m_x,m_y)} = (-)^{m_x} u^0_{(m_x,m_y)}, \quad u^0_{(m_x,-m_y)} = (-)^{m_y} u^0_{(m_x,m_y)}, \quad u^0_{(m_y,m_x)} = (-)^{m_x m_y} u^0_{(m_x,m_y)}. \tag{E.31}$$

The mean field ansatz we obtain is

$$u_{\boldsymbol{i},\boldsymbol{i}+\hat{\boldsymbol{x}}} = i\alpha\tau^0, \qquad u_{\boldsymbol{i},\boldsymbol{i}+\hat{\boldsymbol{y}}} = (-)^{i_x} i\alpha\tau^0. \tag{E.32}$$

Inserting these hopping terms into Eq. (E.5) (and dropping the constant) we obtain

$$H'_\pi = -i\alpha \sum_{\boldsymbol{i}} \left(\psi^\dagger_{\boldsymbol{i}} \psi_{\boldsymbol{i}+\hat{\boldsymbol{x}}} + (-)^{i_x} \psi^\dagger_{\boldsymbol{i}} \psi_{\boldsymbol{i}+\hat{\boldsymbol{y}}} + h.c. \right). \tag{E.33}$$

We now show that the low-energy theory is precisely the Dirac Hamiltonian. In momentum space, we find

$$H'_\pi = 2\alpha \int_{-\pi/2}^{\pi/2} \frac{dk_x}{2\pi} \int_{-\pi/2}^{\pi/2} \frac{dk_y}{2\pi} \, \Psi^\dagger_{\boldsymbol{k}} \left(\sin k_x \tilde{\tau}^3 \mu^3 \tau^0 + \sin k_y \tilde{\tau}^1 \mu^3 \tau^0 \right) \Psi_{\boldsymbol{k}} \tag{E.34}$$

where $\Psi_{\boldsymbol{k}} = \left(\psi_{\boldsymbol{k}}, \psi_{\boldsymbol{k}+\boldsymbol{Q}_x+\boldsymbol{Q}_y}, \psi_{\boldsymbol{k}+\boldsymbol{Q}_x}, \psi_{\boldsymbol{k}+\boldsymbol{Q}_y} \right)^T$ with $\boldsymbol{Q}_x = (\pi, 0)$ and $\boldsymbol{Q}_y = (0, \pi)$, and

$$\tilde{\tau}^3\mu^3 = \begin{pmatrix} 1 & 0 & 0 & 0 \\ 0 & -1 & 0 & 0 \\ 0 & 0 & -1 & 0 \\ 0 & 0 & 0 & 1 \end{pmatrix}, \quad \tilde{\tau}^1\mu^3 = \begin{pmatrix} 0 & 0 & 1 & 0 \\ 0 & 0 & 0 & -1 \\ 1 & 0 & 0 & 0 \\ 0 & -1 & 0 & 0 \end{pmatrix}, \quad \tilde{\tau}^0\mu^1 = \begin{pmatrix} 0 & 1 & 0 & 0 \\ 1 & 0 & 0 & 0 \\ 0 & 0 & 0 & 1 \\ 0 & 0 & 1 & 0 \end{pmatrix}. \tag{E.35}$$

Equivalently, writing $\Psi_{\boldsymbol{k}} = (\psi_{1,1,\boldsymbol{k}}, \psi_{1,2,\boldsymbol{k}}, \psi_{2,1,\boldsymbol{k}}, \psi_{2,2,\boldsymbol{k}})^T$, we can identify the $\tilde{\tau}^\ell$'s with Pauli matrices acting on the first index of $\Psi_{\boldsymbol{k}}$ and the μ^ℓ's with Pauli matrices acting on the second. Finally, to make contact with the expression in Sec. 6.2.2, we express H'_π in terms of

$$\tilde{\Psi}_{\boldsymbol{k}} = e^{i\pi\tilde{\tau}^2\mu^3/4} \Psi_{\boldsymbol{k}}. \tag{E.36}$$

The resulting mean field Hamiltonian is

$$\begin{aligned} H'_\pi &= -2\alpha \int_{-\pi/2}^{\pi/2} \frac{dk_x}{2\pi} \int_{-\pi/2}^{\pi/2} \frac{dk_y}{2\pi} \, \tilde{\Psi}^\dagger_{\boldsymbol{k}} \left(\sin k_x \tau^1 \mu^0 \sigma^0 - \sin k_y \tau^3 \mu^0 \sigma^0 \right) \\ &\cong 2\alpha \int \frac{d^2k}{(2\pi)^2} \, \tilde{\Psi}^\dagger \left(k_x \gamma^0 \gamma^x + k_y \gamma^0 \gamma^y \right) \tilde{\Psi}_{\boldsymbol{k}} \end{aligned} \tag{E.37}$$

where we've rewritten the gauge-charged τ^ℓ's as σ^ℓ's (as done in the main body of the text) and used the fact that $\gamma^\mu = (\tilde{\tau}^y, i\tilde{\tau}^z, i\tilde{\tau}^x)$. It is clear that once dynamic gauge fields are included, this is equivalent to $\mathcal{L}_{\mathrm{QCD}_3}$ in Eq. (6.28).

E.3.2 U1Cn0n1 mean field Hamiltonian

We now use the ansatz for Eq. (E.13) to determine the lattice Hamiltonian corresponding to the gapped spin liquid phase D_f. We show that it is precisely H'_π plus a term which breaks the SU(2) symmetry to U(1): $H_{D_f} = H'_\pi + H_1$.

Eq. (E.13) indicates that all bonds must be of the form

$$u_{\boldsymbol{i},\boldsymbol{i}+\boldsymbol{m}} = (-)^{i_x m_y}\left(iu^0_{\boldsymbol{m}}\tau^0 + (-)^{i_x+i_y}u^3_{\boldsymbol{m}}\tau^3\right). \tag{E.38}$$

Further, hermiticity of the Hamiltonian requires $u^\dagger_{\boldsymbol{ij}} = u_{\boldsymbol{ji}}$ and therefore

$$(-)^{i_x m_y}\left(-iu^0_{\boldsymbol{m}}\tau^0 + (-)^{i_x+i_y}u^3_{\boldsymbol{m}}\tau^3\right) = (-)^{i_x m_y}(-)^{m_x m_y}\left(iu^0_{-\boldsymbol{m}}\tau^0 + (-)^{i_x+i_y}(-)^{m_x+m_y}u^3_{-\boldsymbol{m}}\tau^3\right), \tag{E.39}$$

implying that

$$u^0_{\boldsymbol{m}} = -(-)^{m_x m_y}u^0_{-\boldsymbol{m}}, \qquad u^3_{\boldsymbol{m}} = (-1)^{m_x+m_y}(-)^{m_x m_y}u^3_{-\boldsymbol{m}}. \tag{E.40}$$

Similarly, to satisfy Eq. (E.7), $u_{\boldsymbol{ij}}$ must be invariant under 180^0 rotations:

$$u_{\boldsymbol{i},\boldsymbol{i}+\boldsymbol{m}} = W_{px}P_xW_{py}P_y[u_{\boldsymbol{i},\boldsymbol{i}+\boldsymbol{m}}] = (-)^{i_x m_y}(-)^{m_x m_y}\Big[-(-)^{m_x+m_y}iu^0_{\boldsymbol{m}}\tau^0 + (-)^{i_x+i_y}u^3_{\boldsymbol{m}}\tau^3\Big], \tag{E.41}$$

where we've used the previous expression to relate $u^\ell_{\boldsymbol{m}}$ and $u^\ell_{-\boldsymbol{m}}$. It follows that $u^0_{\boldsymbol{m}} = 0$ when $(m_x, m_y) = (even, even)$ and that $u^3_{\boldsymbol{m}} = 0$ when $(m_x, m_y) = (odd, odd)$. The ansatz must also be invariant under $\mathcal{T}$:

$$u_{\boldsymbol{i},\boldsymbol{i}+\boldsymbol{m}} = W_t\mathcal{T}[u_{\boldsymbol{i},\boldsymbol{i}+\boldsymbol{m}}] = (-)^{i_x m_y}(-)^{m_x+m_y}\left(-iu^0_{\boldsymbol{m}}\tau^0 + (-)^{i_x+i_y}u^3_{\boldsymbol{m}}\tau^3\right), \tag{E.42}$$

showing that $u^0_{\boldsymbol{m}}$ is non-zero only for $m_x + m_y = odd$ and that $u^3_{\boldsymbol{m}}$ is only non-zero when $m_x + m_y = even$. Together, these give

$$u_{\boldsymbol{i},\boldsymbol{i}+\boldsymbol{m}} = \begin{cases} (-)^{i_x+i_y} u^3_{\boldsymbol{m}}, & (m_x, m_y) = (even, even), \\ (-)^{i_x m_y} i u^0_{\boldsymbol{m}} \tau^0, & m_x + m_y = odd. \end{cases} \tag{E.43}$$

We can also show that the action of P_x, P_y, and P_{xy} implies the following relations:

$$u^\ell_{(m_x,my)} = (-)^{m_x} u^\ell_{(-m_x,m_y)}, \quad u^\ell_{(m_x,my)} = (-)^{m_y} u^\ell_{(m_x,-m_y)}, \quad u^\ell_{(m_x,m_y)} = (-)^{m_x m_y} u^\ell_{(m_y,m_x)}, \tag{E.44}$$

for $\ell = 0, 3$. Using these relations, we find,

$$\begin{aligned} u_{\boldsymbol{i},\boldsymbol{i}+\hat{\boldsymbol{x}}} &= i\alpha\tau^0, & u_{\boldsymbol{i},\boldsymbol{i}+2\hat{\boldsymbol{x}}} &= (-)^{i_x+i_y}\beta\tau^3, & u_{\boldsymbol{i},\boldsymbol{i}} &= (-)^{i_x+i_y} a_0\tau^3, \\ u_{\boldsymbol{i},\boldsymbol{i}+\hat{\boldsymbol{y}}} &= (-)^{i_x} i\alpha\tau^0, & u_{\boldsymbol{i},\boldsymbol{i}+2\hat{\boldsymbol{x}}} &= (-)^{i_x+i_y}\beta\tau^3. \end{aligned} \tag{E.45}$$

As expected, the nearest-neighbour bonds are identical to those we found for the π-flux phase in the previous section. The SU(2) symmetry is already broken to U(1) by the inclusion of the next-nearest neighbour bonds and so this is all we consider.

As in the previous section, the mean field Hamiltonian is obtained by inserting these hopping terms into Eq. (E.5):

$$\begin{aligned} H_{D_f} &= H'_\pi + H_1, \\ H_1 &= \sum_{\boldsymbol{i}} (-)^{i_x+i_y} \left[\beta \left(\psi^\dagger_{\boldsymbol{i}} \tau^3 \psi_{\boldsymbol{i}+2\hat{\boldsymbol{x}}} + \psi^\dagger_{\boldsymbol{i}} \tau^3 \psi_{\boldsymbol{i}+2\hat{\boldsymbol{y}}} + h.c. \right) - a_0^3 \psi^\dagger_{\boldsymbol{i}} \tau^3 \psi_{\boldsymbol{i}} \right], \end{aligned} \tag{E.46}$$

where H'_π is given above in Eq. (E.34). In momentum space, this becomes

$$\begin{aligned} H_{D_f} = \int_{-\pi/2}^{\pi/2} \frac{dk_x}{2\pi} \int_{-\pi/2}^{\pi/2} \frac{dk_y}{2\pi} \Psi^\dagger_{\boldsymbol{k}} \Big[& 2\alpha \left(\sin k_x \tilde{\tau}^3 \mu^3 \tau^0 + \sin k_y \tilde{\tau}^1 \mu^3 \tau^0 \right) \\ & - \left(2\beta \left[\cos 2k_x + \cos 2k_y \right] - a_0 \right) \tilde{\tau}^0 \mu^1 \tau^3 \Big] \Psi_{\boldsymbol{k}} \end{aligned} \tag{E.47}$$

where we've used the same notation as in the previous section: $\Psi_{\boldsymbol{k}} = \left(\psi_{\boldsymbol{k}}, \psi_{\boldsymbol{k}+\boldsymbol{Q}_x+\boldsymbol{Q}_y}, \psi_{\boldsymbol{k}+\boldsymbol{Q}_x}, \psi_{\boldsymbol{k}+\boldsymbol{Q}_y}\right)^T$ with $\boldsymbol{Q}_x = (\pi, 0)$ and $\boldsymbol{Q}_y = (0, \pi)$, and the matrices defined in Eq. (E.35). In terms of $\tilde{\Psi}_{\boldsymbol{k}} = e^{i\pi\tilde{\tau}^2\mu^3/4}\Psi_{\boldsymbol{k}}$:

$$H_{D_f} = \int_{-\pi/2}^{\pi/2} \frac{dk_x}{2\pi} \int_{-\pi/2}^{\pi/2} \frac{dk_y}{2\pi}\, \tilde{\Psi}^\dagger_{\boldsymbol{k}} \Big[2\alpha \left(\sin k_x \tilde{\tau}^1 \mu^0 \sigma^0 - \sin k_y \tilde{\tau}^3 \mu^0 \sigma^0 \right) - \left(2\beta \left[\cos 2k_x + \cos 2k_y \right] - a_0 \right) \tilde{\tau}^2 \mu^2 \sigma^3 \Big] \tilde{\Psi}_{\boldsymbol{k}}, \tag{E.48}$$

where, again, we've rewritten the SU(2) matrices τ^ℓ as σ^ℓ in accord with the continuum notation. Expanding H_{D_f} about $\boldsymbol{k} = (0, 0)$, we obtain

$$H_{D_f} \cong \int \frac{d^2k}{(2\pi)^2}\, \tilde{\Psi}^\dagger \Big[-2\alpha \left(k_x \gamma^0 \gamma^x + k_y \gamma^0 \gamma^y \right) + \left(4\beta - a_0 \right) \gamma^0 \mu^y \sigma^z \Big] \tilde{\Psi}_{\boldsymbol{k}} \tag{E.49}$$

where $\gamma^\mu = (\tilde{\tau}^y, i\tilde{\tau}^z, i\tilde{\tau}^x)$. We conclude that the term which reduces the SU(2) symmetry down to U(1) is precisely equivalent to $\bar{\psi}\mu^y\sigma^z\psi \sim \mathrm{tr}\left(\sigma^z \bar{X} \mu^y X\right)$.

E.3.3 U1Bx11n mean field Hamiltonian

In this subsection, we demonstrate that U1Bx11n has *no* lattice analogue. Referring to Eq. E.15, we see that gauge and translational symmetry requires

$$u_{\boldsymbol{i},\boldsymbol{i}+\boldsymbol{m}} = (-)^{i_x m_y} \left(i u^0_{\boldsymbol{m}} \tau^0 + u^3_{\boldsymbol{m}} \tau^3 \right). \tag{E.50}$$

We relate $u^{0,3}_{-\boldsymbol{m}} = u^{0,3}_{\boldsymbol{m}}$ using the fact that $u^\dagger_{\boldsymbol{i},\boldsymbol{i}+\boldsymbol{m}} = u_{\boldsymbol{i}+\boldsymbol{m},\boldsymbol{i}}$:

$$u^0_{-\boldsymbol{m}} = -(-)^{m_x m_y} u^0_{\boldsymbol{m}}, \qquad\qquad u^3_{-\boldsymbol{m}} = (-)^{m_x m_y} u^1_{\boldsymbol{m}}. \tag{E.51}$$

Then, acting on $u_{\boldsymbol{i},\boldsymbol{i}+\boldsymbol{m}}$ with $P_x P_y$ and $\mathcal{T}$ gives

$$\begin{aligned} W_{px} P_x W_{py} P_y [u_{\boldsymbol{i},\boldsymbol{i}+\boldsymbol{m}}] &= (-)^{i_x m_y} (-)^{m_x m_y} (-)^{m_x + m_y} \left(-i u^0_{\boldsymbol{m}} \tau^0 + u^3_{\boldsymbol{m}} \tau^3 \right), \\ \mathcal{T}[u_{\boldsymbol{i},\boldsymbol{i}+\boldsymbol{m}}] &= (-)^{i_x m_y} (-)^{m_x + m_y} \left(-i u^0_{\boldsymbol{m}} \tau^0 - u^3_{\boldsymbol{m}} \tau^3 \right). \end{aligned} \tag{E.52}$$

Equating these expressions with $u_{\boldsymbol{i},\boldsymbol{i}+\boldsymbol{m}}$ implies that $u^0_{\boldsymbol{m}} \neq 0$ only for $m_x + m_y = odd$, as for SU2Bn0 and U1Cn0n1; it can be shown that they must satisfy identical constraints as the τ^0-bonds allowed by these PSG's. In particular, the nearest-neighbour values are identical to those in Eq. (E.32). Conversely, there are no consistent solutions for $u^3_{\boldsymbol{m}}$: it always vanishes and is therefore unable to break the SU(2) gauge symmetry to U(1).

E.3.4 Z2Bxx1z mean field Hamiltonian

We choose a gauge such that Eq. (E.18) describes the PSG of Z2Bxx1z. Translational symmetry and gauge invariance implies that

$$u_{\boldsymbol{i},\boldsymbol{i}+\boldsymbol{m}} = (-)^{i_x m_y}\left(i u^0_{\boldsymbol{m}}\tau^0 + u^1_{\boldsymbol{m}}\tau^1 + (-)^{i_x+i_y}\left[u^2_{\boldsymbol{m}}\tau^2 + u^3_{\boldsymbol{m}}\tau^3\right]\right). \tag{E.53}$$

Hermiticity then requires

$$u^0_{-\boldsymbol{m}} = -(-)^{m_x m_y} u^0_{\boldsymbol{m}}, \qquad u^1_{-\boldsymbol{m}} = (-)^{m_x m_y} u^1_{\boldsymbol{m}}, \qquad u^{2,3}_{-\boldsymbol{m}} = (-)^{m_x m_y}(-)^{m_x+m_y} u^3_{\boldsymbol{m}}. \tag{E.54}$$

Under the action of $P_x P_y$ and $\mathcal{T}$ the ansatz transforms as

$$\begin{aligned} W_{px}P_x W_{py}P_y[u_{\boldsymbol{i},\boldsymbol{i}+\boldsymbol{m}}] &= (-)^{i_x m_y}(-)^{m_x m_y}\Big(-(-)^{m_x+m_y} i u^0_{\boldsymbol{m}}\tau^0 + (-)^{m_x+m_y} u^2_{\boldsymbol{m}}\tau^1 \\ &\qquad + (-)^{i_x+i_y}\left[u^2_{\boldsymbol{m}}\tau^2 + u^3_{\boldsymbol{m}}\tau^3\right]\Big), \\ \mathcal{T}[u_{\boldsymbol{i},\boldsymbol{i}+\boldsymbol{m}}] &= (-)^{i_x m_y}(-)^{m_x+m_y}\left(-i u^0_{\boldsymbol{m}}\tau^0 - u^1_{\boldsymbol{m}}\tau^1 + (-)^{i_x+i_y}\left[u^2_{\boldsymbol{m}}\tau^2 + u^3_{\boldsymbol{m}}\tau^3\right]\right). \end{aligned} \tag{E.55}$$

These relations imply that $u^1_{\boldsymbol{m}} = 0$ for all $\boldsymbol{m}$, $u^0_{\boldsymbol{m}} \neq 0$ only for $m_x + m_y = 0$, and that $u^{2,3}_{\boldsymbol{m}} \neq 0$ only for $(m_x, m_y) = (even, even)$. By studying the action of P_x, P_y, and P_{xy}, we obtain the

following relations:

$$\begin{aligned}
u^0_{(-m_x,m_y)} &= (-)^{m_x} u^0_{(m_x,m_y)}, \quad & u^2_{(-m_x,m_y)} &= -u^2_{(m_x,m_y)}, \quad & u^3_{(-m_x,m_y)} &= u^3_{(m_x,m_y)}, \\
u^0_{(m_x,-m_y)} &= (-)^{m_y} u^0_{(m_x,m_y)}, \quad & u^2_{(m_x,-m_y)} &= -u^2_{(m_x,m_y)}, \quad & u^3_{(m_x,-m_y)} &= u^3_{(m_x,m_y)}, \\
u^0_{(m_y,m_x)} &= u^0_{(m_x,m_y)}, \quad & u^2_{(m_y,m_x)} &= -u^2_{(m_x,m_y)}, \quad & u^3_{(m_y,m_x)} &= u^3_{(m_x,m_y)}.
\end{aligned} \tag{E.56}$$

These show that $u^{0,3}_{\boldsymbol{m}}$ are restricted to take the same values as in Eq. (E.45) for the gapped U(1) spin liquid, leaving the $u^2_{\boldsymbol{m}}$ bonds to break the U(1) gauge symmetry down to $\mathbb{Z}_2$. It turns out that its first non-zero value occurs at sixth nearest-neighbour:

$$\begin{aligned}
u_{\boldsymbol{i},\boldsymbol{i}+2\hat{\boldsymbol{x}}+4\hat{\boldsymbol{y}}} &= (-)^{i_x+i_y}\gamma\tau^2, \quad & u_{\boldsymbol{i},\boldsymbol{i}+2\hat{\boldsymbol{x}}-4\hat{\boldsymbol{y}}} &= -(-)^{i_x+i_y}\gamma\tau^2, \\
u_{\boldsymbol{i},\boldsymbol{i}+4\hat{\boldsymbol{x}}+2\hat{\boldsymbol{y}}} &= -(-)^{i_x+i_y}\gamma\tau^2, \quad & u_{\boldsymbol{i},\boldsymbol{i}+4\hat{\boldsymbol{x}}-2\hat{\boldsymbol{y}}} &= (-)^{i_x+i_y}\gamma\tau^2.
\end{aligned} \tag{E.57}$$

The contribution of these bonds to the Hamiltonian is

$$H_2 = \gamma \sum_{\boldsymbol{i}} (-)^{i_x+i_y} \left[\psi^\dagger_{\boldsymbol{i}} \tau^2 \psi_{\boldsymbol{i}+2\hat{\boldsymbol{x}}+4\hat{\boldsymbol{y}}} - \psi^\dagger_{\boldsymbol{i}} \tau^2 \psi_{\boldsymbol{i}+2\hat{\boldsymbol{x}}-4\hat{\boldsymbol{y}}} - \psi^\dagger_{\boldsymbol{i}} \tau^2 \psi_{\boldsymbol{i}+4\hat{\boldsymbol{x}}+2\hat{\boldsymbol{y}}} + \psi^\dagger_{\boldsymbol{i}} \tau^2 \psi_{\boldsymbol{i}+4\hat{\boldsymbol{x}}-2\hat{\boldsymbol{y}}} - h.c. \right], \tag{E.58}$$

and the minimal Hamiltonian needed to describe Z2B$xx1z$ is $H_{A_f} = H_{D_f} + H_2$. In momentum space, we have

$$H_2 = 4\gamma \int_{-\pi/2}^{\pi/2} \frac{dk_x}{2\pi} \int_{-\pi/2}^{\pi/2} \frac{dk_y}{2\pi} \left(\sin 4k_x \sin 2k_y - \sin 2k_x \sin 4k_y\right) \Psi^\dagger_{\boldsymbol{k}} \tilde{\tau}^0 \mu^2 \tau^2 \Psi_{\boldsymbol{k}}, \tag{E.59}$$

where $\Psi_{\boldsymbol{k}}$ in defined in Eq. (E.36), and the action of the Pauli matrices $\tilde{\tau}^\ell$ and μ^ℓ is given in Eq. (E.35) and below. Once more, we change notation such that Pauli matrices acting on colour space, τ^ℓ, becomes σ^ℓ's and express H_2 in terms of the transformed fermion operator,

	Group relations	fermionic	vison	twist	bosonic
1	$T_y^{-1}T_xT_yT_x^{-1}$	-1	-1	1	1
2	$P_y^{-1}T_xP_yT_x^{-1}$	-1	-1	1	1
3	$P_y^{-1}T_yP_yT_y$	-1	1	1	-1
4	P_y^2	-1	1	-1	1
5	$T_x^{-1}(\mathcal{T}P_x)^{-1}T_x(\mathcal{T}P_x)$	-1	1	1	-1
6	$T_y^{-1}(\mathcal{T}P_x)^{-1}T_y(\mathcal{T}P_x)$	1	-1	1	-1
7	$P_y^{-1}(\mathcal{T}P_x)^{-1}P_y(\mathcal{T}P_x)$	-1	-1	1	1
8	$(\mathcal{T}P_x)^2$	-1	1	1	-1

Table E.2: Symmetry fractionalization and twist factors for the fermionic and bosonic spinon and the vison in the phase $\mathbb{Z}_2$ spin liquid with current-loop order. By comparing with the result in Ref. 23, are able to verify the equivalent of C_f and C_b.

$\tilde{\Psi}_{\boldsymbol{k}} = e^{i\pi\tilde{\tau}^2\mu^3/4}\Psi_{\boldsymbol{k}}$:

$$\begin{aligned} H_2 &= 4\gamma \int_{-\pi/2}^{\pi/2} \frac{dk_x}{2\pi} \int_{-\pi/2}^{\pi/2} \frac{dk_y}{2\pi} \left(\sin 4k_x \sin 2k_y - \sin 2k_x \sin 4k_y\right) \tilde{\Psi}_{\boldsymbol{k}}^\dagger \tau^y \mu^y \sigma^y \tilde{\Psi}_{\boldsymbol{k}}, \\ &\cong -16\gamma \int \frac{d^2k}{(2\pi)^2} \tilde{\Psi}_{\boldsymbol{k}}^\dagger \Big[k_x k_y \left(k_x^2 - k_y^2\right) \gamma^0 \mu^y \sigma^y\Big] \tilde{\Psi}_{\boldsymbol{k}}. \end{aligned} \tag{E.60}$$

Notably, H_2 does *not* correspond to any of the continuum operators in the action we study in the main text, in particular $\mathrm{tr}\left(\sigma^a \bar{X} \partial_0 X\right) \sim \bar{\psi}\sigma^a\partial_0\psi$. Instead, in the continuum language, H_2 is proportional to $\bar{\psi}\mu^y\sigma^y\partial_x\partial_y\left(\partial_x^2 - \partial_y^2\right)\psi \sim \mathrm{tr}\left(\sigma^y \bar{X}\mu^y\partial_x\partial_y\left[\partial_x^2 - \partial_y^2\right]X\right)$. This is discussed in Sec. 6.4.1.

E.4 Symmetry fractionalization of current-loop ordered spin liquid

We can also use symmetry fractionalization to verify that the phase C_f corresponds to C_b. There are now only eight group relations, and these are listed in Table E.2. The PSG of the reduced symmetry group is defined by the gauge transformations

$$\begin{aligned} V_{tx} &= i\sigma^y, & V_{py} &= i\sigma^x, \\ V_{tx} &= i\sigma^y, & V_{tpx} &= i\sigma^z, \end{aligned} \tag{E.61}$$

	$\mathcal{T}$	P_x	P_y	T_x	T_y
z_α	$i\sigma^y z$	z	z	$i\sigma^y z^*$	$i\sigma^y z^*$
Q_x	Q_x	$-Q_x$	Q_x	Q_x^*	Q_x^*
P	$-P$	P	P	P^*	P^*

Table E.3: Symmetry action on the bosonic spinon and Higgs fields in the bosonic dual to the theories studied here, as presented in Eq. (6.4) and Eq. (6.7) [23]. The spinon here is written as a two-component spinor, $z = (z_\uparrow, z_\downarrow)^T$ and that $i\sigma^y$ acts on these indices. We note that $\mathcal{T}[z^*] = -i\sigma^y z^*$ and that $T_{x,y}[z^*] = i\sigma^y z$.

where the subscript *tpx* denotes the joint group action of $\mathcal{T}P_x$. With these, we determine the fermionic symmetry fractionalization using the methods described in Sec. 6.4.1. The results are shown in Table E.2 under the column labeled "fermionic."

Both the symmetry fractionalization of the vison and the twist factors for the reduced symmetry relations can be worked out from the ones already given; Table E.2 lists these under the columns "vison" and "twist" respectively.

In order to determine the bosonic symmetry fractionalization, we borrow notation from Ref. 23. In Table E.3, the symmetry transformation properties of the bosonic spinon and Higgs fields in Eqs. (6.4) and (6.7) are reproduced. It will be convenient to express the bosonic spinon in terms of the four-component field $\mathcal{Z} = (z, z^*)^T = \left(z_\uparrow, z_\downarrow, z_\uparrow^*, z_\downarrow^*\right)^T$. We then let Pauli matrices τ^ℓ act on this new index, while σ-matrices will act on the spin indices as before. The U(1) gauge transformations are expressed as $\mathrm{U}(1)_g : \mathcal{Z} \to e^{i\theta\tau^z}\mathcal{Z}$. In this language, the symmetry transformations are expressed as

$$\mathcal{T}[\mathcal{Z}] = i\sigma^y\tau^z\mathcal{Z}, \qquad P_{x,y}[\mathcal{Z}] = \mathcal{Z}, \qquad T_{x,y}[\mathcal{Z}] = i\sigma^y\tau^x\mathcal{Z}. \tag{E.62}$$

Using these, we obtain the numbers in the column of Table E.2 labeled "boson."

Finally, we multiply the twist, vison, and boson columns and obtain the numbers in the fermion column, thereby verifying the equivalence of C_f and C_b.

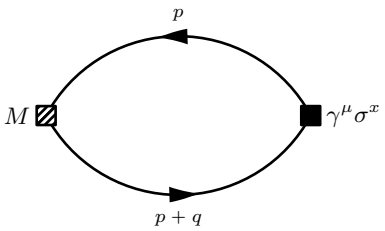

Figure E.1: Fermion bubble to calculate flux response.

E.5 Linear response to nontrivial flux

In this appendix, we calculate the relation in Eq. (6.52) in imaginary time. The residual U(1) gauge field a_μ couples to the current $J^\mu = \bar{\psi}\gamma^\mu\sigma^x\psi$. The response function of an operator O is $\chi^\mu_{\mathrm{O}} = \langle \mathrm{O}(x)J^\mu(x')\rangle$, and the linear response equation in momentum space is simply $\langle \mathrm{O}(q)\rangle = \chi^\mu_{\mathrm{O}}(p)A_\mu(q)$ (we specify to operators whose vacuum expectation values vanish in the absence of perturbations). Assuming $\mathrm{O} = \mathrm{tr}\left(\bar{X}MX\right)$, $\chi^\mu_0(q)$ is represented by the Feynman diagram in Fig. E.1 at leading order. We evaluate this as

$$\chi^\mu_{\mathrm{O}}(q) = -\int \frac{d^3p}{(2\pi)^3}\mathrm{tr}\left[M\frac{\not{p}+im\sigma^x\mu^y}{p^2+m^2}\gamma^\mu\sigma^x\frac{\not{p}+\not{q}+im\sigma^x\mu^y}{(p+q)^2+m^2}\right]. \tag{E.63}$$

If $M \propto \sigma^x$, it can be shown that the leading order term is quadratic in q. A q-linear piece is obtained by assuming that $\mathrm{tr}\,(M\sigma^x) = 0$, in which case

$$\begin{aligned}\chi^\mu_{\mathrm{O}}(q) &= -m\int \frac{d^3p}{(2\pi)^3}\frac{1}{[p^2+m^2]\,[(p+q)^2+m^2]}\left\{p_\alpha\mathrm{tr}\,[M\gamma^\alpha\gamma^\mu\mu^y] + (p+q)_\alpha\mathrm{tr}\,[M\mu^y\gamma^\mu\gamma^\alpha]\right\}\\ &= \frac{m}{8\pi}\frac{iq_\alpha}{|q|}\arctan\left(\frac{|q|}{2m}\right)A_\mu(q)\left(\mathrm{tr}\,[\mu^yM\gamma^\alpha\gamma^\mu] - \mathrm{tr}\,[M\mu^y\gamma^\mu\gamma^\alpha]\right).\end{aligned} \tag{E.64}$$

This is only non-zero for $M = \mu^y\gamma^\nu$. Expanding the inverse tangent in small q, we find

$$\chi^\mu_\nu(q) \cong -\frac{1}{\pi}\epsilon^{\nu\alpha\mu}q_\alpha A_\mu(q) \cong \frac{i}{\pi}\epsilon^{\mu\nu\alpha}\partial_\alpha A_\beta(q). \tag{E.65}$$

Returning to real time, we obtain the result in Eq. (6.52).

References

[1] A. Abanov and P. Wiegmann, "Theta-terms in nonlinear sigma-models," Nuclear Physics B **570**, 685 (2000), arXiv:hep-th/9911025 [hep-th] .

[2] I. Affleck and J. B. Marston, "Large-n limit of the Heisenberg-Hubbard model: Implications for high-T_c superconductors," Phys. Rev. B **37**, 3774 (1988).

[3] I. Affleck, Z. Zou, T. Hsu, and P. W. Anderson, "SU(2) gauge symmetry of the large-U limit of the Hubbard model," Phys. Rev. B **38**, 745 (1988).

[4] V. Alexandrov, P. Coleman, and O. Erten, "Kondo Breakdown in Topological Kondo Insulators," Phys. Rev. Lett. **114**, 177202 (2015).

[5] V. Alexandrov, M. Dzero, and P. Coleman, "Cubic Topological Kondo Insulators," Phys. Rev. Lett. **111**, 226403 (2013).

[6] D. Amit and V. Martin-Mayor, *Field Theory, the Renormalization Group, and Critical Phenomena: Graphs to Computers* (2005).

[7] P. W. Anderson, "Localized Magnetic States in Metals," Phys. Rev. **124**, 41 (1961).

[8] P. W. Anderson, "The Resonating Valence Bond State in La_2CuO_4 and Superconductivity," Science **235**, 1196 (1987).

[9] T. Appelquist and R. D. Pisarski, "High-temperature Yang-Mills theories and three-dimensional quantum chromodynamics," Phys. Rev. D **23**, 2305 (1981).

[10] D. P. Arovas and A. Auerbach, "Functional integral theories of low-dimensional quantum Heisenberg models," Phys. Rev. B **38**, 316 (1988).

[11] A. Auerbach, *Interacting electrons and quantum magnetism* (Springer, New York, NY, 2012).

[12] F. A. Bais, P. van Driel, and M. de Wild Propitius, "Quantum symmetries in discrete gauge theories," Phys. Lett. B **280**, 63 (1992).

[13] L. Balents, "Spin liquids in frustrated magnets," Nature **464**, 199 (2010).

[14] M. Barkeshli, "Transitions between chiral spin liquids and $\mathbb{Z}_2$ spin liquids," arXiv preprint arXiv:1307.8194 (2013).

[15] M. Barkeshli, H. Yao, and S. A. Kivelson, "Gapless spin liquids: Stability and possible experimental relevance," Phys. Rev. B **87**, 140402 (2013), arXiv:1208.3869 [cond-mat.str-el] .

[16] G. Baskaran and P. W. Anderson, "Gauge theory of high-temperature superconductors and strongly correlated Fermi systems," Phys. Rev. B **37**, 580 (1988).

[17] B. A. Bernevig and T. L. Hughes, *Topological Insulators and Topological Superconductors* (Princeton University Press, 2013).

[18] B. A. Bernevig, T. L. Hughes, and S.-C. Zhang, "Quantum Spin Hall Effect and Topological Phase Transition in HgTe Quantum Wells," Science **314**, 1757 (2006).

[19] V. Borokhov, A. Kapustin, and X. Wu, "Topological Disorder Operators in Three-Dimensional Conformal Field Theory," Journal of High Energy Physics **2002**, 049 (2002), arXiv:hep-th/0206054 [hep-th] .

[20] P. Nikolić, "Two-dimensional heavy fermions on the strongly correlated boundaries of Kondo topological insulators," Phys. Rev. B **90**, 235107 (2014).

[21] S. Chatterjee, Y. Qi, S. Sachdev, and J. Steinberg, "Superconductivity from a confinement transition out of a fractionalized Fermi liquid with $\mathbb{Z}_2$ topological and Ising-nematic orders," Phys. Rev. B **94**, 024502 (2016), arXiv:1603.03041 [cond-mat.str-el] .

[22] S. Chatterjee and S. Sachdev, "Insulators and metals with topological order and discrete symmetry breaking," Phys. Rev. B **95**, 205133 (2017), arXiv:1703.00014 [cond-mat.str-el] .

[23] S. Chatterjee, S. Sachdev, and M. S. Scheurer, "Intertwining topological order and broken symmetry in a theory of fluctuating spin-density waves," Phys. Rev. Lett. **119**, 227002 (2017).

[24] G. Chen, A. Essin, and M. Hermele, "Majorana spin liquids and projective realization of SU(2) spin symmetry," Phys. Rev. B **85**, 094418 (2012), arXiv:1112.0586 [cond-mat.str-el] .

[25] J.-Y. Chen, J. H. Son, C. Wang, and S. Raghu, "Exact boson-fermion duality on a 3d euclidean lattice," Phys. Rev. Lett. **120**, 016602 (2018).

[26] W. Chen, M. P. A. Fisher, and Y.-S. Wu, "Mott transition in an anyon gas," Phys. Rev. B **48**, 13749 (1993).

[27] X. Chen, Z.-C. Gu, Z.-X. Liu, and X.-G. Wen, "Symmetry protected topological orders and the group cohomology of their symmetry group," Phys. Rev. B **87**, 155114 (2013), arXiv:1106.4772 [cond-mat.str-el] .

[28] S. M. Chester, M. Mezei, S. S. Pufu, and I. Yaakov, "Monopole operators from the $4-\epsilon$ expansion," Journal of High Energy Physics **2016**, 15 (2016).

[29] S. M. Chester and S. S. Pufu, "Anomalous dimensions of scalar operators in QED$_3$," Journal of High Energy Physics **2016**, 1 (2016).

[30] A. V. Chubukov, S. Sachdev, and T. Senthil, "Quantum phase transitions in frustrated quantum antiferromagnets," Nuclear Physics B **426**, 601 (1994).

[31] B. Coqblin and J. R. Schrieffer, "Exchange interaction in alloys with cerium impurities," Phys. Rev. **185**, 847 (1969).

[32] J. D'Emidio and R. K. Kaul, "First-order superfluid to valence-bond solid phase transitions in easy-plane SU(n) magnets for small n," Phys. Rev. B **93**, 054406 (2016).

[33] J. D'Emidio and R. K. Kaul, "New easy-plane $\mathbb{C}\mathrm{I}^{N-1}$ fixed points," Phys. Rev. Lett. **118**, 187202 (2017).

[34] J. D. Denlinger, J. W. Allen, J.-S. Kang, K. Sun, B.-I. Min, D.-J. Kim, and Z. Fisk, "SmB$_6$ Photoemmission: Past and Present," JPS Conf. Proc. **3**, 017038 (2014).

[35] S. Depenbrock, I. P. McCulloch, and U. Schollwöck, "Nature of the spin-liquid ground state of the $s = 1/2$ heisenberg model on the kagome lattice," Phys. Rev. Lett. **109**, 067201 (2012).

[36] P. Di Francesco, P. Mathieu, and D. Sénéchal, *Conformal field theory* (Springer, New York, NY, 2012).

[37] S. Doniach, "The Kondo lattice and weak antiferromagnetism," Physica B+C **91**, 231 (1977).

[38] E. Dyer, M. Mezei, and S. S. Pufu, "Monopole Taxonomy in Three-Dimensional Conformal Field Theories," ArXiv e-prints (2013), arXiv:1309.1160 [hep-th] .

[39] A. Dymarsky, Z. Komargodski, A. Schwimmer, and S. Theisen, "On scale and conformal invariance in four dimensions," Journal of High Energy Physics **2015**, 171 (2015).

[40] M. Dzero, K. Sun, P. Coleman, and V. Galitski, "Theory of topological Kondo insulators," Phys. Rev. B **85**, 045130 (2012).

[41] M. Dzero, K. Sun, V. Galitski, and P. Coleman, "Topological Kondo Insulators," Phys. Rev. Lett. **104**, 106408 (2010).

[42] M. Dzero, J. Xia, V. Galitski, and P. Coleman, "Topological kondo insulators," Annual Review of Condensed Matter Physics **7**, 249 (2016), https://arxiv.org/abs/1506.05635 .

[43] A. M. Essin and M. Hermele, "Classifying fractionalization: Symmetry classification of gapped $\mathbb{Z}_2$ spin liquids in two dimensions," Phys. Rev. B **87**, 104406 (2013), arXiv:1212.0593 [cond-mat.str-el] .

[44] M. S. Foster and I. L. Aleiner, "Graphene via large N: A renormalization group study," Phys. Rev. B **77**, 195413 (2008).

[45] M. Freedman, C. Nayak, K. Shtengel, K. Walker, and Z. Wang, "A class of P, T-invariant topological phases of interacting electrons," Annals of Physics **310**, 428 (2004), arXiv:cond-mat/0307511 [cond-mat.str-el] .

[46] L. Fu and C. L. Kane, "Topological insulators with inversion symmetry," Phys. Rev. B **76**, 045302 (2007).

[47] L. Fu, C. L. Kane, and E. J. Mele, "Topological insulators in three dimensions," Phys. Rev. Lett. **98**, 106803 (2007).

[48] L. Fu, S. Sachdev, and C. Xu, "Geometric phases and competing orders in two dimensions," Phys. Rev. B **83**, 165123 (2011), arXiv:1010.3745 [cond-mat.str-el] .

[49] S. D. Geraedts and O. I. Motrunich, "Monte Carlo study of a U(1) × U(1) system with π-statistical interaction," Phys. Rev. B **85**, 045114 (2012).

[50] T. Giamarchi, *Quantum Physics in One Dimension*, International Series of Monographs on Physics (Clarendon Press, 2003).

[51] T. Grover and T. Senthil, "Topological spin hall states, charged skyrmions, and superconductivity in two dimensions," Phys. Rev. Lett. **100**, 156804 (2008).

[52] T. Grover and A. Vishwanath, "Quantum phase transition between integer quantum Hall states of bosons," Phys. Rev. B **87**, 045129 (2013), arXiv:1210.0907 [cond-mat.str-el] .

[53] F. D. M. Haldane, "O(3) Nonlinear σ Model and the Topological Distinction between Integer- and Half-Integer-Spin Antiferromagnets in Two Dimensions," Phys. Rev. Lett. **61**, 1029 (1988).

[54] T. H. Hansson, V. Oganesyan, and S. L. Sondhi, "Superconductors are topologically ordered," Annals of Physics **313**, 497 (2004), arXiv:cond-mat/0404327 [cond-mat.supr-con] .

[55] K. Harada, T. Suzuki, T. Okubo, H. Matsuo, J. Lou, H. Watanabe, S. Todo, and N. Kawashima, "Possibility of deconfined criticality in SU(n) Heisenberg models at small N," Phys. Rev. B **88**, 220408 (2013).

[56] A. B. Harris, "Effect of random defects on the critical behaviour of ising models," Journal of Physics C: Solid State Physics **7**, 1671 (1974).

[57] M. Z. Hasan and C. L. Kane, "*Colloquium*: Topological insulators," Rev. Mod. Phys. **82**, 3045 (2010).

[58] M. B. Hastings, "Dirac structure, RVB, and Goldstone modes in the kagomé antiferromagnet," Phys. Rev. B **63**, 014413 (2001), cond-mat/0005391 .

[59] M. B. Hastings, "Lieb-Schultz-Mattis in higher dimensions," Phys. Rev. B **69**, 104431 (2004), arXiv:cond-mat/0305505 [cond-mat.str-el] .

[60] Y.-C. He, M. P. Zaletel, M. Oshikawa, and F. Pollmann, "Signatures of Dirac cones in a DMRG study of the kagome Heisenberg model," Phys. Rev. X **7**, 031020 (2017).

[61] M. Hermele, Y. Ran, P. A. Lee, and X.-G. Wen, "Properties of an algebraic spin liquid on the kagome lattice," Phys. Rev. B **77**, 224413 (2008), arXiv:0803.1150 [cond-mat.str-el] .

[62] M. Hermele, T. Senthil, and M. P. A. Fisher, "Algebraic spin liquid as the mother of many competing orders," Phys. Rev. B **72**, 104404 (2005).

[63] M. Hermele, T. Senthil, and M. P. A. Fisher, "Erratum: Algebraic spin liquid as the mother of many competing orders [Phys. Rev. B **72** , 104404 (2005)]," Phys. Rev. B **76**, 149906 (2007).

[64] M. Hermele, T. Senthil, M. P. A. Fisher, P. A. Lee, N. Nagaosa, and X.-G. Wen, "Stability of U(1) spin liquids in two dimensions," Phys. Rev. B **70**, 214437 (2004), cond-mat/0404751 .

[65] C. Hickey, L. Cincio, Z. Papić, and A. Paramekanti, "Haldane-Hubbard Mott Insulator: From Tetrahedral Spin Crystal to Chiral Spin Liquid," Phys. Rev. Lett. **116**, 137202 (2016), arXiv:1509.08461 [cond-mat.str-el] .

[66] G. 't Hooft, "Magnetic monopoles in unified gauge theories," Nucl. Phys. B **79**, 276 (1974).

[67] P.-S. Hsin and N. Seiberg, "Level/rank duality and Chern-Simons-matter theories," Journal of High Energy Physics **2016**, 95 (2016).

[68] Y. Huh, M. Punk, and S. Sachdev, "Vison states and confinement transitions of Z_2 spin liquids on the kagome lattice," Phys. Rev. B **84**, 094419 (2011).

[69] Y. Huh and P. Strack, "Stress tensor and current correlators of interacting conformal field theories in 2+1 dimensions: fermionic Dirac matter coupled to U(1) gauge field," Journal of High Energy Physics **2015**, 147 (2015).

[70] J. Iaconis and L. Balents, "Many-body effects in topological Kondo insulators," Phys. Rev. B **91**, 245127 (2015).

[71] Y. Iqbal, F. Becca, and D. Poilblanc, "Projected wave function study of $\mathbb{Z}_2$ spin liquids on the kagome lattice for the spin-$\frac{1}{2}$ quantum heisenberg antiferromagnet," Phys. Rev. B **84**, 020407 (2011).

[72] Y. Iqbal, F. Becca, S. Sorella, and D. Poilblanc, "Gapless spin-liquid phase in the kagome spin-$\frac{1}{2}$ heisenberg antiferromagnet," Phys. Rev. B **87**, 060405 (2013).

[73] Y. Iqbal, W.-J. Hu, R. Thomale, D. Poilblanc, and F. Becca, "Spin liquid nature in the Heisenberg J_1-J_2 triangular antiferromagnet," Phys. Rev. B **93**, 144411 (2016), arXiv:1601.06018 [cond-mat.str-el] .

[74] Y. Iqbal, D. Poilblanc, and F. Becca, "Spin-1/2 Heisenberg J_1-J_2 antiferromagnet on the kagome lattice," Phys. Rev. B **91**, 020402 (2015), arXiv:1410.7359 [cond-mat.str-el] .

[75] R. Jackiw and S. Templeton, "How super-renormalizable interactions cure their infrared divergences," Phys. Rev. D **23**, 2291 (1981).

[76] R. A. Jalabert and S. Sachdev, "Spontaneous alignment of frustrated bonds in an anisotropic, three-dimensional Ising model," Phys. Rev. B **44**, 686 (1991).

[77] C.-M. Jian, Z. Bi, and C. Xu, "Lieb-schultz-mattis theorem and its generalizations from the perspective of the symmetry-protected topological phase," Phys. Rev. B **97**, 054412 (2018).

[78] C.-M. Jian, A. Rasmussen, Y.-Z. You, and C. Xu, "Emergent Symmetry and Tricritical Points near the deconfined Quantum Critical Point," (2017), arXiv:1708.03050 [cond-mat.str-el] .

[79] H.-C. Jiang, Z. Wang, and L. Balents, "Identifying topological order by entanglement entropy," Nature Physics **8**, 902 (2012), arXiv:1205.4289 [cond-mat.str-el] .

[80] J. Jiang, S. Li, T. Zhang, Z. Sun, F. Chen, Z. R. Ye, M. Xu, Q. Q. Ge, S. Y. Tan, X. H. Niu, M. Xia, B. P. Xie, Y. F. Li, X. H. Chen, H. H. Wen, and D. L. Feng, "Observation of possible topological in-gap surface states in the Kondo insulator SmB_6 by photoemission," Nat Commun **4** (2013).

[81] S. Jiang, P. Kim, J. H. Han, and Y. Ran, "Competing Spin Liquid Phases in the S=$\frac{1}{2}$ Heisenberg Model on the Kagome Lattice," ArXiv e-prints (2016), arXiv:1610.02024 [cond-mat.str-el] .

[82] S. Kachru, M. Mulligan, G. Torroba, and H. Wang, "Nonsupersymmetric dualities from mirror symmetry," Phys. Rev. Lett. **118**, 011602 (2017), arXiv:1609.02149 [hep-th] .

[83] V. Kalmeyer and R. B. Laughlin, "Equivalence of the resonating-valence-bond and fractional quantum Hall states," Phys. Rev. Lett. **59**, 2095 (1987).

[84] C. L. Kane and E. J. Mele, "Z_2 Topological Order and the Quantum Spin Hall Effect," Phys. Rev. Lett. **95**, 146802 (2005).

[85] A. Karch and D. Tong, "Particle-Vortex Duality from 3d Bosonization," Phys. Rev. **X6**, 031043 (2016), arXiv:1606.01893 [hep-th] .

[86] N. Karthik and R. Narayanan, "No evidence for bilinear condensate in parity-invariant three-dimensional QED with massless fermions," Phys. Rev. D **93**, 045020 (2016), arXiv:1512.02993 [hep-lat] .

[87] N. Karthik and R. Narayanan, "Scale invariance of parity-invariant three-dimensional qed," Phys. Rev. D **94**, 065026 (2016), arXiv:1606.04109 [hep-lat] .

[88] N. Karthik and R. Narayanan, "Flavor and topological current correlators in parity-invariant three-dimensional qed," Phys. Rev. D **96**, 054509 (2017).

[89] R. K. Kaul, "Spin nematics, valence-bond solids, and spin liquids in SO(n) quantum spin models on the triangular lattice," Phys. Rev. Lett. **115**, 157202 (2015).

[90] R. K. Kaul and S. Sachdev, "Quantum criticality of U(1) gauge theories with fermionic and bosonic matter in two spatial dimensions," Phys. Rev. B **77**, 155105 (2008), arXiv:0801.0723 [cond-mat.str-el] .

[91] K. Kaveh and I. F. Herbut, "Chiral symmetry breaking in three-dimensional quantum electrodynamics in the presence of irrelevant interactions: A renormalization group study," Phys. Rev. B **71**, 184519 (2005).

[92] D. J. Kim, T. Grant, and Z. Fisk, "Limit Cycle and Anomalous Capacitance in the Kondo Insulator SmB_6," Phys. Rev. Lett. **109**, 096601 (2012).

[93] D. J. Kim, S. Thomas, T. Grant, J. Botimer, Z. Fisk, and J. Xia, "Surface hall effect and nonlocal transport in smb6: Evidence for surface conduction," Scientific Reports **3**, 3150 EP (2013).

[94] A. Y. Kitaev, "Fault-tolerant quantum computation by anyons," Annals of Physics **303**, 2 (2003), arXiv:quant-ph/9707021 .

[95] A. Y. Kitaev, "Anyons in an exactly solved model and beyond," Annals of Physics **321**, 2 (2006), arXiv:cond-mat/0506438 [cond-mat.mes-hall] .

[96] S. A. Kivelson, D. S. Rokhsar, and J. P. Sethna, "2e or not 2e : Flux Quantization in the Resonating Valence Bond State," Europhys. Lett. **6**, 353 (1988).

[97] I. R. Klebanov, S. S. Pufu, S. Sachdev, and B. R. Safdi, "Entanglement entropy of 3-d conformal gauge theories with many flavors," Journal of High Energy Physics **5**, 36 (2012), arXiv:1112.5342 [hep-th] .

[98] J. Knolle and N. R. Cooper, "Quantum oscillations without a fermi surface and the anomalous de haas–van alphen effect," Phys. Rev. Lett. **115**, 146401 (2015), arXiv:1507.00885 [cond-mat.str-el] .

[99] A. V. Kotikov, V. I. Shilin, and S. Teber, "Critical behavior of $(2+1)$-dimensional QED: $1/N_f$ corrections in the landau gauge," Phys. Rev. D **94**, 056009 (2016).

[100] A. V. Kotikov and S. Teber, "Critical behavior of $(2+1)$-dimensional QED: $1/N_f$ corrections in an arbitrary nonlocal gauge," Phys. Rev. D **94**, 114011 (2016).

[101] A. B. Kuklov, M. Matsumoto, N. V. Prokof'ev, B. V. Svistunov, and M. Troyer, "Deconfined criticality: Generic first-order transition in the su(2) symmetry case," Phys. Rev. Lett. **101**, 050405 (2008).

[102] A. M. Läuchli, J. Sudan, and R. Moessner, "The $S = 1/2$ Kagome Heisenberg Antiferromagnet Revisited," arXiv e-prints (2016), arXiv:1611.06990 [cond-mat.str-el] .

[103] E. Lieb, T. Schultz, and D. Mattis, "Two soluble models of an antiferromagnetic chain," Annals of Physics **16**, 407 (1961).

[104] J. Lou, A. W. Sandvik, and N. Kawashima, "Antiferromagnetic to valence-bond-solid transitions in two-dimensional SU(n) heisenberg models with multispin interactions," Phys. Rev. B **80**, 180414 (2009).

[105] F. Lu, J. Zhao, H. Weng, Z. Fang, and X. Dai, "Correlated Topological Insulators with Mixed Valence," Phys. Rev. Lett. **110**, 096401 (2013).

[106] Y.-M. Lu, "Symmetric $\mathbb{Z}_2$ spin liquids and their neighboring phases on triangular lattice," Phys. Rev. B **93**, 165113 (2016), arXiv:1505.06495 [cond-mat.str-el] .

[107] Y.-M. Lu, G. Y. Cho, and A. Vishwanath, "Unification of bosonic and fermionic theories of spin liquids on the kagome lattice," Phys. Rev. B **96**, 205150 (2017).

[108] A. W. W. Ludwig, M. P. A. Fisher, R. Shankar, and G. Grinstein, "Integer quantum Hall transition: An alternative approach and exact results," Phys. Rev. B **50**, 7526 (1994).

[109] J.-W. Mei, J.-Y. Chen, H. He, and X.-G. Wen, "Gapped spin liquid with F_2 topological order for the kagome heisenberg model," Phys. Rev. B **95**, 235107 (2017).

[110] M. A. Metlitski and R. Thorngren, "Intrinsic and emergent anomalies at deconfined critical points," ArXiv e-prints (2017), arXiv:1707.07686 [cond-mat.str-el] .

[111] M. A. Metlitski, A. Vishwanath, and C. Xu, "Duality and bosonization of (2+1)-dimensional Majorana fermions," Phys. Rev. B **95**, 205137 (2017), arXiv:1611.05049 [cond-mat.str-el] .

[112] R. Moessner and S. L. Sondhi, "Ising models of quantum frustration," Phys. Rev. B **63**, 224401 (2001).

[113] R. Moessner and S. L. Sondhi, "Resonating valence bond phase in the triangular lattice quantum dimer model," Phys. Rev. Lett. **86**, 1881 (2001).

[114] J. E. Moore and L. Balents, "Topological invariants of time-reversal-invariant band structures," Phys. Rev. B **75**, 121306 (2007).

[115] O. I. Motrunich and A. Vishwanath, "Emergent photons and transitions in the O(3) sigma model with hedgehog suppression," Phys. Rev. B **70**, 075104 (2004).

[116] D. F. Mross, J. Alicea, and O. I. Motrunich, "Explicit derivation of duality between a free dirac cone and quantum electrodynamics in $(2+1)$ dimensions," Phys. Rev. Lett. **117**, 016802 (2016).

[117] G. Murthy and S. Sachdev, "Action of hedgehog instantons in the disordered phase of the (2 + 1)-dimensional CP^{N-1} model," Nuclear Physics B **344**, 557 (1990).

[118] J. Murugan and H. Nastase, "Particle-vortex duality in topological insulators and superconductors," JHEP **05**, 159 (2017), arXiv:1606.01912 [hep-th] .

[119] A. Nahum, J. T. Chalker, P. Serna, M. Ortuño, and A. M. Somoza, "3d loop models and the CP^{n-1} sigma model," Phys. Rev. Lett. **107**, 110601 (2011).

[120] A. Nahum, J. T. Chalker, P. Serna, M. Ortuño, and A. M. Somoza, "Deconfined quantum criticality, scaling violations, and classical loop models," Phys. Rev. X **5**, 041048 (2015).

[121] A. Nahum, P. Serna, J. T. Chalker, M. Ortuño, and A. M. Somoza, "Emergent SO(5) Symmetry at the Néel to Valence-Bond-Solid Transition," Phys. Rev. Lett. **115**, 267203 (2015), arXiv:1508.06668 [cond-mat.str-el] .

[122] M. Neupane, N. Alidoust, S.-Y. Xu, T. Kondo, Y. Ishida, D. J. Kim, C. Liu, I. Belopolski, Y. J. Jo, T.-R. Chang, H.-T. Jeng, T. Durakiewicz, L. Balicas, H. Lin, A. Bansil, S. Shin, Z. Fisk, and M. Z. Hasan, "Surface electronic structure of the topological Kondo-insulator candidate correlated electron system SmB_6," Nat Commun **4** (2013).

[123] I. Paul, C. Pépin, and M. R. Norman, "Multiscale fluctuations near a Kondo breakdown quantum critical point," Phys. Rev. B **78**, 035109 (2008).

[124] W. A. Phelan, S. M. Koohpayeh, P. Cottingham, J. W. Freeland, J. C. Leiner, C. L. Broholm, and T. M. McQueen, "Correlation between Bulk Thermodynamic Measurements and the Low-Temperature-Resistance Plateau in SmB_6," Phys. Rev. X **4**, 031012 (2014).

[125] J. Polchinski, "Scale and conformal invariance in quantum field theory," Nuclear Physics B **303**, 226 (1988).

[126] A. Polyakov, "Compact gauge fields and the infrared catastrophe," Phys. Lett. B **59**, 82 (1975).

[127] A. Polyakov, "Quark confinement and topology of gauge theories," Nuclear Physics B **120**, 429 (1977).

[128] A. M. Polyakov, "Particle spectrum in quantum field theory," JETP Lett. **20**, 194 (1974).

[129] A. M. Polyakov, *Gauge Fields and Strings*, Contemporary concepts in physics (Taylor & Francis, 1987).

[130] A. P. Polychronakos, "Abelian Chern-Simons theories in 2 + 1 dimensions," Annals of Physics **203**, 231 (1990).

[131] A. C. Potter, C. Wang, M. A. Metlitski, and A. Vishwanath, "Realizing topological surface states in a lower-dimensional flat band," Phys. Rev. B **96**, 235114 (2017), arXiv:1609.08618 [cond-mat.str-el] .

[132] S. S. Pufu, "Anomalous dimensions of monopole operators in three-dimensional quantum electrodynamics," Phys. Rev. D **89**, 065016 (2014), arXiv:1303.6125 [hep-th] .

[133] S. Pujari, F. Alet, and K. Damle, "Transitions to valence-bond solid order in a honeycomb lattice antiferromagnet," Phys. Rev. B **91**, 104411 (2015).

[134] S. Pujari, K. Damle, and F. Alet, "Néel-state to valence-bond-solid transition on the honeycomb lattice: Evidence for deconfined criticality," Phys. Rev. Lett. **111**, 087203 (2013).

[135] X.-L. Qi and S.-C. Zhang, "Topological insulators and superconductors," Rev. Mod. Phys. **83**, 1057 (2011).

[136] Y. Qi and L. Fu, "Detecting crystal symmetry fractionalization from the ground state: Application to Z_2 spin liquids on the kagome lattice," Phys. Rev. B **91**, 100401 (2015), arXiv:1501.00009 [cond-mat.str-el] .

[137] Y. Q. Qin, Y.-Y. He, Y.-Z. You, Z.-Y. Lu, A. Sen, A. W. Sandvik, C. Xu, and Z. Y. Meng, "Duality between the deconfined quantum-critical point and the bosonic topological transition," Phys. Rev. X **7**, 031052 (2017).

[138] A. Ralko, M. Ferrero, F. Becca, D. Ivanov, and F. Mila, "Dynamics of the quantum dimer model on the triangular lattice: Soft modes and local resonating valence-bond correlations," Phys. Rev. B **74**, 134301 (2006).

[139] Y. Ran, M. Hermele, P. A. Lee, and X.-G. Wen, "Projected-Wave-Function Study of the Spin-1/2 Heisenberg Model on the Kagomé Lattice," Phys. Rev. Lett. **98**, 117205 (2007), cond-mat/0611414 .

[140] W. Rantner and X.-G. Wen, "Electron Spectral Function and Algebraic Spin Liquid for the Normal State of Underdoped High T_c Superconductors," Phys. Rev. Lett. **86**, 3871 (2001), cond-mat/0010378 .

[141] W. Rantner and X.-G. Wen, "Spin correlations in the algebraic spin liquid: Implications for high-T_c superconductors," Phys. Rev. B **66**, 144501 (2002).

[142] N. Read and B. Chakraborty, "Statistics of the excitations of the resonating-valence-bond state," Phys. Rev. B **40**, 7133 (1989).

[143] N. Read and S. Sachdev, "Valence-bond and spin-Peierls ground states of low-dimensional quantum antiferromagnets," Phys. Rev. Lett. **62**, 1694 (1989).

[144] N. Read and S. Sachdev, "Spin-Peierls, valence-bond solid, and Néel ground states of low-dimensional quantum antiferromagnets," Phys. Rev. B **42**, 4568 (1990).

[145] N. Read and S. Sachdev, "Large N expansion for frustrated quantum antiferromagnets," Phys. Rev. Lett. **66**, 1773 (1991).

[146] A. N. Redlich, "Gauge Non-invariance and Parity Non-conservation of Three-Dimensional Fermions," Phys. Rev. Lett. **52**, 18 (1984).

[147] A. N. Redlich, "Parity violation and gauge non-invariance of the effective gauge field action in three dimensions," Phys. Rev. D **29**, 2366 (1984).

[148] D. S. Rokhsar and S. A. Kivelson, "Superconductivity and the Quantum Hard-Core Dimer Gas," Phys. Rev. Lett. **61**, 2376 (1988).

[149] B. Roy, J. D. Sau, M. Dzero, and V. Galitski, "Surface theory of a family of topological Kondo insulators," Phys. Rev. B **90**, 155314 (2014).

[150] R. Roy, "Z_2 classification of quantum spin hall systems: An approach using time-reversal invariance," Phys. Rev. B **79**, 195321 (2009).

[151] S. Rychkov, *EPFL Lectures on Conformal Field Theory in D≥3 Dimensions* (Springer, 2017) arXiv:1601.05000 [hep-th] .

[152] S. N. Saadatmand and I. P. McCulloch, "Symmetry fractionalization in the topological phase of the spin-$\frac{1}{2}$ J_1-J_2 triangular heisenberg model," Phys. Rev. B **94**, 121111 (2016), arXiv:1606.00334 [cond-mat.str-el] .

[153] S. Sachdev, "Kagome and triangular-lattice Heisenberg antiferromagnets: Ordering from quantum fluctuations and quantum-disordered ground states with unconfined bosonic spinons," Phys. Rev. B **45**, 12377 (1992).

[154] S. Sachdev, "Nonzero-temperature transport near fractional quantum Hall critical points," Phys. Rev. B **57**, 7157 (1998), cond-mat/9709243 .

[155] S. Sachdev, *Quantum phase transitions* (Cambridge University Press, 2011).

[156] S. Sachdev and R. Jalabert, "Effective lattice models for two dimensional quantum antiferromagnets," Mod. Phys. Lett. B **04**, 1043 (1990).

[157] S. Sachdev and N. Read, "Large N expansion for frustrated and doped quantum antiferromagnets," Int. J. Mod. Phys. B **5**, 219 (1991), arXiv:cond-mat/0402109 [cond-mat.str-el] .

[158] S. Sachdev and M. Vojta, "Translational symmetry breaking in two-dimensional antiferromagnets and superconductors," J. Phys. Soc. Jpn **69**, Supp. B, 1 (1999), arXiv:cond-mat/9910231 [cond-mat.str-el] .

[159] A. W. Sandvik, "Evidence for deconfined quantum criticality in a two-dimensional heisenberg model with four-spin interactions," Phys. Rev. Lett. **98**, 227202 (2007).

[160] A. W. Sandvik, "Continuous quantum phase transition between an antiferromagnet and a valence-bond solid in two dimensions: Evidence for logarithmic corrections to scaling," Phys. Rev. Lett. **104**, 177201 (2010).

[161] A. W. Sandvik, S. Daul, R. R. P. Singh, and D. J. Scalapino, "Striped phase in a quantum xy model with ring exchange," Phys. Rev. Lett. **89**, 247201 (2002).

[162] J. R. Schrieffer and P. A. Wolff, "Relation between the Anderson and Kondo Hamiltonians," Phys. Rev. **149**, 491 (1966).

[163] M. Schuler, S. Whitsitt, L.-P. Henry, S. Sachdev, and A. M. Läuchli, "Universal signatures of quantum critical points from finite-size torus spectra: A window into the operator content of higher-dimensional conformal field theories," Phys. Rev. Lett. **117**, 210401 (2016), arXiv:1603.03042 [cond-mat.str-el] .

[164] N. Seiberg, T. Senthil, C. Wang, and E. Witten, "A Duality Web in 2+1 Dimensions and Condensed Matter Physics," Annals Phys. **374**, 395 (2016), arXiv:1606.01989 [hep-th] .

[165] A. Sen and A. W. Sandvik, "Example of a first-order Néel to valence-bond-solid transition in two dimensions," Phys. Rev. B **82**, 174428 (2010).

[166] T. Senthil, L. Balents, S. Sachdev, A. Vishwanath, and M. P. A. Fisher, "Quantum criticality beyond the Landau-Ginzburg-Wilson paradigm," Phys. Rev. B **70**, 144407 (2004), cond-mat/0312617 .

[167] T. Senthil and M. P. A. Fisher, "$\mathbb{Z}_2$ gauge theory of electron fractionalization in strongly correlated systems," Phys. Rev. B **62**, 7850 (2000), arXiv:cond-mat/9910224 [cond-mat.str-el] .

[168] T. Senthil and M. P. A. Fisher, "Competing orders, nonlinear sigma models, and topological terms in quantum magnets," Phys. Rev. B **74**, 064405 (2006), arXiv:cond-mat/0510459 [cond-mat.str-el] .

[169] T. Senthil, S. Sachdev, and M. Vojta, "Fractionalized Fermi Liquids," Phys. Rev. Lett. **90**, 216403 (2003).

[170] T. Senthil, A. Vishwanath, L. Balents, S. Sachdev, and M. P. A. Fisher, "Deconfined Quantum Critical Points," Science **303**, 1490 (2004), cond-mat/0311326 .

[171] T. Senthil, M. Vojta, and S. Sachdev, "Weak magnetism and non-Fermi liquids near heavy-fermion critical points," Phys. Rev. B **69**, 035111 (2004).

[172] H. Shao, W. Guo, and A. W. Sandvik, "Quantum criticality with two length scales," Science **352**, 213 (2016).

[173] D. Simmons-Duffin, "TASI lectures on the conformal bootstrap," arXiv:1602.07982 (2016).

[174] B. S. Tan, Y.-T. Hsu, B. Zeng, M. C. Hatnean, N. Harrison, Z. Zhu, M. Hartstein, M. Kiourlappou, A. Srivastava, M. D. Johannes, T. P. Murphy, J.-H. Park, L. Balicas, G. G. Lonzarich, G. Balakrishnan, and S. E. Sebastian, "Unconventional Fermi surface in an insulating state," Science **349**, 287 (2015).

[175] A. Tanaka and X. Hu, "Many-Body Spin Berry Phases Emerging from the π-Flux State: Competition between Antiferromagnetism and the Valence-Bond-Solid State," Phys. Rev. Lett. **95**, 036402 (2005), arXiv:cond-mat/0501365 [cond-mat.str-el] .

[176] S. Templeton, "Summation of coupling-constant logarithms in three-dimensional QED," Phys. Rev. D **24**, 3134 (1981).

[177] S. Templeton, "Summation of dominant coupling constant logarithms in QED_3," Physics Letters B **103**, 134 (1981).

[178] A. Vishwanath and T. Senthil, "Physics of three-dimensional bosonic topological insulators: Surface-deconfined criticality and quantized magnetoelectric effect," Phys. Rev. X **3**, 011016 (2013).

[179] C. Wang, A. Nahum, M. A. Metlitski, C. Xu, and T. Senthil, "Deconfined Quantum Critical Points: Symmetries and Dualities," Phys. Rev. X **7**, 031051 (2017), arXiv:1703.02426 [cond-mat.str-el] .

[180] F. Wang and A. Vishwanath, "Spin-liquid states on the triangular and kagomé lattices: A projective-symmetry-group analysis of schwinger boson states," Phys. Rev. B **74**, 174423 (2006).

[181] X. G. Wen, "Vacuum degeneracy of chiral spin states in compactified space," Phys. Rev. B **40**, 7387 (1989).

[182] X. G. Wen, "Topological orders in rigid states," International Journal of Modern Physics B **04**, 239 (1990).

[183] X. G. Wen, "Mean-field theory of spin-liquid states with finite energy gap and topological orders," Phys. Rev. B **44**, 2664 (1991).

[184] X.-G. Wen, "Quantum orders and symmetric spin liquids," Phys. Rev. B **65**, 165113 (2002), arXiv:cond-mat/0107071 [cond-mat.str-el] .

[185] X.-G. Wen, "Quantum Orders in an Exact Soluble Model," Phys. Rev. Lett. **90**, 016803 (2003), arXiv:quant-ph/0205004 .

[186] X.-G. Wen, *Quantum field theory of many-body systems: from the origin of sound to an origin of light and electrons* (Oxford University Press, 2004).

[187] X. G. Wen and Q. Niu, "Ground-state degeneracy of the fractional quantum Hall states in the presence of a random potential and on high-genus Riemann surfaces," Phys. Rev. B **41**, 9377 (1990).

[188] X. G. Wen, F. Wilczek, and A. Zee, "Chiral spin states and superconductivity," Phys. Rev. B **39**, 11413 (1989).

[189] S. Whitsitt and S. Sachdev, "Transition from the $\mathbb{Z}_2$ spin liquid to antiferromagnetic order: Spectrum on the torus," Phys. Rev. B **94**, 085134 (2016), arXiv:1603.05652 [cond-mat.str-el] .

[190] A. Wietek and A. M. Läuchli, "Chiral spin liquid and quantum criticality in extended $s = \frac{1}{2}$ Heisenberg models on the triangular lattice," Phys. Rev. B **95**, 035141 (2017), arXiv:1604.07829 [cond-mat.str-el] .

[191] K. G. Wilson, "Renormalization group and critical phenomena. I. Renormalization group and the kadanoff scaling picture," Phys. Rev. B **4**, 3174 (1971).

[192] K. G. Wilson, "Renormalization group and critical phenomena. II. Phase-space cell analysis of critical behavior," Phys. Rev. B **4**, 3184 (1971).

[193] K. G. Wilson and M. E. Fisher, "Critical exponents in 3.99 dimensions," Phys. Rev. Lett. **28**, 240 (1972).

[194] E. Witten, "Quantum field theory and the Jones polynomial," Communications in Mathematical Physics **121**, 351 (1989).

[195] S. Wolgast, C. Kurdak, K. Sun, J. W. Allen, D.-J. Kim, and Z. Fisk, "Low-temperature surface conduction in the Kondo insulator SmB_6," Phys. Rev. B **88**, 180405 (2013).

[196] C. Xu, "Three-dimensional symmetry-protected topological phase close to antiferromagnetic néel order," Phys. Rev. B **87**, 144421 (2013).

[197] C. Xu and L. Balents, "Quantum phase transitions around the staggered valence-bond solid," Phys. Rev. B **84**, 014402 (2011), arXiv:1103.1638 [cond-mat.str-el] .

[198] C. Xu and S. Sachdev, "Square-lattice algebraic spin liquid with SO(5) symmetry," Phys. Rev. Lett. **100**, 137201 (2008).

[199] C. Xu and S. Sachdev, "Global phase diagrams of frustrated quantum antiferromagnets in two dimensions: Doubled chern-simons theory," Phys. Rev. B **79**, 064405 (2009).

[200] C. Xu and Y.-Z. You, "Self-dual quantum electrodynamics as boundary state of the three-dimensional bosonic topological insulator," Phys. Rev. B **92**, 220416 (2015).

[201] N. Xu, C. E. Matt, E. Pomjakushina, X. Shi, R. S. Dhaka, N. C. Plumb, M. Radović, P. K. Biswas, D. Evtushinsky, V. Zabolotnyy, J. H. Dil, K. Conder, J. Mesot, H. Ding, and M. Shi, "Exotic kondo crossover in a wide temperature region in the topological kondo insulator smb_6 revealed by high-resolution arpes," Phys. Rev. B **90**, 085148 (2014).

[202] N. Xu, X. Shi, P. K. Biswas, C. E. Matt, R. S. Dhaka, Y. Huang, N. C. Plumb, M. Radović, J. H. Dil, E. Pomjakushina, K. Conder, A. Amato, Z. Salman, D. M. Paul, J. Mesot, H. Ding, and M. Shi, "Surface and bulk electronic structure of the strongly correlated system SmB_6 and implications for a topological Kondo insulator," Phys. Rev. B **88**, 121102 (2013).

[203] S. Yan, D. A. Huse, and S. R. White, "Spin-Liquid Ground State of the S = 1/2 Kagome Heisenberg Antiferromagnet," Science **332**, 1173 (2011), arXiv:1011.6114 [cond-mat.str-el] .

[204] F. Yang and H. Yao, "Frustrated resonating valence bond states in two dimensions: Classification and short-range correlations," Phys. Rev. Lett. **109**, 147209 (2012), arXiv:1204.6381 [cond-mat.str-el] .

[205] X. Yang and F. Wang, "Schwinger boson spin-liquid states on square lattice," Phys. Rev. B **94**, 035160 (2016), arXiv:1507.07621 [cond-mat.str-el] .

[206] J. Ye, "Effects of weak disorders on quantum Hall critical points," Phys. Rev. B **60**, 8290 (1999).

[207] J. Ye and S. Sachdev, "Coulomb Interactions at Quantum Hall Critical Points of Systems in a Periodic Potential," Phys. Rev. Lett. **80**, 5409 (1998), cond-mat/9712161 .

[208] M. P. Zaletel, Y.-M. Lu, and A. Vishwanath, "Measuring space-group symmetry fractionalization in $_2$ spin liquids," Phys. Rev. B **96**, 195164 (2017), arXiv:1501.01395 [cond-mat.str-el] .

[209] X. Zhang, N. P. Butch, P. Syers, S. Ziemak, R. L. Greene, and J. Paglione, "Hybridization, Inter-Ion Correlation, and Surface States in the Kondo Insulator SmB_6," Phys. Rev. X **3**, 011011 (2013).

[210] X.-F. Zhang, Y.-C. He, S. Eggert, R. Moessner, and F. Pollmann, "Continuous easy-plane deconfined phase transition on the kagome lattice," ArXiv e-prints (2017), arXiv:1706.05414 [cond-mat.str-el] .

[211] W. Zheng, J.-W. Mei, and Y. Qi, "Classification and Monte Carlo study of symmetric $\mathbb{Z}_2$ spin liquids on the triangular lattice," (2015), arXiv:1505.05351 [cond-mat.str-el] .

[212] Z. Zhu and S. R. White, "Spin liquid phase of the S =1/2 J_1-J_2 Heisenberg model on the triangular lattice," Phys. Rev. B **92**, 041105 (2015), arXiv:1502.04831 [cond-mat.str-el] .

[213] I. J. Zucker, "Exact results for some lattice sums in 2, 4, 6 and 8 dimensions," Journal of Physics A: Mathematical, Nuclear and General **7**, 1568 (1974).